DEVELOPMENT OF SOLAR COOKER WITH TEMPERATURE CONTROLLED THERMAL ENERGY STORAGE UNITS

Thesis

Submitted in partial fulfilment of the requirements for the degree of

DOCTOR OF PHILOSOPHY

By

ANIL KUMAR B C

DEPARTMENT OF MECHANICAL ENGINEERING

NATIONAL INSTITUTE OF TECHNOLOGY KARNATAKA

SURATHKAL, MANGALORE-575 025

February 2023

DECLARATION

I hereby declare that the Research Thesis entitled "**Development of solar cooker with temperature controlled thermal energy storage units**" which is being submitted to **the National Institute of Technology Karnataka, Surathkal** in partial fulfillment of the requirements for the award of the Degree of **Doctor of Philosophy** in **Mechanical Engineering** is a bonafide report of the research work carried out by me. The material contained in this Research Thesis has not been submitted to any other Universities or Institutes for the award of any degree.

Register Number: **197076ME001**

Name of the Research Scholar: **ANIL KUMAR B C**

Signature of the Research Scholar:

Department of Mechanical Engineering

Place: NITK-Surathkal

Date: 02-02-2023

i

CERTIFICATE

This is to certify that the Research Thesis entitled "**Development of solar cooker with temperature controlled thermal energy storage units**" submitted by **Mr. Anil Kumar B C (Register Number: 197076ME001)** as the record of the research work carried out by him, *is accepted as the Research Thesis submission* in partial fulfilment of the requirements for the award of the Degree of **Doctor of Philosophy**.
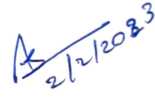
Research Guides

Dr. Ranjith M

Assistant Professor

Department of Mechanical Engineering

Dr. Anish S

Associate Professor

Department of Mechanical Engineering

Chairman-DRPC

Date: 20.2.2023

iii

ACKNOWLEDGEMENT

ABSTRACT

Solar cookers (SCs) have been a research focus worldwide because of their numerous advantages, such as no running costs, non-polluting nature, and ample availability of solar energy. Different sensible and latent heat storage materials are used to extend the usability of SCs in the late evening hours. Recently, the latent heat of phase change materials (PCMs) used as thermal energy storage (TES) medium has become remarkable because of its high energy density and constant temperature operating characteristics. In light of this, the main objective of the present study is to design, optimize, fabricate, and perform an experimental investigation of solar box cooker (SBC) with constant temperature heat storage unit incorporating PCM. Prediction models are also developed to forecast the component temperatures of SBC.

As a preliminary work, three geometries of SBCs are developed and tested to familiarize the test procedures and performance assessment. A rectangular-shaped SBC (RSBC) is fabricated by incorporating an optimum mixture of sensible heat storage materials below the absorber plate. The optimum cooker surface area is estimated with analytical heat loss and design equations solved through an iterative procedure implemented in MATLAB. Next, a cylindrical-shaped SBC (CSBC) is designed and fabricated using the minimum entropy generation (MEG) method and iterative design procedure. The experimental investigation is carried out to check the effectiveness of the frustum of a decahedron-shaped reflector on the performance of CSBC. Through experiments, it is observed that the absorber plate attains peak temperature of about 138°C-150°C. Finally, the performance of trapezoidal shaped SBC (TSBC) fitted with four outer reflectors is assessed using water and glycerol as cooking load. The TSBC shows maximum absorber plate temperature of 171°C, making this an A-grade SBC. Comparing standardized cooking power and energy efficiency, TSBC fitted with four outer reflectors performs more than CSBC equipped with decahedron-shaped reflectors. The analysis of annualized life cycle cost and pay-back period show that TSBC is more economically feasible than CSBC.

The next stage study focuses on developing prediction model for SBCs through computational and machine learning (ML) approaches. The objective is to forecast the component temperatures of SBC through ML techniques such as random forest (RF), k-Nearest Neighbor (k-NN), linear regression, and decision tree. A numerical model based on thermal balance is used to generate the data set for the ML algorithm. Heat transfer model is developed by considering all the components of SBC such as absorber plate, glazing cover, cooking pot, lid, air cavity, and cooking load. The total heat loss from the SBC to the surroundings is estimated by considering heat loss from the absorber plate to the ambient through all faces of the cooker. The absorber plate receives solar irradiance through the double-glazing covers. Among this, some heat energy is absorbed, and the rest is rejected via convection heat transfer to inner air cavity, radiation heat transfer to second glass, and conductive heat loss through bottom of absorber plate via insulation and casing. Experiments on the TSBC are conducted to validate the numerical model. The temperatures of different components obtained through numerical modeling agree with experimental values with less than 7% maximum error. The RF model outperformed the other models and has great accuracy in predicting the thermal parameters of SBC.

The third stage study focuses on the design optimization of PCM based TES unit for SBC. A computational procedure is developed to estimate the optimum mass of PCM and dimensions of the TES unit. MATLAB code is written to implement the iterative procedure, simplifying exhaustive calculations required for optimizing and designing the TES unit. The computational procedure is validated by the present experimental study and also compared with previous works. A modified TES unit containing PCM as heat storage medium surrounding cooking vessel is designed and fabricated with the iterative procedure. The TES units developed in this study have the provisions for filling the PCM on all sides, including the lid, enhancing the heat storage. The present work also aims to design, fabricate and test different geometries of TES units using paraffin wax as the PCM. After six hours of the test, the cooking load temperature in all geometries of TES units reached the melting point of PCM. TES units with cylindrical shapes perform best among hexagon and square designs.

The selection of optimum PCM is also important for effective heat storage in SCs. Therefore, the present work aims to select the optimum PCM among the alternatives for the TES unit incorporated in SBC. Based on the melting temperature, the PCMs are pre-screened among the alternatives used in earlier works. The optimum PCM is selected with multi-criteria decision-making (MCDM) techniques like TOPSIS, EDAS, and MOORA. The criteria weights required for the optimization algorithm are found by using AHP, ENTROPY, and CRITIC methods. All MCDM techniques show that erythritol is the best alternative for the TES medium incorporated in the SBC. The iterative solution procedure also selects erythritol as the best alternative since it requires less quantity than other PCMs.

In the last stage, the performance of optimized TES units is experimentally assessed using SBC. The performance parameters of the RSBC having iron grits, sand, brick powder, and charcoal powder in the optimum ratio (mass) of 1:2:2:3 respectively as heat storage material is investigated. It is found that water temperature in the developed TES incorporated RSBC is maintained above 70°C till 6 PM in a day. The performance test on CSBC is carried out with the optimized cooking vessel surrounded by the TES unit filled with paraffin wax as the PCM. The results show that the TES maintains water temperature between 55°C-60°C during evening hours. Finally, the optimized TES unit containing erythritol as PCM is tested with TSBC using glycerol and water as cooking load. Glycerol and water show more than 115°C and 90°C, respectively, during night hours by absorbing latent heat energy from the TES unit.

As a summary, this study focused on the design, fabrication, and experimental assessment of the performance of a novel solar box cooker with thermal energy storage unit using phase change material. It includes optimum design of solar box cooker and thermal energy storage unit, computational, and machine learning approaches for the prediction model development. The optimum phase change material is selected based on the multi criteria decision making techniques and computational procedure. As per literature study no other work incorporates

computational, experimental, and machine learning aspects of solar cooker assessment. Researchers can predict solar cooker performance through the study without requiring elaborate experiments, which saves both time and money. This study will inspire researchers to explore the possibilities of optimization, numerical and machine learning approaches for solar thermal conversion applications.

Keywords: Solar box cooker, Thermal energy storage, Machine learning, Phase change material, Multi-criteria decision-making, Cooking load.

TABLE OF CONTENTS

LIST OF FIGURES

LIST OF TABLES

NOMENCLATURE

A	Area (m^2)
C	Specific heat (J/kg K)
D_i	Inner diameter of cylindrical TES unit (m)
D_o	Outer diameter of cylindrical TES unit (m)
d	Diameter of cooking pot (m)
F_1	First figure of merit
F_2	Second figure of merit
h_{conv}	Convection heat transfer coefficient (W/m^2K)
h_{rad}	Radiation heat transfer coefficient (W/m^2K)
G	Solar irradiance (W/m^2)
Gr	Grashoff number
G_{sc}	Solar constant (W/m^2)
H	Altitude or elevation above sea level (m)
I	Global solar radiation (W/m^2)
k	Thermal conductivity (W/m K)
L	Length of solar cooker (m)
L_i	Inner length of square and hexagonal TES unit (m)
L_o	Outer length of square and hexagonal TES unit (m)
l	Height of cooking pot (m)
m	Mass (kg)
N_c	Number of glazing covers
Nu	Nusselt number
P	Cooking power (W)
Pr	Prandtl number
P_s	Standardized cooking power (W)
Q	Heat loss from the container (J)
$\dot{Q}_{abs}$	Rate of heat absorption (W)
$\dot{Q}_{conv}$	Rate of convective heat transfer (W)
$\dot{Q}_{rad}$	Rate of radiative heat transfer (W)
$\dot{Q}_{cond}$	Rate of conductive heat transfer (W)

Ra	Rayleigh number
r_i	Inner radius of cylindrical TES unit (m)
r_o	Outer radius of cylindrical TES unit (m)
S_{gen}	Entropy generation rate (W/m K)
T	Temperature (K)
t	Time (s)
t_h	Thickness (m)
U_L	Overall heat transfer coefficient (W/m^{2}K)
U_B	Bottom heat loss coefficient (W/m^{2}K)
U_S	Side heat loss coefficient (W/m^{2}K)
v	Wind velocity (m/s)

Greek symbols

α	Absorption coefficient
β	Angular inclination (degree)
ε	Emissivity
δ	Declination angle (degree)
ρ	Density (kg/m^3)
ϕ	Latitude (degree)
τ	Transmission coefficient
λ	Latent heat of fusion of PCM (J/kg K)
υ	Kinematic viscosity (m^2/s)
η	Efficiency
θ	Dimensionless temperature
$θ_z$	Solar zenith angle (degree)
σ	Stefan Boltzmann constant (W/m^{2}K^4)
ω	Hour angle (degree)

Subscripts

air	Inner air cavity
amb	Ambient
av	Average
b	Beam component

bottom	Bottom side
d	Diffusive component
en	Energy
ex	Exergy
g	Glass material
g_1	First glazing cover
g_2	Second glazing cover
gen	Generation
inner	Inner wall
ins	Insulation material
L	Loss
lid	Lid of cooking vessel
load	Cooking load
max,ap	Maximum for absorber plate
mp	Melting point
outer	Outer wall
p	Absorber plate
pcm	Phase change material
pot	Cooking pot
s	Steel
st	Stagnant condition
surr	Surroundings
v	Wind
w	Water
wall	Wall of solar box cooker

1. INTRODUCTION

Cooking is one of the most basic activities for every human worldwide. It is accomplished with heat energy produced by burning suitable fuel. A large portion of total energy consumption is used for cooking in most developing and developed countries. Energy sources often used for cooking include firewood, cow dung, crop wastes, charcoal, kerosene, electricity, liquefied petroleum gas (LPG), coal, and natural gas. Many developing countries still lack access to commercial fuels such as natural gas, LPG, and electricity. People are forced to use solid fuels (firewood, agricultural waste, dung) and kerosene for cooking. According to the latest report by the international energy agency (IEA), around 2.6 billion people cook over open fires with kerosene and solid fuels, which results in more than 3.8 million premature deaths each year. About 69% of rural families depend on firewood for cooking, leading to deforestation, global warming, and indoor air pollution in India. Cooking with solid fuels also has notable effects on global climate change by the emission of greenhouse gases (CO_2, CH_4, and NO_x) and black carbon, which share about 1 to 3% of human-created global warming. Therefore, traditional cooking with solid fuels needs to be replaced with clean fuels to mitigate environmental and health issues. But, the accessibility of clean cooking fuels is less than two-thirds of households in the world. The increased consumption, ever-increasing price of fossil fuels, and environmental pollution drive the need for renewable energy sources for cooking. Moreover, the current global energy crisis calls for alternative energy sources, particularly in developing countries. Solar energy technologies hold great promise in this regard. Solar energy has become more prominent in the worldwide debate on energy and the environment.

According to the geographic information system (GIS) data from the National Renewable Energy Laboratory (NREL), many developing countries, including India, have plentiful solar energy with long-term average global horizontal irradiance (GHI) of around 4 to 6 kWh/m^2 per day and 250 to 300 sunny days per year. Solar radiation can be best utilized for cooking in rural and urban areas as it can easily fulfill the demand and supply chain. Therefore, solar energy will be a substitute for wood and other polluting sources of energy for cooking in developing and developed countries.

Solar cookers (SCs) convert solar irradiance into heat energy required for cooking. SCs are not a new concept, but they have been modified over time. However, there is still scope for improving efficiency, lowering costs, enhancing portability, and adaptability to different environmental conditions. Solar cooking has been a major research interest for the past few decades worldwide due to many advantages: zero running cost, non-polluting character, and ample availability. However, lack of awareness among the developing countries may inhibit the growth of market for SCs. Therefore, many research initiatives and promotional schemes are needed to market SCs as an alternative to conventional cooking devices successfully.

1.1. Solar cooker

French-Swiss scientist Horace de Saussure introduced the box-type solar cooker in 1767, which became an initiative to start solar cooking technology. In 1945, Ghosh designed the first commercialized SC. Many modifications have been made to SCs over the last four to five decades worldwide (Aramesh et al. 2019; Arunachala and Kundapur 2020; Herez et al. 2018). SCs are classified mainly into two kinds subject to heat transfer to the cooking vessel: direct and indirect. The cooking process is carried under sunlight in direct type SCs, while heat is transferred to the cooking pot with some heat transfer fluid (HTF) in indirect type. The detailed classification is depicted in Figure 1.1.

Direct SCs are mainly classified as the panel, concentrating, and box types. In solar panel cookers, the cooking vessel is set on the focal point of the reflective panel. The performance of the panel cooker is very low, particularly on days of lesser solar radiation. Concentrating SC utilizes the cooking energy directly from the sun without any obstruction between solar irradiance and the cooking vessel. It includes parabolic reflector, cooking vessel kept at its focus, and support with tracking mechanism for changing the direction. The reflector concentrates solar irradiance onto the cooking vessel and attains high temperatures. The main limitation is changing the orientation based on the sun's rays to achieve high temperature and efficiency. Large size, price, and risk of burns are also some of the disadvantages of concentrating SC. Box type solar cooker is the most commonly used as it is safe and straightforward to operate. The direct and diffuse radiation strikes the surface of the absorber plate and cooking

vessel via the glass cover. Since the concentration factor is low for the solar box cooker (SBC), no tracking mechanism is needed.
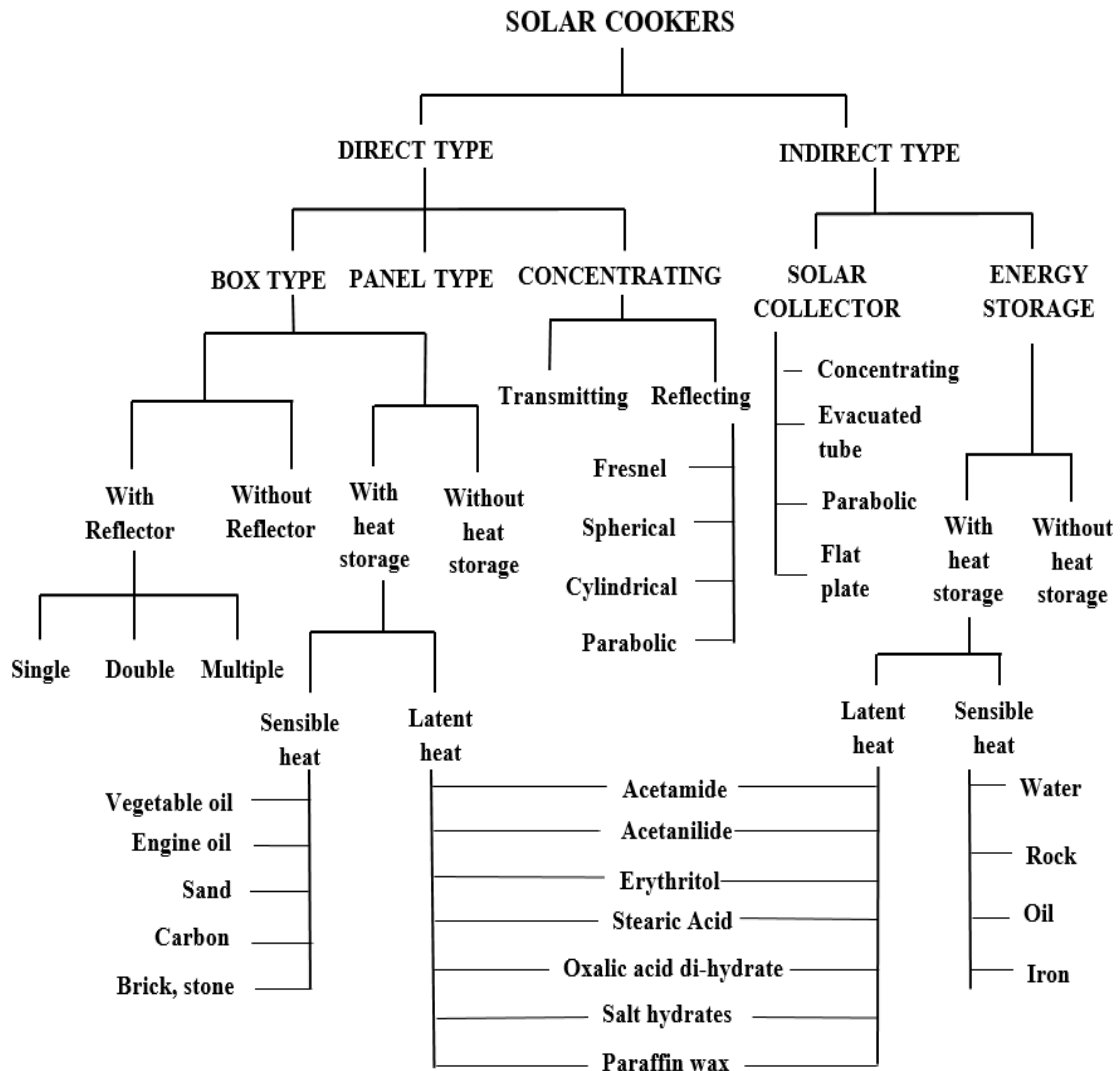
Figure 1.1 Classification of solar cooker

Indirect SC consists of collector for absorbing and accumulating heat energy for cooking. A small pump circulates the HTF, which transfers heat from the solar collector to the cooking vessel. These cookers are categorized based on the type of collector used: flat plate, evacuated tube, and compound parabolic. These cookers have the benefit of being socially acceptable because they can be used for indoor cooking. They are, however, more expensive to fabricate. Recently, many

modifications to the direct and indirect SCs indicate the importance of more advanced and novel research in solar cooking technology.

Among different classes of solar cookers, SBCs are successfully marketed in many parts of the world. Many designs and prototypes of SBCs have been reported over the last few years (Aramesh et al. 2019; Arunachala and Kundapur 2020). The SBC is discussed in depth further below.

1.2. Solar box cooker

Solar box cooker (Figure 1.2) consists of double-walled box with a single- or double-glazing cover at the top. The insulating materials such as glass wool or rock wool fill the gap between the inner and outer wall. The absorber plate is kept at the bottom surface of SBC. The material for the absorber plate is selected so that absorptivity is so high as to absorb maximum solar radiation. The cooking vessel covered with a lid is placed on the absorber plate. The absorber plate and cooking vessel are painted black to absorb maximum solar irradiance. The working of SBC is based on the formation of greenhouse effect inside the box. Solar irradiance proceeds through the glass cover and is absorbed by the absorber plate and cooking vessel. Since the inner wall is made up of reflective material, it reflects the irradiance on the surface of absorber plate and cooking vessel. As the glass is opaque to higher wavelength radiation such as infrared waves emitted by the absorber plate, the inner cavity of the cooker will trap the heat radiation. Here, glazing cover provides greenhouse effect that allows the progress of irradiance into the cooker cavity but prevents it from escaping. The insulation provided at lateral and bottom side of the cooker prevents the loss of heat to the surroundings.
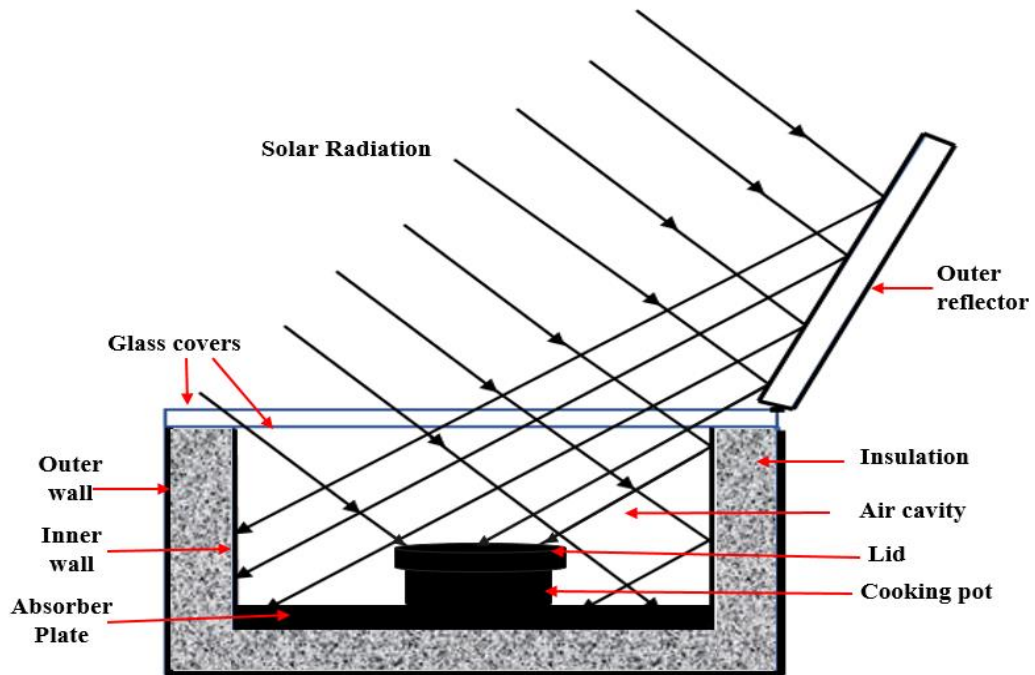
Figure 1.2 Schematic of solar box cooker

The concept behind all kinds of SBCs is the same, but their performance differs due to external or internal modifications such as the number of outer reflectors, double exposure, absorber plate configuration, finned vessel, finned absorber plate, twin chamber, hybrid SC and hybrid cooking pot etc. Furthermore, there have been recent advancements and enhanced performance to SBCs because of new design modifications. Apart from design modifications, various test procedures and performance assessment parameters were proposed for standardization of SBC which includes cooker characteristic number, first and second figures of merit, cooking power, energy and exergy efficiency, new figure of merit, and effective concentration ratio. Even though several performance indicators are introduced, SBCs are graded based on the first and second figures of merit proposed by Mullick et al. (1987).

The ratio between optical efficiency and heat loss factor gives the first figure of merit for thermal performance of SBC as measured from stagnation test without load (Mullick et al. 1987). SBCs are recommended with high optical efficiency and low heat loss factors. The product of optical efficiency, heat exchange efficiency factor, and heat capacity ratio gives the second figure of merit (Mullick et al. 1987).

Concerning the second figure of merit, higher heat exchange efficiency factor and optical efficiency with lower heat capacity of both the cooker interior and the cooking vessel are desirable for SBC. As per the IS 13429 (Part 1):2000, SBCs are of two grades: A-grade (first figure of merit > 0.12) and B-grade (first figure of merit > 0.11). Also, the second figure of merit should be higher than 0.4 for both categories.

The performance of SBC in any climatic conditions is affected by every element of the cooker, such as box geometry, absorber plate, glazing system, cooking vessel, heat storage, external and internal reflector, and insulation material. Solar irradiance entering the cooker is one of the significant factors affecting the SBC performance. The augmentation of incident solar irradiance on the cooker surface can be accomplished by fitting outer reflectors to the SBC. The absorber plate, whose surface area should be optimal, is another important part of SBC. It absorbs maximum solar energy and transfers it to the cooking load by conduction and radiation mode of heat transfer. Optimizing the cooker surface area minimizes the overall heat loss coefficient, resulting in optimal performance. Therefore, determining the optimum size of the absorber plate to gain maximum temperature for cooking load is of paramount importance. The minimum entropy generation (MEG) principle, also known as thermodynamics of irreversible processes, can be used for optimizing heat-interacting devices, such as SBCs. A system that works with MEG will result in the least destruction of availability or minimum loss of useful work (Torres-Reyes et al. 2001). In SBCs, irreversibility occurs due to the finite temperature difference between the sun and absorber plate or between the absorber plate and cooking load.

The commonly used box geometries for SBCs are rectangular, cylindrical, trapezoidal, and rectangular with inclined glass covers. Rectangular SBC with inclined glass cover performs more than the horizontal one as more solar irradiance intercepts onto the cooker surface (Yettou et al. 2015). Kurt et al. (2008a) experimentally found that cylindrical SBC shows high thermal efficiency and low boiling time than the rectangular type. Therefore, it is required to assess the performance parameters of different geometries of SBC experimentally.

In addition to experimental evaluations, numerical analysis of heat transfer involved in SBC was performed to predict the performance parameters. It is accomplished by predicting the temperature at each component of SBC, such as absorber plate, glazing cover, cooking vessel, air cavity, inner and outer wall, and cooking load. The numerical analysis was based on thermal balance equations at each component but differed in solution methodology like the fourth order Runge-kutta method (Binark and Turkmen 1996), Newton-Raphson method (Guidara et al. 2017), and the number of components considered. The numerical studies that have been reported so far have used experimentally determined solar irradiance to solve thermal balance equations. Numerical simulations that incorporate all elements of SBC with changing solar irradiance as a function of day, time, and location are lacking in the literature. The machine learning (ML) models can easily predict the performance without further doing simulations to test the same kind of SC at different geographical locations. The data obtained from numerical simulations can be used to develop ML models for prediction. The data-driven techniques are rarely used, and the majority of them are based on artificial neural networks (ANN) or their modifications. ML models other than ANN have not been explored for solar thermal energy utilization appliances. Also, many popular ML methods like ANN is unstable and unreliable. As a result of this instability, small changes in the input data could significantly impact the predicted values. In the early 1990s, ensemble learning was developed to overcome these problems. In addition to improving stability, ensemble-based ML methods reduce variance and bias by combining the results of several individual models. In this direction, the development of tree and ensemble-based ML prediction models for SC is of significance.

ML is a commonly used form of artificial intelligence, and it continues to be popular and attractive as it finds new applications every day. In ML, the system learns from itself and then estimates the unknown outputs. Training success and selection of attributes are crucial factors that influence the performance of ML algorithms. The two classes of ML are supervised and unsupervised learning. In supervised learning, input and output data are provided. On the other hand, only the input data is provided in the case of unsupervised learning. Regression is one class of supervised learning,

and it shows a line or curve that connects all data points on the actual-predictor graph with shortest vertical distance between them. Linear regression, decision trees, random forests, support vector machines (SVM), k-nearest neighbor (k-NN), and ANN are the regression techniques extensively employed in ML.

The use of SBC is limited as cooking is not possible due to irregular clouds obscuring the sky during the day or at late night. It is possible to cook indoor and late night by incorporating some thermal energy storage (TES) materials in SBC. Variety of sensible and latent heat storage materials were tested, making it possible to cook after sunset. TES that links between the energy generation and utilization has become research interest in the recent years. Particularly, latent heat storage (LHS) unit employing phase change materials (PCMs) is of great importance in the renewable energy applications. A more in-depth discussion of SBC incorporated with TES units is provided below.

1.3. Solar box cooker with thermal energy storage

The evening or night cooking is possible with the provision of heat storage facility in SBCs. The provision of TES facilities will enhance the usage of SBCs. The SBC can store heat in the form of sensible or latent heat or both. In sensible heat storage (SHS), heat energy is stored by increasing the temperature of storage material. The primary drawbacks of sensible heat storage materials (SHSMs) are low specific heat capacity and cooking efficiency since the temperature of the storage material drops while discharge. The generally used SHSMs in SBCs are sand, vegetable oil, engine oil, carbon, stone pebbles, iron grits, and iron balls. Neither bricks nor charcoal has been tested as heat storage materials for SBCs. Bricks and charcoal have high specific heat capacity compared to sand, stone pebbles, and iron grits. Furthermore, determining the optimal mixture of SHSMs is another important aspect of SBC.

The energy stored during phase change is used for cooking in LHS system. Generally, PCMs are used to store heat energy in the latent form. PCM as TES medium have gained significant attention in recent years due to their high energy density and constant temperature characteristics, making them suitable for SCs. They have the property that the temperature becomes constant throughout phase change ie, melting,

or solidification (Figure 1.3). During the melting process, PCM absorbs large quantity of heat from the surrounding area, and when the temperature decreases, the material solidifies and releases heat. SBC having LHS unit designs are of two kinds. The first type of design uses heat energy from LHS materials (LHSMs) placed beneath the absorber plate (Buddhi and Sahoo 1997; Nahar 2003). The LHS unit is integrated with cooker parts and not with the cooking pot in this design. Nyahoro et al. (1997) kept LHSMs at the top of the absorber plate. In the work of Buddhi and Sahoo (1997), LHSMs were placed under the absorber plate having fin arrangement. During sunny hours, irradiance absorbed by the cooking pot and absorber plate is transferred to the cooking load. But, during sundown time, thermal energy stored in LHSMs is transferred to the cooking pot via conduction. In the second type of design, the LHS unit is integrated with the cooking pot instead of the cooker. Cooking pots incorporating the LHS system contain concentric cylindrical vessels filled with PCMs.
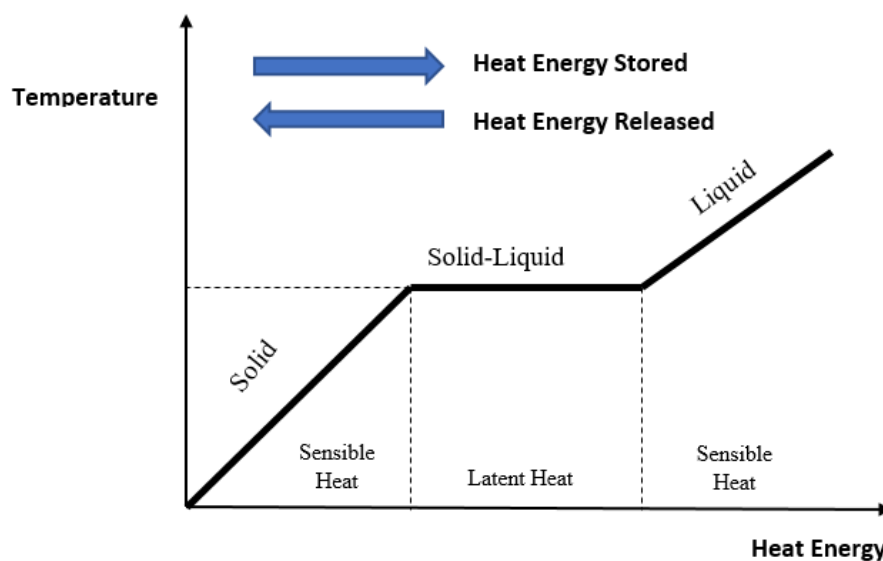
Figure 1.3 Melting and solidification process in PCM

The constant temperature retained during solidification is utilized to design and develop temperature-controlled TES. Hence it is required to optimize and design the TES unit for maintaining constant temperature for a particular period. TES units should be filled with PCM in liquid form as it has greater volume than solid. Also,

designed quantity of PCM should be inserted into the TES units to permit the material to solidify and expand throughout the cycle. If there is extra PCM, latent heat will not be fully absorbed, reducing the system's efficiency. Thus, it is necessary to find the optimum quantity of PCM and design the container to maintain constant temperature for certain period. No previous works on the computation of optimum mass of PCM and design of LHS unit for SBC is reported. The design procedure involves typically tedious calculations of theoretical heat loss and design equations. When different geometries and PCMs are considered, calculations become exhaustive. Therefore, it is essential to develop a computational procedure to solve these equations, simplifying the calculations required for designing TES unit. The TES units used in SC are generally incorporated with the cooking pot, filled with PCM along the lateral side only. It is possible to improve heat transfer to the cooking load by placing PCM at the bottom and lateral sides and the lid of the pot.

The PCM selected for storing solar thermal energy should have thermo-physical properties such as high latent heat of fusion, high specific heat, and high thermal conductivity at the desired operating temperature. Also, they should be chemically stable, non-toxic, non-flammable, and should not degrade after each cycle of melting or freezing. A lot of research works were carried out over the last few decades by considering all the cooker configurations and desirable properties of PCM (Nkhonjera et al. 2017; Omara et al. 2020). Many researchers performed testing of SBC with different PCMs such as magnesium nitrate hexahydrate, stearic acid, acetamide, acetanilide, paraffin wax, erythritol, oxalic acid dihydrate, and magnesium chloride hexahydrate. However, the optimum selection of PCM is essential for the efficient utilization of SBC integrated with TES unit. Multi-criteria decision-making (MCDM) technique is used to select the best of a set of alternatives by evaluating them with reference to different attributes. The MCDM methods have high potential for optimizing material selection. Various MCDM methods were applied in sustainable and renewable energy development sectors (Mardani et al. 2015; Lee and Chang, 2018). But very few studies were reported on the use of MCDM tools for the optimum selection of PCM. MCDM techniques make it possible to select the best PCM among the alternatives for the TES unit incorporated in the SC. The commonly used MCDM

methods are the analytic hierarchy process (AHP), technique for order preference by similarity to ideal solution (TOPSIS), complex proportional assessment (COPRAS), evaluation based on distance from average solution (EDAS), combinative distance-based assessment (CODAS), and multi-objective optimization by ratio analysis (MOORA).

1.4. Outline of the thesis

The rest of the thesis is organized as below,

Chapter 2 presents an extensive literature review of the current study. The literature review focuses on analysing SCs based on experimental and numerical investigations. A review of SCs with thermal energy storage is also included in this chapter.

Chapter 3 discusses experimental observations related to SBCs. The study involves designing, fabricating, and evaluating rectangular, cylindrical, and trapezoidal shaped SBCs. Experiments involving the inclusion of outer reflectors are reported. A section on statistical, uncertainty, and economic analysis are also presented in this chapter.

Chapter 4 discusses the methods and results of the numerical and machine learning-based prediction model for the SBC. For temperature prediction, the fourth order Runge-Kutta method is used to solve the thermal balance equations at each component of SBC. An experimental study validates the developed model. Based on the numerical results, prediction models are developed using machine learning techniques such as random forest, linear regression, decision tree, and k-NN.

Chapter 5 addresses the optimization of TES systems for SBCs. A computational procedure is developed for the optimum design of the TES unit, validated by experimental studies. It also presents MCDM methods such as TOPSIS, EDAS, and MOORA to select the optimum PCM for TES integrated SBC.

Chapter 6 discusses the performance studies of thermal energy storage integrated SBCs. It includes the analysis of SBC incorporated with an optimum mixture of SHSMs. The methods and results of the performance evaluation of an optimized TES unit integrated with SBC is also presented in this chapter.

Finally, **Chapter 7** presents the significant findings and conclusions of the experimental, numerical, and machine learning-based evaluations of SBCs integrated with optimized thermal energy storage system.

2. LITERATURE REVIEW

It was well known to scientists of the 18th century that glass could trap heat from the sun by creating a greenhouse effect. However, French-Swiss scientist Horace de Saussure used this theory to cook food, which resulted in solar cooking. Solar cooking has undergone a great deal of modification and exploration to improve efficiency and ease of use. A broad review regarding experimental and numerical studies of solar cooker (SC) including thermal energy storage (TES) is given below.

2.1. Experimental study

The experimental studies are carried out to assess the performance of SCs with some modifications made to the existing ones. Numerous test procedures and standards have been proposed for evaluating and comparing SCs.

The test procedure for solar box cooker (SBC) based on stagnation temperature and solar insolation was proposed by Vaishya et al. (1985). They suggested a number that represents the characteristics of SC. Mullick et al. (1987) modified the characteristic number called first and second figures of merit of thermal performance. They also proposed test procedure for the performance evaluation and standardization of SBCs. Several experiments were performed to obtain two figures of merit for predicting the thermal performance. They concluded as follows: (i) Two figures of merit are relatively independent of the climatic variables and pertain to the cooker. High value of first figure of merit indicates good optical efficiency and low heat loss factor. A high value of second figure of merit indicates good heat exchange efficiency factor, good optical efficiency and low heat capacity of the cooker interiors and vessels compared to a full load of water, (ii) Boiling time is a strong function of climatic variables and (iii) A time factor can be evaluated, which is a measure in standard heating hours of the combined effect of two figures of merit in a given standard climate. Later, (Funk 2000) proposed the international standard procedure for testing SCs of different designs. The cooking power curve analyzed in the test procedure interprets the capacity and heat retention ability of SC. Ozturk (2004) conducted theoretical and experimental study to develop an energy and exergy model for predicting solar cooker performance. The time-variations of these efficiencies

were calculated based on the applied formulae and measurement data. In SBCs, significant amount of heat energy is lost to the surroundings through all the faces. The total heat loss is computed by finding various heat loss coefficients from the absorber plate to the ambient. A simple thermal analysis to evaluate the natural convective heat transfer coefficient between absorber plate and inner glass cover for the SBC is presented by Kumar (2004a). They inferred that, the correlations for rectangular enclosure cannot be used for trapezium to compute the convective heat transfer coefficient. Kumar (2004b) also developed correlation for top heat loss coefficient as a function of cooking load and ambient temperature, and wind speed for SBC by conducting indoor and outdoor experimentation. From the proposed correlation, heating characteristic curve for different quantities of water, solar radiation and wind speed were obtained. (Kumar 2005) presented a method to find the optical efficiency and heat capacity of the SBC using linear regression analysis of experimentally obtained second figure of merit values for different cooking load. Purohit and Purohit (2009) experimentally analyzed the effects of instrumentation on first and second figures of merit of SBC. They found that attainable accuracy and absolute error in the evaluation of second figure of merit is more critical than first figure of merit. Purohit (2010) evaluated the overall error in determining the performance parameters of box type and parabolic cookers due to instrumentation. The maximum effect of instrumentation error is obtained for the second figure of merit, optical efficiency factor and standardized cooking power. Another performance parameter called the effective concentration ratio (ECR) which is an indication of the usefulness of the outer reflectors in the opto-thermal performance of SBCs was proposed by Sagade et al. (2018). ECR is a design-dependent parameter, and therefore, it does not change with environmental, meteorological, and operational parameters. Collares-Pereira et al. (2018) proposed revised testing procedures and new figures of merit for SBCs having augmented mirrors and inclined glass covers. A new parameter called heat retention time for SCs was introduced by Sagade et al. (2019). Heat retention time enable the users in the selection of appropriate design of SCs by comparing the performance for a particular location. They also presented open sun cooling test which facilitates the user to check the ability of a particular design of SC to cook the food under unexpected weather conditions. Recently, Ebersviller and Jetter (2020)

tested three classes of SCs namely panel, box and parabolic type based on ASAE (American Society of Agricultural Engineers) standard and reported suggestions for improving test and evaluation methods.

Researchers have also explored the economics and environmental implications of SCs in recent decades. Kanndpal and Mathur (1986) presented an economic evaluation of SBC based on payback period, net present value, and break-even number of cooked meals. Since then, many researchers have adapted this method (Kumar et al. 1996; Nahar 2001; Panwar et al. 2013; Kumar et al. 2022). Indora and Kandpal (2018) have carried out techno-economic assessments of two SCs for institutional use. Their approach can evaluate any direct SC design using a simple methodology. Mendoza et al. (2019) analyzed the potential sustainability benefits of using house made SCs instead of microwaves in developed countries with suitable climatic conditions. For this analysis, they fabricated three types of SC using reused household materials and compared the lifecycle environmental and economic performance with the conventional microwaves. They suggested that high use intensity of long serving SCs along with microwaves as backup could reduce the environmental impact by up to 65% including global warming and annual costs by up to 40% when compared with the microwaves alone. The study by Mostafaepour et al. (2021) employed structural equation model (SEM) to explore variables and risks associated with the production and usage of SCs. SCs were ranked using factor analysis and inferred that capital, technology, infrastructure, interactions, and financial support affect the success of SCs.

Although, the theory underlying all types of SBCs is the same, their performance varies because of the modifications made to them. One of the important design modifications was fitting outer reflector with SBC to enhance the solar irradiance incident on the cooker cavity. Algifri and Towaie (2001) proposed a method for determining the reflector performance and orientation factor for a single reflector SBC using the sun's elevation angle, the solar surface azimuth angle, and the reflector tilt angle. Nahar (2001) studied two-reflector hot SBC of rectangular shape with transparent insulation material and compared it with single reflector. In the morning, one mirror faces south and the other faces east, while in the afternoon, the cooker is

rotated 90°, again facing south and west. The SC did not move, but SBC was tracked towards the sun every hour. Accordingly, their results indicate that tracking towards the sun for three hours can be eliminated by adding a reflector. Ekechukwu and Ugwuoke (2003) studied the performance of SBC augmented with a single plane reflector. Their findings justify the modification of traditional SBC designs. Guidara et al. (2017) studied trapezoidal-shaped SBC fitted with four reflectors. A four-reflector design increased optical efficiency of the SC, leading to an improvement of 0.07 to 0.14 in the first figure of merit and temperature increase of 133.6 °C for the absorber plate. Accordingly, the second figure of merit was in the range of 0.34 to 0.39. Coccia et al. (2017) developed SBC with dodecagonal reflectors and studied its performance. Higher optical efficiency and thermal insulation enabled it to cook at high temperatures. The performance of SBC also depends on the shape of the box. The commonly employed box geometries are rectangular, rectangular with inclined glass cover, trapezoidal and cylindrical. Kurt et al. (2008a) experimentally found that cylindrical SBC has larger thermal efficiency and reduced boiling time compared to rectangular type. Since the cylinder side area is more efficient than the rectangle, heat loss from sideways is less for the cylindrical box geometry. Yettou et al. (2015) experimentally showed that rectangular SBC with inclined glass cover performs better than the horizontal as it provides more solar irradiance on to the cooker surface via large interception area.

Recent studies also show the advancements and enhanced performance of SBCs because of design modifications. Saxena and Agarwal (2018) developed and tested hybrid SBC incorporated with trapezoidal duct, halogen lamp and low power fan which enables to cook the food in small duration. Cuce (2018a) experimentally and numerically investigated the effects of three micro porous absorber configurations (triangular, semi-circular, and trapezoidal) in cylindrical SBC. The results show that micro porous absorber gives better thermal performance than the ordinary one. Also, it was found that trapezoidal absorber gives maximum performance as it has more linear length compared to other configurations. Siddique et al. (2020) experimentally assessed the performance of combined SC cum dryer. The hybrid system consists of trapezoidal-shaped cooker with rectangular dryer chamber placed at the top to cook

and dry separately. Under the same ambient condition, they observed two different temperature ranges for the cooker (80°C-135°C) and the dryer compartment (35°C - 65°C). The first and second figures of merit of the cooker are respectively 0.11 and 0.303. An intermediate SBC with hybrid cooking pot having a glass lid at the top is tested for thermal performance by conducting heating and open sun cooling test by Sagade et al. (2020). Khallaf et al. (2020) developed and tested the performance of SBC named as Quonset SC (QSC) with transparent fiberglass reinforced plastic glazing cover. They found that characteristic boiling time is about 50% slower for boiling 1 kg of water with the QSC compared to SBCs. Engoor et al. (2020) improved the thermal performance of SBC by incorporating two Fresnel lens magnifiers. By integrating the Fresnel lens magnifier, first and second figures of merit and cooking power enhanced from 0.11 to 0.12, 0.43 to 0.45, and 43.83 W to 46.87 W, respectively. Shanmugan et al. (2020) carried out experimentation to study the effects of absorber plate coating of stepped SBC with different ratios of SiO_2/TiO_2 nanoparticles for performance enhancement. Vengadesan and Senthil (2021) experimentally investigated the effects of adding fins to the cooking vessel of SBC. They used four different cooking pots, both finned and un-finned, with fin lengths ranging from 25 mm to 45 mm. Sensible heating test reveals that the finned cooking vessel performs better than the un-finned. Mawire et al. (2021) compared SBC with and without reflector and parabolic dish SC under different water loads of 1 kg, 1.5 kg, 2 kg, 2.5 kg, and 3 kg based on exergy and energy performance parameters. The results reveal that the SBC with reflector has the highest average energy and exergy efficiency and is independent of the water load. Arif et al. (2021) conducted comparative study to investigate the effects of changing position of cooking pot on absorber plate, mirror and aluminium reflector, as well as the number of cooking pots on the performance of two geometrically similar SBCs. Using mirror and aluminium reflector, respectively, the cooking load temperature increases by 25.5% and 23.4%. With increasing numbers of cooking pots and loads, the second figure of merit rises linearly. Recently, Ruivo et al. (2022) investigated the suitability of using linear regression for the estimation of performance parameters of panel and box type SC.

Besides SBC, modifications were also made to other types of SCs as detailed below. A parabolic SC with synthetic oil SAE-40 as heat transfer fluid (HTF) integrated with heat storage unit is modeled and tested by Mbodji and Ali-Hajji (2017). Kumar et al. (2018) presented the study of heat loss in parabolic dish-type SC. They introduced new parameter termed performance index of cooking pot indicating how well the productive energy of cooking pot reaches concentration ratio of SC. Goswami et al. (2019) tested and compared the energy and exergy efficiency of thin plate parabolic SC having aluminium cooking pot coated with and without activated carbon. Abd-Elhady et al. (2019) reported that inserting copper wires and nanographene particles in thermal oil will increase the natural convection heat transfer in the evacuated tube SC. Ahmed et al. (2020) compared the performance of reflective materials like stainless steel, aluminium foil, and Mylar tape in the parabolic SC and found Mylar tape is more efficient. Hosseinzadeh et al. (2020a) investigated the effects of the flow rate of nanofluid and mass fraction of nanoparticles on the performance of indirect SC. Hosseinzadeh et al. (2020b) evaluated the energy and exergy efficiency of the indirect SC with nanoparticles SiO_2, TiO_2, and SiC added with thermal oil as HTF. The SC developed by Atmane et al. (2021) uses photovoltaic (PV) energy formed by PV panels, power blocks, and controls, as well as thermal resistances. In comparison to traditional SCs, the performance results show significant improvements in cooking temperature, boil duration, and heating speed by 178%, 83.3%, and 943 %. Thermal efficiency of 86% was achieved, which is a significant improvement over conventional cooker. Singh (2021) presented solar-based, electronically controlled indoor cooking system by developing solar parabolic dish concentrator, mechanical support, sun-tracking mechanism, HTF system, and heater plate fitted with heating coil. In this system, solar PV panel continuously charges 12 V battery through charge controller. The battery then powers the solar tracker and DC motor-pump set, circulating HTF via heating coil. Tawfik et al. (2021) proposed new SC equipped with tracking type parabolic reflector (TBPR) at the bottom. They carried out thermal performance assessment of first figure of merit (F_1), cooker opto-thermal ratio (COR), and ECR. Their study found COR 0.165 for the cooker with TBPR and 0.123 for the one without and overall efficiencies of 10.7% and 12.5% respectively. With TBPR, the cooker reached intermediate temperatures between 140-150°C, and F_1 and ECR

were 0.119 and 1.34. Coccia et al. (2021) designed, fabricated, and tested low-cost concentrating SC equipped with lens-mirror system that directs solar energy to the bottom of cooking pot. It has high geometrical concentration ratio of 40.97 and is tested with water and silicone oil as cooking loads. Tibebu and Hailu (2021) designed and fabricated dual-axis sun-tracking SC using locally available materials. Apaolaza-Pagoaga et al. (2021a) used the ASAE S580.1 procedure to analyze two funnel cookers and proposed new method to account for the effects of minor design changes. Al-Nehari et al. (2021) developed tiltable box-type SC and obtained the first and second figure of merit, cooking power, and maximum stagnation temperature of 0.1354 °Cm^2/W, 0.4934, 63.53 W, and 172.75 °C. Apaolaza-Pagoaga et al. (2021b) studied the performance of two identical solar funnel cookers using glycerin as cooking load. Sagade et al. (2021) proposed thermal method for the determination of ECR of concentrating type SC. Kanyowa et al. (2021) investigated experimentally and analytically the performance of Scheffler dish-type solar thermal cooking system capable of preparing 6000 meals every day. Ruivo et al. (2021) investigated solar funnel cookers using ASAE S580.1 standard procedure. Some procedures were proposed to improve the measurement's quality and reliability. They also compared the effect of two different pot lids on standardized cooking power. Recently, the effect of partial loads on a funnel cooker thermal performance was carried by Apaolaza-Pagoaga et al. (2023). Experiments were conducted on two identical funnel cookers, and results indicate that the standardised power drops by about 15% of the original value when the water volumetric load fraction drops by 25%, for both cooker operations, with and without glass enclosure. They designed a new cooking vessel which improves the performance at partial loads, i.e., a 25.4% increase in cooker power.

2.2. Prediction models

Extensive research has been done using numerical analysis to study the heat transfer involved in SBC for the determination of performance parameters. It is accomplished by predicting the temperatures at each component of SBC, such as absorber plate, glazing cover, cooking vessel, air cavity, inner and outer wall, and cooking load.

Binark and Turkmen (1996) developed a mathematical model based on the heat transfer processes involved in SBC and solved numerically using fourth order Runge-kutta method. They validated numerical model with experimental results. Ozturk (2004) conducted theoretical and experimental study to develop energy and exergy model for predicting SC performance. Soria-Verdugo (2015) proposed heat transfer model of SBC based on the solar radiation and external temperature, which is validated by experiments. The required convective heat transfer coefficients were obtained from experiments. Guidara et al. (2017) numerically and experimentally investigated the thermal performance of SBC with four outer reflectors. A mathematical model is developed based on thermal balances validated by experimental results. The equations are solved using Newton-Raphson method. They used experimentally obtained solar irradiance for the numerical model. Zafar et al. (2019) numerically investigated the design of double-glazed SBC with flat foldable external reflector at top and front and an internal reflector at the bottom of L-shaped absorber plate. They validated the model using experimental results and investigated the effects of various design parameters on the performance of cooker such as glazing spacing, thickness, effects of vertical component of absorber plate and internal reflector. Chatelain et al. (2019) presented nodal model based on energy balance equation for SC which predicts the temperature of cooking vessel. Also, the model parameters are evaluated using optimization technique based on genetic algorithm. A box-type SC made up of unused recyclable materials was examined theoretically and experimentally by Neto et al. (2021). Based on thermal balance equations, mathematical model was developed to estimate the temperatures of absorber plate, air cavity inside the cooker, and glass surface. Recently, Verma et al. (2022) presented analytical model to quantify the effects of various parameters on the performance of SBC coupled with sensible heat storage (SHS) system. For the analysis, they introduced new user-controlled parameters such as the cooking vessel area fraction for day and night.

All the above-mentioned research were based on solving thermal balance equations at each element of the SBC. In addition to this, some alternative prediction models were also developed to predict the performance of SC. Kurt et al. (200b) used artificial

neural network (ANN) method for temperature prediction of different components in SBC. Simulations of thermal behavior of SBC have been done using Cramer's rule (Venugopal et al. 2012). The optimization of exergy efficiency of double exposure SC has been done by Zamani et al. (2017) using response surface method (RSM). Hosseinzadeh et al. (2020c) investigated the performance of portable evacuated tube SC along with stainless steel tank analytically and compared with the experimental results. Also, evaluated the effect of design and weather parameters on the performance of cooker. Thy used Taguchi method for optimizing the useful thermal power of the cooker and inferred that solar radiation is the most effective parameter. Mukaro (2021) developed an ANN model to predict SC efficiency, power and exergy efficiency, using experimentally observed variables as inputs, such as time of day, solar radiation intensity, ambient, water, and cooker temperatures. Bhavani et al. (2021) used fuzzy logic and experimental study to examine the thermal performance of SBC with absorber plate covered with Cr_2O_3–MoS_2–Fe_2O_3 nanocomposite.

2.3. Solar cooker integrated with thermal energy storage

Cooking is possible only during daytime when solar intensity is more with conventional SBC. A large amount of heat is lost from the cooker cavity via conduction, convection and radiation which results in reduced effectiveness of cooker. SBCs are most efficient for cooking in daytime and are limited to use in late evening. This inherent drawback can be overcome by using heat storage materials. Thermal energy can be stored in the SC as sensible or latent heat.

Sensible heat storage materials (SHSMs) were tested in SBCs by placing them beneath the absorber plate for evening cooking. Nahar (2003) developed hot box SC with used engine oil as the heat storage medium. They obtained the same stagnation temperature with or without heat storage medium but 23°C higher during the night in storage SC. Agrawal and Yadav (2015) carried thermal analysis of SHS units containing sand, stone pebbles, iron grits, and iron balls integrated with SC theoretically and compared with experimental data. A parabolic dish type solar collector is used to concentrate irradiance on to the cooker. The SHSMs are filled around the cooking pot having diameter 13 cm and height 11 cm. Saxena and Karaklicik (2017) developed SC with optimum mixture of SHSMs such as sand and

carbon. Cuce (2018) tested the performance of cylindrical SBC having bayburt stone as heat storage material. Milikias et al. (2020) tested the performance of SBC incorporated with SHSMs such as concrete and black stone.

Variety of latent heat storage materials (LHSMs) were also tested, making it possible to cook after sunset. The solidification heat is used for cooking in the evening hours by materials with LHS, such as phase change materials (PCMs). Many researchers have investigated SBC with different PCMs numerically and experimentally.

Ramadan et al. (1988) presented the concept of PCM for off-sunshine cooking by designing flat plate SC with focusing plane mirrors. They tested the performance of SC with cylindrical copper cooking pot surrounded by 5 mm thickness of sand. They suggested to use salt hydrate Ba $(OH)_2$ $8H_2O$ having melting point 78°C as a layer surrounding the cooking pot for indoor cooking. The overall energy efficiency of the cooker is found to be 28.4% and performed indoor cooking for 3 hours/day. Domanski et al. (1995) conducted the performance assessment of SC with cooking vessel containing stearic acid and magnesium nitrate hexahydrate as LHS medium. They assessed the performance of the cooker concerning the charging and discharging hours of PCM. They reported that the SBC with LHS unit employing PCM during discharging has efficiency 3 to 4 times more than the steam and heat pipe SCs. Buddhi and Sahoo (1997) carried performance evaluation of SBC by incorporating LHS unit beneath the absorber plate. They tested with 3.2 kg stearic acid as LHSM. It took more time to cook due to slow heat transfer from LHS unit to the cooking pot. However, they showed that PCMs can be used as the heat storage medium for SCs. Sharma et al. (2000) tested SC with acetamide as LHS medium. They provided cylindrical storage unit around the cooking vessel, enhancing the heat transfer between LHSM and cooking load. The cooking pot integrated with the LHS unit consists of two concentric cylinders of diameters 18 and 25 cm and height 8 cm. The annular gap is filled with 2 kg of PCM. By experimentation, they concluded that incorporating LHS has no effects on the cooker performance during noontime. Also, they suggested to use PCM with melting point between 105 and 110°C for the night cooking. Buddhi et al. (2003) tested SC having single and triple reflectors incorporated with the LHS system. They used acetanilide as LHSM. The LHS unit

comprises two hollow concentric cylinders made up of aluminium with diameters 20 and 30 cm and height of 12.5 cm. The annular gap is filled with 2.25 kg and 4 kg of PCM for testing SC with single and triple reflectors, respectively. From test results, it is clear that the provision of three reflectors in the SC increases the irradiance to perform evening cooking with LHS unit containing PCM. They could cook up to 8 PM by incorporating 4.0 kg acetanilide in the LHS unit. Chen et al. (2008) investigated the effect of thermo-physical properties of heat exchanger container materials and PCMs, the thickness of container materials, initial PCM temperatures, and boundary wall temperatures on the melt fraction of different PCMs numerically. Stearic acid and acetamide were suggested as storage media in an SBC for late-night cooking. They also reported that the thermal conductivity of the container material and the PCM's effective thermal conductivity should be considered when choosing the container material and the PCM. Yuksel et al. (2012) tested rectangular SBC with paraffin wax as LHS material. The absorber plate placed at the bottom of SBC is made of two aluminium sheets of thickness 3 mm. The space between two aluminium sheets is filled with 5 kg paraffin wax and 3.5 kg metal shavings. The metal shavings will provide good conduction and melting/freezing properties in paraffin wax. They investigated the effects of paraffin wax and reflector angles on the performance of the cooker. Experimental results obtained an effective reflector angle of 30°, and energy efficiency improved by 18.35%. Paraffin wax attained maximum temperature between 75.1 and 80.5°C. Arabacigil et al. (2015) designed, fabricated, and tested the SBC with three-step inner reflectors and varying outer reflector angles. They also tested the performance of SBC by filling 5 kg of paraffin wax and 3.5 kg of metal shavings beneath the absorber plate during sundown hours. The outer and inner box has dimensions 64.3 cm x 52 cm x 29 cm and 40.6 cm x 37.4 cm x 12.1 cm respectively. The outer and inner boxes are 10 mm thick wood and 3 mm aluminium sheet, respectively. The space between the inner and outer box is filled with glass wool of 8 mm thickness to reduce heat loss to the surroundings. Geddam et al. (2015) conducted experimentation to increase the TES capacity of SBC using aluminium cooking vessel filled with paraffin wax as PCM. The test results show that the PCM storage unit containing paraffin wax keeps the SC hot for 4 hours. Yadav et al. (2015) reported that by incorporating PCMs with SHSMs like sand and pebbles in a SC

performs better than with iron grits and balls. Adetifa and Aremu (2016) investigated the effects of heat storage materials like benzoic and stearic acid and palm oil on the performance of double exposure type SBC. They filled 4.5 kg of benzoic acid, 4 kg of stearic acid, and 6 liters of palm oil in the annular cavity of the cooking pot. They found that using benzoic acid results in more cooking power and the second figure of merit than palm oil and stearic acid. Vigneswaran et al. (2017) tested SBC with oxalic acid di-hydrate as PCM. The heat storage unit consists of two concentric cylindrical aluminium containers having outer and inner diameters 25.5 and 17.5 cm, respectively. The annular space is filled with 2.9 kg of PCM. The discharge efficiency of the PCM storage unit containing oxalic acid di-hydrate is 57 % during off-sunshine cooking with SC. This shows that the PCM transfers thermal energy effectively to the cooking load.

Coccia et al. (2020) tested portable type SBC with LHS unit containing erythritol as PCM and cooking load as water and silicone oil. The SBC consists of wooden box with zinc-coated steel frame as the cooking chamber inside. The TES unit consists of two cylindrical steel pots with outer and inner pot diameters of 23 cm and 19 cm. The two pots are connected with four bolts, and 2.5 kg of PCM is filled in the annular space. The mean load cooling time for the temperature range of 125-100°C is 351.6 % more than the cooker without TES. Saxena et al. (2020) modified SBC fitted with copper tube containing LHS materials, which enhanced thermal efficiency and cooking power. Twelve numbers of cylindrical copper tubes of 0.5 mm thick, diameter 2 cm and length 47.1 cm are fastened on the absorber plate for holding the PCM. By testing the modified SBC, they obtained higher performance parameters such as efficiency, overall heat loss coefficient, and cooking power, respectively as 53.81%, 5.11 W/m^2 $^{\circ}$C, and 68.81 W. Cuce et al. (2020) tested SC with propolis as LHS medium. The melting temperature of propolis is 47°C and by placing 8 kg of propolis under the absorber plate maintained the cooking above 40°C during evening hours. Palanikumar et al. (2021) carried out thermal performance study (experimentally and theoretically) on three kinds of SCs such as SBC with waste cooking oil and $C_4H_4O_3$ as PCMs (SBC-PCM), novel SBC with (SBC-NPCM) and without nanocomposite PCM (SBC-WNPCM). The results showed that using

absorber plate coated with $MgAl_2O_4$/Ni-doped, Fe_2O_3 nanoparticles combined with PCM raises interior temperature of the cooker to 164.12°C. Furthermore, the absorber plate temperature was 163.74°C, 147°C, and 113.34°C for SBC-NPCM, SBC-PCM, and SBC-WNPCM, respectively, under solar irradiance of 1037 W/m^2. Recently, Mawire et al. (2022) compared the storage and heat utilization efficiencies of two identical TES pots using different heat storage materials. Using five different cooking loads (0.5, 1.0, 1.5, 2.0, 2.5 kg), they compared the performance with erythritol and sunflower oil as TES medium. A low-cost SBC with extended fins and heat storage medium was developed by Kumar et al. (2022). They placed about 144 numbers of small aluminium capsules containing PCM on the absorber plate.

For concentrating and indirect type SCs, the TES unit is incorporated within the cooking vessel. The cooking vessel with TES unit is placed at the focal point of the solar collector and liberates heat in late hours. Sharma et al. (2005) developed SC with an evacuated tube solar collector and erythritol as LHSM. The TES unit consists of two hollow concentric cylinders with inner and outer dimensions, respectively 30.4 cm and 44.1 cm, and height 42 cm. The annular gap is filled with 45 kg of erythritol. The cooking vessel of diameter 29.7 cm and height 30 cm is inserted inside the LHS unit. The PCM temperatures reached more than 110°C. Their recommendation was to use erythritol as an effective PCM in solar cooking. Lecuona et al. (2013) designed and fabricated TES unit with two concentric cylindrical pots of inner and outer diameters 22 cm and 28.5 cm, respectively for parabolic SC. The inner and outer pot heights are respectively 14 and 17 cm. The annular space between two cylinders was filled with paraffin wax and erythritol as LHS medium. Nayak et al. (2016) carried out performance assessment of SC integrated with the LHS system and evacuated tube solar collector. The TES unit consists of hollow concentric aluminum cylinders with inner and outer dimensions, respectively 25 cm and 35 cm and height 30 cm. The annular space is filled with 3 kg acetanilide and 2.5 kg stearic acid as PCMs. An efficiency of 60-65% in the collector and 30% in the cooker is observed with acetanilide as PCM. As compared to stearic acid, acetanilide yielded better results for all the loadings in the cooker. Panchal and Sadasivuni (2018) did the performance analysis of SCs having sensible and latent heat storage materials by augmenting solar

radiation with scheffler reflector. They placed 1.5 L capacity pressure cooker as cooking pot at the centre of two concentric cylindrical pots of inner and outer dimensions 23.1 cm and 28.7 cm, respectively. The inner and outer space is filled with acetamide and SHSMs such as sand, pebbles, and iron balls. Test results showed that sand-acetamide and pebbles-acetamide pair of sensible and latent heat storage incorporated cooking pots outperform iron-balls-acetamide. Bhave and Thakare (2018) conducted performance test on concentrating type solar cooker with LHS unit containing magnesium chloride hexahydrate as PCM. The LHS unit consists of double-walled cylindrical vessel of inner dimension 13 cm and height 15 cm through which the PCM tubes are placed. The PCM tubes are aluminum with length 10 cm and internal diameter 1.6 cm (Fig. 22). The storage space is filled with HTF, which submerges the PCM tubes fully and in contact with the bottom and sides of the cooking vessel. A total of 21 tubes containing 0.48 kg magnesium chloride hexahydrate and 660 ml of HTF is filled in the TES space. A cooking vessel of diameter 11 cm and height 4 cm is inserted into the TES device supported using a flange. Their experiment showed that the cooker could store a charge of heat in 50 minutes and cook 140 g of rice in 30 minutes with the heat from the stored charge. Kedida et al. (2019) modeled and tested parabolic SC integrated with pebble bed thermal storage. They placed the cooking vessel on the top of the TES unit with diameter of 30 cm and height of 90 cm. A study by Abu-Hamdeh and Alnefaie (2019) evaluated thermal performance of solar stove that utilized acetamide as heat storage agent. The PCM is packed into the cylindrical capsule known as solar coal. Solar radiation was focused onto the aluminium container filled with PCM using parabolic reflector. Bhave and Kale (2020) developed heat storage cum cooking device with the aid of potassium and sodium nitrate mixture. Fins made of aluminium are welded at the bottom of the cooking pot for heat transfer enhancement of PCM. A double-walled stainless-steel vessel is used as PCM storage, in which the external annular cavity is evacuated. The cooking vessel is incorporated with PCM storage container by using larger flange. They also presented mathematical modelling of heat transfer and compared it with the experimental results. According to the cooking performance results, 0.6 kg of rice was cooked from one charge in two batches, each taking 20 minutes. Mawire et al. (2020) experimentally compared two kinds of TES cooking

pots having sunflower oil as SHSM and erythritol as LHS material using parabolic dish solar cooker. The TES unit consists of cylindrical stainless-steel vessels with inner and outer diameters, respectively 25 cm and 32 cm, and inner and outer depths, respectively 7.8 cm and 11 cm. The quantities of sunflower oil and erythritol filled in the annular cavities are 3.750 and 3.780 L, respectively. The corresponding mass of erythritol and sunflower oil are respectively 5.438 and 3.438 kg. The two vessels are kept inside the insulating wonder bag slow cooker for the performance analysis during sundown hours. They found that sunflower oil shows lesser cooking time and higher maximum storage temperatures than erythritol storage cooking vessels during the daytime. However, during sundown hours, the erythritol storage pot offers better performance than the oil storage. Kajumba et al. (2020) developed and tested cooking unit integrated with TES by utilizing sunflower as HTF and heat storage medium. Senthil (2021) carried thermal performance study on parabolic dish SC incorporated with TES unit containing paraffin wax as PCM.

Many review articles were also reported on the developments of SCs incorporated with heat storage materials. Sharma et al. (2009) reviewed the SC incorporated with PCMs. A review on SCs integrated with sensible and latent heat storage materials was carried by Panchal et al. (2017). Nkhonjera et al. (2017) carried review on the heat storage units, materials, and performance of SCs incorporated with TES units. They suggested to optimize the geometry and heat transfer characteristics of TES units. The recent advances in the application of PCMs in solar thermal energy systems like solar thermal power plants, solar air heaters, solar water heaters, and SCs were reported by (Pandey et al. 2018). A review article on the desirable and undesirable qualities of different types of PCM required for SCs was presented by Thirugnanam et al. (2020). Omara et al. (2020) reviewed the applications of PCMs as TES mediums to improve the performance of SCs during evening cooking.

2.4. Research gap and critical Review

A review on SCs has been made. Several authors have analyzed experimentally the performance of SCs including design modifications and proposal of new thermal performance parameters and test procedures. Others have focused on predicting the

temperatures of different elements in SC through heat transfer models. SCs incorporated with TES for off-sunshine cooking were also reported by many authors.

The literature review sheds light on the fact that performance of SBC in any climatic conditions is affected by every element of the cooker system, such as box shape, absorber plate, glass cover, cooking pot, thermal storage medium, outer and inner reflectors, insulation material and thickness etc. However, absorber plate is the most important part as it absorbs maximum solar energy and transfers it to the cooking load by conduction and radiation mode of heat transfer. Therefore, it is essential to determine the optimum area of absorber plate so as to attain maximum temperature for cooking load. Optimizing the cooker surface area minimizes overall heat loss coefficient, resulting in maximum performance. As per the literature review, no works have been reported on the determination of optimum area of absorber plate. Solar irradiance entering the cooker cavity is another important parameter which needs to be enhanced by fitting outer reflector to the SBC. An up-to-date review of literature reveals that no work has been reported on cylindrical solar box cooker (CSBC) fitted with outer reflector. Performance comparison of different geometries of SBC is not reported as of now. It is essential to compare the performance of cylindrical and trapezoidal shaped SBCs experimentally.

Several studies have been conducted on SCs, including numerical and experimental investigations. Experimental research evaluates the performance of SCs and determines the practicability. Since the performance of SC depends on solar irradiance, it is essential to conduct the test at different times, days, and locations. Performing experiments involves a great deal of time, money, and human resources. Additionally, the environmental conditions can fluctuate during the experiments, giving inappropriate performance results. The numerical studies of SC that have been reported so far have used experimentally determined solar irradiances to solve thermal balance equations. Numerical simulations that incorporate all elements of SBC with changing solar irradiance as a function of day, time, and location are lacking in the literature. The major parameters which effects on the heat transfer due to solar energy in SBC are the absorptivity, emissivity, transmissivity, specific heat capacity and density of the glass, absorber plate and cooking vessel materials. The machine

learning (ML) models can easily predict the performance without further doing simulations to test the same kind of SC at different geographical locations. In this direction, the development of ML-based prediction models for SC is of significance. The data-driven techniques are rarely used, and most of them are based on artificial neural network (ANN) or their modifications. ML models other than ANN have not been explored for solar thermal energy utilization appliances. Also, many popular ML methods like ANN is unstable and unreliable. ML models like random forest (RF), linear regression, k-nearest neighbor (k-NN), and decision trees are helpful in estimating the performance parameters of SBCs with known parameters, material properties, and location data.

Different kinds of SCs with PCM storage have been developed over the last few decades. But no studies have stated the determination of the optimum quantity of PCM and dimensions of the TES container for maintaining constant temperature for a particular duration. Also, through literature survey, it is clear that no studies have reported the optimal geometry and heat transfer characteristics for TES units for SBCs. Optimum selection of PCM is also essential for the efficient heat storage in the TES unit. Various multi-criteria decision-making (MCDM) methods were applied in sustainable and renewable energy development sectors. But very few studies were reported on the use of MCDM tools for the optimum selection of PCM. Further, as per literature study it is clear that TES units surrounding the cooking vessel are usually filled with PCM along the lateral side (Sharma et al. 2000; Buddhi et al. 2003; Vigneswaran et al. 2017; Lecuona et al. 2013; Bhave and Kale 2020; Mawire et al. 2020). But, if we could provide the facility for filling the PCM at the lateral and bottom part of the cooking pot and on the lid, cooking performance will be enhanced as heat is transferred to the load through all sides of the pot.

Motivated by previous studies and research gaps, the following objectives are formulated.

2.5. Objectives

The prime objective of the present work is to design, optimize, develop and test a SBC with temperature-controlled TES unit using PCMs. Through this work, it is

planned to carry out experimental, numerical and machine learning based analysis. The primary objectives are:

- Design, fabrication, and experimental investigation on the thermal performance of rectangular, cylindrical, and rectangular with inclined glass cover type SBC fitted with outer reflectors.
- To develop prediction models for the SBC using computational and machine learning techniques.
- To investigate the optimum geometry and dimensions of latent heat storage (LHS) units for SBC by developing computational procedure.
- To select optimum PCM among the alternatives to be used for the LHS unit integrated with SBC using MCDM techniques.
- To carry out experimental investigation on the performance assessment of SBC integrated with optimized TES system.

3. EXPERIMENTAL ANALYSIS OF VARIOUS SHAPED SOLAR BOX COOKERS

This thesis is mainly concerned with developing solar box cooker (SBC) with thermal energy storage (TES) system using phase change material (PCM). It involves developing computational and optimization procedures to accomplish this objective. Experiments are conducted on different SBCs to familiarize them with the test procedure and performance assessment. This section presents the design, fabrication, and performance evaluation of rectangular, cylindrical, and trapezoidal shaped SBCs. A more detailed discussion is presented in the following sections.

3.1. Background

Thermal performance study by experimental investigations on various types of SBCs were conducted and presented by many authors. A lot of such works have been done to study the performances of different box cookers by obtaining performance parameters namely figures of merit (F_1 and F_2), energy and exergy efficiency, cooking power etc.

This chapter analyses the performance of different geometries of SBCs. The SBCs are fabricated and tested as per Indian standards IS 13429. As a preliminary study, rectangular-shaped SBC (RSBC) is designed with the aid of analytical heat loss and design equations solved using an iterative procedure. The RSBC is fabricated and tested for performance assessment. The effect of providing a single reflector to the RSBC is also investigated. Next, the principle of minimum entropy generation (MEG) method is used to optimize the design of cylindrical-shaped SBC (CSBC). The experimental study on CSBC fitted with decahedron-shaped outer reflector (CSBC-FDR) is conducted. Then, a trapezoidal-shaped SBC (TSBC) is designed, fabricated, and tested for performance evaluations. The effect of providing four outer reflectors to the TSBC is also carried out.

3.2. Methodology

The description about design parameters, experimental set up and test procedures are presented in this section. It also presents the performance evaluation methods, statistical, uncertainty and economic analysis of SBCs.

3.2.1. Design of solar box cooker

Iterative design procedure

The optimum area of absorber plate for SBC can be computed with the aid of analytical heat loss and design equations using an iterative solution procedure. The absorber plate area is calculated based on the mass of water to be boiled using the energy balance equation as:

$$A_p = \frac{m_w c_w (T_{w2} - T_{w1})}{t[G_{av}\alpha_p\tau_g - U_L(T_p - T_a)]} \tag{3.1}$$

The heat lost to the atmosphere from SBC depends on the difference in temperature between the absorber plate and outside air. Therefore, cooker loses more heat when the absorber plate temperature is maximum. The absorber plate temperature is assumed initially and found by the iterative procedure solved using Matlab.

Total heat loss from the absorber plate to the surrounding is estimated by considering heat loss coefficients from the plate to the ambient through all faces of the cooker (Figure 3.1). This can be expressed as overall heat loss coefficient (U_L) which involves heat losses through bottom, top and lateral sides which is given by,

$$U_L = U_T + U_B + U_S \tag{3.2}$$

here, U_T is the top loss coefficient for SBC with double glass cover which can be written in terms of heat transfer coefficients as (Samdarshi and Mullick (1991)):

$$\frac{1}{U_T} = \left(\frac{1}{h_{rpg1} + h_{cpg1}}\right) + \left(\frac{1}{h_{rg1g2} + h_{cg1g2}}\right) + \left(\frac{1}{h_{rg2a} + h_w}\right) + \frac{2t_g}{k_g} \tag{3.3}$$

Samdarshi and Mullick (1991) proposed an analytical equation for the top loss by substituting the coefficients from the approximate solution into the above equation as:

$$\frac{1}{U_T} = \left[\frac{5.78\{(T_p - T_{g1})\cos\beta\}^{0.27}}{\left(\frac{T_p + T_{g1}}{2}\right)^{0.31} L_{pg1}{}^{0.21}} + \frac{\sigma(T_p^2 + T_{g1}^2)(T_p + T_{g1})}{\frac{1}{\varepsilon_p} + \frac{1}{\varepsilon_g} - 1}\right]^{-1} + \left[\frac{5.78\{(T_{g1} - T_{g2})\cos\beta\}^{0.27}}{\left(\frac{T_{g1} + T_{g2}}{2}\right)^{0.31} L_{g1g2}{}^{0.21}} + \right.$$

$$\left. \frac{\sigma(T_{g1}^2 + T_{g2}^2)(T_{g1} + T_{g2})}{\frac{2}{\varepsilon_g} - 1}\right]^{-1} + \left[h_w + \sigma\varepsilon_g(T_{g2}^2 + T_a^2)(T_{g2} + T_a)\right]^{-1} + \frac{2t_g}{k_g} \qquad (3.4)$$

The wind heat transfer coefficient (h_w) is estimated by using (Guidara et al. 2017),

$$h_w = 5.7 + 3.8 \, w \qquad (3.5)$$

With fixed values of ambient temperature (T_a) and solar irradiance (G), top loss coefficient depends only on absorber plate temperature T_p. The glazing temperatures (T_{g1} and T_{g2}) are determined by iterative procedure.

The correlation for top heat loss coefficient (U_T) for SBC also given by Channiwala and Doshi (1989) as:

$$U_T = \left[\frac{2.8}{\frac{1}{\varepsilon_p} + \frac{1}{N_c^{0.025}\varepsilon_g} - 1} + 0.825(x_m)^{0.21} + aV^b - 0.5(N_c^{0.95} - 1)\right]\left[T_{pm} - T_a\right]^{0.2} \qquad (3.6)$$

The expressions for 'a' and 'b' are given by Channiwala and Doshi (1989) which is as follows:

$$a = [0.6 - 0.05(N_c - 1)] \qquad (3.7)$$

$$b = [1.1 - 0.1(N_c - 1)] \qquad (3.8)$$

The top heat loss coefficient is calculated using equation (3.6) with the mean absorber plate and ambient temperatures.

Bottom heat loss coefficient (U_B) is calculated using the equation:

$$\frac{1}{U_B} = \frac{t_{ins}}{k_{ins}} + \frac{t_{st}}{k_{st}} \qquad (3.9)$$

Side heat loss occur by conduction and is a function of thermal conductivity and dimensions of the casing such as length, width, and height (spacing between the bottom and the glass cover). Side heat loss depends on thermal conductivity of the

insulation material and the housing. Calculation of U_s aims to reduce collector sizing which minimizes the heat lost through the sides. Equations (3.10) and (3.11) are respectively for the side heat loss coefficients for rectangular and cylindrical box geometry.

$$\frac{1}{U_S} = \frac{1}{4\ L\ L_{pg1}}\left[\frac{t_{ins}}{k_{ins}} + \frac{t_{st}}{k_{st}}\right] \tag{3.10}$$

$$\frac{1}{U_S} = \left(\frac{d}{2}\right)\left[\frac{\ln\left\{1+\left(\frac{2\ t_{ins}}{d}\right)\right\}}{k_{ins}}\right] \tag{3.11}$$

U_S is calculated by assuming the side length of absorber plate (L) initially and then by iterative procedure using Matlab.
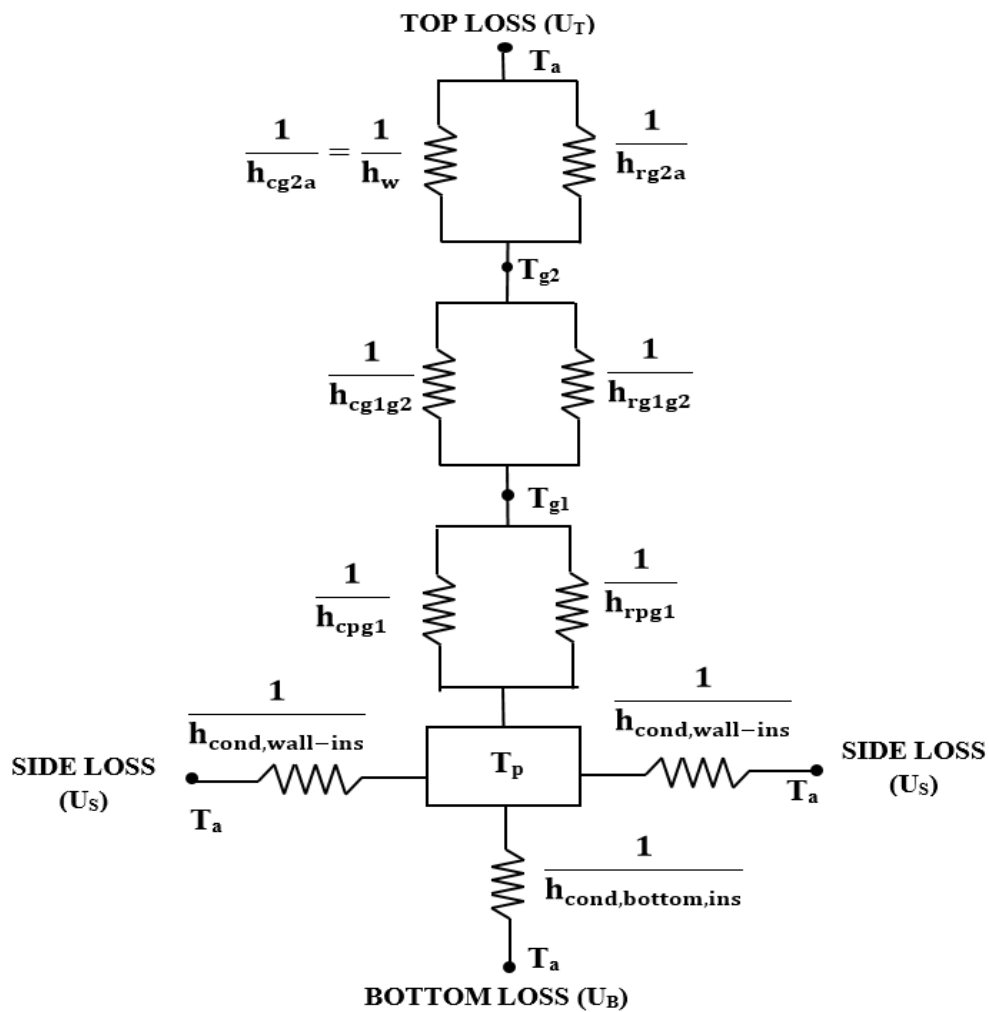
Figure 3.1 Network diagram of thermal resistance in a solar cooker

Minimum entropy generation method

Optimal SBC design is also possible by applying minimum entropy generation (MEG) principle, which minimizes loss of useful work or destruction of availability. MEG (also called thermodynamics of irreversible processes) can be used for thermal optimization of heat transferring devices (Bejan et al. 1981). In SBCs, irreversibility occurs due to finite temperature differences between the sun and absorber plate or between absorber plate and cooking load.

The energy balance for SBC with incoming solar energy, useful heat energy and losses to surroundings is written as:

$$U_L A_p \left(T_p - T_a\right) = G\left(\tau_g{}^2 \alpha_p\right) A_p - \left(\frac{m_w C_w}{t}\right)\left(T_{w2} - T_{w1}\right) \tag{3.12}$$

The maximum possible absorber plate temperature ($T_{p, max}$) of SBC at any given irradiance can be obtained by taking useful heat energy as zero. Therefore, all incoming irradiance is lost to the surroundings. Thus equation (3.12) becomes,

$$U_L A_p \left(T_{p,max} - T_a\right) = G\left(\tau_g{}^2 \alpha_p\right) A_p \tag{3.13}$$

Rearranging and defining $T_{p, max}$ in dimensionless form as,

$$\theta_{max,ap} = \frac{T_{p,max}}{T_a} = 1 + \frac{G\left(\tau_g{}^2 \alpha_p\right)}{U_L T_a} \tag{3.14}$$

But, during the operation of SBC, vessel containing cooking load is placed on top of the absorber plate for time duration t (sec). The exergy destruction from the sun to absorber plate at apparent sun temperature (6000 K), and absorber plate to cooking load (at its varying temperature) and surroundings (at ambient temperature) is quantified as entropy generation rate (Chauhan et al. 2019).

The entropy balance for closed system is given by,

$$\dot{S}_{gen} = \frac{m_w C_w \ln\left(\frac{T_{w2}}{T_{w1}}\right)}{t} - \left(\frac{-Q_L}{T_a} + \frac{Q_{in}}{T_{sun}}\right) \tag{3.15}$$

For SBC, it can be written as:

$$\dot{S}_{gen} = \left(\frac{m_w C_w}{t}\right) \ln\left(\frac{T_{w2}}{T_{w1}}\right) + \frac{G(\tau_g^2 \alpha_p)A_p - \left(\frac{m_w C_w}{t}\right)(T_{w2} - T_{w1,})}{T_a} - \frac{G(\tau_g^2 \alpha_p)A_p}{T_{sun}} \tag{3.16}$$

In dimensionless form it is reduced to:

$$\frac{\dot{S}_{gen} T_a}{G(\tau_g^2 \alpha_p)A_p} = \frac{\left(\frac{m_w C_w}{t}\right)T_a}{G(\tau_g^2 \alpha_p)A_p}\left[\ln\left(\frac{\theta_f}{\theta_i}\right) - \theta_f + \theta_i\right] - \frac{1}{\theta_{sun}} + 1 \tag{3.17}$$

Entropy Generation Number (EGN) is given by,

$$EGN = \frac{\dot{S}_{gen} T_a}{G(\tau_g^2 \alpha_p)A_p} \tag{3.18}$$

and Energy Capacity Rate Number (ECN) is given by,

$$ECN = \frac{\left(\frac{m_w C_w}{t}\right)T_a}{G(\tau_g^2 \alpha_p)A_p} \tag{3.19}$$

Therefore, equation (3.17) is rewritten as,

$$EGN = ECN\left[\ln\left(\frac{\theta_f}{\theta_i}\right) - \theta_f + \theta_i\right] - \frac{1}{\theta_{sun}} + 1 \tag{3.20}$$

Taking $\theta_i = 1$ (ie $T_{w1} = T_a$), the EGN becomes (Bejan et al. 1981; Chauhan et al. 2019),

$$EGN = ECN[\ln(\theta_f) - \theta_f + 1] - \frac{1}{\theta_{sun}} + 1 \tag{3.21}$$

ECN can be expressed in dimensionless form of peak absorber plate and final cooking load temperature as: (Torres-Reyes et al. 2001; Bejan et al. 1981)

$$ECN = \frac{1}{(\theta_{max,ap} - 1)}\frac{1}{\ln\left(\frac{\theta_{max,ap} - \theta_i}{\theta_{max,ap} - \theta_f}\right)} \tag{3.22}$$

The procedure for preliminary design of SBC based on MEG is as follows:

Step 1: Obtain the average values of G and T_a.

Step 2: Determine the required final temperature of cooking load (T_f).

Step 3: Find maximum absorber plate temperature by obtaining the correlation.

Step 4: Find the minimum EGN for $\theta_{max, ap}$ and θ_f.

Step 5: Determine ECN for $\theta_{max,ap}$ and θ_f using equation (3.22).

Step 6: Obtain the value of U_L from equation (3.14).

Step 7: Determine the absorber plate area (A_p) using equation (3.19) and ECN found in step 5 (known values of m_w and t).

3.2.2. Experimental setup

Rectangular SBC

Design of RSBC is carried out based on the desired requirements such as average solar irradiance, mass of water to be boiled and final water temperature. The overall heat loss coefficient and absorber plate area are found by solving the heat loss and energy balance equation (Table 3.1). Absorber plate area is estimated for achieving final cooking load temperature of 100°C in two hours. The top heat loss coefficient U_T based on the requirement is found to be 3.65W/m²K which is more than the side and bottom heat loss coefficient. This is due to more convective and radiative losses from the top of the cooker. In SBC, the top heat loss factor depends on absorber plate temperature, wind heat transfer coefficient and ambient temperature (Mullick et al. 1997). Recently, Saxena et al. (2020) obtained overall heat loss coefficient (U_L=5.11W/m²K) for a modified SBC incorporated with PCM infused tubes which is higher than the present study (U_L=4.72 W/m²K).

Table 3.1 Design parameters of RSBC

Sl No.	Specifications	Value
1	Top heat loss coefficient, U_T (W/m²K)	3.65
2	Side heat loss coefficient, U_S (W/m²K)	0.48
3	Bottom heat loss coefficient, U_B (W/m²K)	0.59
4	Overall heat loss coefficient, U_L (W/m²K)	4.72
5	Absorber plate area, A_P (m²)	0.342

The RSBC is fabricated based on the design parameters. It consists of rectangular box made up of steel having outer dimensions (650 mm x 650 mm), inner dimensions

(600 mm x 600 mm) and height 250 mm with double-glazed glass of spacing 15 mm at the top (Figure 3.2). An insulation of glass wool with thickness 50mm is provided at the bottom surface and 25mm thickness provided at the lateral surfaces to minimize the conduction losses (Kumar, 2004). The absorber plate made up of aluminium sheet painted with matte black is placed at the bottom of inner box to absorb the solar radiant energy falling on it and to transfer heat to the cooking pot placed on it. As the thermal conductivity of aluminium is 237W/mK, it is suitable for transferring heat to the cooking pot in a fast manner. A single reflector is also provided at the top to boost the solar radiation which penetrates through the glazing. The dimension of the reflector is same as that of the aperture of the cooker which is 600 mm x 600 mm with an allowance for the ease of closing the cooker.

Figure 3.2 Experimental setup for RSBC

Cylindrical SBC

The design of CSBC is carried out using the principle of MEG method and iterative design procedure. Monthly average value of solar irradiance (G) and ambient temperature (T_a) are taken as 850 W/m^2 and 30°C respectively. The required final temperature of cooking load is assumed to be 100°C. Initial temperature of cooking load (T_{w1}) is assumed to be equal to ambient and desired time (t) for boiling water is

90 minutes. The absorptivity (α_p) of absorber plate material and transmissivity of glass (τ_g) is taken as 0.95 and 0.9 respectively.

The correlation between dimensionless temperatures θ_f and $\theta_{max,ap}$ is obtained from regression analysis (Figure 3.3). The correlation is given by,

$$\theta_f = 0.636\,\theta_{max,ap} + 0.381 \tag{3.23}$$

The value of regression coefficient (R^2) is found to be 0.97. From the regression equation (3.23), dimensionless peak absorber plate temperature ($\theta_{max,ap}$) is obtained as 1.33. According to equations (3.21) and (3.22), EGN is shown as a function of final cooking load temperature, using maximum absorber plate temperature as parameter (Figure 3.4). After determining dimensionless maximum absorber plate temperature, corresponding curve in Figure 3.4 is selected, and minimum EGN is calculated. The value of minimum EGN is obtained as 0.891. Figure 3.5 illustrates ECN as a function of θ_f, with $\theta_{max,ap}$ as parameter, according to equation (3.22). Here, ECN is found after selecting the curve corresponding to dimensionless maximum absorber plate temperature shown in Figure 3.5. Optimum ECN is obtained as 2.516. Figure 3.6 shows peak absorber plate temperature as a function of overall heat loss coefficient (U_L) for different solar irradiance. The curve corresponds to average solar irradiance is selected, and U_L is obtained as 6.54 W/m^{2}K. Finally, absorber plate area (A_p) is calculated as 0.143 m^2 with the aid of equation (3.19) and optimum ECN value. The absorber plate area found by iterative solution procedure is 0.145 m^2 which is in close agreement with the results of MEG method. Hence, the CSBC is fabricated with absorber plate of diameter 43 cm.
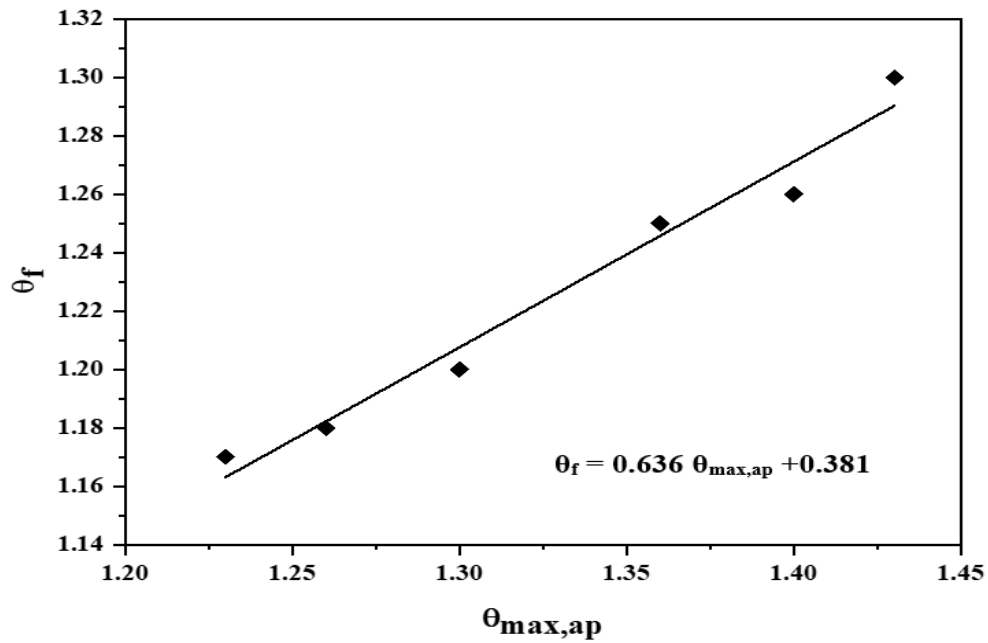
Figure 3.3 Relationship between cooking load final and absorber plate maximum temperature for MEG condition

$$\theta_f = 0.636\, \theta_{max,ap} + 0.381$$
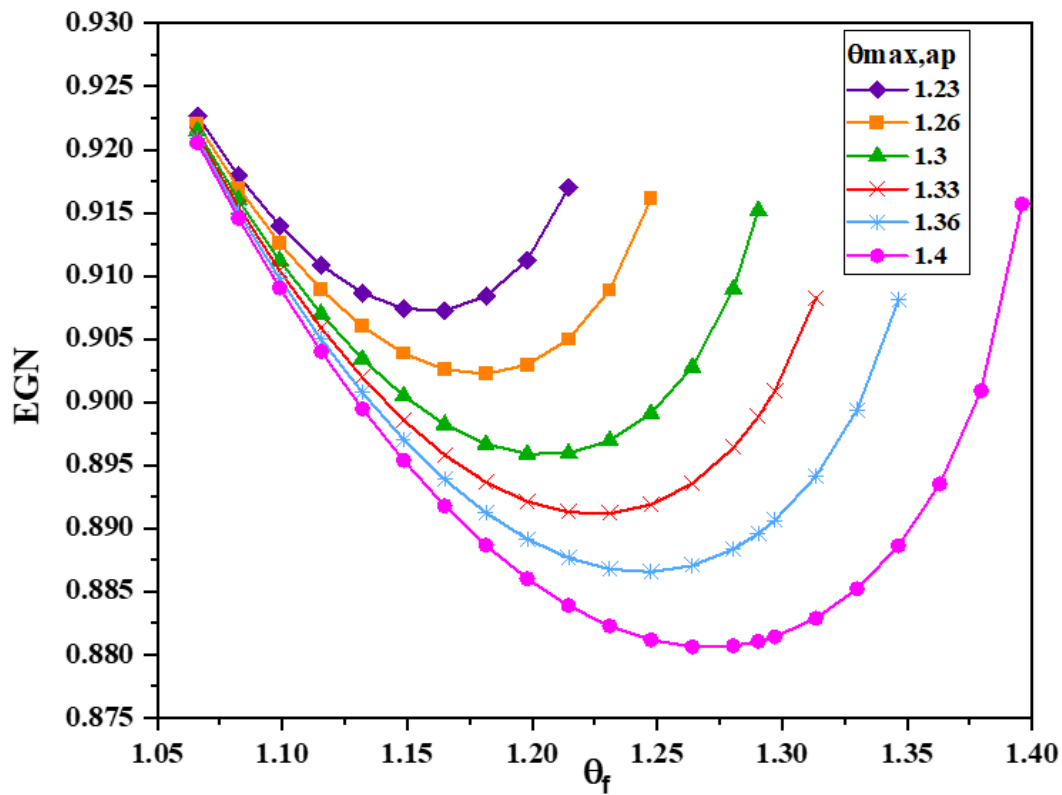
Figure 3.4 EGN as a function of final temperature of cooking load for different values of $\theta_{max,ap}$
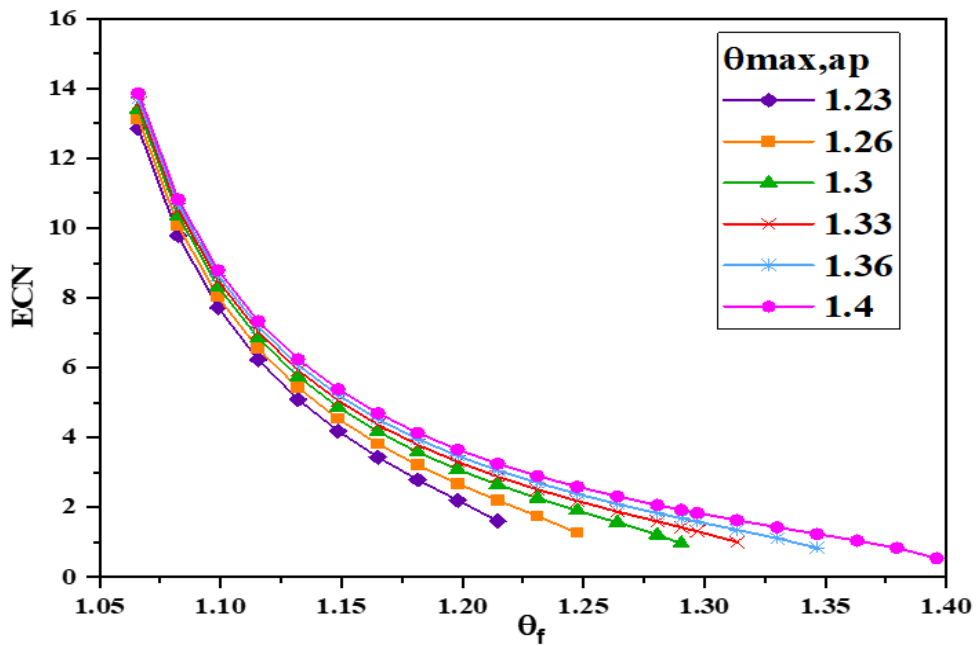
Figure 3.5 ECN as a function of final cooking load temperature for different values of $\theta_{max, ap}$
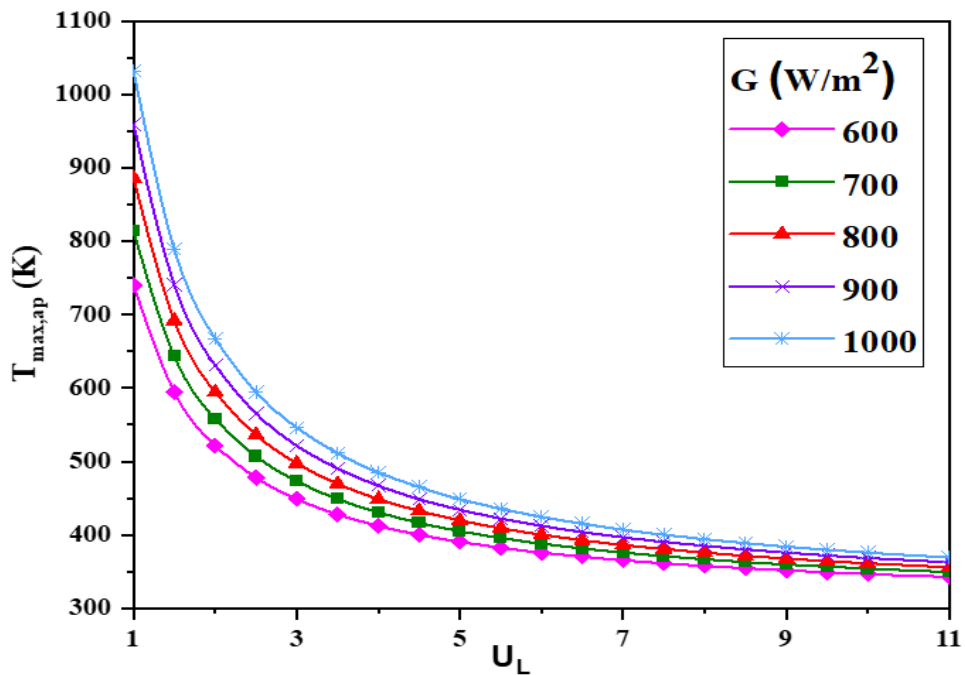
Figure 3.6 Peak temperature of absorber plate as a function of overall heat loss coefficient for different solar irradiance

The CSBC (Figure 3.7a) developed in this work comprises mild steel cylindrical box with external diameter 53 cm, internal diameter 43 cm, and height 30 cm with double glass cover at the top. The gap between two layers is filled with glass wool of

thickness 5 cm as insulation (Cuce 2018b) to reduce heat transfer with the surroundings. Aluminum absorber plate of diameter 43 cm, thickness 2 mm, and black in color is fixed at the base of cooker's inner cavity. Glass wool insulation with 5 cm thickness is provided below the absorber plate to reduce heat transfer through bottom surface. A small door is provided on lateral surface of the cooker rather than at top as in conventional SBC (Cuce 2018b). Hence, glazing covers at the top are permanently fixed without leakage at edges, which reduces heat loss through top of cooker cavity.

Figure 3.7 (a) Cylindrical box solar cooker with cooking vessel (b) cooker fitted with decahedron reflector
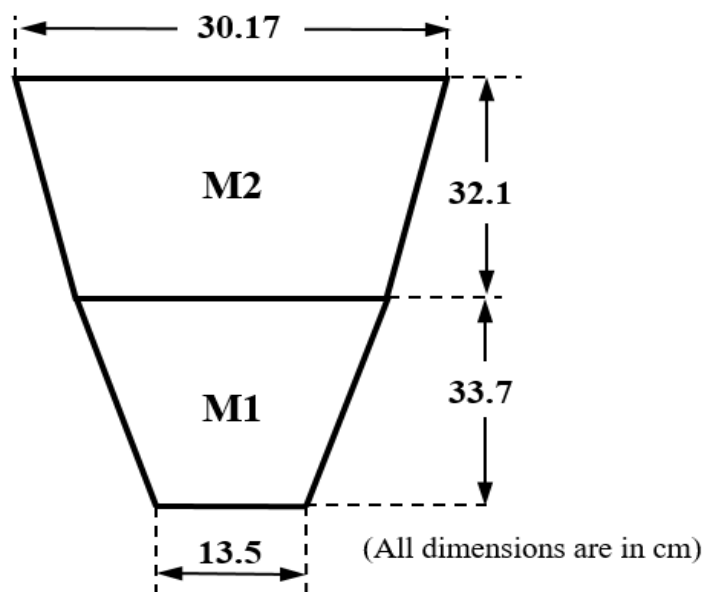
Figure 3.8 schematic of single reflector

Decahedron-shaped reflector made up of plane mirrors is also provided to increase solar radiation penetration though glazing (Figure 3.7b). The reflector has ten identical pieces of double row mirrors, trapezoidal in shape. The mirror's upper (32.1cm long) and lower (33.7 cm long) portions make an angle of 70° and 63°, respectively, with the horizontal surface. Dimensions of reflector are calculated based on aperture area of the cooker (Figure 3.8).

Trapezoidal shaped SBC

The TSBC (Figure 3.9) developed in this study is a double-walled box made of multi-wood and covered with glazing covers at the top. The design parameters are detailed in Table 3.2. The glazing covers are made up of 5 mm thick glass and are inclined upwards at an angle of 30° with horizontal surface. The upper and lower glazing cover have dimensions of 600 mm x 500 mm and 570 mm x 470 mm respectively. Glass wool thickness of 50 mm is used as insulation (Cuce 2018b) in the annular space between the outer and inner boxes to reduce heat transfer between the cooker and the surroundings. A black matte square-shaped aluminum absorber plate, dimension 475 mm x 3 mm thickness, is fixed to the bottom of the inner cavity of the cooker. The absorber plate has area 0.2256 m^2, which is set based on the MEG method and the iterative solution procedure. The present TSBC can occupy 3 to 4 cooking vessels having diameters 15 to 20 cm which in turn can cook the food for a family of 4 to 5 members in a day. The cooker has advantage of being easy to build and use, ease of construction, the ease of movement and transportation, and the use of common and inexpensive materials. The bottom of the absorber plate is covered with layer of glass wool insulation to prevent heat loss to the surroundings. On interior surface of inner box, aluminium foils are glued so as to reflect the solar radiation on to the absorber plate. Four removable reflectors made up of plain mirrors with thickness 3 mm are fixed at outer edges of the box. A mechanism for changing the angle of inclination (15°, 30° and 45° with vertical) of reflectors is also provided. Like CSBC, here also lateral surface of the cooker is provided with small opening rather than top of the cooker (Guidara et al. 2017). Figures 3.10 (a) and (b) respectively depicts the experimental setup for SBC without and with external reflectors.
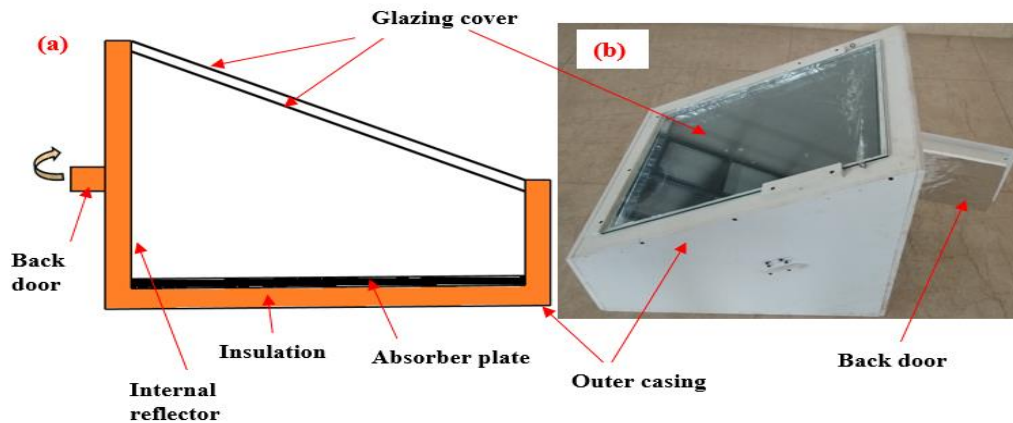
Figure 3.9 Trapezoidal-shaped SBC (a) Schematic (b) Pictorial

Table 3.2 Geometrical parameters of components in TSBC

Parameters	Description
Outer casing material	Multi wood
Thickness	12 mm
Dimensions: Trapezoidal	520 mm x 570 mm x 500 mm x 220 mm
Back side	520 mm x 500 mm
Double glazing material	Glass
Thickness	5 mm
Dimensions: Upper glass	600 mm x 500 mm
Lower glass	570 mm x 470 mm
Spacing between glazing covers	15 mm
Angle of inclination	30º
Absorber plate material	Aluminium
Thickness	3 mm
Dimensions	475 mm x 475 mm
Insulation material	Glass wool
Thickness	50 mm
Outer reflector material	Mirror
Thickness	3 mm
Dimensions: Front and back side	500 mm x 500 mm
Trapezoidal side	600 mm x 500 mm
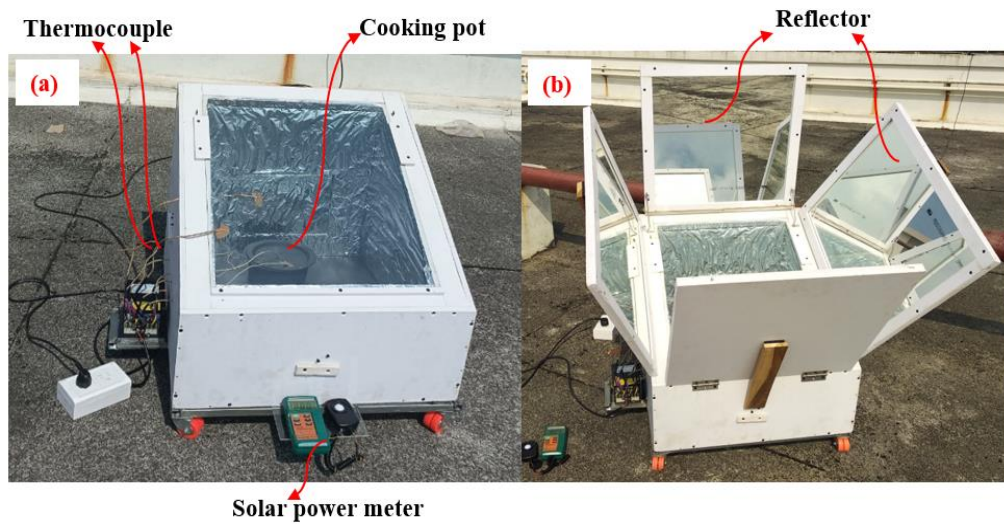
Figure 3.10 Experimental setup (a) TSBC without reflector (b) TSBC with reflector

3.2.3. Experimental study

The experimental study includes stagnation and sensible heating tests. As per IS 13429 (Part 3):2000 test standard, minimum three tests should be carried out to evaluate first and second figures of merit. In the present study, six tests are conducted for both stagnation and sensible heating. Solar irradiance and temperatures of absorber plate, inner air cavity, glazing cover, cooking load, and ambient air are measured at every 10-minute time interval from 10.00 AM to 4.00 PM on each test day. Energy, exergy and cooking power analysis are performed based on the temperature and solar irradiance measurements during sensible heating test.

Stagnation test

The first figure of merit (F_1) is found out by stagnation test (Mullick et al, 1987) on the developed SBCs. During this test, cooker is placed open to sunlight with no-load condition. Temperatures of absorber plate, ambient air, and cooker cavity are measured using thermocouples at each interval of time till the stagnation condition is obtained. The first figure of merit is calculated as, (Mullick et al, 1987)

$$F_1 = \frac{T_{ps} - T_{as}}{G_s} \tag{3.24}$$

Sensible heat test

The sensible heat test or load test is carried out to find the second figure of merit (F_2) (Mullick et al, 1987). For this, water contained in cooking vessel is kept in the cooker and time taken for rising the temperature of water from T_{w1} (60 to 65°C) to T_{w2} (90 to 95°C) is noted. The second figure of merit is calculated as, (Mullick et al, 1987)

$$F_2 = \frac{F_1 m_w c_w}{At} \ln\left[\frac{1-\frac{1}{F_1}\left(\frac{T_{w1}-T_a}{G}\right)}{1-\frac{1}{F_1}\left(\frac{T_{w2}-T_a}{G}\right)}\right] \tag{3.25}$$

Energy analysis

This indicates the maximum energy which can be transformed from solar radiation to useful heat energy. The output energy of the cooker divided by solar energy gives energy efficiency (Ozturk, 2004).

$$\eta_{energy} = \frac{m_w c_w [T_f - T_i]}{GAt} \tag{3.26}$$

Exergy analysis

It is the energy component available in the transformation of solar energy. Exergy output of water divided by the solar radiation gives the exergy efficiency and is given by (Ozturk, 2004),

$$\eta_{exergy} = \frac{m_w c_w\left[(T_f - T_i) - T_a \ln\left[\frac{T_f}{T_i}\right]\right]}{\left[1-\left(\frac{4T_a}{3T_S}\right)\right]AGt} \tag{3.27}$$

where $T_S = 5800K$

Cooking power analysis

Cooking power is the rate of thermal energy which is productive during heating time and is calculated by (Funk 2000),

$$P = \frac{m_w c_w [T_f - T_i]}{t} \tag{3.28}$$

Standardized cooking power is the cooking power which is corrected to standard insolation of 700 W/m^2 and is given by (Funk 2000),

$$P_s = \frac{m_w c_w [T_f - T_i]\, 700}{t\, G} \tag{3.29}$$

Instruments used

The experimental procedure for performance tests is conducted as per international standards IS 13429. A calibrated solar power meter (± 10 W/m^2 accuracy) having a range of 2000 W/m^2 with 0.1 W/m^2 resolution is used to measure the intensity of solar irradiance (G). The temperatures of absorber plate, air cavity, water and glazing are measured using K-type (Chromel-Alumel) thermocouple with an accuracy of 2°C. Measurements are taken at every 10-minute interval from 10 AM to 4 PM Indian Standard Time (IST) during each experiment. Mass of water is measured by using an electronic balance (accuracy 0.001kg).

3.2.4. Uncertainty analysis

Uncertainty is the best estimate of the magnitude of the unknown error. Suppose 'R' is the result of a measurement which depends on the independent variables X_1, X_2, ...X_n. Then the uncertainty in the result is given by, (Purohit, 2010)

$$W_R = \left[\left(\frac{\partial R}{\partial X_1} W_1\right)^2 + \left(\frac{\partial R}{\partial X_2} W_2\right)^2 + \cdots \ldots \ldots . \left(\frac{\partial R}{\partial X_n} W_n\right)^2\right]^{1/2} \tag{3.30}$$

Where, W_1, W_2, W_3....... Wn are the uncertainties in the independent variables X_1, X_2, X_3.......X_n.

Percentage of uncertainty in energy efficiency, exergy efficiency, F_1 and F_2 are calculated by using the following equations:

Energy efficiency

Uncertainty in energy efficiency is given by, (Purohit, 2010)

$$W_{\eta_{en}} = \left[\left(\frac{\partial \eta_{en}}{\partial m_w} W_{m_w}\right)^2 + \left(\frac{\partial \eta_{en}}{\partial T_f} W_{T_f}\right)^2 + \left(\frac{\partial \eta_{en}}{\partial T_i} W_{T_i}\right)^2 + \left(\frac{\partial \eta_{en}}{\partial G} W_G\right)^2 + \left(\frac{\partial \eta_{en}}{\partial A} W_A\right)^2 +$$

$$\left(\frac{\partial \eta_{en}}{\partial t} W_t\right)^2\right]^{\frac{1}{2}} \tag{3.31}$$

Equation (3.31) is reduced to percentage of uncertainty in energy efficiency as:

$$\frac{W_{\eta_{en}}}{\eta_{en}} = \left[\left(\frac{W_{m_w}}{m_w}\right)^2 + \left(\frac{W_{T_f}}{T_f-T_i}\right)^2 + \left(\frac{-W_{T_i}}{T_f-T_i}\right)^2 + \left(\frac{-W_G}{G}\right)^2 + \left(\frac{-W_A}{A}\right)^2 + \left(\frac{-W_t}{t}\right)^2\right]^{1/2} \tag{3.32}$$

Exergy efficiency

Uncertainty in exergy efficiency is given by, (Purohit, 2010)

$$W_{\eta_{ex}} = \left[\left(\frac{\partial \eta_{ex}}{\partial m_w}W_{m_w}\right)^2 + \left(\frac{\partial \eta_{ex}}{\partial T_f}W_{T_f}\right)^2 + \left(\frac{\partial \eta_{ex}}{\partial T_i}W_{T_i}\right)^2 + \left(\frac{\partial \eta_{ex}}{\partial T_a}W_{T_a}\right)^2 + \left(\frac{\partial \eta_{ex}}{\partial G}W_G\right)^2 + \right.$$

$$\left.\left(\frac{\partial \eta_{ex}}{\partial A}W_A\right)^2 + \left(\frac{\partial \eta_{ex}}{\partial t}W_t\right)^2\right]^{\frac{1}{2}} \tag{3.33}$$

Equation (3.33) is reduced to percentage of uncertainty in exergy efficiency as:

$$\frac{W_{\eta_{ex}}}{\eta_{ex}} = \left[\left(\frac{W_{m_w}}{m_w}\right)^2 + \left(\frac{\left(1-\frac{T_a}{T_f}\right)W_{T_f}}{\left(T_f-T_i-T_a\ln\left(T_f/T_i\right)\right)}\right)^2 + \left(\frac{-\left(1-\frac{T_a}{T_i}\right)W_{T_i}}{\left(T_f-T_i-T_a\ln\left(T_f/T_i\right)\right)}\right)^2 + \right.$$

$$\left.\left(\frac{-\ln\left(\frac{T_f}{T_i}\right)W_{T_a}}{\left(T_f-T_i-T_a\ln\left(T_f/T_i\right)\right)\left(1-\frac{4T_a}{3T_s}\right)}\right)^2 + \left(\frac{-W_G}{G}\right)^2 + \left(\frac{-W_A}{A}\right)^2 + \left(\frac{-W_t}{t}\right)^2\right]^{1/2} \tag{3.34}$$

First figure of merit

Uncertainty in F_1 is given by (Purohit, 2010)

$$W_{F1} = \left[\left(\frac{\partial F_1}{\partial T_{as}}W_{T_{as}}\right)^2 + \left(\frac{\partial F_1}{\partial T_{ps}}W_{T_{ps}}\right)^2 + \left(\frac{\partial F_1}{\partial G_s}W_{G_s}\right)^2\right]^{1/2} \tag{3.35}$$

Equation (3.35) is reduced to percentage of uncertainty in F_1 as:

$$\frac{W_{F1}}{F_1} = \left[\left(\frac{-W_{T_{as}}}{T_{ps}-T_{as}}\right)^2 + \left(\frac{W_{T_{ps}}}{T_{ps}-T_{as}}\right)^2 + \left(\frac{-W_{G_s}}{G_s}\right)^2\right]^{1/2} \tag{3.36}$$

Second figure of merit

Uncertainty in F_2 is given by (Purohit, 2010)

$$W_{F2} = \left[\left(\frac{\partial F_2}{\partial F_1}W_{F_1}\right)^2 + \left(\frac{\partial F_2}{\partial m_w}W_{m_w}\right)^2 + \left(\frac{\partial F_2}{\partial T_{w1}}W_{T_{w1}}\right)^2 + \left(\frac{\partial F_2}{\partial T_{w2}}W_{T_{w2}}\right)^2 + \right.$$

$$\left.\left(\frac{\partial F_2}{\partial T_a}W_{T_a}\right)^2 \left(\frac{\partial F_2}{\partial G}W_G\right)^2 + \left(\frac{\partial F_2}{\partial A}W_A\right)^2 + \left(\frac{\partial F_2}{\partial t}W_t\right)^2\right]^{1/2} \tag{3.37}$$

Equation (3.37) is reduced to percentage of uncertainty in F_2 as:

$$\frac{W_{F_2}}{F_2} = \left[\left(\frac{W_{m_w}}{m_w}\right)^2 + \left(\frac{-W_A}{A}\right)^2 + \left(\frac{-W_t}{t}\right)^2 + \right.$$

$$\left(\frac{W_{T_a}(T_{w1}-T_{w2})}{(F_1 G-(T_{w1}-T_a))(F_1 G-(T_{w2}-T_a))\left(\ln\left[\frac{1-\frac{1}{F_1}\left(\frac{T_{w1}-T_a}{G}\right)}{1-\frac{1}{F_1}\left(\frac{T_{w2}-T_a}{G}\right)}\right]\right)}\right)^2 +$$

$$\left(\frac{-W_{T_{w1}}}{(F_1 G-(T_{w1}-T_a))\left(\ln\left[\frac{1-\frac{1}{F_1}\left(\frac{T_{w1}-T_a}{G}\right)}{1-\frac{1}{F_1}\left(\frac{T_{w2}-T_a}{G}\right)}\right]\right)}\right)^2 + \left(\frac{W_{T_{w2}}}{(F_1 G-(T_{w2}-T_a))\left(\ln\left[\frac{1-\frac{1}{F_1}\left(\frac{T_{w1}-T_a}{G}\right)}{1-\frac{1}{F_1}\left(\frac{T_{w2}-T_a}{G}\right)}\right]\right)}\right)^2 +$$

$$\left(\frac{W_{F_1}}{F_1}\left\{1 + \frac{F_1 G(T_{w1}-T_{w2})}{(F_1 G-(T_{w1}-T_a))(F_1 G-(T_{w2}-T_a))\left(\ln\left[\frac{1-\frac{1}{F_1}\left(\frac{T_{w1}-T_a}{G}\right)}{1-\frac{1}{F_1}\left(\frac{T_{w2}-T_a}{G}\right)}\right]\right)}\right\}\right)^2 + \left(\frac{-W_G}{G}\left\{1 + \right.\right.$$

$$\left.\left.\left.\frac{F_1 G(T_{w1}-T_{w2})}{(F_1 G-(T_{w1}-T_a))(F_1 G-(T_{w2}-T_a))\left(\ln\left[\frac{1-\frac{1}{F_1}\left(\frac{T_{w1}-T_a}{G}\right)}{1-\frac{1}{F_1}\left(\frac{T_{w2}-T_a}{G}\right)}\right]\right)}\right\}\right)^2\right]^{1/2} \tag{3.38}$$

Where $W_{\eta en}$, $W_{\eta ex}$, W_{F1}, W_{F2}, W_{mw}, W_{Tf}, W_{Ti}, W_G, W_A, W_t are the uncertainty in energy efficiency, exergy efficiency, F_1, F_2, mass of water, final temperature of water, initial temperature of water, solar irradiance, area of absorber plate and time taken for rise of water temperature respectively.

3.2.5. Statistical Analysis

The statistical parameters studied in the present work are stated as follows:

Arithmetic Mean

Ratio of sum of all the measured readings and number of measurements is the arithmetic mean of several readings as given below (Purohit and Purohit, 2009).

$$\bar{x} = \frac{\sum_{i=1}^{n} x_i}{n} \tag{3.39}$$

Standard Deviation

Square root of the average of the squares of the deviation of the measured readings from the average value is standard deviation (Purohit and Purohit, 2009).

$$\sigma = \sqrt{\frac{\sum_{i=1}^{n}(x_i - \bar{x})^2}{n-1}} \qquad (3.40)$$

Confidence interval

It indicates the probability that the average value will be within certain number of standard deviation values. For 99% confidence level, confidence interval is written as, (Purohit and Purohit, 2009).

$$\bar{x} = \bar{x} \pm 2.58 \left(\frac{\sigma}{\sqrt{n}}\right) \qquad (3.41)$$

3.2.6. Economic Analysis

Annualized life cycle cost (ALCC)

Different economic criteria were used to evaluate and optimize solar energy systems (Duffie and Beckman, 2013), including least cost solar energy, life-cycle costs (LCC), and life-cycle savings. LCC represents sum of all the costs incurred by the system over its life span expressed in present value. It consists of initial investment (C_c), the present value of operation and maintenance costs ($C_{m, pv}$), and replacement's present value (C_r) (Duffie and Beckman, 2013) as given by equation (3.42).

$$LCC = C_c + C_{m,pv} + C_r \qquad (3.42)$$

Here, initial investments include costs of each component of the system and installation cost.

Where, installation cost is taken as 20% of initial system cost.

Operation and maintenance cost (C_m) includes taxes, insurance, maintenance, recurring costs etc. which is taken as some percentage (say 2%) of initial investment (Kolhe et al. 2002). All future costs of operation and maintenance have a present value calculated by,

$$C_{m,pv} = (pwf)C_m \qquad (3.43)$$

Where, pwf is the present worth factor obtained by (Duffie and Beckman, 2013),

$$\text{pwf} = \frac{(1+i)^t - 1}{i(1+i)^t} \tag{3.44}$$

where, 'i' is the percentage yearly rate of interest and 't' is the life expectancy in years.

Annualized life cycle cost (ALCC) is the total LCC expressed in terms of cost per year and is calculated by (Duffie and Beckman, 2013),

$$\text{ALCC} = \frac{\text{LCC}}{\text{pwf}} \tag{3.45}$$

Payback period (PP)

The payback period (PP) is estimated for SBC which is replaced with liquefied petroleum gas (LPG) stove. The PP is computed based on the cost of SBC and amount of saved money (SM).

The SM per year is computed by, (Herez et al. 2018)

$$\text{SM} = P_t \, M_{LPG} C_{LPG} \tag{3.46}$$

where, P_t is the percentage of time where the SBC is used, M_{LPG} is the mass of LPG consumed per year and C_{LPG} the price of 1 kg of LPG.

The PP is calculated by, (Herez et al. 2018)

$$\text{PP} = \frac{C_{SC}}{\text{SM}} \tag{3.47}$$

Where, C_{SC} is the total cost of SBC.

3.3. Results and discussions

3.3.1. Rectangular SBC

Stagnation and sensible heating tests are conducted on RSBC to familiarize the test procedures and performance assessment of SCs. From stagnation test, the average value of F_1 for RSBC is found to be 0.085 which is lower than 0.12(A-grade). According to Mullick et al. (1987), a cooker having high optical efficiency and low

heat loss has higher F_1 value. The developed RSBC exhibits low F_1 value probably due the presence of heat storage materials below the absorber plate. These materials absorb the major heat from the absorber plate and stores as sensible heat. The sensible heating test (load test) with cooking load (ie water) is carried out during the second and third week of March 2019 and the corresponding temperature profile recorded is shown in Figure 3.11. The peak absorber plate temperature is noted as 106°C and it is obtained between 1.30 PM and 2.30 PM. The water temperature is obtained as 98°C between 2.30 PM and 3.30 PM. From sensible heat test, second figure of merit is found to be 0.319. A low value of F_2 (<0.4) means poor heat exchange efficiency, poor optical efficiency and more heat capacity of the cooker interiors and vessels compared to full load of water (Mullick et al., 1987). The SBC incorporated with PCM infused tubes developed by Saxena et al. (2020) shows a larger value of F_1 (0.12-0.13) compared to the present work (0.08). However, the range of F_2 value (0.27-0.37) for the cooker reported in (Saxena et al. (2020)) and present work (0.29-0.36) are in close agreement. Also, recently developed SC having dome shaped glazing cover made of fibre glass reinforced plastic (Khallaf et al., 2020) shows a lesser F_1 (0.0657) value compared to the present RSBC.
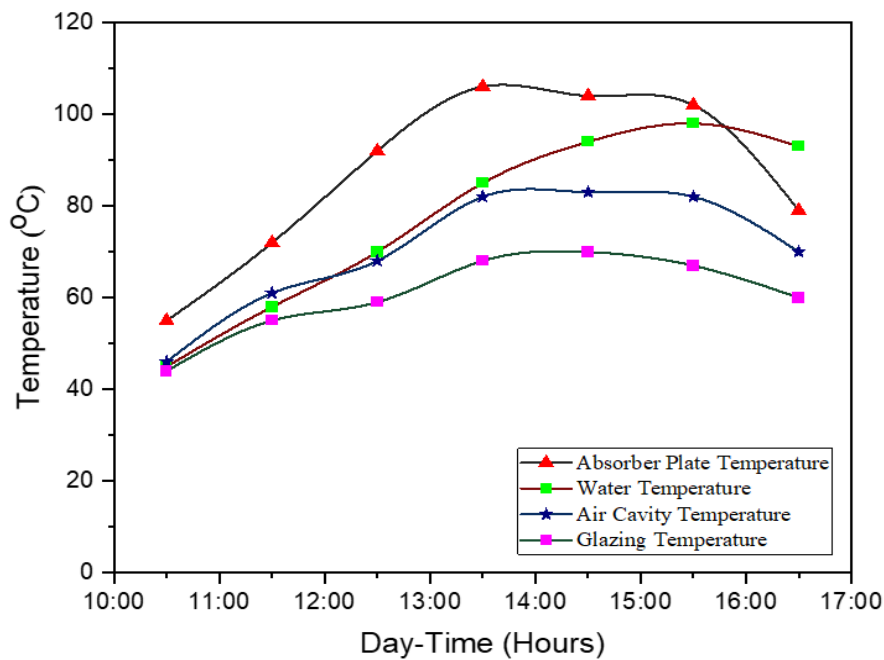
Figure 3.11 Variation of different temperatures with time (Based on experiments conducted on May 2019)

3.3.2. Cylindrical SBC

Stagnation test

The stagnation test on the developed CSBC-FDR is carried out to find F_1 value. The summary of measured data and calculated first figure of merit is shown in Table 3.3. For a particular day (26th April 2019), stagnation temperature of 140.3°C is obtained as maximum value for the absorber plate corresponding to solar irradiance 865 W/m^2 at around 1.00 PM. The corresponding ambient air temperature is measured as 31.4°C, and F_1 is found to be 0.126. Through all stagnation tests, average value of F_1 is found to be 0.131. As a result, the CSBC is classed as A-grade SC. Since first figure of merit implies the ratio of optical efficiency and overall heat loss coefficient, the developed CSBC has high optical efficiency and low heat loss factor (Mullick et al. 1987). Figure 3.12 shows solar irradiance variation and temperatures of absorber plate, glazing cover, inner air cavity, and ambient air measured during the test. The maximum absorber plate temperature attained by SC under certain climatic conditions depends on the total thermal losses of inner cavity. The temperature of internal air cavity also contributes to the cooking process by natural convection. This temperature is much lesser than absorber plate due to heat loss from inside air to the surroundings through top glazing. Experiments are carried on the CSBC fitted with and without decahedron reflectors to evaluate the effects of providing outer reflector. Results show that external reflectors proved to be an important addition to the SBC. The temperature profile recorded during stagnation test for the cooker with and without reflectors is depicted in Figure 3.13. Using decahedron-shaped reflectors, the maximum temperature of the absorber plate is increased by 40.56%. The peak temperature gained by the absorber plate without reflector during stagnation test (2nd May 2019) is 107°C. However, incorporating decahedron reflector, absorber plate attains maximum temperature of 150.4°C on 3rd May 2019. Further, analyzing the tests carried out in March and April 2019, it is observed that CSBC without reflector has lower absorber plate temperature than the one fitted with reflector. Since absorber plate temperature significantly contributes to cooking power and thermal performance, the CSBC-FDR shows better result.

Table 3.3 Summary of stagnation test

Day	G_s (W/m^2)	T_{ps}(°C)	T_{as}(°C)	F_1(°C/(W/m^2))
26th March 2019	876	146.5	32.4	0.130
27th March 2019	844	148.0	32.5	0.137
22nd April 2019	877	141.9	31.0	0.126
26th April 2019	865	140.3	31.4	0.126
3rd May 2019	889	150.4	32.1	0.133
9th March 2019	902	149.3	30.2	0.132
Mean value of F_1				0.131 ± 0.004
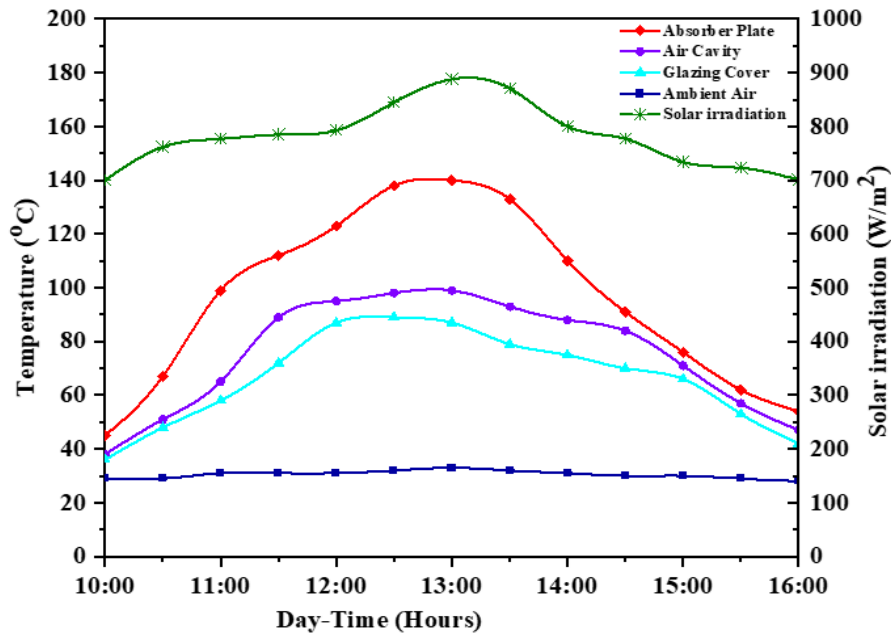
Figure 3.12 Variation of solar irradiance and different temperature with time of during stagnation test (based on the data collected on 26th April 2019)

The maximum air temperature in the inner chamber increased from 83.2°C to 106.4°C, which is nearly 28.8% improvement compared to CSBC without external reflector. Furthermore, when outer reflector is fitted to the CSBC, temperature of lower glazing cover increases by 32.2%. Accordingly, the maximum temperature of lower glass rises from 72.4°C to 95°C. Because of air gap (that separates upper glass from lower) and direct exposure of upper glass to ambient air, this enhancement has less effect on the maximum temperature of upper glass. Therefore, the outer reflector

fitted with CSBC enhances temperatures of every component except upper glass and hence improves overall performance.
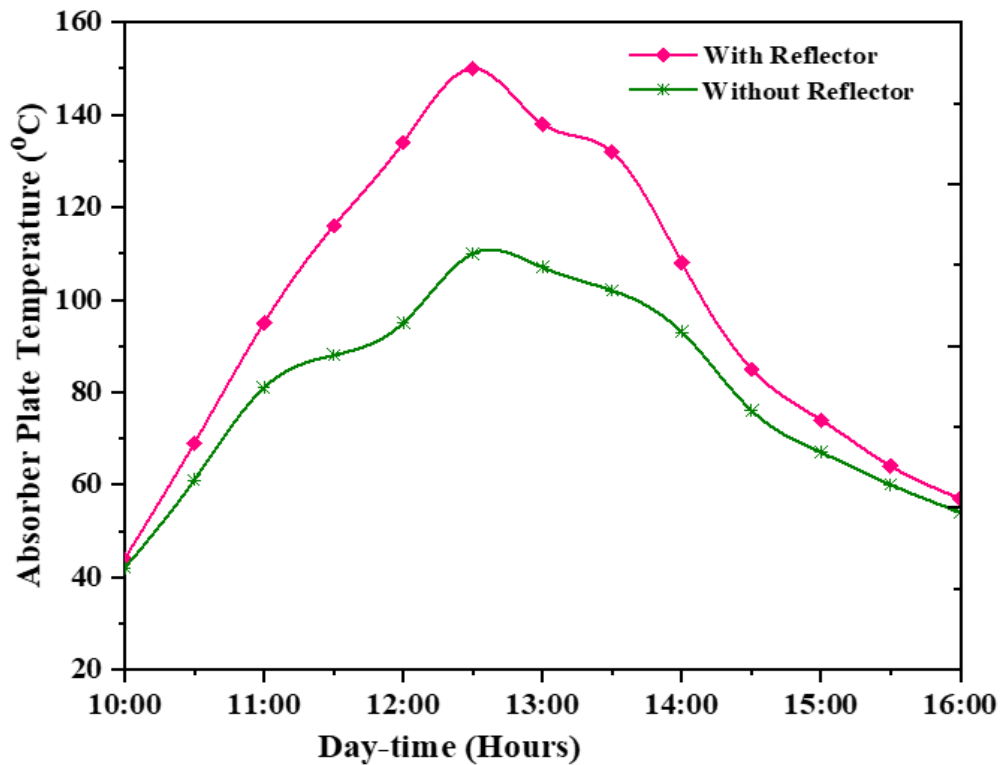
Figure 3.13 Absorber plate temperature variation with time for the cylindrical solar cooker without reflector (2nd May 2019) and with reflector (3rd May 2019)

Load test

Load test is performed to determine the F_2 of the CSBC-FDR. Six load tests are conducted with 1 kg of water as cooking load. The summary of the tests is shown in Table 3.4. Figure 3.14 shows variation of solar irradiance and water and ambient temperatures measured during the experiment conducted on 13th May 2019. Experiments started at 10 AM, and measurements for every 10-minute time interval are recorded. The water temperature reached 65°C at 11:22 AM, and corresponding solar irradiance and ambient temperature are observed to be 789W/m² and 31°C, respectively. Later, water temperature attained 95°C at 12:40 PM, and the solar irradiance and ambient temperature are found to be 845W/m² and 33.4°C, respectively. The F_2 calculated for the above test data is 0.41, and average value from all sensible heating tests is found to be 0.39. Therefore, the CSBC has higher heat

exchange efficiency factor (F′) and optical efficiency but low heat capacity of cooker interiors and vessel. Also, average values of thermal efficiency (η_{energy}) and exergy efficiency (η_{exergy}) are 21.6% and 3.01%, respectively.

The boiling time and second figure of merit obtained for the CSBC are compared with (Guidara et al. 2017) under similar operating and environmental conditions. The boiling time for 1kg of water during sensible heating test on 13th May 2019 is 78 minutes. The average solar irradiance and ambient temperature during the test are 818 W/m^2 and 32.7^{o}C, respectively. Guidara et al. (2017) reported cooking time of 68 minutes for the sensible heating test on trapezoidal SBC to boil 1kg of water at average solar irradiance of 828W/m^2 with ambient temperature 33°C. This boiling time is 10 minutes slower than the present study, even though the environmental cooking conditions are similar. This may be due to larger absorber surface area (0.4678m^2) than the CSBC (0.146m^2). However, there is close agreement between F_2 values (0.34-0.39) for the SBC stated in (Guidara et al. 2017) and present study (0.32-0.41). The CSBC with F_1 (0.126-0.137) and F_2 (0.32-41) satisfies the requirements of A-grade SBC.

Table 3.4 Summary of sensible heating test

Day	G (W/m^2)	T_{w1}(^{o}C)	T_{w2}(^{o}C)	T_a(^{o}C)	t(s)	F_2
28th March 2019	835	63	90	33.1	4800	0.32
29th March 2019	806	61	93	32.4	4900	0.41
23rd April 2019	825	62	92	31.0	4725	0.39
27th April 2019	782	65	93	31.1	4860	0.41
5th May 2019	809	61	91	33.0	4632	0.39
13th May 2019	818	65	95	32.7	4680	0.41
Mean value of F_2						0.39 ± 0.034
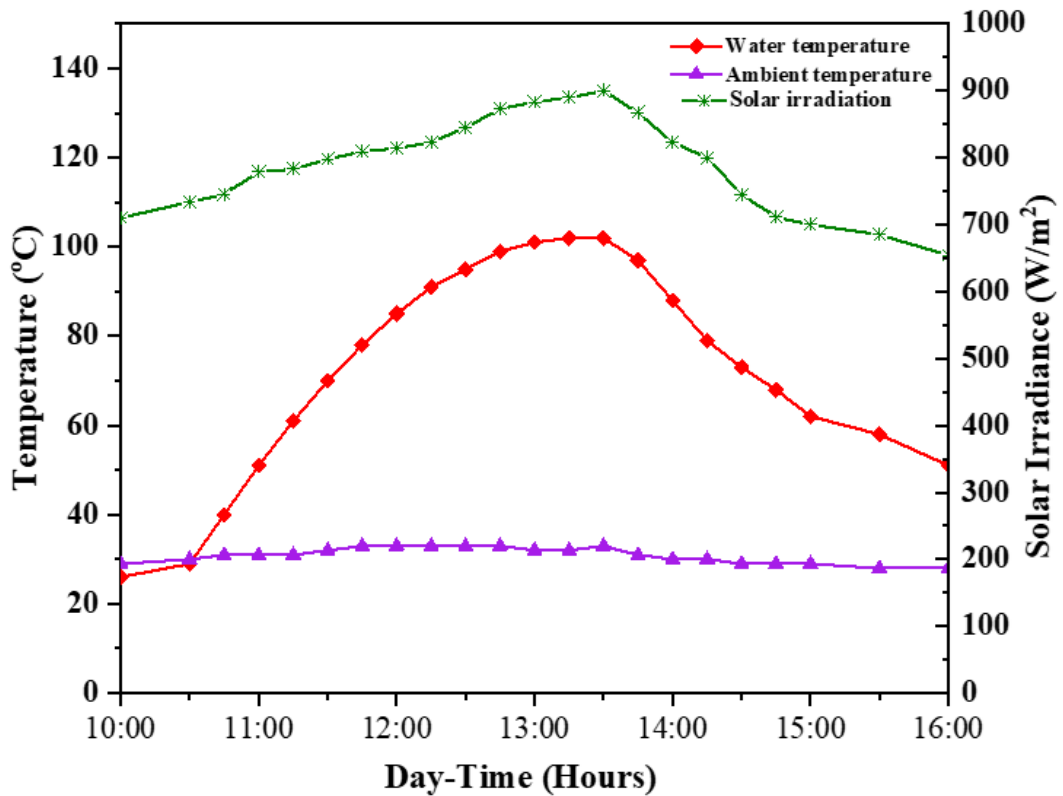
Figure 3.14 Variation of water temperature and solar irradiance with time (13th May 2019)

Cooking power

To study the impact of outer reflector on CSBC's performance, standardized cooking power is calculated following the international testing procedure. The standardized cooking power and corresponding temperature difference between water and ambient air (ΔT) are calculated for every 10-minute time interval during sensible heat test. The correlation between P_s and ΔT is obtained from regression analysis of test data for the load test conducted on 13th May 2019 (Fig. 3.15). The correlation is given by,

$$P_s = 61.729 - 0.729\Delta T \tag{3.48}$$

The value of regression coefficient (R^2) is found to be 0.92 which satisfies the testing standard (>0.75) proposed by (Funk 2000). As indicated by its low slope, the CSBC-FDR exhibits good thermal insulation. The results indicate that as temperature difference increased, cooking power decreased. It is primarily because temperature of water increased faster at the beginning of experiment. Eventually, increase in water

temperature subsides, resulting in reduced temperature difference. The standardised cooking power (P_s) at 50°C is calculated as 25.28 W.
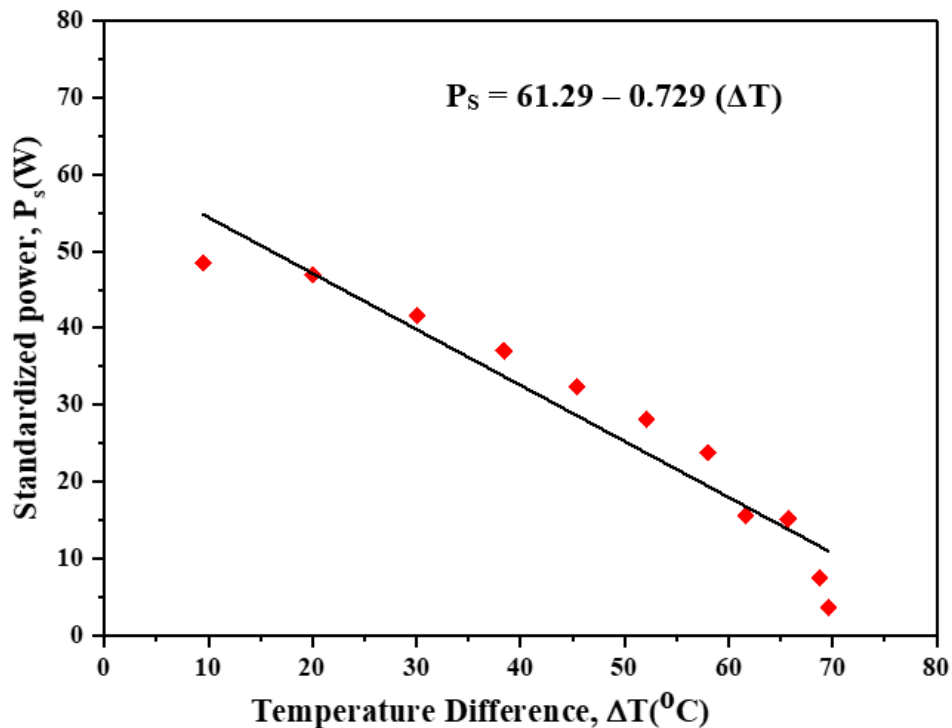
Figure 3.15 Relation between the standardized cooking power and the temperature difference for the CSBC-FDR (13th May 2019)

Overall heat loss coefficient

Overall heat loss coefficient (U_L) is found to be 8.97 W/m^{2}K using the experimental data obtained during sensible heating test on 13th May 2019. For SBC modified by placing PCM infused tubes, Saxena et al. (2020) reported U_L of 5.11 W/m^{2}K, which is lower than the present study. This is because of PCM as a thermal energy storage in the SC. Numerically and experimentally obtained top heat loss coefficients (U_T) in the present study are 7.9 W/m^{2}K and 8.13 W/m^{2}K respectively. The results show variation of 2.9% between experimentally and numerically obtained top loss coefficients. Because of more heat losses through top of the cooker via convection and radiation, which relies on wind heat transfer coefficient, absorber plate and ambient temperatures, top loss coefficient is comparatively higher than the side and bottom.

Cooking performance test

The real cooking performance of the developed CSBC-FDR is conducted on 20th May 2019. Cooking vessel containing 500 g of water is kept on the cooker which is exposed to direct solar irradiance on roof of the building. After 80 minutes, water started boiling. Then, 100 g of rice is poured in to boiling water and covered the cooking pot with lid. It took another 20 minutes to cook the rice fully. Therefore, total of 100 minutes is taken to cook 100 g of rice.

3.3.3. Trapezoidal SBC

Stagnation test

Six stagnation tests are conducted on the TSBC to determine its F_1 value. Table 3.5 summarizes the measured data and calculated F_1 values based on experiments performed between December 2021 and March 2022. Figure 3.16 illustrates temperature variation of the absorber plate and the surroundings and solar irradiance fluctuations during the stagnation test conducted on 18th January 2022. Accordingly, the maximum absorber plate temperature for solar irradiance intensity of 1018 W/m^2 at 1 PM is 171°C. F_1 is calculated to be 0.135 for ambient air temperature of 33°C. According to all stagnation tests, F_1 averages out to 0.13.

Table 3.5 Stagnation test results

Day	I_{st} (W/m^2)	$T_{p,st}$ (^{o}C)	$T_{a,st}$ (^{o}C)	F_1 (^{o}C/(W/m^2))
27th December 2021	1005	165	33	0.131
17th January 2022	885	146	32	0.129
18th January 2022	1018	171	33	0.135
14th February 2022	954	155	32	0.129
18th February 2022	924	149	32	0.127
7th March 2022	989	158	33	0.126
Mean value of F_1				0.130 ± 0.0034

Because F_1 refers to the ratio of optical efficiency and overall heat loss coefficient, the developed TSBC is optically efficient and has low heat loss factor (Mullick et al. 1987). Based on the tests conducted in January and February 2022, it is found that

TSBC without reflector has lower temperature for absorbing plates than one with reflector. As the absorbing plate temperature has decisive effect on the cooking power and thermal performance of the TSBC, the device fitted with outer reflector shows the best results.
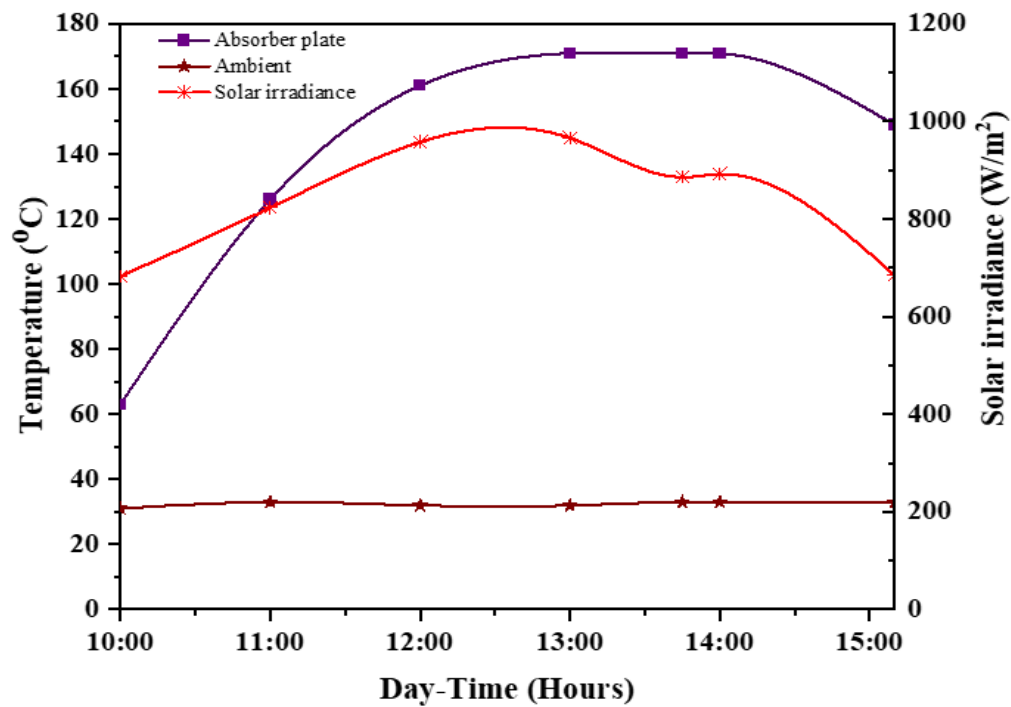
Figure 3.16 Solar irradiance, absorber plate and surrounding temperature measured in stagnation test for SBC (according to the data obtained on 18th January 2022)

Load test

Load tests are carried out during January, February, and March 2022 with 1 kg of water to determine F_2 of TSBC. Table 3.6 summarizes the results of the load test with F_2 values. Figure 3.17 illustrates the changes in solar irradiance, ambient, and water temperatures as a result of experiments performed on 19th January 2022. Water attained 65°C temperature at 10:44 AM, along with irradiance 823 W/m^2 and ambient temperature 32°C. By 11:21 AM, water reached 95°C with solar irradiance 951 W/m^2 and ambient temperature 33°C. Using the above test data, F_2 is 0.449, and all load tests average 0.423. As a result, the TSBC provides better heat transfer and optical efficiency while retaining lower heat capacity for the pot and cooker interiors.

This study also compares the boiling time and F_2 of (Guidara et al. 2017) for similar environmental conditions. In the present study on TSBC, load test conducted on 19th January 2022 takes 70 minutes to boil 1 kg of water. The averaged values of solar irradiance and surrounding temperature are 843 W/m^2 and 32°C, respectively, during the test. In the study of (Guidara et al. 2017), TSBC with absorber surface area of 0.4678 m^2 was subjected to load test. At an ambient temperature of 33°C and an average solar irradiance of 828 W/m^2, 1kg of water boils in 68 minutes. In both cases, boiling time is almost identical. According to present TSBC, the boiling water time is eight minutes shorter than in CSBC as discussed in the previous section. Furthermore, the F_2 values (0.32-0.41) for the CSBC are low compared to the TSBC (0.39-0.45).

Table 3.6 Load test (water as cooking load) results

Day	I (W/m^2)	T_{w1}(^{o}C)	T_{w2}(^{o}C)	T_a(^{o}C)	t(s)	F_2
19th January 2022	927	65	95	33	2220	0.449
28th January 2022	910	64	95	32	2460	0.436
30th January 2022	968	63	94	33	2364	0.398
2nd February 2022	885	65	95	31	2560	0.435
4th February 2022	911	64	93	32	2410	0.409
3rd March 2022	982	65	95	33	2224	0.408
Mean value of F_2						0.423 ± 0.02

Figure 3.18 shows the temperature variations of different components in TSBC and cooking load (glycerol) during sensible heating test conducted on 25th January 2022. On this day, solar irradiance averaged 840 W/m^2 and surrounding atmosphere temperature 32°C. The glycerol temperature reached 162°C at 2.15 PM and remains above 139°C at 4 PM. Similarly, variations in temperature of different components and solar irradiance during load test with air as working substance is depicted in Figure 3.19. The air cavity in the cooking vessel reaches its peak temperature of 168°C at 2.00 PM with average solar irradiance 796 W/m^2 and surrounding temperature 32°C. A time-varying plot of cooking load temperatures (air, glycerol, and water) during sensible heating is shown in Figure 3.20. Unlike water (4.22 kJ/kg

K) and glycerol (2.42 kJ/kg K), cooking pot containing no load shows the highest temperature as air has the lowest specific heat capacity. Since air has low heat-retaining capacity, temperature decreases more quickly than glycerol and water.
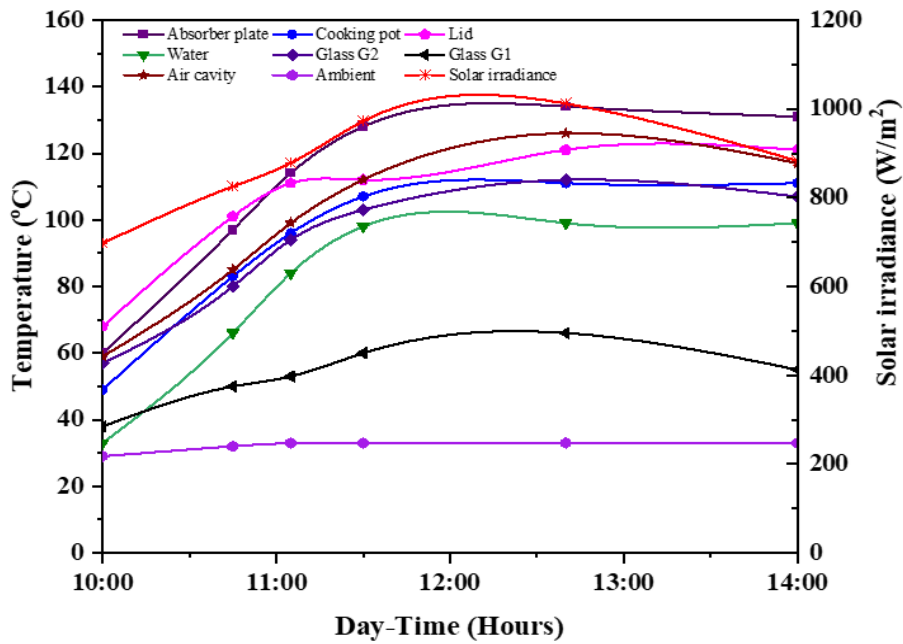
Figure 3.17 Variation of temperature and solar irradiance during sensible heating test with water as cooking load (19th January 2022)
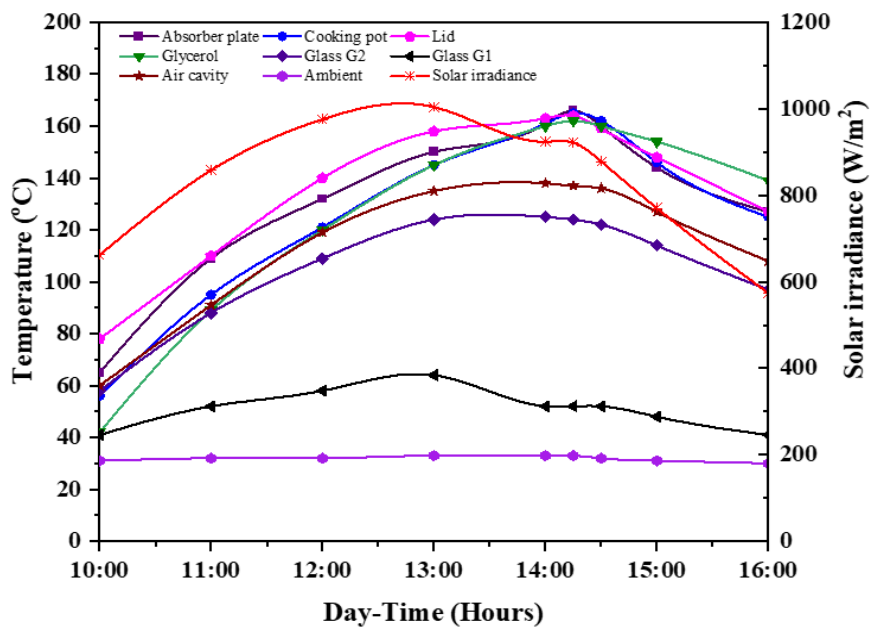
Figure 3.18 Variation of temperature and solar irradiance during sensible heating test with glycerol as cooking load (25th January 2022)

62
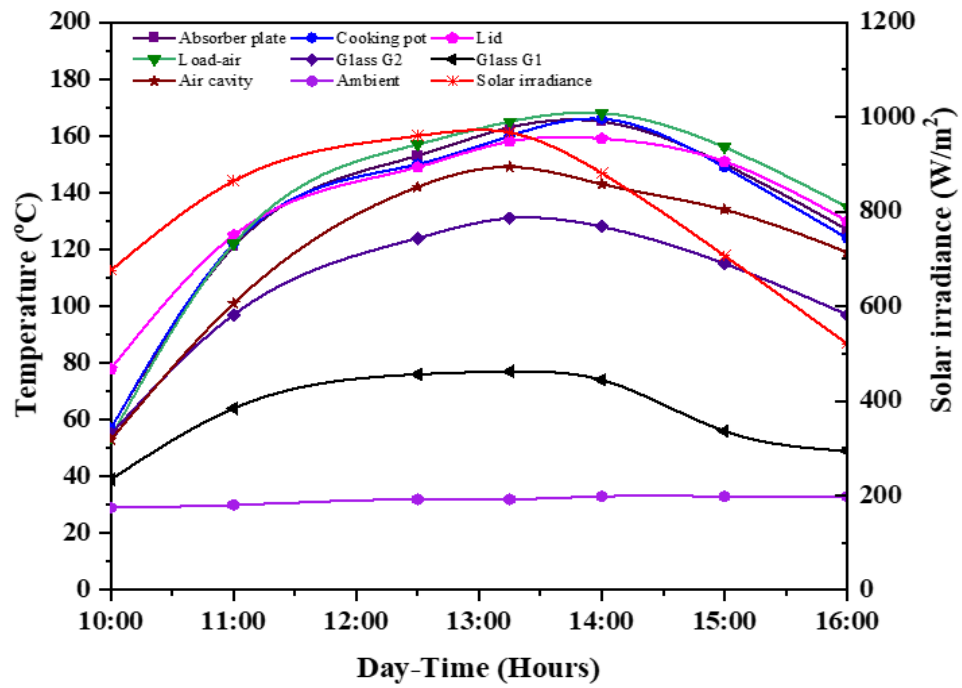
Figure 3.19 Variation of temperature and solar irradiance during sensible heating test with no-load condition (20th January 2022)
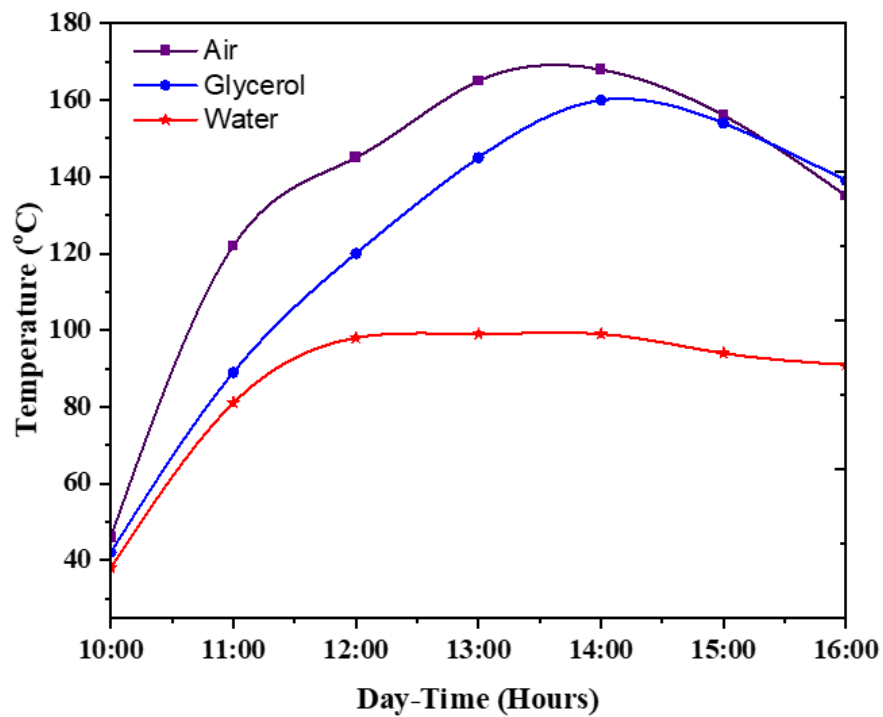
Figure 3.20 Variation of cooking load temperature with time

Standardized cooking power

Figure 3.21 depicts the temperature variations in absorber plate, water and the surroundings and fluctuations in solar irradiance with time during load test conducted on 23rd February 2022. The water temperature reached 96°C at 11:50 AM and remains constant during next two hours. For every 10-minute interval during test, P$_s$ and the associated temperature difference between water and the ambient air (ΔT) are determined. According to the regression analysis of experimental data obtained on 23rd February 2022, Ps and ΔT are correlated (Fig. 3.22). The correlation is as follows:

$$P_s = 69.79 - 0.83\ \Delta T \tag{3.49}$$

The regression coefficient (R^2) is 0.91, which meets the testing standard (>0.75) proposed by (Funk 2000).
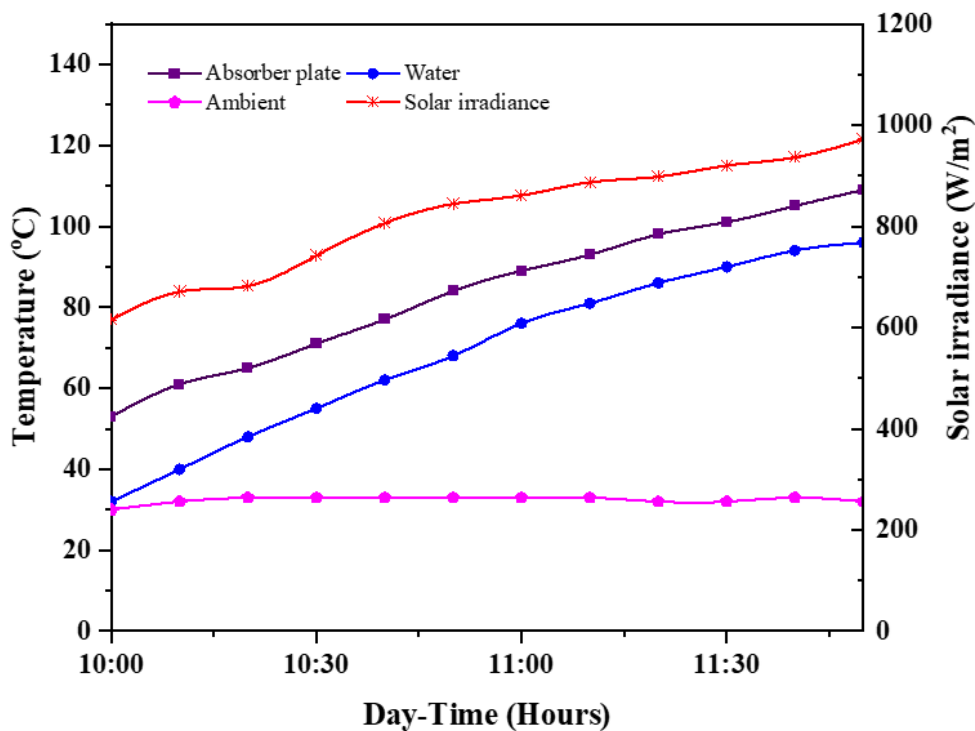
Figure 3.21 Variation of temperature and solar irradiance during load test with water (23rd February 2022)
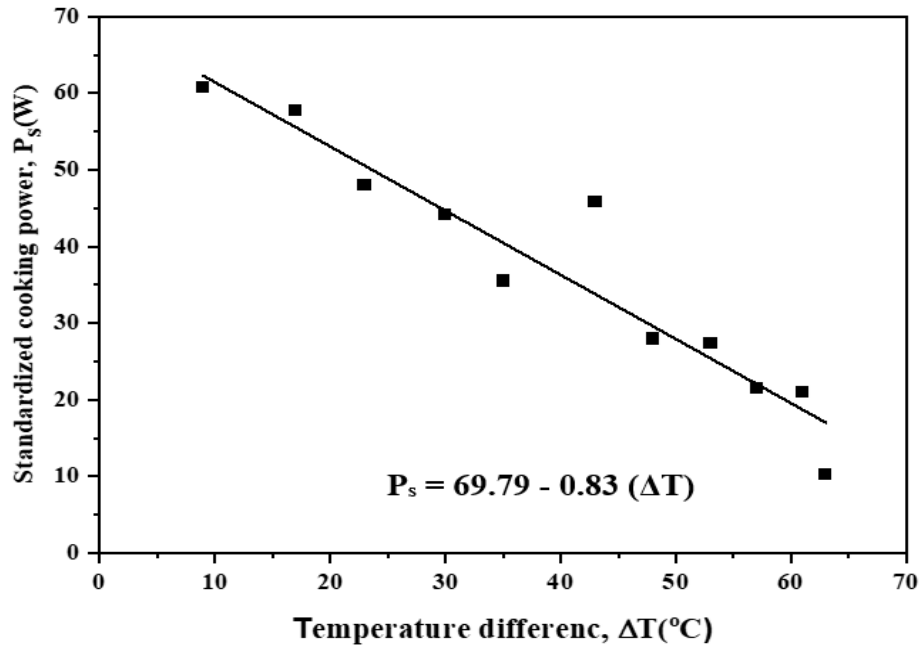
Figure 3.22 Relation between standardized cooking power and temperature difference (23rd February 2022)

3.3.4. Comparative study of SBCs based on cooking power

Different SBCs are compared concerning standardized cooking power, energy efficiency, and first figure of merit (Table 3.7). The correlations obtained for cooking power for the CSBC and TSBC in the present study are almost similar to that of (El-sebaii and Ibrahim 2005) tested for the cooking load of 1 kg of water contained in single cooking pot. It is found that standardized cooking power at 50°C and energy efficiency for the CSBC (25.28 W, 21.6%) and TSBC (28.29 W, 25.5%) are more than those obtained by (El-Sebaii and Ibrahim 2005; Riva et al. 2017; Mukaro and Tinarwo 2008). However, SC developed by (Saxena et al. 2020) shows more significant value of P_s (68.81W) and η_{energy} (53.81%) compared to present work. This can be due to larger absorber area and inclusion of PCM-infused tubes in the SC. The present TSBC and CSBC shows a slight decrease in P_s compared to the Quonset SC having dome-shaped fiber reinforced plastic glass cover (Khallaf et al. 2020). This may be due to larger inner air cavity volume, which accumulates more heat onto the cooking vessel in Quonset dome-shaped SBC. Their reported value of F_1 is 0.066, which is much less than the standard value of 0.12 for A-grade SC.

Table 3.7 Comparison of cooking power and energy efficiency of different SCs

Reference	Description of SC	A_p (m²)	P_s at 50ºC (W)	Regression equation	R^2	η_{en} (%)	F_1
El-Sebaii and Ibrahim 2005	RSBC with outer reflector	0.27	20.8	58.7-0.758 ΔT	0.97	9.7	0.13
Mukaro and Tinarwo 2008	TSBC with two inclined internal reflectors.	0.144	11	22.41-0.239 ΔT	0.8	15	-
Saxena et al. 2020	RSBC with PCM infused tubes and outer reflector.	0.25	68.8	-	-	53.8	0.13
Khallaf et al. 2020	Quonset SC with dome shaped glazing cover of fiber glass reinforced plastic.	0.24	29.9	42.37-0.248 ΔT	0.9	35	0.066
Riva et al. 2017	RSBC with four reflectors.	-	8.6	34.10-0.51 ΔT	0.93	8.13	-
Weldu et al. 2019	TSBC (copper absorber plate) with single reflector	0.115	39.5	62.235-0.454 ΔT	0.86	33.9	0.127
Harmim et al. 2013	SBC with compound parabolic concentrator	0.478	78.9	136.28-1.142 ΔT	0.94	-	0.152
Mahavar et al. 2012	RSBC with single reflector	0.167	30	103.5-1.474 ΔT	0.95	-	0.116
Present study	CSBC with decahedron shaped reflector.	0.146	25.3	61.729-0.729 ΔT	0.92	21.6	0.131
	TSBC with four outer reflectors	0.225	28.3	69.79-0.83 ΔT	0.91	25.5	0.13

The standardized cooking power and energy efficiency of SBC developed by Weldu et al. (2019) are 39.54 W and 33.89 %, higher than the present work despite smaller absorber plate area. This can be due to the fact that three inner sidewalls of their SBC are inclined at an angle of 105° to the cooker's base, allowing additional solar rays to enter the cooking vessel beside the sun and reflector. However, F_1 value and maximum absorber plate temperature obtained for CSBC (0.13 and 150ºC) and TSBC (0.13 and 171ºC) in the present study are more than their work (0.127 and 148.7ºC).

They used copper as absorber plate material because of its low thermal resistance and superior corrosion resistance. For the SBC with compound parabolic concentrator as outer reflector and absorber plate in the form of step, cooking power and F_1 are 78.9 W and 0.152 (Harmim et al. 2013) and are considerably larger than those found in the present study. Also, in this case, surface area of the absorber plate (0.478 m^2) is three times larger than that of CSBC and two times that of TSBC. Comparing with the findings of Mahavar et al. (2012), there is insignificant decrease in cooking power. When compared with similar previous works, it is clear that CSBC with smaller absorber plate area will perform well when integrated with booster reflectors. The present work involves permanent glazing cover provided on the cooker since it has back-door for placing cooking vessels. As a result, more heat is trapped within the cooker cavity because top glazing cover minimizes heat loss via convection. Therefore, the current design of CSBC and TSBC have higher inside air temperature than already developed SCs. Based on P_s and energy efficiency found in the present work, TSBC fitted with four outer reflectors performs more than CSBC-FDR.

3.3.5. Statistical analysis

The average value, standard deviation and 99% confidence interval for F_1 and F_2 are found based on the works carried out by Purohit (2010) and are shown in Table 3.8. It is found that there is some scattering between the values of F_1 which may be because of variations in the climatic conditions like solar irradiance and ambient temperature. The deviation is found in the third decimal point of F_1. From the full load test with water, second figure of merit F_2 is determined for SBCs under different climatic conditions. In contrast with F_1, the deviation in the F_2 values is higher due to the involvement of more variables in the determination of F_2.

3.3.6. Uncertainty analysis

Table 3.9 shows the uncertainty values in the results of performance parameters of SCs due to the uncertainties in the instruments used for the measurements of temperature, solar irradiance, mass of water and time during the testing. The attainable accuracy or uncertainty in the F_1 value is found to be about 1.24%, 1.28% and 1.18% respectively for RSBC, CSBC and TSBC. Whereas uncertainty in F_2 are respectively 2.48%, 3.01%, and 2.76%. Uncertainty in F_2 is much more than that of F_1

because of more parameters involved in the determination of F_2 value. Hence, more instrumental uncertainty will result while determining F_2 value. Also, uncertainty in the values of energy and exergy efficiency are also given in table 3.9.

Table 3.8 Statistical analysis of performance parameters

Parameters	SBC	Mean value	Standard deviation	99% confidence interval
First figure of merit, F_1	RSBC	0.085	0.002	0.083≤0.085≤0.087
	CSBC	0.131	0.004	0.126≤0.131≤0.135
	TSBC	0.130	0.003	0.126≤0.130≤0.133
Second figure of merit, F_2	RSBC	0.319	0.029	0.291≤0.319≤0.348
	CSBC	0.390	0.034	0.360≤0.390≤0.420
	TSBC	0.426	0.020	0.402≤0.426≤0.444

Table 3.9 Uncertainty analysis of performance parameters

Parameters	SBC	Mean value	Uncertainty (%)
First figure of merit, F_1	RSBC	0.085	1.24
	CSBC	0.131	1.28
	TSBC	0.13	1.18
Second figure of merit, F_2	RSBC	0.319	2.48
	CSBC	0.39	3.01
	TSBC	0.426	2.76
Energy efficiency, η_{energy}	RSBC	16.1	2.49
	CSBC	21.93	2.79
	TSBC	25.47	2.62
Exergy efficiency, η_{exergy}	RSBC	0.61	2.84
	CSBC	3.04	3.09
	TSBC	3.64	2.92

3.3.7. Economic Analysis

The economic analysis of CSBC and TSBC is carried out based on ALCC and the payback period. The LPG price and Indian Rupee (₹) to US dollar ($) exchange rates used in the present analysis are based on the 6th October 2021.

ALCC

Table 3.10 summarizes the material and manufacturing costs for the developed cylindrical and trapezoidal SBCs. The total capital cost for the TSBC is $94.58 (₹7,050.00). Whereas for the CSBC, initial cost is $120.08 (₹8950.00). The economic analysis of the SBC is carried with reference to the LCC as given in Table 16. ALCC of $14.3 (₹1,066.00) and $18.16 (₹1354.00) are obtained respectively for the TSBC and CSBC which is economically feasible. For the analysis, present worth factor (pwf) is taken as 8.51 by considering yearly rate of interest as 10% and life expectancy of 20 years. As there is no replacement of any of the component, present value of replacement (C_r) is taken as zero.

Table 3.10 Material and manufacturing cost of CSBC and TSBC

Sl. No	Item	Cost (₹)	
		CSBC	TSBC
1	Aluminium sheet (Absorber plate)	700.00	900.00
2	Material (Box and outer reflector support)	2500.00	2,100.00
3	Insulation (Glass wool)	500.00	600.00
4	Glass	300.00	400.00
5	Mirror (Outer reflector)	2000.00	800.00
6	Aluminium foil (Inner reflector)	50.00	50.00
7	Paint (Black)	100.00	100.00
8	Cooking pot	300.00	300.00
9	Labour	2200.00	1,500.00
10	Miscellaneous	300.00	300.00
11	Total cost	8950.00	7,050.00

Table 3.11 Computation of ALCC of CSBC and TSBC

Sl. No	Particulars	Cost (₹)	
		CSBC	TSBC
1	Initial system cost (cost of solar box cooker, cooking vessel)	8,950.00	7,050.00
2	Installation cost @10% of initial system cost	895.00	705.00
3	Initial investment, C_c (Initial system cost + installation cost)	9,845.00	7,755.00
4	Operation and maintenance cost, C_m @ 2% of initial investment	197.00	155.00
5	Future costs of operation and maintenance, $C_{m,pv}$	1,676.00	1,320.00
6	Life cycle cost, LCC	11,521.00	9,075.00
7	Annualized life cycle cost, ALCC	1,354.00	1,066.00

Payback period

PP is calculated based on 14.2 kg LPG cylinder cost on the Indian market. The subsidized price is approximately $12.07 (₹900.00) on 6[th] October 2021. Table 3.12 shows the consumption of LPG (kg/year) and its cost ($/year) for four people in a family. The computed SM and PP also depicted in Table 3.12. For cooking 1 kg of food, it is assumed that 15 MJ of energy is required. The total energy content in commercially available 14.2 kg LPG cylinder is 639 MJ (Calorific value of LPG is 45 MJ/kg). Assuming 240 clear sunny days in a year, approximately six cylinders of LPG is consumed. For P_t =0.5, payback period for TSBC and CSBC are respectively 2.61 and 3.31. Therefore, TSBC is more cost-effective option than CSBC.

Table 3.12 Payback period for SBC (P_t = 0.5)

SBC	Quantity of LPG consumed (kg/year)	Cost of LPG ($/year)	SM ($/year)	C_{SC} ($)	PP (Year)
TSBC	85.2	72.45	36.22	94.58	2.61
CSBC	85.2	72.45	36.22	120.08	3.31

PP is shown as a function of P_t in Figure 3.23. It is clear that PP is inversely proportional to P_t. For example, in case of TSBC, when P_t is 0.3 corresponding PP is 4.35 years, whereas when P_t is 0.7 the PP is about 1.86 years, ie, if TSBC is allowed to use 70% of the total cooking time, PP is reduced to 1.86 years.
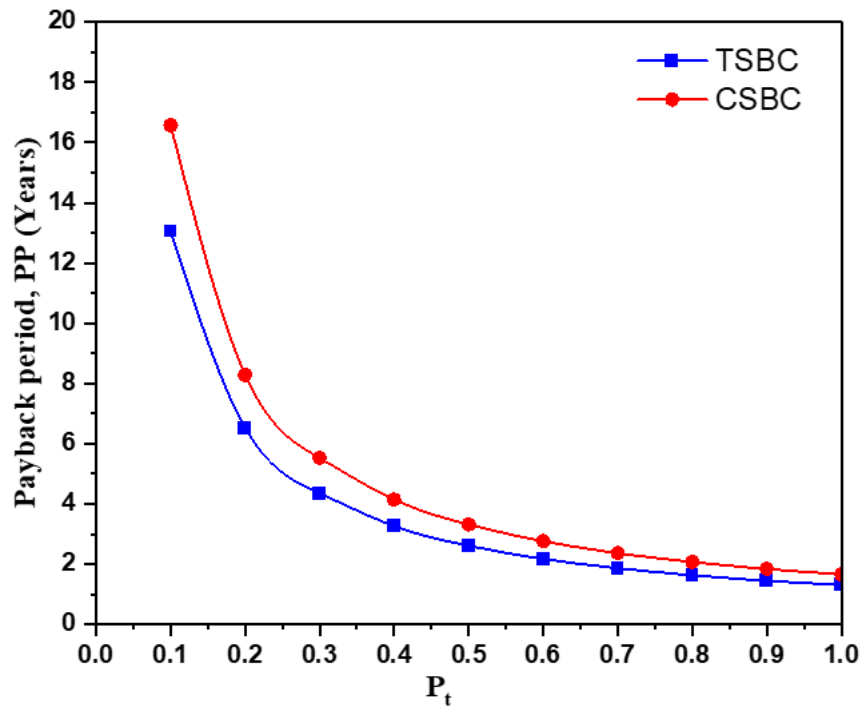
Figure 3.23 Variation of PP as function of P_t

3.4 Summary

Rectangular SBC

The optimum cooker surface area for RSBC is calculated using analytical heat loss equations and energy balance equation. The heat loss factors are calculated by an iterative procedure using MATLAB programming. Based on the anticipated average value of solar irradiance and mass of water to be boiled, the absorber plate area is found to be 0.36 m^2. An RSBC having an outer reflector is constructed according to the design considerations. From experimental investigations, the Figures of merit F_1 and F_2 are obtained as 0.085 and 0.319 respectively which is lower than that of A-grade solar cooker because of absorption of major amount of heat by the sensible heat storage materials from the absorber plate.

Cylindrical SBC

The performance evaluation of CSBC fitted with decahedron-shaped outer reflector is carried out. The CSBC is designed and fabricated based on principle of minimum entropy generation (MEG) method. Experimental investigation is conducted to check the effectiveness of decahedron reflector on cooker's performance, including stagnation, sensible heat, and cooking performance tests. The average values of F_1 and F_2 are found to be 0.13 and 0.39, respectively, which satisfies the requirements of A-grade SBC as per the Bureau of Indian Standards (BIS). The thermal efficiency (η_{energy}), exergy efficiency (η_{exergy}), and standardized cooking power (P_S) are found to be 21.93 %, 3.04 %, 24.84 W, respectively. The developed CSBC shows better performance in terms of standardized cooking power and energy efficiency than the conventional rectangular shaped SBCs.

Trapezoidal SBC

The TSBC is designed and fabricated in the next stage. The absorber plate area of 0.2256 m^2 is set based on the MEG method and iterative solution procedure. Tests are performed on the TSBC with and without outer reflectors. The absorber plate temperature increases 37.9% when passing from one configuration to another. It shows maximum absorber plate temperature of 171°C under mean solar irradiance and surrounding temperature of 841.8 W/m^2 and 32°C, respectively. The cooker with outer reflectors is more optically efficient, as indicated by the first figure of merit of 0.135. Different SBCs are compared concerning standardized cooking power, energy efficiency, and the first figure of merit. TSBC fitted with four outer reflectors performs more than the CSBC fitted with decahedron reflector.

Next, the statical and uncertainty analysis of RSBC, CSBC and TSBC has been carried out. The average value, standard deviation and 99% confidence interval for F_1 and F_2 are found. It is found that the deviation and uncertainty in the F_2 values is higher than that of F_1 due to the involvement of more variables in the determination of F_2. Hence, more instrumental uncertainty will result while determining F_2 value. As per the economic analysis of CSBC and TSBC based on ALCC and the payback period, TSBC is more cost effective than CSBC.

4. PREDICTION MODEL DEVELOPMENT FOR SBC USING COMPUTATIONAL AND MACHINE LEARNING TECHNIQUES

To predict the performance parameters of SBC, prediction models are developed using computational and machine learning (ML) techniques. A combined prediction model is developed that accounts for all heat transfer involved in each component of SBC. Experimental validation of the numerical model is conducted using the trapezoidal-SBC (TSBC) discussed in the previous chapter. More details are presented in the following sections.

4.1. Background

In addition to experimental studies, many researchers have used numerical heat transfer analyses to predict the temperatures at different elements of SBCs. The various components include absorber plate, glass cover, air cavity, cooking vessel, and load. The heat balance equations are the basis for all numerical analysis but differ in the solution methodologies. In addition, researchers used artificial neural networks (ANN), to predict the thermal efficiency parameters of the SBC. Kurt et al. (2008) used ANN to predict the temperatures of SBC components, including absorber plate, air cavity, and pot water. Data sets for the model were derived from experimental investigations of SBC under different climatic conditions. The experimental data set consists of 126 values, out of which 96 values were used for training and 30 for testing the model. They showed ANN also a viable alternative to numerical simulations in the SC. Recently, Mukaro (2021) developed an ANN model to predict the performance parameters of the SC, such as output power, cooker efficiency, exergy output, and exergy efficiency. Inputs to the model were ambient and cooker temperatures, the volume of water, the intensity of incident solar radiation, and the time of day. The data driven techniques other than ANN have not been explored for solar thermal energy utilization appliances. Also, many popular ML methods like ANN are unstable and unreliable (Brieman, 1996). Alternatively, tree and ensemble learning models reduce variance and bias by combining the results of several individual models. Hence, in the present study, decision trees and ensemble learning

models such as random forests are used to estimate the performance parameters of SBCs with known design parameters, material properties, and location data.

This chapter presents the prediction model development for SBC by combining numerical simulation and ML techniques. This study uses ML techniques such as random forest, decision tree, linear regression, and k-nearest neighbor (k-NN). For this, first, a numerical model based on thermal balances at different components of SBC is developed to generate the input data required for ML models. The numerical model accounts for all modes of heat transfer, which predicts the temperatures of all the elements of SBC. Next, the numerical model is validated by conducting experiments on TSBC from January to March 2022. The numerical model considers varying heat transfer coefficients and theoretical solar irradiance, thus providing an accurate solution. Finally, the effects of input variables such as latitude and longitude on the output cooking load temperature are studied with the aid of the developed ML model.

4.2. Methodology

4.2.1. Numerical modelling

Numerical modelling of SBC is carried out by solving thermal balance equations at every element; absorbing plate, glass covers, cooking pot and lid, inner air cavity, and load (Figure 4.1). The geometrical dimensions and physical properties of glass covers, absorber plate, cooking pot and lid used for the numerical simulation and experimental study are shown in Table 4.1-4.3. Numerical modelling is helpful to predict temperatures at each time step with solar irradiance (I) and surrounding temperature (T_{surr}) as inputs.
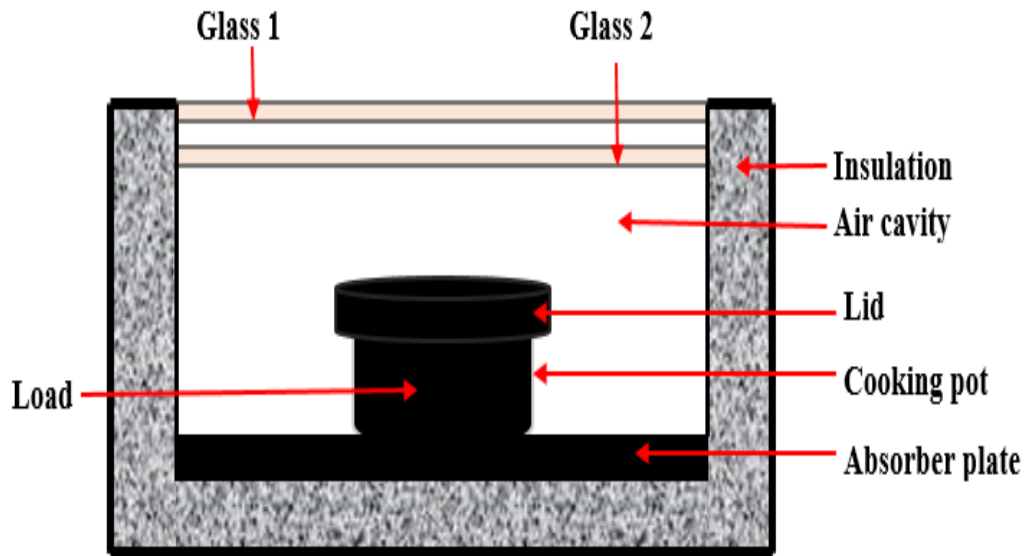
Figure 4.1 Schematic of SBC with cooking vessel

Table 4.1 Geometrical dimensions and physical properties of glass covers

Description	Symbol	Value
Surface area of glass 1 (m^2)	A_{g1}	0.3
Surface area of glass 2 (m^2)	A_{g2}	0.267
Thickness (mm)	th_g	5
Spacing between glazing covers (mm)	L_{g1g2}	15
Angle of inclination (degree)	β	30
Absorptivity	α_g	0.1
Transmissivity	τ_g	0.9
Density (kg/m^3)	ρ_g	2530
Specific heat capacity (J/kgK)	C_g	840
Emissivity	$\boldsymbol{\varepsilon}_g$	0.92

Table 4.2 Geometrical dimensions and physical properties of absorbing plate

Description	Symbol	Value
Surface area (m^2)	A$_p$	0.2256
Thickness (mm)	th$_p$	3
Absorptivity	α$_p$	0.95
Density (kg/m^3)	ρ$_p$	2700
Specific heat capacity (J/kgK)	C$_p$	900
Emissivity	ε_p	0.95

Table 4.3 Geometrical dimensions and physical properties of cooking pot and lid

Description	Symbol	Value
Diameter of pot (mm)	d	180
Height of pot (mm)	L$_{pot}$	80
Base area of pot (m^2)	A$_{potbottom}$	0.0254
Side area of pot (m^2)	A$_{potside}$	0.045
Base area of lid (m^2)	A$_{lid}$	0.0266
Thickness of lid (mm)	th$_{lid}$	2
Thickness of pot (mm)	th$_{pot}$	1
Absorptivity	α$_{pot}$	0.95
Density (kg/m^3)	ρ$_{pot}$	2700
Specific heat capacity (J/kgK)	C$_{pot}$	900
Emissivity	ε_{pot}	0.95

Thermal modelling

The thermal network diagram for the heat transfer model is shown in Figure 4.2. Heat transfer model is developed by considering all the components of SBC such as absorber plate, glazing cover, cooking pot, lid, air cavity, and cooking load. Firstly, thermal balance equations for all the components are derived and are discretized using the finite difference method which is given below.
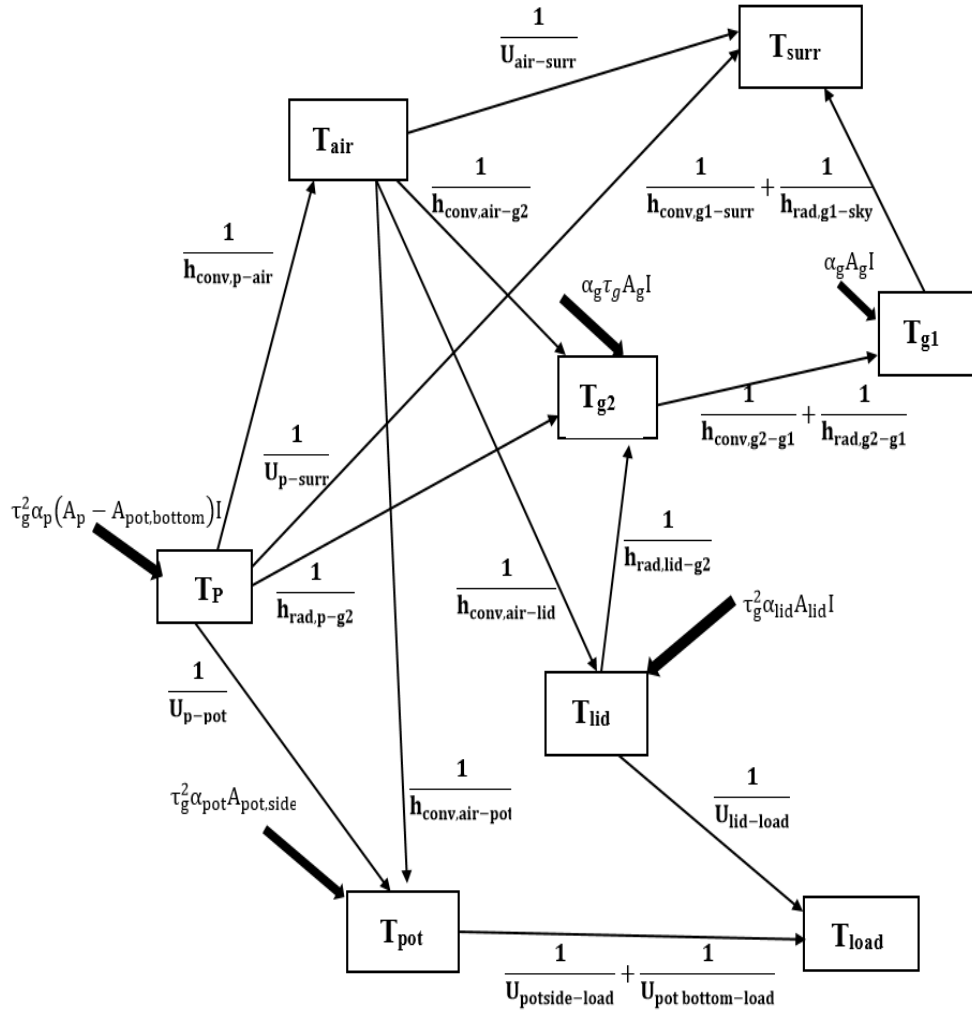
Figure 4.2 Thermal network diagram

Absorber Plate

Two glass covers placed on the top of the cooker transmit incident solar radiation onto the absorber plate. Therefore, the absorber plate receives solar irradiance multiplied by the square of glass transmissivity. In this process, some heat energy is absorbed. At the same time, rest is rejected via convection heat transfer to inner air cavity, radiation heat transfer to second glass surface, and heat loss through bottom of absorber plate via insulation and casing. As cooking vessel rests on top of the absorber plate, conductive heat is transferred between plate and base of pot. The equation for thermal balance and its discretization are given below.

$$m_p c_p \frac{dT_p}{dt} = \dot{Q}_{abs,p} - \dot{Q}_{conv,p-air} - \dot{Q}_{rad,p-g2} - \dot{Q}_{cond,p-pot} - \dot{Q}_{cond,p-surr} \qquad (4.1)$$

$$T_p^{n+1} = T_p^n + \frac{\Delta t(A_p - A_{potbottom})}{m_p c_{p,p}} \left[\tau_g^2 \alpha_p I + h_{conv,p-air} T_{air} + h_{rad,p-g2} T_{g2} + \right.$$

$$\left(\frac{A_p}{A_p - A_{potbottom}} \right) U_{p-surr} T_{surr} + \left\{ \left(\frac{A_{potbottom}}{A_p - A_{potbottom}} \right) U_{p-pot} \right\} T_{pot} - \left(h_{conv,p-air} + \right.$$

$$\left. \left. h_{rad,p-g2} + U_{p-surr} \left(\frac{A_p}{A_p - A_{potbottom}} \right) + U_{p-pot} \left(\frac{A_{potbottom}}{A_p - A_{potbottom}} \right) \right) T_p \right]^n \tag{4.2}$$

Air cavity

The air cavity in the inner box is in contact with the absorbing plate, cooking pot, lid, and lower glass cover. The air cavity gains heat energy from the absorber plate by convection, which then transfers to second glass, pot, and lid. Additionally, heat will be lost from air cavity to the surroundings through sideways insulations and casing. The air will accumulate the remaining heat. The equation for thermal balance of air cavity and its discretization are as follows:

$$m_{air} c_{air} \frac{dT_{air}}{dt} = \dot{Q}_{conv,p-air} - \dot{Q}_{conv,air-surr} - \dot{Q}_{conv,air-g2} - \dot{Q}_{conv,air-pot} -$$

$$\dot{Q}_{conv,air-lid} \tag{4.3}$$

$$T_{air}^{n+1} = T_{air}^n + \frac{\Delta t}{m_{air} c_{p,air}} \left[h_{conv,p-air} \left(A_p - A_{pot,bottom} \right) T_p + \right.$$

$$U_{wall-surr} A_{wall} T_{surr} + h_{conv,air-g2} A_{g2} T_{g2} + h_{conv,air-pot} A_{pot,side} T_{pot} +$$

$$h_{conv,air-lid} A_{lid} T_{lid} - \left(h_{conv,p-air} \left(A_p - A_{pot,bottom} \right) + U_{wall-surr} A_{wall} + \right.$$

$$\left. \left. h_{conv,air-g2} A_{g2} + h_{conv,air-pot} A_{pot,side} + h_{conv,air-lid} A_{lid} \right) T_{air} \right]^n \tag{4.4}$$

Glass 2

The second glass cover receives solar irradiance transmitted by the first glass. In other words, incident solar irradiance multiplied by the transmissivity of first glass will reach the second glass. In addition, there is heat transfer from absorber plate and lid of the cooking pot to second glass via radiation. The second glass is also heated by convection from inner air cavity. In this heat transfer system, a portion is absorbed by the second glass, and the rest is lost to first glass via convection and radiation. The heat balance equation for the second glazing cover with its discretization are as follows:

$$m_{g2}c_g\frac{dT_{g2}}{dt} = \dot{Q}_{abs,g2} + \dot{Q}_{conv,air-g2} + \dot{Q}_{rad,p-g2} + \dot{Q}_{rad,lid-g2} - \dot{Q}_{conv,g2-g1} -$$
$$\dot{Q}_{rad,g2-g1} \tag{4.5}$$

$$T_{g2}^{n+1} = T_{g2}^n + \frac{\Delta t\, A_{g2}}{m_{g2}c_{p,g}}\left[\tau_g\alpha_g I + h_{conv,air-g2}T_{air} + h_{rad,p-g2}\left(\frac{A_p - A_{pot,bottom}}{A_{g2}}\right)T_p +\right.$$
$$h_{rad,lid-g2}\left(\frac{A_{lid}}{A_{g2}}\right)T_{lid} + \left(h_{conv,g2-g1} + h_{rad,g2-g1}\right)T_{g1} - \left(h_{conv,air-g2} +\right.$$
$$\left.\left. h_{rad,lid-g2}\left(\frac{A_{lid}}{A_{g2}}\right) + h_{rad,p-g2}\left(\frac{A_p - A_{pot,bottom}}{A_{g2}}\right) + h_{conv,g2-g1} + h_{rad,g2-g1}\right)T_{g2}\right]^n \tag{4.6}$$

Glass 1

Solar radiation reaches the first glazing cover, accumulating some and transmitting the remaining irradiance to the inner box. The heat is transferred between first and second glass by convection and radiation. Furthermore, there will be heat loss from first glass through convection with the ambient air and radiation with the sky. The thermal balance equation for first glass cover and its discretization are as follows:

$$m_{g1}c_g\frac{dT_{g1}}{dt} = \dot{Q}_{abs,g1} + \dot{Q}_{conv,g2-g1} + \dot{Q}_{rad,g2-g1} - \dot{Q}_{conv,g1-surr} - \dot{Q}_{rad,g1-sky}$$
$$\tag{4.7}$$

$$T_{g1}^{n+1} = T_{g1}^n + \frac{\Delta t\, A_{g1}}{m_{g1}c_{p,g}}\left[\alpha_g I + h_{conv,g1-surr}T_{surr} + h_{rad,g1-sky}T_{sky} +\right.$$
$$\left(\frac{A_{g2}}{A_{g1}}\right)\left(h_{conv,g2-g1} + h_{rad,g2-g1}\right)T_{g2} - \left(h_{conv,g1-surr} + h_{rad,g1-sky} +\right.$$
$$\left.\left(\frac{A_{g2}}{A_{g1}}\right)h_{conv,g2-g1} + \left(\frac{A_{g2}}{A_{g1}}\right)h_{rad,g2-g1}\right)T_{g1}\right]^n \tag{4.8}$$

Cooking Pot

Solar radiation reaches the cooking pot via glazing cover and reflective inner walls. Furthermore, there is conduction and convection between the cooking pot, absorber plate, and air cavity. During cooking, a portion of heat is accumulated by the pot and remaining is transferred to load. The thermal balance equation for the cooking pot and its discretization are as follows:

$$m_{pot}c_{pot}\frac{dT_{pot}}{dt} = \dot{Q}_{abs,pot} + \dot{Q}_{cond,p-pot} + \dot{Q}_{conv,air-pot} - \dot{Q}_{conv,pot\,side-load} -$$
$$\dot{Q}_{conv,pot,bottom-load} \tag{4.9}$$

$$T_{pot}^{n+1} = T_{pot}^n + \frac{\Delta t}{m_{pot}c_{p,pot}}\left[\tau_g^2\alpha_{pot}IA_{pot,side} + A_{pot,bottom}U_{p,pot}T_p + \right.$$

$$A_{pot,side}h_{conv,air-pot}T_{air} + A_{pot,side}h_{conv,pot\,side,load}T_{load} +$$

$$h_{conv,pot\,bottom-load}A_{pot,bottom}T_{load} - \left(U_{p-pot}A_{pot,bottom} + A_{pot,side}h_{conv,air-pot} + \right.$$

$$\left. A_{pot,side}h_{conv,pot\,side,load} + A_{pot,bottom}h_{conv,pot\,bottom-load}\right)T_{pot}\bigg]^n \qquad (4.10)$$

Lid

Solar irradiance reaches the lid through glazing covers at the top. In addition, lid exchanges heat with air cavity. The lid accumulates a part of heat and transfers the other to the load. Through radiation, rest of heat is lost through the walls and second glass. The thermal balance equation for the lid and its discretization are as follows:

$$m_{lid}c_{lid}\frac{dT_{lid}}{dt} = \dot{Q}_{abs,lid} + \dot{Q}_{conv,air-lid} - \dot{Q}_{conv,lid-load} - \dot{Q}_{rad,lid-g2} \qquad (4.11)$$

$$T_{lid}^{n+1} = T_{lid}^n + \frac{\Delta t A_{lid}}{m_{lid}c_{p,lid}}\left[\tau_g^2\alpha_{lid}I + h_{conv,air-lid}T_{air} + h_{conv,lid-load}T_{load} + \right.$$

$$h_{rad,lid-g2}T_{g2} - \left(h_{conv,air-lid} + h_{conv,lid-load} + h_{rad,lid-g2}\right)T_{lid}\bigg]^n \qquad (4.12)$$

Load

Cooking loads (glycerol) receive heat from the walls of cooking pot and lid via convection. The heat balance equation for the cooking load is as follows:

$$m_{laod}c_{load}\frac{dT_{load}}{dt} = \dot{Q}_{conv,pot\,side-load} + \dot{Q}_{conv,pot,bottom-load} + \dot{Q}_{conv,lid-load} \qquad (4.13)$$

Discretization of the equation (13) gives:

$$T_{load}^{n+1} = T_{load}^n +$$

$$\frac{\Delta t}{m_{load}c_{p,load}}\left[\left(h_{conv,pot\,side-load}A_{load} + h_{conv,pot,bottom-load}A_{pot,bottom}\right)T_{pot} + \right.$$

$$h_{conv,lid-load}A_{lid}T_{lid} - \left(h_{conv,pot\,side-load}A_{load} + h_{conv,pot,bottom-load}A_{pot,bottom} + \right.$$

$$\left. h_{conv,lid-load}A_{lid}\right)T_{load}\bigg]^n \qquad (4.14)$$

Initial conditions are set for the temperatures of different components of SBC in ºC as given below.

T_p (0) = 30; T_{lid} (0) = 30; T_{g1} (0) = 30; T_{g2} (0) = 30; T_{air} (0) = 30; T_{pot} (0) = 30; T_{load} (0) = 28; T_{surr} = 30.

The discretized equations are solved numerically using fourth-order Runge-Kutta method. Figure 4.3 illustrates the numerical solution procedure implemented using MATLAB code.
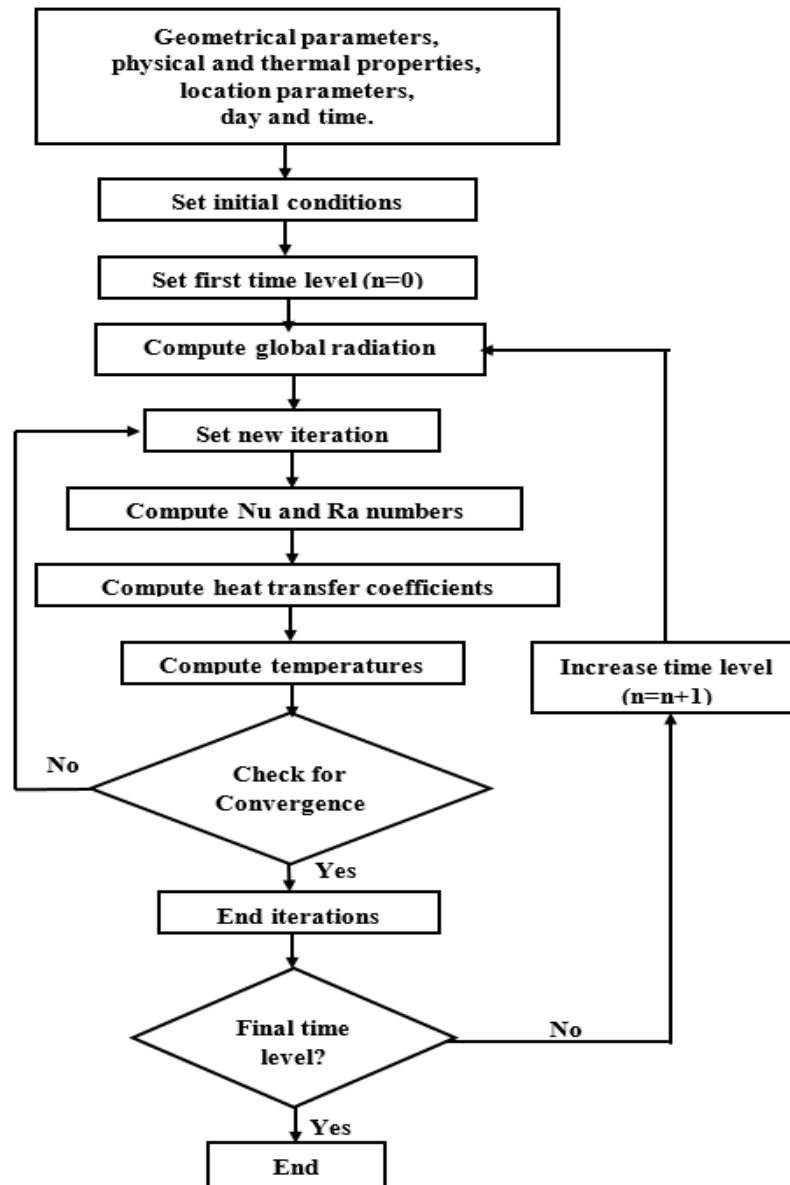
Figure 4.3 Numerical solution procedure

Heat transfer coefficients

Heat transfer coefficients required for the numerical solution depend on the temperature of different components, the thermal properties of materials, and environmental conditions. Calculating fluctuating heat transfer coefficients is

essential for finding the accurate temperature for each element. At each iteration heat transfer coefficients are computed using respective correlations found in the literature.

The convective heat transfer coefficient between aluminium absorber plate and inner cavity air is calculated using equation, (Guidara et al. 2017)

$$h_{conv,p-air} = 1.32 \left(\frac{T_p - T_{air}}{L}\right)^{1/4} \tag{4.15}$$

The radiation heat transfer coefficient between absorber plate and second glass is determined using the expression as follows:

$$h_{rad,p-g2} = \frac{\sigma(T_p + T_{g2})(T_p^2 + T_{g2}^2)}{\left(\frac{1}{\varepsilon_p}\right) + \frac{A_p}{A_{g2}}\left(\frac{1-\varepsilon_g}{\varepsilon_g}\right)} \tag{4.16}$$

The convective heat transfer coefficient between two glass covers is computed by finding Nusselt number which is obtained through the Hollands equation (Hollands et al. 1976), as given below.

$$h_{conv,g2-g1} = \frac{Nu_{g2-g1} k_{air}}{L_{g1g2}} \tag{4.17}$$

$$Nu_{g2-g1} = 1 + 1.44 \left(1 - \frac{1708}{Ra_{g2-g1}\cos\beta}\right)^+ \left(1 - \frac{1708(\sin(1.8\,\beta))^{1.6}}{Ra_{g2-g1}\cos\beta}\right) + \left(\left(\frac{Ra_{g2-g1}\cos\beta}{5830}\right)^{1/3} - 1\right)^+ \tag{4.18}$$

$(-)^+$ are set to zero, if they are negative.

The convective heat transfer coefficient between inner air cavity and second glass cover is calculated using equation, (Guidara et al. 2017)

$$h_{conv,air-g2} = 0.1291 \, Ra^{0.304} \frac{k_{air}}{L_{air}} \tag{4.19}$$

Where L_{air} is mean thickness of inner air gap which is given by,

$$L_{air} = \frac{L_{face} + L_{back}}{2} \tag{4.20}$$

The convective heat transfer coefficient between first glass and the surroundings is expressed in terms of wind velocity as given below (Guidara et al. 2017).

$$h_{conv,g1-surr} = 5.7 + 3.8 \, v \tag{4.21}$$

The radiation heat transfer coefficient between first glass cover and sky is computed using equation, (Duffie and Beckman 2013)

$$h_{rad,g1-sky} = \varepsilon_{g1} \, \sigma \left(T_{sky} + T_{g1}\right)\left(T_{sky}^2 + T_{g1}^2\right) \tag{4.22}$$

Where, temperature of sky is calculated by, (Adelard et al. 1998)

$$T_{sky} = 0.0552 \, T_{surr}^{1.5} \tag{4.23}$$

Overall heat transfer coefficient through walls and bottom of SBC are calculated using the following expressions,

$$U_{wall,surr} = \frac{1}{\frac{th_{inner}}{k_{inner}} + \frac{th_{ins}}{k_{ins}} + \frac{th_{outer}}{k_{outer}} + \frac{1}{h_{conv,outer-surr}}} \tag{4.24}$$

$$U_{p-surr} = \frac{1}{\frac{th_p}{kp} + \frac{th_{ins}}{k_{ins}} + \frac{th_{outer}}{k_{outer}} + \frac{1}{h_{conv,outer-surr}}} \tag{4.25}$$

Where, convective heat transfer coefficient between outer wall and surroundings is obtained using equation (4.21).

The Convective heat transfer coefficient between inner cavity air and lateral surface of cooking pot is calculated using the following expressions: (Churchill and Chu 1975)

$$h_{conv,air-pot} = \frac{Nu_{air-pot} k_{air}}{L_{pot}} \tag{4.26}$$

$$Nu_{air-pot} = \left[0.825 + \frac{0.387 Ra_{air,pot}^{1/6}}{\left[1 + \left(\frac{0.492}{pr}\right)^{9/16}\right]^{8/27}}\right]^2 \tag{4.27}$$

Whereas convective heat transfer coefficient between lid and inside air is calculated using following correlations (Churchill and Chu 1975).

$$h_{conv,air-lid} = \frac{Nu_{air-lid}k_{air}}{L_c} \tag{4.28}$$

$$Nu_{air-lid} = 0.54 \, Ra^{0.25} \quad if \, 10^4 \leq Ra \leq 10^7$$

$$Nu_{air-lid} = 0.15 \, Ra^{0.333} \quad if \, 10^7 \leq Ra \leq 10^{11} \tag{4.29}$$

The convective heat transfer coefficient between lateral surface of cooking pot and load is calculated using the following correlations.

$$h_{conv,pot \, side-load} = \frac{4 \, Nu_{pot \, side-load} \, k_{load}}{3 \, L_{pot}} \tag{4.30}$$

$$Nu_{pot \, side-load} = 0.508 \, pr^{0.5}(0.952 + pr)^{0.25}Gr^{0.25} \quad if \, Ra < 10^9$$

$$Nu_{pot \, side-load} = 0.10 \, Ra^{0.333} \quad if \, Ra > 10^9 \tag{4.31}$$

The convective heat transfer coefficient between bottom surface of cooking pot and load is computed using equation (4.28). Whereas convective heat transfer coefficient between lid and load is obtained using the correlations as given below.

$$h_{conv,lid-load} = \frac{Nu_{lid-load}k_{air}}{L_c} \tag{4.32}$$

$$Nu_{lid-load} = 0.27 \, Ra^{0.25} \quad if \, 10^5 \leq Ra \leq 10^{10} \tag{4.33}$$

Estimation of global radiation

The estimation of total radiation falling on a horizontal surface at a particular location is required for the numerical prediction of temperatures at different solar cooker components. The inputs for estimating the total irradiance at any local time are the latitude (ϕ), longitude (L_{long}), altitude (H), and standard meridian (L_{st}) for the location under consideration. The global or total radiation falling on the horizontal surface can be calculated by using the following equation (Kaushika et al. 2014).

$$I = I_b + I_d \tag{4.34}$$

Where I_b and I_d are respectively the beam and diffuse components of solar radiation falling on the surface and are computed using the equations as given below (Duffie and Beckman 2013).

$$I_b = Z_b I_o \cos \theta_z \tag{4.35}$$

$$I_d = Z_d I_o \cos \theta_z \tag{4.36}$$

The empirical relation for finding the value of Z_b is presented by (Hottel 1976) as:

$$Z_b = a_o + a_1 \exp\left(\frac{-k}{\cos \theta}\right) \tag{4.37}$$

(Liu and Jordan 1960) presented an empirical relationship between the transmission coefficients for beam and diffuse radiation for the clear days as,

$$Z_d = 0.271 - 0.294 Z_b \tag{4.38}$$

The empirical constants a_o, a_1, and k are the functions of the altitude of the location. After standard tropical climate correction, these constants are expressed by the following relations for standard atmosphere with 23 km visibility at an altitude less than 2.5 km (Hottel 1976).

$$a_0 = 0.95[0.4237 - 0.00821(6 - H)^2] \tag{4.39}$$

$$a_1 = 0.98[0.5055 + 0.00595(6.5 - H)^2] \tag{4.40}$$

$$k = 1.02[0.2711 + 0.01858(2.5 - H)^2] \tag{4.41}$$

The extra-terrestrial irradiance (I_o) incident on the plane normal to the radiation on the nth day of the year is found out using the equation (Duffie and Beckman 2013)

$$I_o = I_{sc}[1.000110 + 0.034221 \cos B + 0.001280 \sin B + 0.000719 \cos 2B +$$
$$0.000077 \sin 2B] \tag{4.42}$$

$$B = (n - 1)\frac{360}{365} \tag{4.43}$$

Where I_{sc} is the solar constant (1367 w/m^2), and n is the day of the year.

Solar zenith angle is the angle of incidence of beam radiation on a horizontal surface which can be found by using the equation (Duffie and Beckman 2013)

$$\cos \theta_z = \cos \phi \cos \delta \cos \omega + \sin \phi \sin \delta \tag{4.44}$$

Here, δ and ω are respectively the declination and hour angle measured in degree which are calculated using the following relations (Duffie and Beckman 2013).

$$\delta = \frac{180}{\pi}[0.006918 - 0.399912\cos B + 0.070257\sin B - 0.006758\cos 2B +$$

$$0.000907\sin 2B - 0.002697\cos 3B + 0.00148\sin 3B] \qquad (4.45)$$

$$\omega = 15\,(t_{solar} - 12) \qquad (4.46)$$

The difference in minutes between solar time and standard or local time is given by the relation (Duffie and Beckman 2013)

$$\text{solar time} - \text{local time} = 4\big(L_{st} - L_{long}\big) + E \qquad (4.47)$$

Here, E is the equation of time in minutes given by (Duffie and Beckman 2013)

$$E = 229.2[0.000075 + 0.001868\cos B - 0.032077\sin B - 0.014615\cos 2B -$$

$$0.04089\sin 2B] \qquad (4.48)$$

4.2.2. Machine learning

Artificial intelligence (AI) is often implemented through ML, and its popularity and appeal continue to grow as more applications are found every day. In ML, the system learns from itself and then estimates the unknown outputs. As a general algorithm, ML can be conceptualized as a function f(x) that generates y from input vector x. Training success and selection of attributes are crucial factors that influence the performance of ML algorithms. Figure 4.4 illustrates ML's broad classification. Linear regression, decision trees, random forests, support vector machines (SVM), k-nearest neighbor (k-NN), and ANN are the regression techniques extensively employed in ML. The present study uses decision tree, k-NN, linear regression, and random forest for the prediction. Most widely used ML methods (e.g., ANN, SVM) have instability issues, and therefore are prone to be unreliable. The instability could lead in large variations in the predicted values due to small changes in the input data. The ensemble-based techniques such as RF is well suited for predicting temperatures as they reduce variance and bias by combining results of several individual models while improving the stability. Recently, RF approach received attention in many applications. In these applications, the authors concluded that the RF model has higher stability and robustness and better success rates with the use of proper training parameters than those of other models. Therefore, a better outcome will be obtained with the implementation of the RF regression algorithm for

the prediction of SC components temperature. Comparing with decision tree, RF is more accurate, and it solves the issue of over fitting. k-NN does not require training, it simply memorizes all the elements in the dataset. It can then give an output based on the distance of the input with the other point in the dataset.

The inputs include latitude, longitude, altitude, date and time, and numerically computed cooking load temperature. Datasets are randomly split as part of the shuffled sampling method, and 70% of total data is used during training and 30% during the testing phases. An open-source machine learning and data visualization tool called Orange is used to develop ML prediction models.

Machine learning techniques

Kernel nearest neighbour (k-NN)

Kernel nearest neighbour (k-NN) is one of the simplest and oldest supervised classification algorithms in ML. Using special number k (number of neighbours) in the whole data set, we can calculate the average or mode of the nearest neighbours and assign new object to the closest class. Euclidean, Mahalanobis, Chebyshev and Manhattan functions allow one to calculate distances between new objects and their neighbours. In this approach, the processing time increases as k and data sets get bigger, and all these distance calculations have to be stored in memory. For this reason, the choice of k is crucial.

Decision tree

Decision tree (DT) is one of the commonly used non-parametric supervised learning methods. Both classification and regression problems can be solved using this method. To make prediction, response or class Y must be derived from input X_1, X_2, ..., X_p. Binary trees are used for this. Every node in the tree is tested with input, say X_i. A sub-branch of tree will be selected based on the test result. The prediction is made after a leaf node is reached. Upon reaching a leaf, this prediction aggregates all training data points. A model is constructed by using each independent variable. The best split is determined by the mean squared error of each variable.

Simple and multiple linear regression

Regression is a well-known ML modeling technique. This technique uses continuous dependent variable and continuous or discrete independent variables. It creates relationship between the independent variable (X) and the dependent variable (Y) using the best fit straight-line method (regression line).
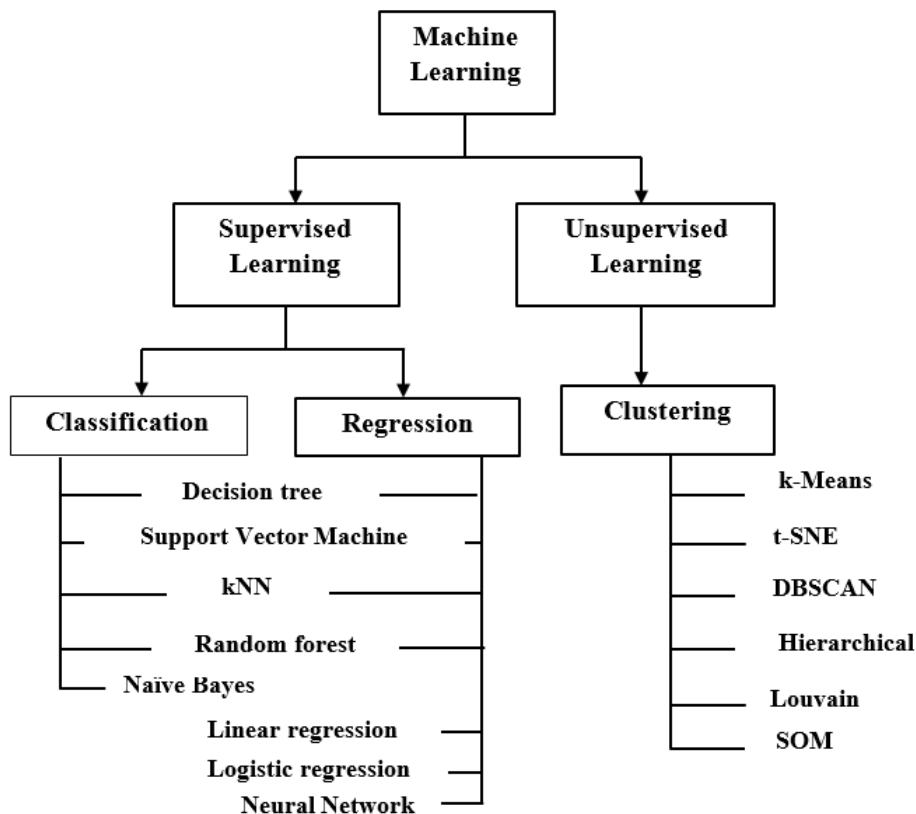
Figure 4.4 Classification of ML algorithms

Random forest

As a regression and classification problem, Breiman (2001) developed the random forest (RF) algorithm. The RF method utilizes ensemble learning for the prediction. Better predictive performance can be obtained using ensemble methods, which combine various ML algorithms. The model comprises many weak decision-tree learners growing simultaneously to decrease bias and variance (Breiman 2001). The method constructs several decision trees during training and uses the mean of the classes to predict all trees. The RF algorithm generates 'forest' that is trained through bagging or bootstrap aggregation. The bagging method is based on the notion that combination of models increases the overall result. In contrast to traditional DT

algorithms, it eliminates the overfitting of datasets and improves precision. Figure 4.5 illustrates structure of RF that classifies or predicts a variable from input data (x) by constructing number of regression trees (K) and averaging the results.
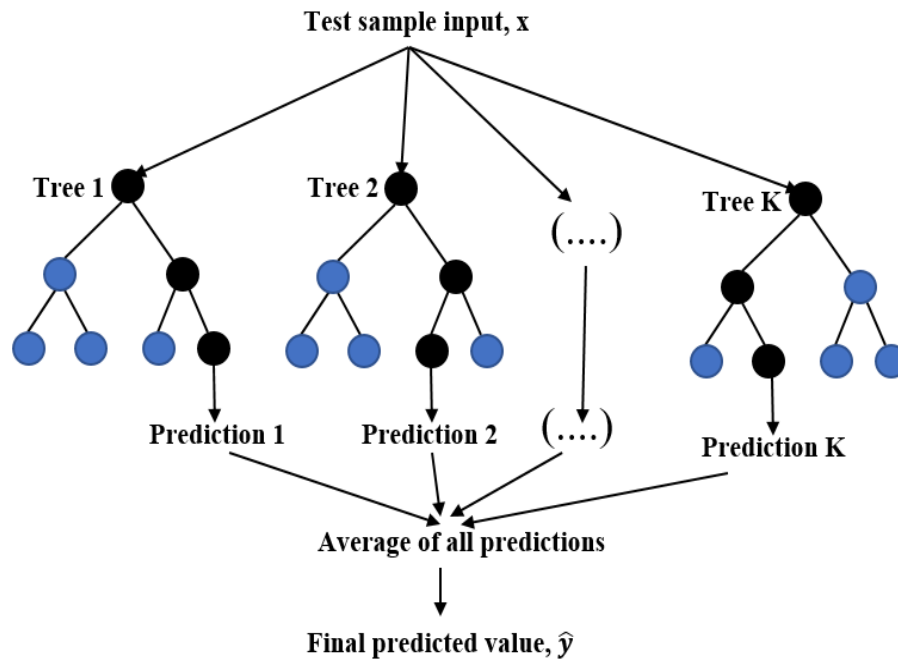
Figure 4.5 Structure of random forest

Data description

The training and testing data for the prediction models are based on the numerically simulated cooking load temperatures. The analysis takes into consideration different geographical locations (Table 4.4). The date, time, location's longitude, latitude, and altitude are the data required for the prediction models. Training data make up 70% of the entire dataset, and the remaining data samples are used for testing. The test variables used in the modeling are as follows:

Latitude: Latitude of a location is the angle made by the radial line joining the location to the center of the earth with the projection of the line on the equatorial plane. Range: $-25.85°$ to $46.51°$.

Longitude: The longitude of a place is its angular distance east or west of the prime meridian. Range: $-79.02°$ to $+80.27°$

Altitude: Altitude is the distance above the sea level. Range: 0.0067 to 2.355 km.

Time of a day: Range- 10:00 AM to 4:00 PM.

Table 4.4 Details of geographical location

Place	Latitude	Longitude	Altitude (km)	Author
Adis Ababa	8.98º N	38.76º E	2.355	Tibebu and Hailu 2021
Adrar	28.02º N	0.264º W	0.258	Harmim et al. 2010
Aligarh	27.89° N	78.08 °E	0.178	Arif et al. 2021
Ancona	43.58° N	13.51° E	0.016	Coccia et al. 2021
Burundi	3.21° S	29.98° E	2.3	Riva et al. 2017
Chennai	13.08° N	80.27° E	0.0067	Vengadesan et al. 2021
Dassanech	4.83° N	36.10° E	0.395	Milikias et al. 2020
Ghardaia	32.49° N	3.64° E	0.572	Yettou et al. 2019
Indore	22.71° N	75.85° E	0.55	Sharma et al. 2000
Kurukshetra	29.96° N	76.87° E	0.274	Yadav et al. 2017
Lausanne	46.51°N	6.63° E	0.495	Chatelain et al. 2019
Ludhiana	30.90° N	75.85° E	0.247	Singh and Sethi, 2018
Madrid	40.42º N	3.7º W	0.657	Soria-verdugo 2015
Mahikeng	25.85º S	25.64º E	1.5	Mawire et al. 2022
Mashhad	36.26° N	59.61° E	0.985	Zamani et al. 2017
Moradabad	28.83° N	78.77° E	0.198	Saxena et al. 2020
New Delhi	28.61º N	77.2º E	0.216	Singh 2021
Nikunja	23.83° N	90.41° E	0.015	Ahmed et al. 2020
North carolina	35.76º N	79.02º W	0.21	Ebersviller and Jetter 2020
Ranchi	23.44° N	85.14° E	0.651	Sagade et al. 2018
Razavi-Khorasan	35.10° N	59.10° E	0.299	Mostafaeipour et al. 2021
Rize	41.02° N	40.51° E	0.006	Cuce 2018
Sanaa city	15.40º N	44.2º E	2.25	Al-Nehari et al. 2021
Sfax	34.73° N	10.76° E	0.008	Guidara et al. 2017
Sohag	26.55° N	31.69° E	0.061	Abd-Elhady et al. 2020
Taxila	33.75° N	72.84° E	0.549	Zafar et al. 2019
Tiruchirappalli	10.79° N	78.70º E	0.088	Engoor et al. 2022
Vijayawada	16.50° N	80.64°E	0.011	Palanikumar et al. 2021

| Zagazig | 30.58° N | 31.50° E | 0.014 | Tawfik et al.2021 |
| Mangalore | 12.91° N | 74.85° E | 0.022 | Present study |

Evaluation of prediction model

Prediction models are evaluated by determining the mean square error (MSE), root mean square error (RMSE), mean absolute error (MAE), and coefficient of determination (R^2). The MAE and MSE are respectively the averages of absolute and squared differences between actual and predicted values in the dataset. Whereas RMSE is the square root of MSE values. The R^2 coefficient indicates how well the values fit in relation to their original values, ranging from 0 to 1. Higher R^2 values indicate better model performance. The following equations are used to calculate MAE, MSE, RMSE, and R^2 values (Ahamd et al. 2018).

$$MAE = \frac{1}{N}\sum_{i=1}^{N}|y_i - \hat{y}| \qquad (4.49)$$

$$MSE = \frac{1}{N}\sum_{i=1}^{N}(y_i - \hat{y})^2 \qquad (4.50)$$

$$RMSE = \left[\frac{1}{N}\sum_{i=1}^{N}(y_i - \hat{y})^2\right]^{\frac{1}{2}} \qquad (4.51)$$

$$R^2 = 1 - \frac{\sum(y_i - \hat{y})^2}{\sum(y_i - \bar{y})^2} \qquad (4.52)$$

Where $\hat{y}, y_i$, and $\bar{y}$ are the predicted, actual, and average value.

4.3. Results and discussion

The results and discussions of numerical modeling and ML prediction are presented in this section. Section 4.3.1 presents validation of the numerical model by comparing with the experimental study on TSBC. Modeling is being done to generate the input data required for ML models. The prediction results of ML models are presented in section 4.3.2.

4.3.1. Validation of numerical model

Sensible heat test with glycerol as cooking load is conducted on 11th January 2022 to obtain the temperatures of different components of SBC. The temperatures of first (T_{g1}) and second glazing cover (T_{g2}), inner air cavity (T_{air}), absorber plate (T_p),

cooking pot (T_{pot}), lid (T_{lid}), glycerol (T_{gly}) and surroundings (T_{surr}) is recorded from 10 AM to 4 PM (Figure 4.6). On this day, solar irradiance averaged 875 W/m^2 and surrounding atmosphere temperature 31°C. The glycerol temperature reached 121°C at 2 PM and remains above 104°C at 4 PM. The corresponding theoretical temperatures are obtained through the numerical model developed in Matlab. The numerical and experimental results for each component are shown in figures 4.7 (a-g). Figures 4.8 (a-g) shows the error which is the difference between experimentally and numerically obtained temperatures at the same point of time. The maximum error for T_p, T_{lid}, T_{g1}, T_{g2}, T_{air}, and T_{pot} are respectively -5.62%, +6.5%, +5.68%, +5.49%, -7.18%, and -6.78%. These errors are below 10%. For the cooking load glycerol, initially error is more and reduces later hours. During first three hours, it shows error more than 10% whereas, for last three hours it is less than 1%. The variation in results is due to the unpredictable climate change during day hours. Also, there may be some unexpected heat loss through the insulation at higher temperatures. The calculated errors are within the acceptable range, which validates the developed numerical model.

For further confirmation of the validation of the numerical solution, experiments were conducted on 25th January 2022 and 12th February 2022. For both days, the error between experimentally and numerically obtained temperatures of all the components is below 10%. A comparison of the numerical and experimentally obtained glycerol temperatures for 25th January 2022 is shown in figure 4.9 (a) and the corresponding error in figure 4.9 (b). Here also, initially, there is a significant difference between numerical and experimental results but later decreases. For the first three hours, the error is more than 13%, whereas, for the last three hours, it is below 5%. However, for all other components of SBC, the error is less than 10%. Similar results are observed for the test conducted on 12th February 2022, as shown in figure 4.10.
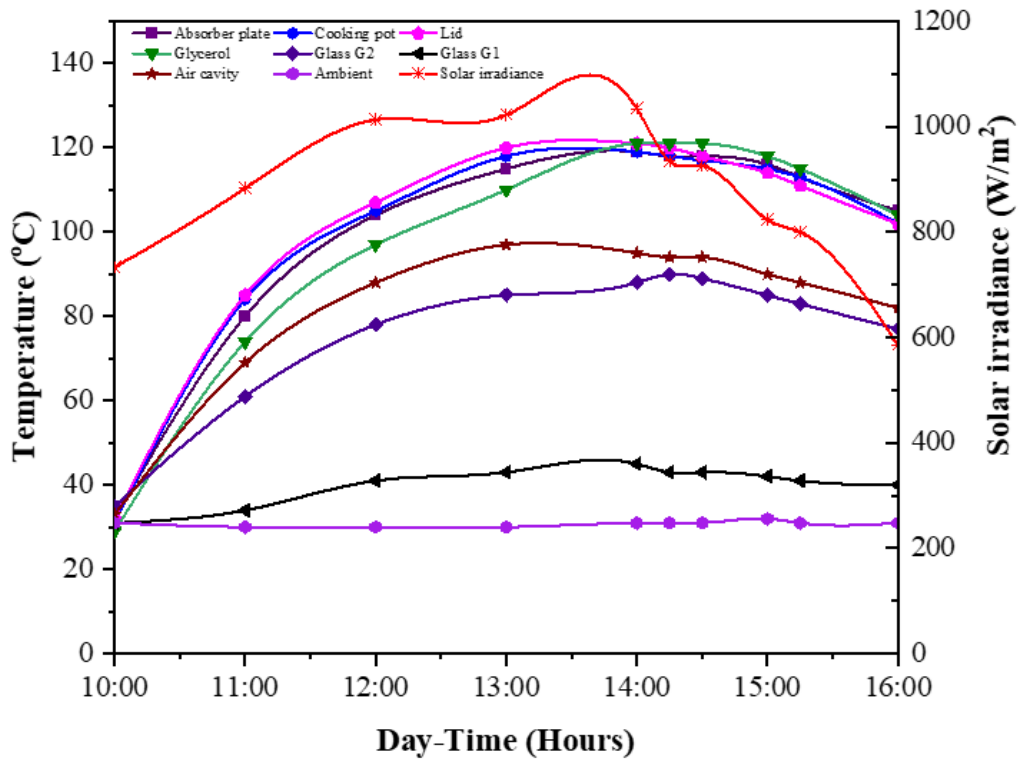
Figure 4.6 Variation of temperature and solar irradiance during sensible heating test with glycerol as cooking load (based on experiment on 11th January 2022)
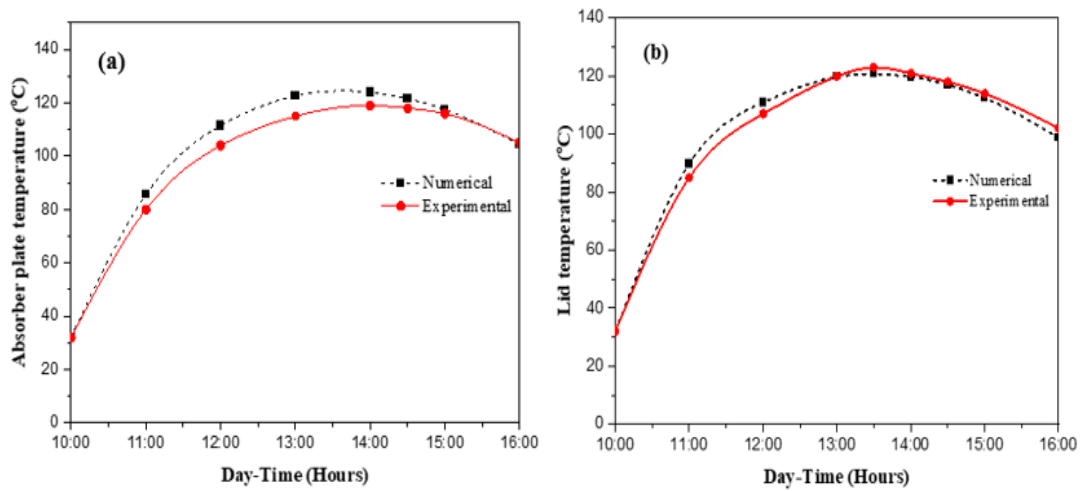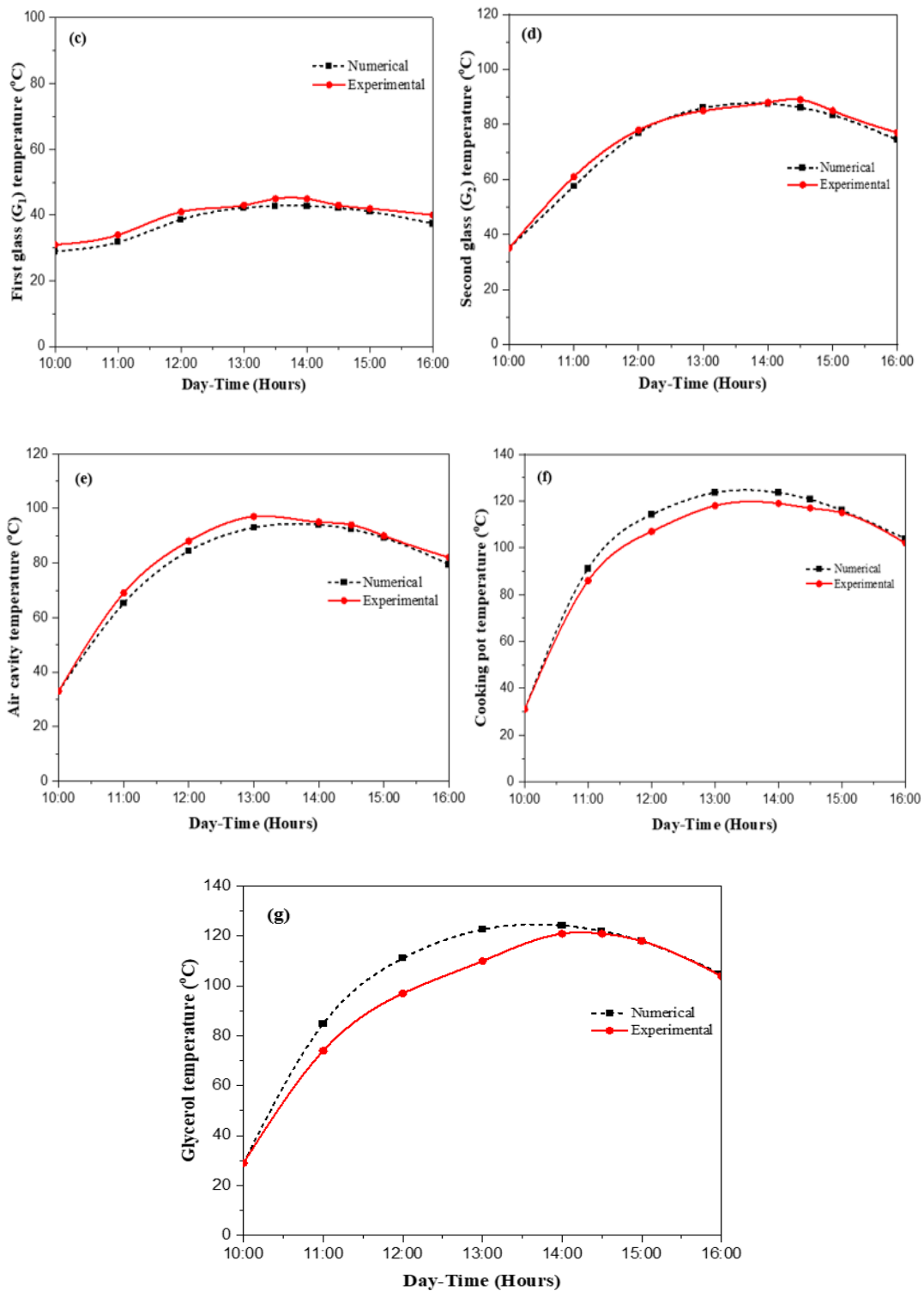
Figure 4.7 Comparison of experimental results with numerical modelling (a) Absorber plate (b) Lid (c) Glazing cover g_1 (d) Glazing cover g_2 (e) Air cavity (f) Cooking pot (g) Glycerol
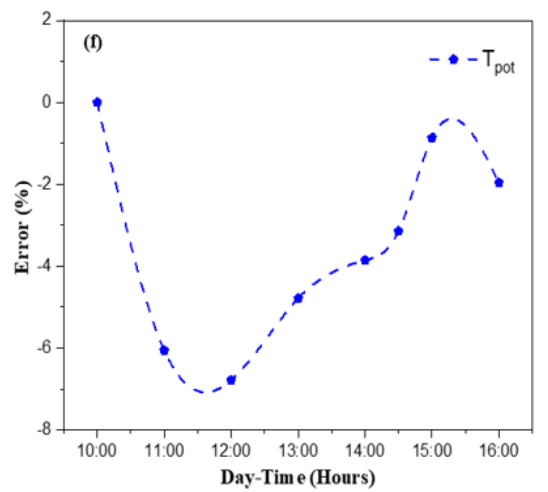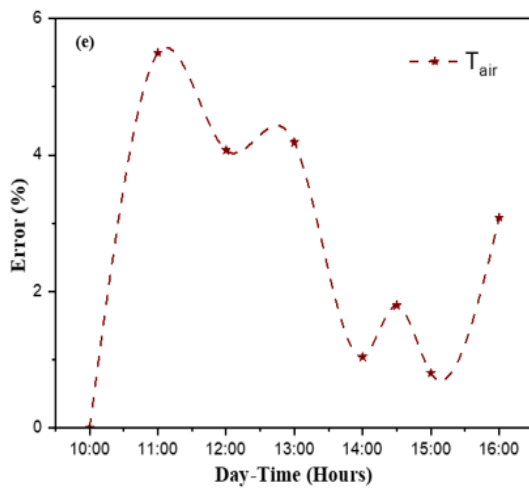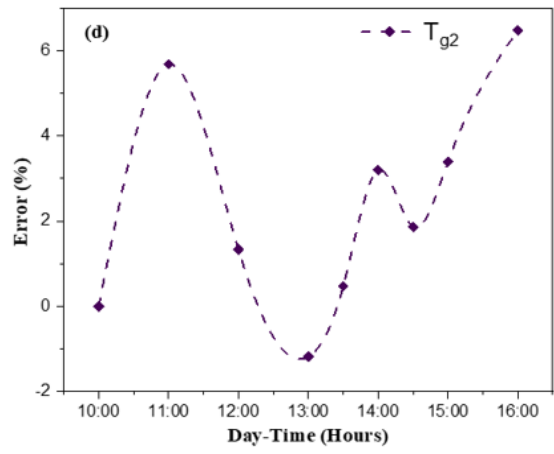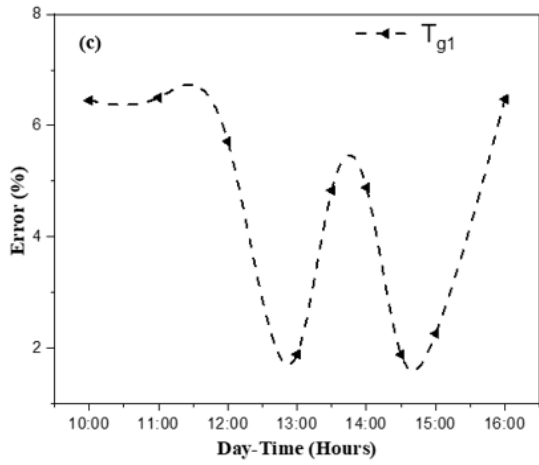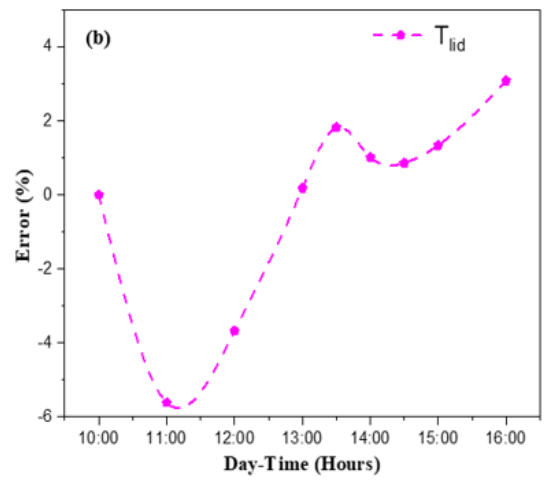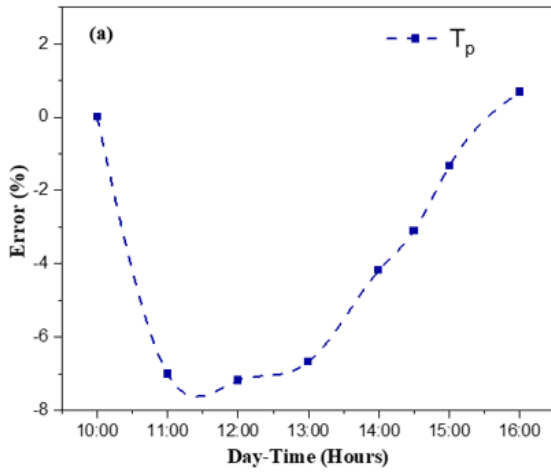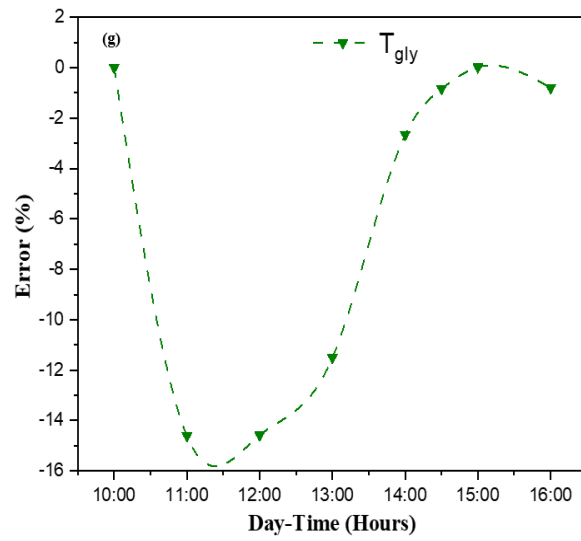
Figure 4.8 Error between experimental and numerical results (a) Absorber plate (b) Lid (c) First glass g$_1$ (d) Second glass g$_2$ (e) Air cavity (f) Cooking pot (g) Glycerol
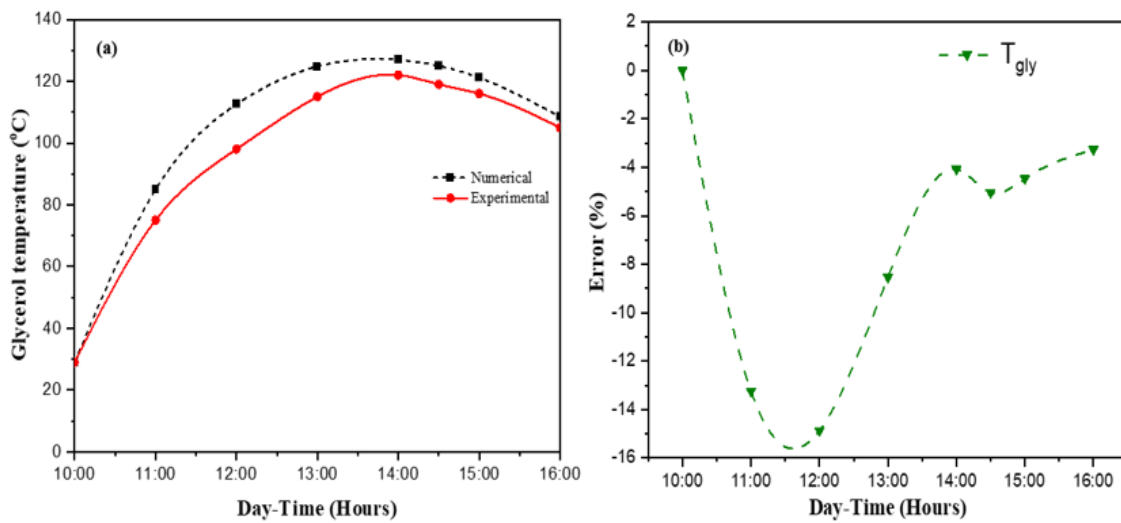
Figure 4.9 Cooking load (glycerol) temperature by experimental and numerical analysis based on the test conducted on 25th January 2022 (a) Comparison (b) Error
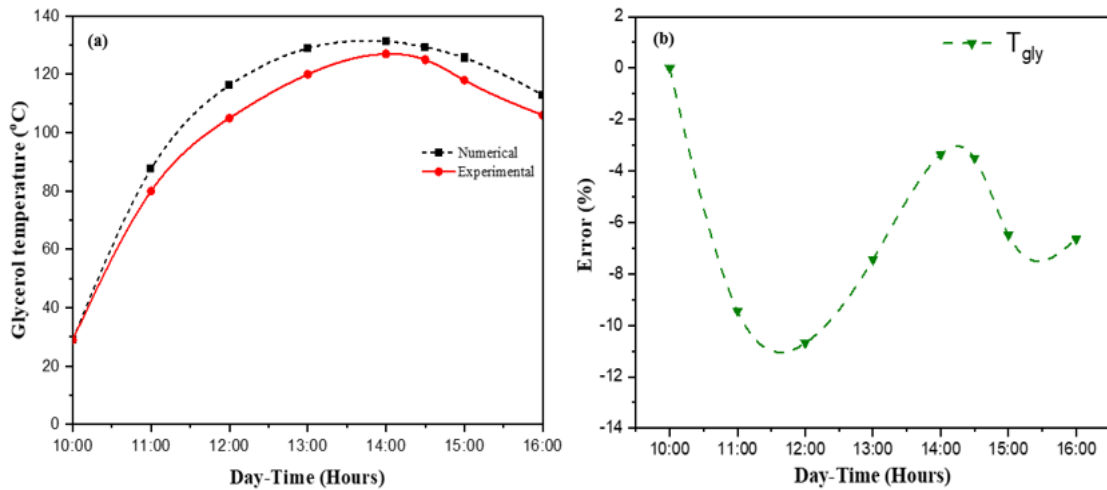
Figure 4.10 Cooking load (glycerol) temperature by experimental and numerical analysis based on the test conducted on 12th February 2022 (a) Comparison (b) Error

Figure 4.11 illustrates the variation of heat transfer coefficients obtained through the numerical study. Radiation heat transfer coefficients ($h_{rad, g2-g1}$ and $h_{rad, g1-sky}$) initially increases with increasing temperature and decreases toward evening. As the cooking vessel is heated up during the initial stage, the lid transfers heat to the cooking load, reducing the convection heat transfer coefficient. Later, during the cooking process, the cooking load reaches the lid temperature, and reverse heat transfer occurs, increasing the convection heat transfer coefficient between the lid and load ($h_{conv, lid-load}$). During the first hour, the convective heat transfer coefficient between air cavity and second glass cover ($h_{conv, air-g2}$) increases and gradually decreases. This is because, in the beginning, glass cover g_2 might have been hotter than the air. The inner air cavity becomes too warm during later hours, transferring heat to the glazing. Similarly, other convection heat transfer coefficients ($h_{conv, g2-g1}$, $h_{conv, p-air}$, $h_{conv, air-pot}$ and $h_{conv, air-lid}$) increase initially, then decrease as the day progresses.
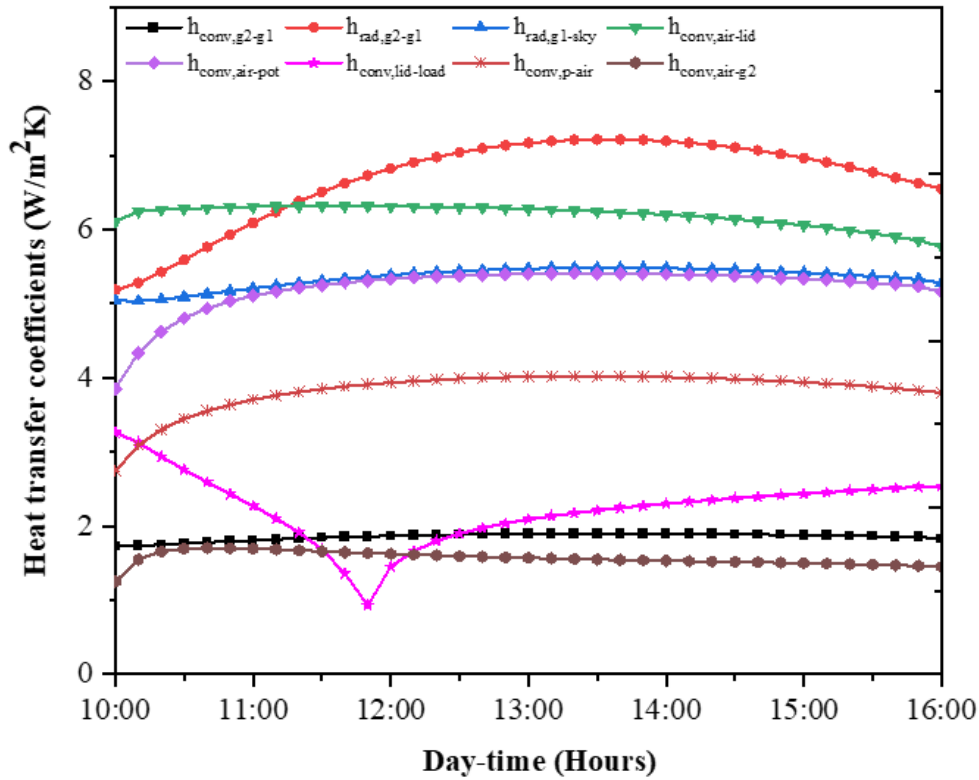
Figure 4.11 Variation of heat transfer coefficients during sensible heat test

4.3.2. Machine learning prediction and discussion

The previous sections discussed the numerical model for the temperature prediction and validation by the experimental investigation on trapezoidal-shaped SBC in Indian weather conditions. This numerical model involves all the different heat transfer modes for every component of SBC. Prediction models based on ML are the alternatives for predicting cooking load temperatures without further simulations. In the present work, prediction models are developed that can predict the cooker performance easily for known design parameters, material properties and location data. This section presents the ML-based prediction results. Dataset with four inputs and a target variable is used in this study. It includes 1080 data points obtained from numerical simulations of trapezoidal-shaped SBCs at 30 geographical locations.

Different ML models such as decision tree (DT), random forest (RF), linear regression (LR), and k-NN are developed to predict the cooking load temperatures of SBC. A plot of predicted versus actual cooking load (glycerol) temperature for different models is shown in figure 4.12 (a-d). The prediction results through the RF

and DT methods depicted in figure 4.12 (a-b) clearly show how the model predicts the temperature with a linear relationship. The RF and DT data are clustered along a line with a few isolated cases that show similar predicted and actual values. However, in other models shown in figure 4.12 (c-d), the deviations from the line are considerably higher, indicating larger error margin. Solar radiation fluctuation may occur during some hours of testing, resulting in greater discrepancies between actual and predicted values. For training the ML models, 1080 instances with 5 variables are used. Table 4.5 shows the prediction results of ML models during testing with 324 instances.
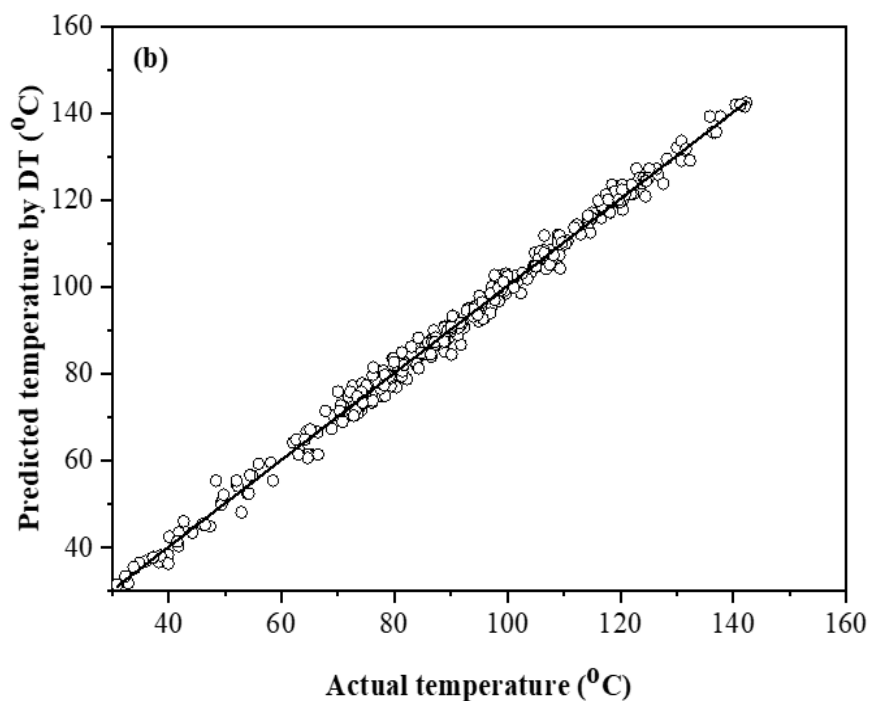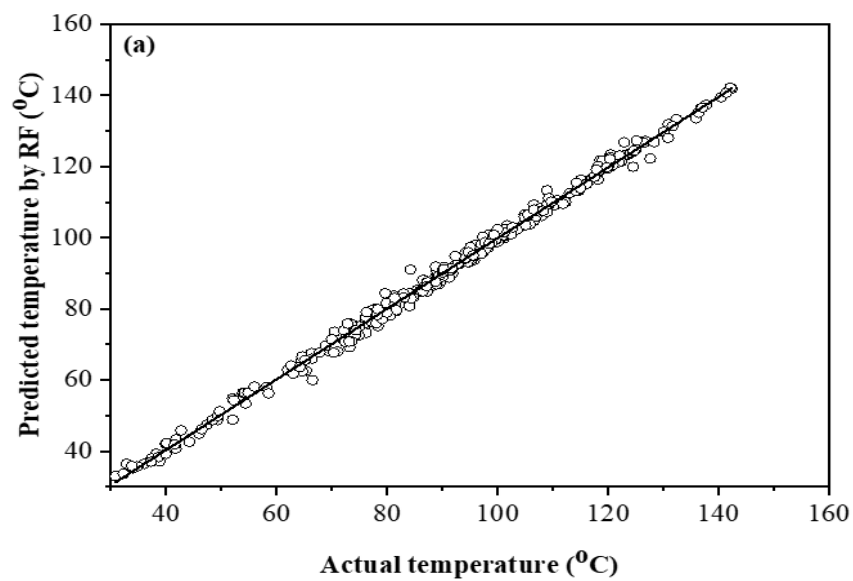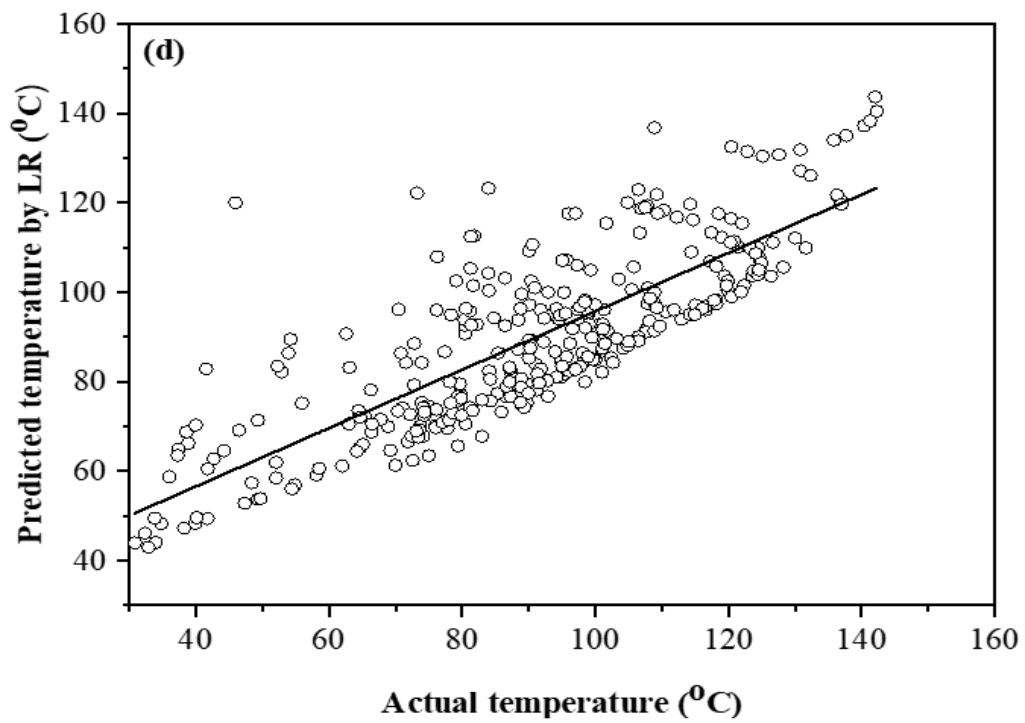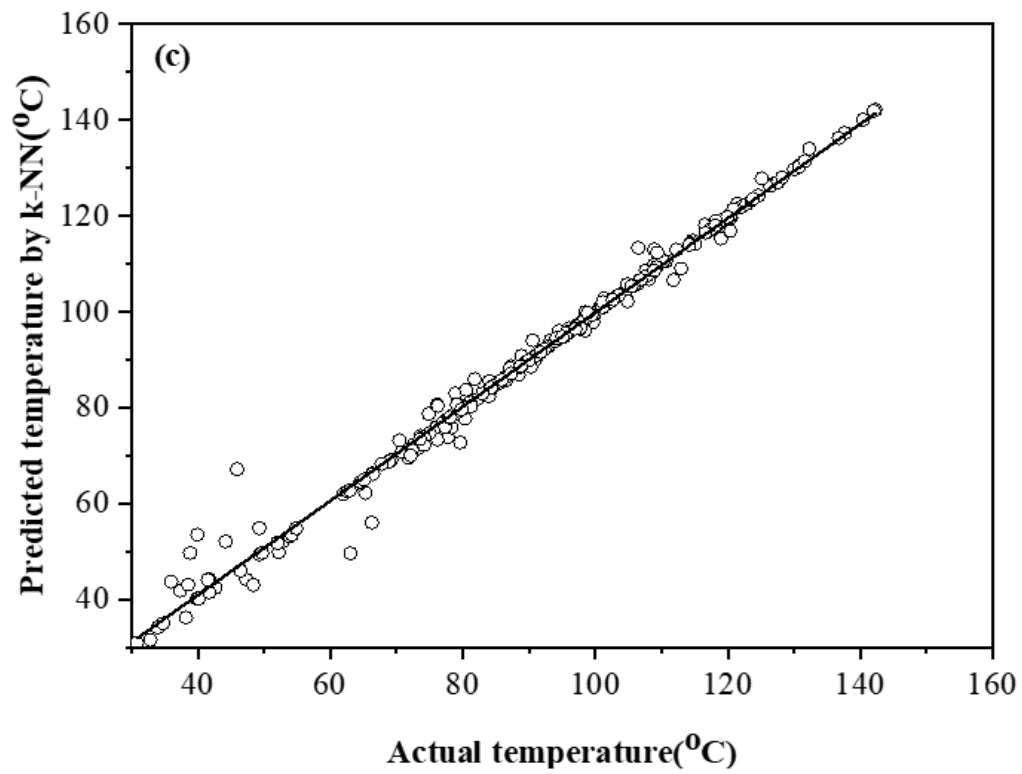
Figure 4.12 Comparison between actual cooking load temperature (T_{gly}) and predicted values (a) Random Forest (b) Decision tree (c) kNN (d) Linear regression

Table 4.5 Testing of ML models using 324 instances.

Sl No.	Latitude (degree)	Longitude (degree)	TIME	Cooking load temperature (ºC)				
				Actual	RF	DT	kNN	LR
1	22.72	75.85	13:40	110.67	110.54	110.55	110.57	95.65
2	15.4	44.2	11:50	107.72	107.68	106.83	107.48	91.81
3	46.5	6.63	11:30	41.72	43.30	40.37	44.22	49.42
4	-3.214	29.97	16:00	108.89	113.30	112.02	113.01	136.89
5	15.4	44.2	11:20	96.18	95.56	95.26	95.87	88.58
6	-25.85	25.64	12:30	137.70	137.40	139.21	137.32	135.12
7	23.83	90.41	10:40	66.25	67.49	66.75	56.00	78.21
8	26.56	31.69	11:50	94.92	93.19	92.10	94.72	81.07
9	36.26	59.61	15:10	80.45	82.55	81.95	80.36	90.78
10	34.74	10.76	15:20	80.43	80.75	78.77	80.34	92.63
.	.	.	.	.	.	.	.	.
.	.	.	.	.	.	.	.	.
315	16.5	80.65	13:20	119.70	119.28	120.03	119.59	119.74
316	36.26	59.61	12:20	79.91	78.09	82.68	83.48	78.90
317	23.83	90.41	13:50	108.19	107.45	107.34	106.98	107.54
318	28.61	77.2	11:20	78.25	76.18	79.76	81.03	79.88
319	34.74	10.76	12:40	88.75	86.34	87.45	88.63	87.65
320	16.5	80.65	11:10	90.25	90.88	93.30	89.91	91.11
321	23.44	85.15	15:50	81.29	83.25	84.92	81.21	83.04
322	23.83	90.41	12:20	104.99	102.14	104.67	102.00	103.53
323	35.75	-79.02	10:10	33.81	35.66	35.58	38.98	35.78
324	8.98	38.76	15:30	114.23	117.74	116.46	114.14	115.40

In the RF model, 11 trees are selected in the forest, and it is found that increasing numbers of trees do not significantly affect the prediction. Then, the performance dependence on the maximum depth of individual trees is analyzed. At depth of 18, the RF model performs with optimum R^2 0.995 and 0.996 respectively during training and testing. It is observed that higher tree counts do not affect performance, while trees smaller than 18 have negative effect. DT also performs best when the maximum

tree depth is limited to 18. The R^2 for k-NN model with Mahalanobis, Euclidian, Manhattan, and Chebyshev distance metrics are 0.988, 0.896, 0.903, and 0.867. The k-NN algorithm with k=2 and Mahalanobis distance provides better results than other metrics. We selected k=2 and Mahalanobis distance metrics for the k-NN algorithm in this study.

A comparison between different models based on their prediction performance is given in Table 4.6. RF, k-NN and DT models have R^2 values greater than 90%. However, the RMSE value for the tree and k-NN models are respectively 2.95 and 3.22, which is larger than that of RF (2.14). The R^2 value for LR is below 90%, displaying large differences between predicted and actual values. The RF with R^2 0.992 and RMSE 2.14 outperformed other developed models. It is clear from the results that the RF model can accurately predict the cooking load temperatures.

Table 4.6 Comparison of prediction performance of different ML models

Model	MSE	RMSE	MAE	R^2
LR	220.52	14.85	11.77	0.629
k-NN	10.36	3.22	1.75	0.983
DT	8.73	2.95	2.05	0.985
RF	4.58	2.14	1.45	0.992

4.3.3. Effect of input variables on target

The effects of input variables (latitude and longitude) on the target (cooking load temperature) are presented below. The design parameters, material properties, and location data influence the performance of SC. However, for a particular SC, performance is determined solely by the location and weather conditions on the day. The inputs for estimating the total irradiance at any local time are the latitude, longitude, altitude, and standard meridian for the location under consideration. The global or total radiation falling on the horizontal surface depends on the latitude, declination, surface azimuth, and hour angle. Whereas hour angle is related to the solar time which further depends on the longitude of location. Therefore, latitude and longitude of location determines the amount of total irradiance falling on the cooker surface which in turn affects the cooking load temperature.

Effect of latitude

Figure 4.13 shows the scatter diagram of latitude versus cooking load temperature. We used all data sets for this illustration. For latitudes below 10°, the maximum cooking load temperature can reach more than 125°C in some instances. In addition, when the latitude is greater than 30°, the cooking load temperature is less than 100°C in all cases. With latitude between 10° and 30°, the target temperature can reach 100°C-125°C. Because of this, the SC performs better in regions where the latitude is below 30°.

Effect of longitude

The scatter plot of longitude versus cooking load temperature is shown in Figure 4.14. The figure indicates that cooking loads can exceed 125°C when longitude is between 25° and 40°. Furthermore, when longitude exceeds 40°, the peak temperature reaches 100 – 125°C. SC is, therefore, more effective at places where longitude is greater than 25°. Hence, the analysis shows that the present trapezoidal shaped solar box cooker is more effective in regions with latitudes less than 30° and longitudes greater than 25°.
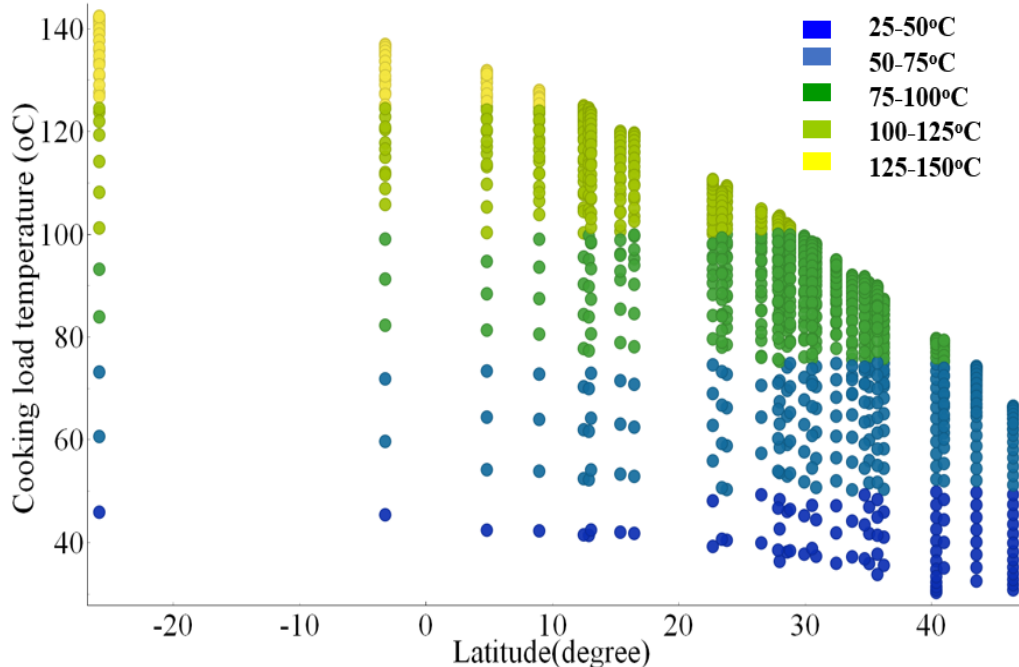
Figure 4.13 Scatter diagram of latitude versus cooking load temperature
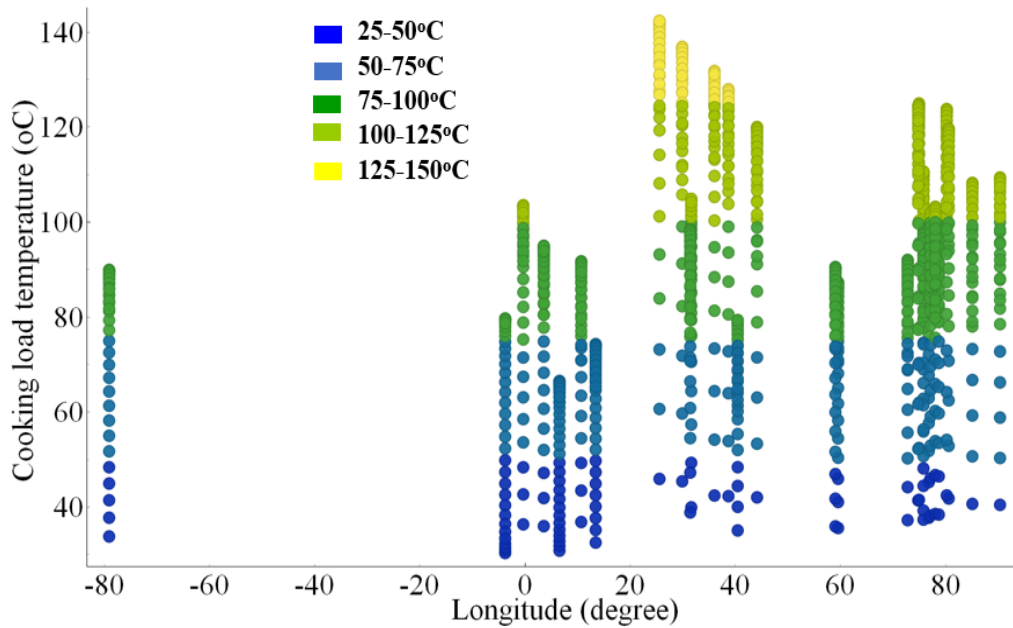
Figure 4.14 Scatter diagram of longitude versus cooking load temperature

4.4 Summary

The use of ML techniques in solar thermal energy conversion applications is significant in the development of effective prediction models. Many data are involved in solar thermal device analysis as it depends on the day, time, and location. Developing an ML-based prediction model is essential to forecast the system performance in a short time, which motivates the present study. Accordingly, prediction models for the SBC are developed using ML techniques such as random forest (RF), decision tree, linear regression, and k-nearest neighbor (k-NN). For this, first, a numerical model based on thermal balances at different components of SBC is developed to generate the input data required for ML models. Experiments are conducted in Indian weather conditions on a trapezoidal-shaped SBC from January to March 2022 to validate the numerical model. Then, the ML prediction models are trained, validated, and tested using the numerical modeling results.

Below are the main findings of the study:

- The numerical model is validated based on experiments conducted on trapezoidal-shaped SBC. Across all component temperatures, the difference

between experimental and numerical results is less than 7%, indicating the accuracy of numerical model.

- Prediction models are evaluated by determining the mean square error (MSE), root mean square error (RMSE), mean absolute error (MAE), and coefficient of determination (R^2). Results shows that RF model outperformed other models with MSE, RMSE, MAE, and R^2 respectively 4.8 (^{o}C), 2.14 (^{o}C), 1.45 (^{o}C) and 0.992. It indicates that RF model can accurately predict the thermal parameters of SBCs with great precision.

- Based on analysis of input variables and their effects in ML modeling, the present SC is more effective in regions with latitudes less than 30° and longitudes greater than 25°.

5. DESIGN OPTIMIZATION OF PCM BASED THERMAL ENERGY STORAGE UNIT FOR SOLAR BOX COOKER

To extend the usability of SBCs in the late evening hours, different thermal energy storage (TES) materials are used. The latent heat of phase change materials (PCMs) used as TES medium has become remarkable because of their high energy density and constant temperature operating characteristics. A computational procedure is developed to simplify the exhaustive calculations required to optimize and design the TES unit employing PCM as heat storage medium. Different geometries (cylindrical, square, and hexagonal) of TES units are developed, and experiments are conducted to validate the computational procedure. The optimum PCM for TES is also selected using multi-criteria decision-making (MCDM) methods. A more detailed discussion is presented in the following sections.

5.1. Background

The evening or night cooking is possible with the heat storage facility in SBCs. Thermal energy can be stored in SBCs as sensible or latent heat. In latent heat storage (LHS) units, energy stored during phase change is used for cooking. Generally, PCMs are used to store energy in the form of latent heat. The cooking pot incorporated with LHS system contains two concentric cylindrical vessels with annular cavity filled with PCM (Figure 5.1). The PCMs contained in the cooking vessel are heated and liquefied by the SBC. In general, the TES units surrounding the cooking vessel are filled with PCM along the lateral side (Sharma et al. 2000; Buddhi et al. 2003; Vigneswaran et al. 2017; Lecuona et al. 2013; Bhave and Kale 2020; Mawire et al. 2020). In the present work, new design of the TES unit is introduced that includes the facility for filling the PCM at the lateral and bottom part of the cooking pot. This will enhance the cooking performance as heat is transferred to the load through all sides of the pot. However, it is required to optimize the geometry and heat transfer properties of TES units to utilize latent heat effectively (Nkhonjera et al. 2017). Accordingly, the present work develops and compares the performance of TES units of different

geometries by conducting experiments. The optimum mass of PCM and dimensions for the TES units are found by developing a computational procedure.
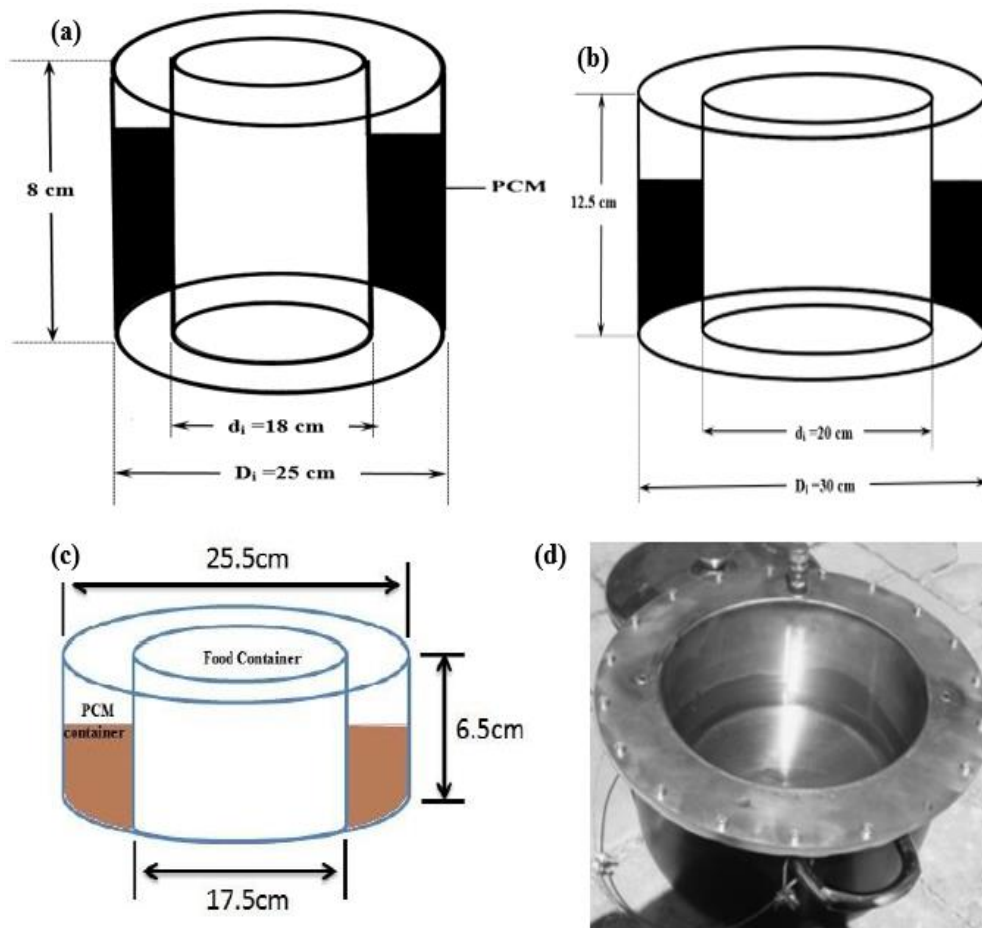
Figure 5.1 Schematic of TES units for SC (a) (Sharma et al. 2000) (b) (Buddhi et al. 2003) (c) (Vigneswaran et al. 2017) (d) (Leucona et al. 2013)

Selection of optimum PCM is very essential for the efficient heat storage in the TES unit. MCDM methods are having high potential in the optimization of material selection (Emovon and Oghenenyerovwho 2020). MCDM methods are used to select the best of a set of alternatives by evaluating them with reference to different attributes. Various MCDM techniques were applied in sustainable and renewable energy development sectors (Mardani et al. 2015). These methods are based on various theories such as reference point, outranking and pairwise comparison procedure. The commonly used techniques are the analytic hierarchy process (AHP), technique for order preference by similarity to ideal solution (TOPSIS), preference

ranking organization method for enrichment evaluations (PROMETHEE), complex proportional assessment (COPRAS), evaluation based on distance from average solution (EDAS), combinative distance-based assessment (CODAS), multi-objective optimization by ratio analysis (MOORA), multi-objective optimization on the basis of simple ratio analysis (MOOSRA) and multi-attribute utility analysis (MAUA). Rathod and Kanzaria (2011) presented TOPSIS and FUZZY-TOPSIS for the optimum selection of PCMs in solar water heater system. They employed AHP method for the determination of criteria weights. Both TOPSIS and FUZZY-TOPSIS techniques give calcium chloride hexa-hydrate as the optimum PCM. Rastogi et al. (2015) presented MCDM tool for the optimum selection of PCM in HVAC applications. They used the ENTROPY method for the determination of criteria weights and Ashby and TOPSIS for the PCM selection. Socaciu et al. (2016) ranked commercial PCMs for the thermal comfort of vehicle occupants with the aid of AHP method. They obtained overall weight of the PCMs with reference to the hierarchies such as objective, seven criteria and ten numbers of alternatives. Xu et al. (2017) employed TOPSIS and AHP for the selection of PCMs in the LHS unit for the solar air conditioning system. (Yang et al. 2018) applied TOPSIS for selecting the best PCM from the pre-screened alternatives. They obtained the criteria weights using AHP and ENTROPY method and then computed the combination weight. The ranking by TOPSIS method is validated by information retrieval. Recently, Gadhave et al. (2020) presented TOPSIS, VIKOR and EXPROM2 for the optimum selection of PCM in the LHS unit for domestic water heating system. The criteria weights used for the optimization problem is the compromised value between the weights obtained through AHP and ENTROPY methods. Based on the rankings, sodium acetate tri-hydrate is found to be the best PCM from the alternatives.

This chapter presents the development of a computational procedure for obtaining the optimum quantity of PCM and dimensions of the TES unit for the SBC. The computational procedure is validated by comparing it with previous works and conducting experimental investigations on different geometries of TES systems using paraffin wax as the PCM. Further, this chapter presents various MCDM techniques for selecting the best PCM among different alternatives for SBCs. PCMs are pre-

screened among the alternatives used in earlier works based on the melting temperature. The optimum PCM is then selected with TOPSIS, EDAS, and MOORA methods. The criteria weights required for the optimization algorithm are found using AHP, ENTROPY, and CRITIC methods. Also, compromised values between the weights obtained through these methods are computed. The methodology adopted in the present study is presented in section 5.2. Section 5.3 presents the validation results of the computational procedure, the comparison of the performance of various geometry options of the TES units, and the optimum PCM based on MCDM methods.

5.2. Methodology

5.2.1. Computational procedure for the design of TES unit

SBC incorporating TES consists of cooking vessel integrated with PCM container to store the thermal energy. The TES system must lose enough latent heat to maintain constant temperature for a particular period. This determines the quantity of PCM needed, which in turn decides container size. To maintain cooking load temperatures at the melting point of PCM, PCM must release latent heat energy equal to energy loss from the container, which can be calculated by,

$$m_{pcm}\lambda = U[T_{mp} - T_a]t \tag{5.1}$$

Using iterative approach, optimum quantity of PCM for different TES unit geometries surrounding the cooking pot is calculated. The shapes for analysis include cylindrical, square, and hexagonal (Figure 5.2(a-c)). Overall heat loss coefficient (U) for each geometry is calculated based on the following equations:

For cylindrical, $\qquad U = \dfrac{1}{\dfrac{1}{2\pi l}\left[\dfrac{1}{h_i r_i} + \dfrac{\ln\left(\frac{r_o}{r_i}\right)}{k_s} + \dfrac{1}{h_o r_o}\right]}$ $\hfill$ (5.2)

For square, $\qquad U = \dfrac{1}{\dfrac{1}{4l}\left[\dfrac{1}{h_i L_i} + \dfrac{2t_s}{k_s\,(L_i + L_o)} + \dfrac{1}{h_o L_o}\right]}$ $\hfill$ (5.3)

For hexagonal, $\qquad U = \dfrac{1}{\dfrac{1}{6l}\left[\dfrac{1}{h_i L_i} + \dfrac{2t_s}{k_s\,(L_i + L_o)} + \dfrac{1}{h_o L_o}\right]}$ $\hfill$ (5.4)
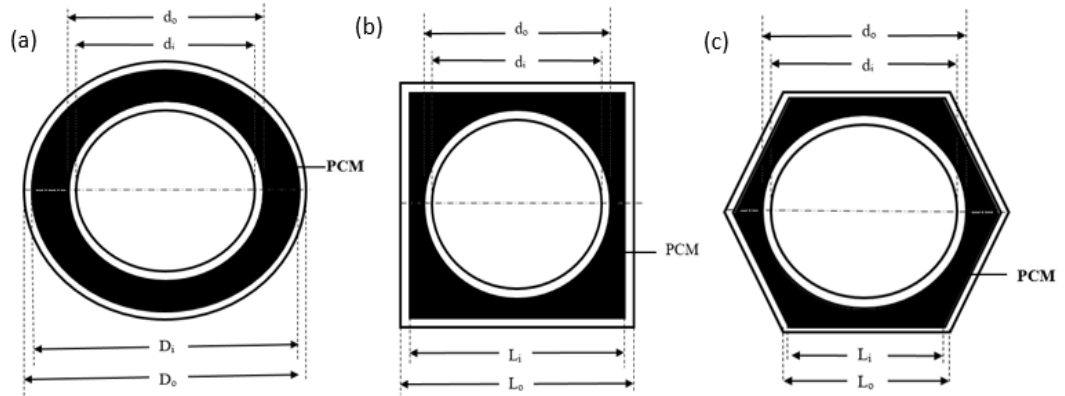
Figure 5.2 Top view of cooking pot integrated with different geometries of TES container (a) cylindrical (b) square (c) hexagonal

By assuming initial temperatures at each nodal point, h_i and h_o are calculated using following equations.

$$h = \frac{4 \, Nu \, k}{3 \, l} \tag{5.5}$$

$$Gr = \frac{g \, \beta \, (\Delta T) \, l^3}{\upsilon^2} \tag{5.6}$$

$$\text{If } Gr \, Pr \, < 10^9, \; Nu = 0.508 \, Pr^{0.5}(0.952 + Pr)^{-0.25} Gr^{0.25} \tag{5.7}$$

$$\text{If } Gr \, Pr \, > 10^9, \; Nu = 0.10 \, (Gr \, Pr)^{0.333} \tag{5.8}$$

After that, D_i and L_i can be computed as follows:

For cylindrical,
$$D_i = \left[\frac{\left(\frac{m_{pcm}}{\rho_l}\right) + \left(\pi \frac{d^2 l}{4}\right)}{\frac{\pi l}{4}} \right]^{\frac{1}{2}} \tag{5.9}$$

For square,
$$L_i = \left[\frac{\left(\frac{m_{pcm}}{\rho_l}\right) + \left(\pi \frac{d^2 l}{4}\right)}{l} \right]^{\frac{1}{2}} \tag{5.10}$$

For hexagonal,
$$L_i = \left[\frac{\left(\frac{m_{pcm}}{\rho_l}\right) + \left(\pi \frac{d^2 l}{4}\right)}{\frac{3l\sqrt{3}}{2}} \right]^{\frac{1}{2}} \tag{5.11}$$

111

D_o and L_o are computed by considering material thickness of containers. The temperatures at internal (T_i) and external (T_o) surfaces are then calculated using equations (5.12-5.17) and compared to the previous value.

For cylindrical,
$$T_i = T_{mp} - \frac{Q}{\pi D_i l\, h_i} \tag{5.12}$$

$$T_o = T_a + \frac{Q}{\pi D_o l\, h_o} \tag{5.13}$$

For square,
$$T_i = T_{mp} - \frac{Q}{4 L_i l\, h_i} \tag{5.14}$$

$$T_o = T_a + \frac{Q}{4 L_o l\, h_o} \tag{5.15}$$

For hexagonal,
$$T_i = T_{mp} - \frac{Q}{6 L_i l\, h_i} \tag{5.16}$$

$$T_o = T_a + \frac{Q}{6 L_o l\, h_o} \tag{5.17}$$

Where, Q is the heat loss from container. Finally, iterative solution finds optimal PCM mass and container dimensions. Figure 5.3 shows flow chart of the computational procedure implemented through MATLAB code.
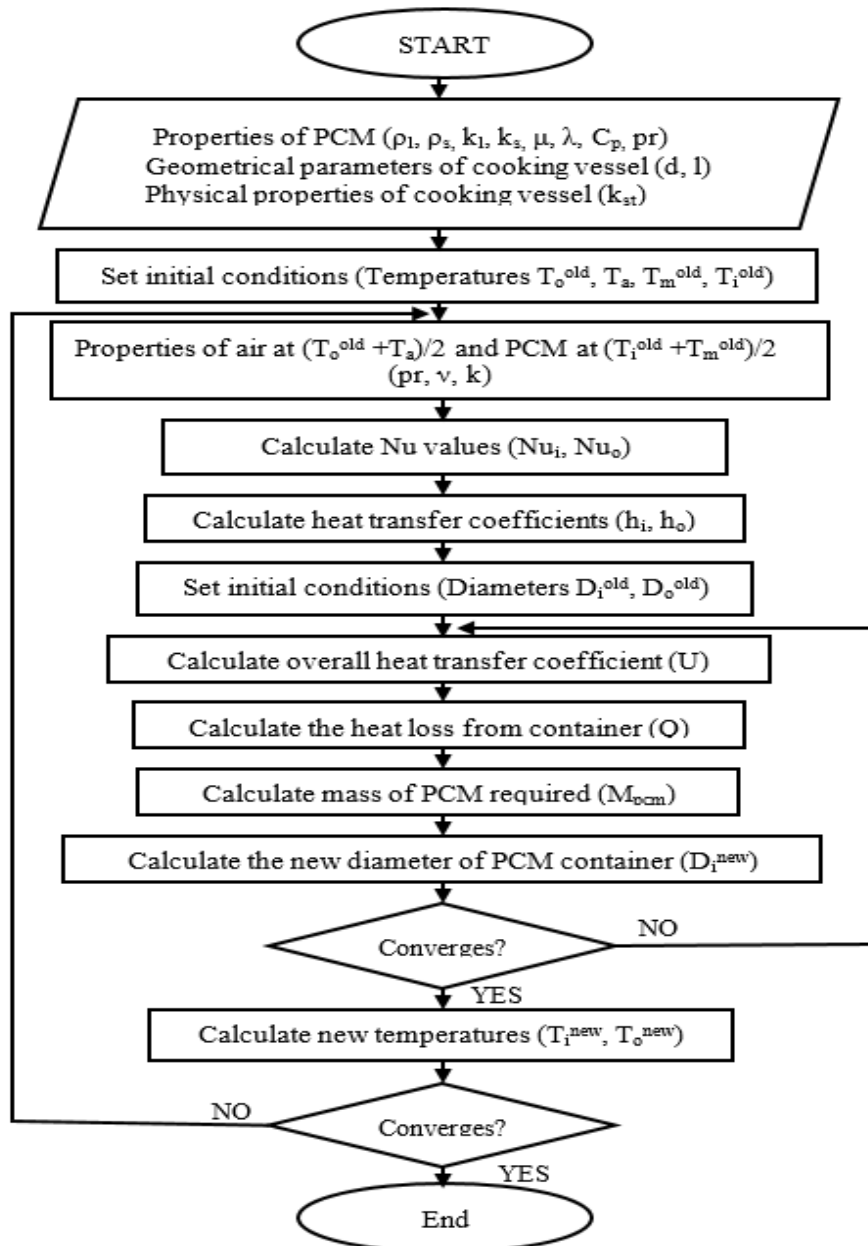
Figure 5.3 Flowchart for the computational procedure

5.2.2. Experimental investigation of TES systems

The experimental study is performed to validate the computational approach for the design of TES containers of all geometries. The thermo-physical parameters of commercial-grade paraffin wax, which is employed as the PCM for heat storage in all geometries, are shown in Table 5.1. The mass of paraffin wax required and dimensions of TES containers of different geometries surrounding the cooking vessel of diameter 16 cm and height 18 cm are calculated using the computational procedure

(Table 5.2). According to findings, optimum PCM required for 6 hours for cylindrical geometry is the least, followed by hexagonal and the most for square. Therefore, cylindrical-shaped TES unit is considered the optimum geometry as it uses the minimum mass of PCM for maintaining constant temperature for a specific duration.

Table 5.1 Thermo-physical parameters of commercial grade paraffin wax

Properties		Values
Melting temperature (°C)		55-60
Latent heat of fusion (kJ/kg)		220
Density (kg/m³)	Solid	818
	Liquid	760
Specific heat (kJ/kg °C)	Solid	2.95
	Liquid	2.51
Thermal conductivity, liquid (W/m°C)		0.22

Table 5.2 Dimensions of different geometries of TES units and required mass of PCM

Geometry	Dimension of TES container (cm)	Mass of PCM (kg)		
		Lateral side	Bottom side + Lid	Total
Cylindrical	18.7	1.01	0.416	1.426
Hexagonal	10.7	1.32	0.452	1.772
Square	17.5	1.44	0.464	1.904

Fabrication of TES Units

The TES units of cylindrical, hexagonal, and square geometries (Figure 5.4) are fabricated using stainless steel sheet of 1 mm thickness. The sheet is cut into the required shapes and dimensions using the automatic CNC machine. Bending and rolling works are carried out using hydraulic press brake bending and rolling machines, respectively. Then the parts are joined by spot/resistance welding at different locations to form the required geometry. Afterward, the joints are entirely welded by the tungsten inert gas (TIG) welding process. Finally, the grinding process is carried out for the smooth and consistent appearance of the welded parts. Two holes

are drilled on the vertical surface of the container facing in the opposite direction for inserting PCM into the cavity. The PCM can be filled in the annular cavity between the inner pot and outer TES container on the lateral side and at the bottom. The lid for all the geometries of TES units is fabricated with provisions for filling the PCM. For this, two holes are provided at the top of the lid in opposite directions.
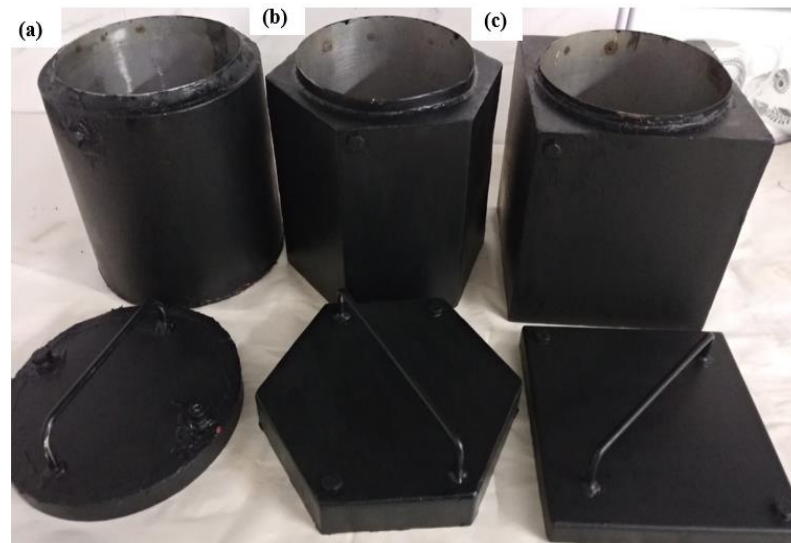
Figure 5.4 Cooking pot with TES unit and lid of different geometry (a) Cylindrical (b) Hexagonal (c) Square

The designed quantity of PCM should be filled into the TES unit to expand and solidify completely in each cycle. The TES unit is first kept vertically and partially placed in hot water during PCM filling. PCM is filled through one of the provisions at the top. At the same time, the other provision on the opposite side was kept open for the escape of air during filling. After filling at the hole level, one of them is closed, and the container is kept in a horizontal position. Then the PCM is filled, and another provision is also closed. The lid is also filled with PCM by following the same procedure. During the complete filling procedure, PCM is maintained in the liquid state by keeping the TES unit in hot water bath.

Experimental study

The experimental setup for the TES unit of hexagonal geometry is shown in Figure 5.5. The temperature of cooking pot surfaces and water is measured by using the K-type thermocouple and an indicator. The container is tested with water for the

performance study. Initially, water is heated up to 100°C and is poured into the vessel fully. Again, water in the vessel is replaced with newly boiled water. Before changing the water, the temperature of the previous water in the container is measured. Also, the temperatures of all the surfaces of the vessel are measured. This process is continued until all the surface temperature reaches the melting temperature of PCM and remains constant after that. This ensures that all PCMs in the container are melted. After PCM gets melted fully, water in the vessel is made empty, and again water at temperature above the melting point of PCM is filled in the vessel and the lid is closed. The temperature at each surface of the vessel is measured in equal intervals of time. After six hours, the water temperature is measured and compared with the expected value.
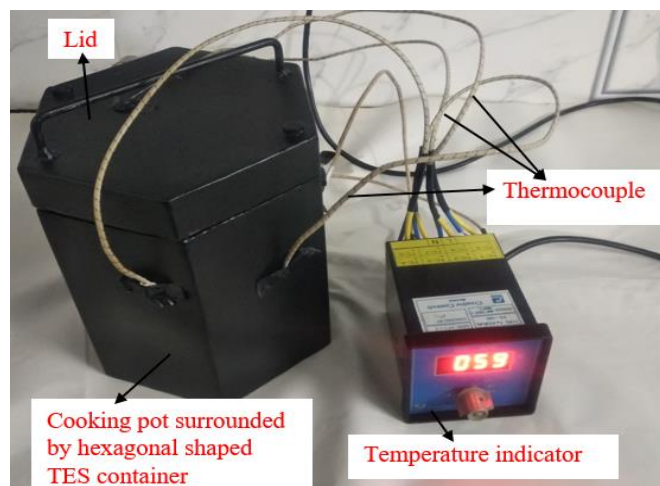
Figure 5.5 Experimental setup

5.2.3. Selection of optimum PCM for SBC

The optimum selection of PCM for the TES unit in SBC can be accomplished by calculating the criteria weights and ranking the alternatives using different MCDM methods. Firstly, the subjective and objective weights of criteria are found by using AHP, ENTROPY and CRITIC methods. Then, compromised weights are determined to account all the three methods by the linear combination. Finally, PCMs are ranked by TOPSIS, EDAS and MOORA method. The flowchart for the methodology is shown in Figure 5.6.
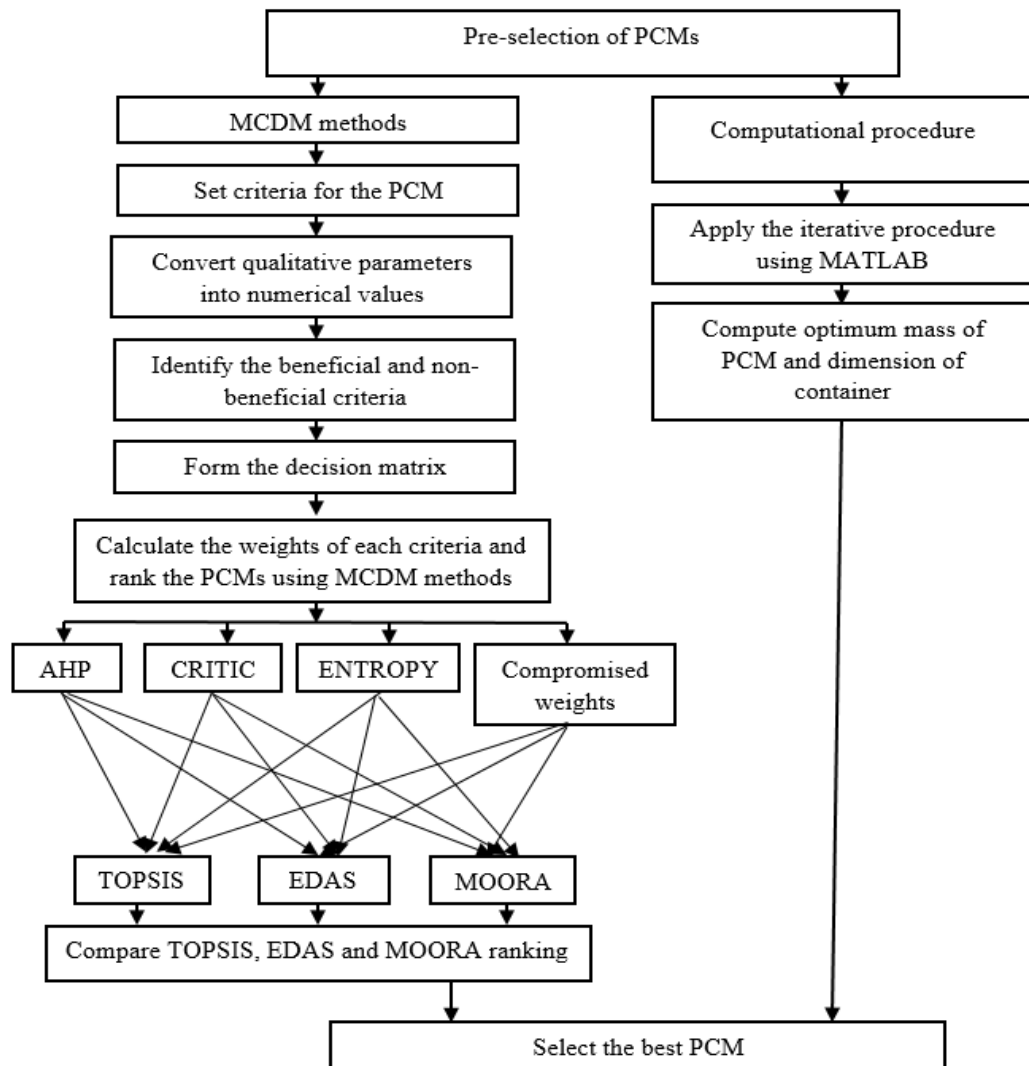
Figure 5.6 Flowchart for the methodology

AHP method for computing subjective weights

Saaty in 1970 developed AHP method to compute the subjective weights for solving multi criteria problems (Karayalcin 1982). The optimal solution is obtained with regard to the significance of various criteria and alternatives. The main drawback is that, as the number of criteria and alternatives increases, this approach would be more complicated. The procedures to be followed in AHP method are given below (Mishra et al. 2018; Sivaraja et al. 2018):

Step 1: Form the hierarchical structure based on the PCM criteria or attributes and alternatives (Figure 5.7).

Step 2: Formulate the pair-wise comparison matrix with reference to Saaty's scale of relative importance as shown in Table 5.3 (Karayalcin 1982).
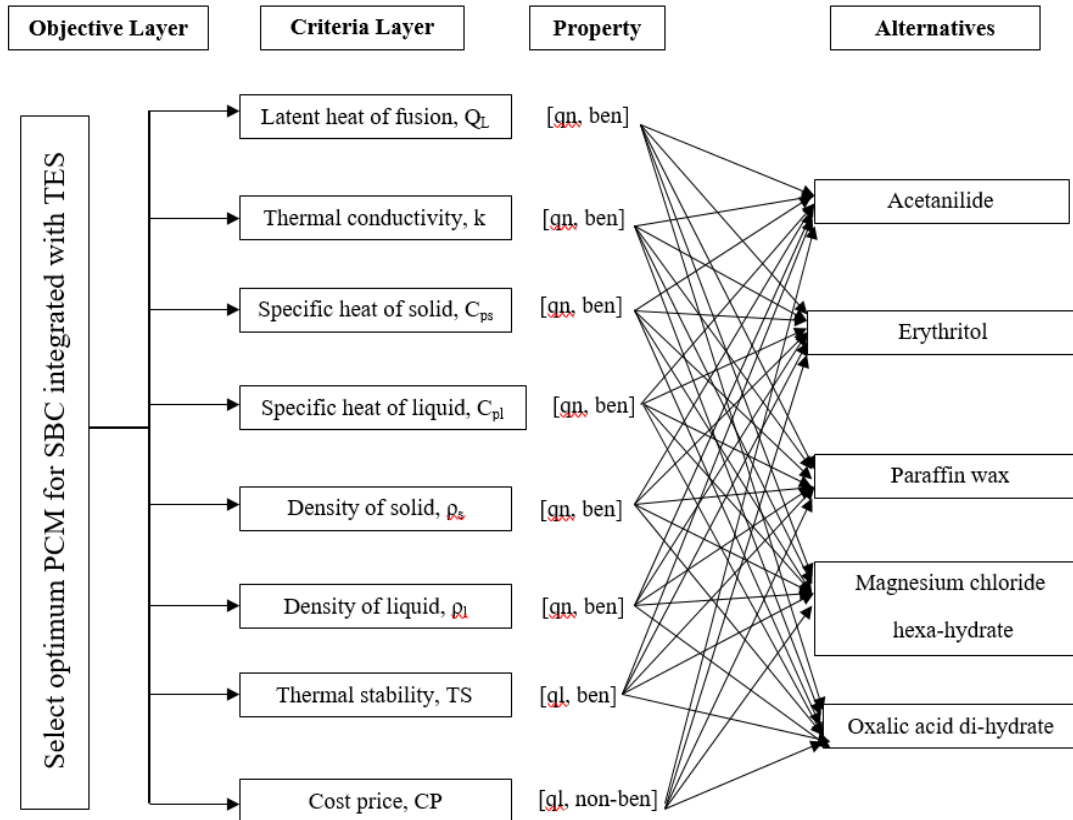
Figure 5.7 Hierarchical structure based on PCM criteria

Table 5.3 Relative significance factors (Karayalcin 1980)

Relative importance	Description
1	Equal importance
3	Moderate importance
5	Strong importance
7	Very strong importance
9	Absolute importance
2,4,6,8	Intermediate values

Step 3: Form the normalized pair-wise matrix and compute all criteria weights ($W_{j,AHP}$).

Step 4: Form the weighted matrix and check for consistency by finding consistency values, index, and ratio. Consistency values are the product of weighted index and each criteria weight.

Consistency index (CI) is calculated by,

$$CI = \frac{\lambda_{max} - n}{n - 1} \tag{5.18}$$

Where, λ_{max} is the average of consistency values and n is the number of criteria.

Consistency ratio (CR) is computed by,

$$CR = \frac{CI}{RI} \tag{5.19}$$

Random index (RI) with respect to the number of criteria is obtained from Table 5.4 (Rathod and Kanzaria 2011). Finally, to check the consistency of weights, obtained CR is compared with the accepted upper bound of 0.1.

$$\begin{cases} \text{If CR} \leq 0.1, & \text{Weights are consistent} \\ \quad \text{CR} > 0.1, & \text{Form new comparison matrix and repeat proedure} \end{cases} \tag{5.20}$$

Table 5.4 Random index values of numbers of criteria (Rathod and Kanzaria 2011)

Number of criteria	Random Index (RI)
3	0.52
4	0.89
5	1.11
6	1.25
7	1.35
8	1.4
9	1.45
10	1.49

ENTROPY method for computing objective weights

Shannon's ENTROPY method is one of the prominent methods for finding the objective weights in multi criteria problems (Lotfi and Fallahnejad 2010). This method makes use of the initial decision matrix to calculate the criteria weights. The procedures to be followed in this method are as follows (Yazdani et al. 2020):

Step 1: Prepare decision matrix.

Step 2: Normalize the decision matrix by using equation (5.21).

$$Z_{ij} = \frac{X_{ij}}{\sum_{i=1}^{n} X_{ij}} \text{ for } i = 1,2,3 \dots n; \ j = 1,2,3 \dots \dots m \tag{5.21}$$

where n is the number of alternatives and m is the number of criteria and X_{ij} is the performance index of ith alternative on j^{th} attribute.

Step 3: Compute the entropy value (e_j) by using the equation,

$$e_j = \frac{-1}{\ln(n)} \sum_{i=1}^{n} z_{ij} \ln(z_{ij}) \tag{5.22}$$

Step 4: Calculate the degree of diversification (d_j) as:

$$d_j = 1 - e_j \tag{5.23}$$

Step 5: Calculate the criteria weight ($W_{j,ENT}$) as:

$$W_{j,ENT} = \frac{d_j}{\sum_{j=1}^{m} d_j} \tag{5.24}$$

CRITIC method for computing objective weights

Diakoulaki et al. (1995) developed the CRITIC technique to find the objective weights of relative importance in MCDM problems. In the contest of decision-making framework of the problem, this approach involves both the severity of the contrast and the conflict. The standard deviation of the normalized criterion values by columns and the correlation coefficients of all pairs of columns are used to evaluate the criteria-contrast. In order to assess the information in the attributes under which alternatives are evaluated, this method relies on an empirical analysis of the decision matrix. The step-by-step procedure to be followed is given below (Diakoulaki et al. 1995):

Step 1: Normalize decision matrix by using the equation as:

$$z_{ij} = \frac{x_{ij} - x_j^{worst}}{x_j^{best} - x_j^{worst}}$$ (5.25)

where, x_j^{best} and x_j^{worst} are respectively the maximum and minimum values for beneficial and minimum and maximum for non-beneficial attributes in the decision matrix. For beneficial criteria, larger values are preferred whereas for non-beneficial, smaller values are preferred.

Step 2: Compute the standard deviation (σ_j) for each criterion.

Step 3: Form a matrix of order m x m by finding the elements (Z_{jk}) as linear correlation between Z_j and Z_k.

Step 4: Find the measure of conflict made by criterion j with respect to the decision condition defined by remaining criteria as,

$$\sum_{k=1}^{m}(1 - r_{jk})$$ (5.26)

Step 5: Find the quantity of information for each criterion as:

$$C_j = \sigma_j \sum_{k=1}^{m}(1 - r_{jk})$$ (5.27)

Step 6: Calculate the weights as,

$$W_{j,CRI} = \frac{C_j}{\sum_{k=1}^{m} C_j}$$ (5.28)

Compromised weights calculation

The weights obtained through AHP ($W_{j,AHP}$), ENTROPY ($W_{j,ENT}$) and CRITIC ($W_{j,CRI}$) methods are converted to compromised weights by linear combination between them. The compromised weights ($W_{j,AE}$) between $W_{j,AHP}$ and $W_{j,ENT}$ are computed using the equation as given below,

$$W_{j,AE} = \frac{W_{j,AHP}W_{j,ENT}}{\sum_{j=1}^{j=n}(W_{j,AHP}W_{j,ENT})}$$ (5.29)

where n is the number of criteria. Similarly, compromised weights ($W_{j,AC}$) between $W_{j,AHP}$ and $W_{j,CRI}$ is obtained as,

$$W_{j,AC} = \frac{W_{j,AHP}W_{j,CRI}}{\sum_{j=1}^{j=n}(W_{j,AHP}W_{j,CRI})} \quad\quad (5.30)$$

Also, compromised weights (W_j) between the weights obtained through all three methods are calculated using,

$$W_j = \frac{W_{j,AHP}W_{j,CRI}W_{j,ENT}}{\sum_{j=1}^{j=n}(W_{j,AHP}W_{j,CRI}W_{j,ENT})} \quad\quad (5.31)$$

TOPSIS method

The TOPSIS method is based on the selection of optimum alternative at the shortest distance from ideal positive and longest distance from ideal negative solution (Trilok and Gnanasekaran 2021). The ideal positive solution maximizes the benefit and minimizes non-beneficial criteria. Whereas the negative ideal solution minimizes the benefits and maximizes non-beneficial criteria. The procedure to reach optimum solution is as follows (Trilok and Gnanasekaran 2021):

Step 1: Formulate the decision matrix

Step 2: Normalize the decision matrix by using equation (5.32),

$$Z_{ij} = \frac{X_{ij}}{\sqrt{\sum_{i=1}^{n}X_{ij}^2}} \quad\quad (5.32)$$

Step 3: Calculate the weighted normalized decision matrix as:

$$Y_{ij} = w_j Z_{ij} \quad\quad (5.33)$$

where, Y_{ij} is the weighted normalized value.

Step 4: Find the ideal positive (best) and negative (worst) value. Ideal best solution (Y_j^+) will be the maximum value for the benefit and the minimum value for the non-beneficial criteria in the weighted normalized matrix. Similarly, ideal worst solution (Y_j^-) is the minimum value for the benefit and the maximum for non-beneficial criteria.

Step 5: Compute Euclidean distance from ideal best and worst solution as:

$$E_i^+ = \left[\sum_{j=1}^{m}\left(Y_{ij} - Y_j^+\right)^2\right]^{0.5} \tag{5.34}$$

$$E_i^- = \left[\sum_{j=1}^{m}\left(Y_{ij} - Y_j^-\right)^2\right]^{0.5} \tag{5.35}$$

Step 6: Calculate the value of relative closeness (RC) to the perfect solution as:

$$RC_i = \frac{E_i^-}{E_i^+ + E_i^-} \tag{5.36}$$

Step 7: Rank the alternatives based on the value of RC.

EDAS method

EDAS is one of the important MCDM techniques for selecting best alternative based on various attributes. In this method, the best alternative will be corresponding to the distance from the average solution (Keshavarz-Ghorabaee et al. 2015). Here, in the first step, positive distance (PDA) and the negative distance from the average (NDA) are to be calculated which indicates the difference between each alternative and average solution. Higher PDA and lower NDA values would therefore imply optimum solution. The procedure to obtain optimum solution is given below (Yazdani et al. 2020):

Step 1: Formulate the decision matrix.

Step 2: Find the average solution ($AV_{,j}$) using equation (5.37),

$$AV_j = \frac{\sum_{i=1}^{n} X_{ij}}{n} \tag{5.37}$$

Step 3: Calculate positive distance from average solution (PDA) by using equation (5.38).

$$PDA_{ij} = \begin{cases} \frac{\max\{0,(X_{ij}-X_{av,j})\}}{X_{av,j}}, & \text{if } j^{th} \text{ attribute is beneficial} \\ \frac{\max\{0,(X_{av,j}-X_{ij})\}}{X_{av,j}}, & \text{if } j^{th} \text{ attribute is non} - \text{beneficial} \end{cases} \tag{5.38}$$

Step 4: Calculate negative distance from average solution (NDA) by using equation (5.39).

$$NDA_{ij} = \begin{cases} \dfrac{\max\{0,(X_{av,j}-X_{ij})\}}{X_{av,j}}, \text{if } j^{th} \text{ attribute is beneficial} \\ \dfrac{\max\{0,(X_{ij}-X_{av,j})\}}{X_{av,j}}, \text{if } j^{th} \text{ attribute is non} - \text{beneficial} \end{cases} \qquad (5.39)$$

Step 4: Calculate the weighted sum of PDA and NDA by using equations (5.40-5.41),

$$SP_i = \sum_{j=1}^{m} w_j\, PDA_{ij} \qquad (5.40)$$

$$SN_i = \sum_{j=1}^{m} w_j\, NDA_{ij} \qquad (5.41)$$

Step 5: Normalize the weighted sum values using equations as given below.

$$NSP_i = \frac{SP_i}{\max_i(SP_i)} \qquad (5.42)$$

$$NSN_i = 1 - \frac{SN_i}{\max_i(SN_i)} \qquad (5.43)$$

Step 6: Calculate the appraisal score (AS_i) by taking average of NSP_i and NSN_i and rank the alternatives.

MOORA method

The MOORA method was developed by Brauers in 2006 to solve different complex decision-making problems in the manufacturing sector. The procedure to be followed in solving the problem is as follows (Sharma et al. 2018):

Step 1: Prepare the decision matrix.

Step 2: Normalize the decision matrix by using equation (5.44),

$$Z_{ij} = \frac{X_{ij}}{\sqrt{\sum_{i=1}^{n} X_{ij}^2}} \text{ for } i = 1,2,3 \dots n; \ j = 1,2,3 \dots \dots m \qquad (5.44)$$

Step 3: Form the weighted normalized decision matrix using,

$$Y_{ij} = w_j\, Z_{ij} \qquad (5.45)$$

Step 4: Calculate normalized assessment value (NAV) of each alternative by subtracting the sum of weighted normalized values of non-beneficial from beneficial criteria as given by,

$$NAV = \sum_{j=1}^{k} Y_{ij} - \sum_{j=k+1}^{m} Y_{ij} \qquad (5.46)$$

where, k and m-k are the number of beneficial and non-beneficial criteria.

Step 5: Rank the alternatives based on the descending value of NAV.

5.3. Results and discussion

5.3.1. Computational procedure for optimum design of TES

A computational procedure is developed for the optimal design of the TES system for SBC. Next, cooking pot integrated with TES units of cylindrical, square, and hexagonal geometries is designed and fabricated using the computational procedure. Then, the computational approach is validated by conducting experiments on TES units using paraffin wax (melting temperature of 55-60°C) as the PCM. The computational procedure is also validated by comparing it to previous experimental studies. Finally, the optimum PCM for the SBC is selected based on the computational procedure.

Validation of computational procedure

A comparison is made between optimal dimensions and quantities of PCMs required for TES unit surrounding the cooking vessel, derived from the computational approach, and those determined from earlier experimental studies (Sharma et al. 2000; Buddhi et al. 2003). Unlike previous works (Sharma et al. 2000; Buddhi et al. 2003) that did not optimize the container diameter or PCM quantity, present results provide optimal value for the duration of constant temperature. Table 5.5 shows TES dimensions and optimum duration calculated using the computational approach. According to (Sharma et al. 2000), they used cylindrical container with 25 cm diameter that surrounded cooking pot with 18 cm diameter and 8 cm height that was exposed to experimentation on the SBC (Figure 5.1 (a)). In this work, optimal PCM required is determined to be 2 kg and the container diameter 25.36 cm to keep steady temperature for 6.6 hours. It appears that diameter of TES unit calculated in the

present approach differs by 1.4% from previous work (Sharma et al. 2000). A similar apparatus is used by Buddhi et al. (2003), which comprises container with diameter of 30 cm and height of 12.5 cm, with 4 kg of acetanilide inside, as shown in figure 5.1 (b). According to the present study, maintaining constant temperature for 4.04 hours requires optimal PCM of 4 kg and container size of 28.63 cm. There is 4.5% variation in the diameter of TES units computed by the present study compared with previous work (Buddhi et al. 2003). Accordingly, comparing the current approach with both works, variation of TES unit dimensions is within ±5%, acceptable. The proposed computational procedure is thus validated. As per the findings of both studies, quantity of PCM necessary to keep steady temperature is time dependent. Earlier works did not specify the length of time for maintaining constant temperature. However, for fabricating SC, it is important to know how much PCM is necessary to store the optimum amounts of heat.

Table 5.5 Comparison of dimension of TES unit with earlier works

| Sl No. | Previous Works | | | | | Present Work | |
	Author	PCM and T_{mp} (ºC)	Cooking vessel dimensions (cm)	m_{pcm} (kg)	D_i (cm)	Time (Hr)	D_i (cm)
1	Sharma et al. 2000	Acetamide 82	d_i =18 l =8	2	25	6.6	25.36
2	Buddhi et al. 2003	Acetanilide 118.9	d_i =20 l=12.5	4	30	4.04	28.63

Optimal geometry selection

Cylindrical, square, and hexagonal shapes are considered for determining optimum TES unit geometry. TES containers are designed by using the computational procedure developed in this study. Two different cooking vessels are considered for the study, one measuring 16 cm in diameter and 20 cm in height with paraffin wax and the other measuring 18 cm and 8 cm with acetamide as PCM. The optimal PCM for constant temperature in the cooking vessel for 6 hours is found through iterative solution procedure. Container size is determined from the estimated quantity of PCM.

In both cases, cylindrical containers encircling the cooking vessel use least PCM (Table 5.6). For this reason, cylindrical geometry is chosen as the best TES unit.

Table 5.6 Geometry comparison of PCM containers

Sl No.	PCM	T_{mp} (°C)	Dimensions of cooking pot (cm)	Cylindrical		Square		Hexagonal	
				D_i (cm)	m_{pcm} (kg)	L_i (cm)	m_{pcm} (kg)	L_i (cm)	m_{pcm} (kg)
1	Paraffin wax	60	$d_i = 16$ $l = 20$	20.1	1.77	19.12	2.5	11.6	2.28
2	Acetamide	82	$d_i = 18$ $l = 8$	24.6	1.77	22.67	2.07	13.7	1.88

Performance comparison of TES units by experimental investigation

In testing, cooking pot is filled with water at temperature higher than melting point of paraffin wax, which is then covered with lid. Every 30 minutes, the surface temperature is recorded. The temperature of the water is also monitored after 6, 7, and 8 hours. The surface temperature of cylindrical TES unit is increased from 43°C to 62°C after 45 minutes. At the same time, lid temperature rises from 38°C to the maximum of 56°C after 1 hour and 15 minutes. Figures 5.8 (a-c) illustrate variation in surface and lid temperatures of cylindrical, square, and hexagonal TES units. For square-shaped TES unit, temperatures are measured at the four side faces denoted as surface 1, 2, 3, and 4, as depicted in Figure 5.8 (b). Similarly, for hexagonal geometry, all the six side faces are considered for temperature measurement denoted by surface 1, 2, 3, 4, 5, and 6, as shown in Figure 5.8 (c). The side faces for square and hexagonal geometry of TES units exhibit nearly equal temperatures at every time. The temperature of surface and lid falls in small units after 1 hour and 45 minutes from the start of the test. This shows that paraffin wax maintains nearly constant temperature during phase change. The TES units of cylindrical, hexagonal, and square geometries are developed based on computational procedure to keep water temperature within the range of 55-60°C for six hours. Figure 5.9 shows variations in water temperature for cylindrical, square, and hexagonal TES units over time. The results show that after 6 hours, all geometries of TES units keep the water temperature

at the same level as the melting point of paraffin wax (55-60°C). The experimental results, therefore, clearly validate the computational approach for all configurations of TES units. The water temperature then decreases for all the geometries and TES unit with square shape is slightly lower than those with cylindrical and hexagonal geometries. Also, the results indicate that cylindrical TES unit performs best among all other geometries.
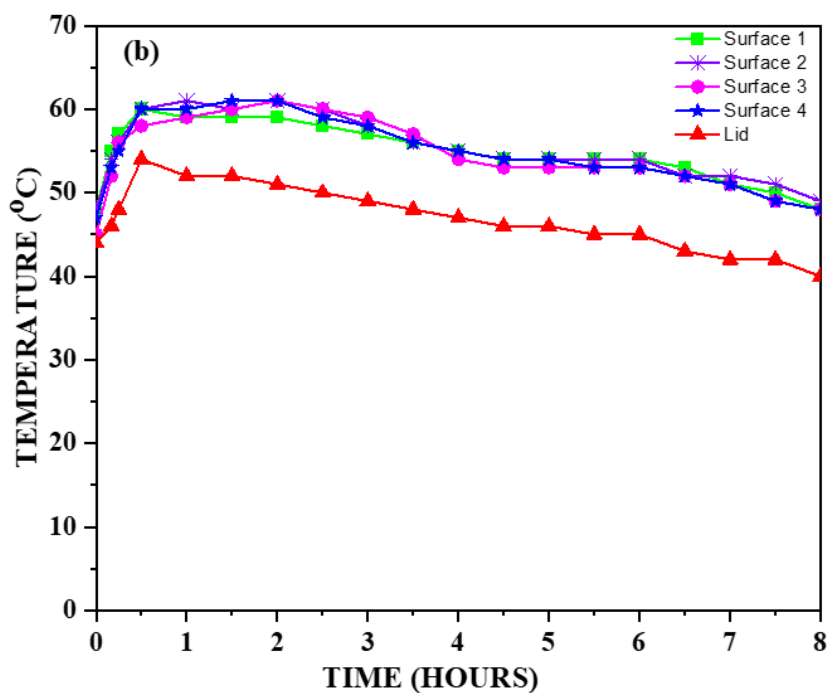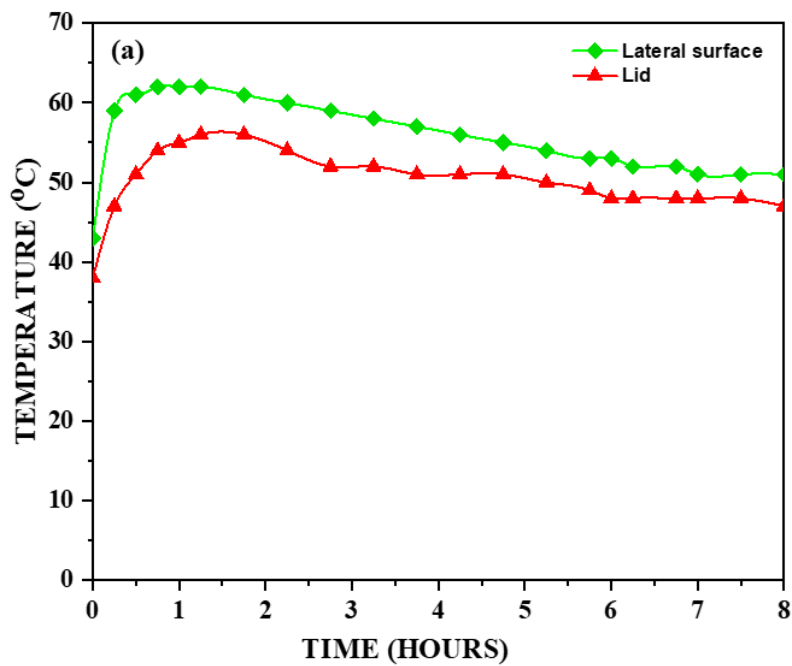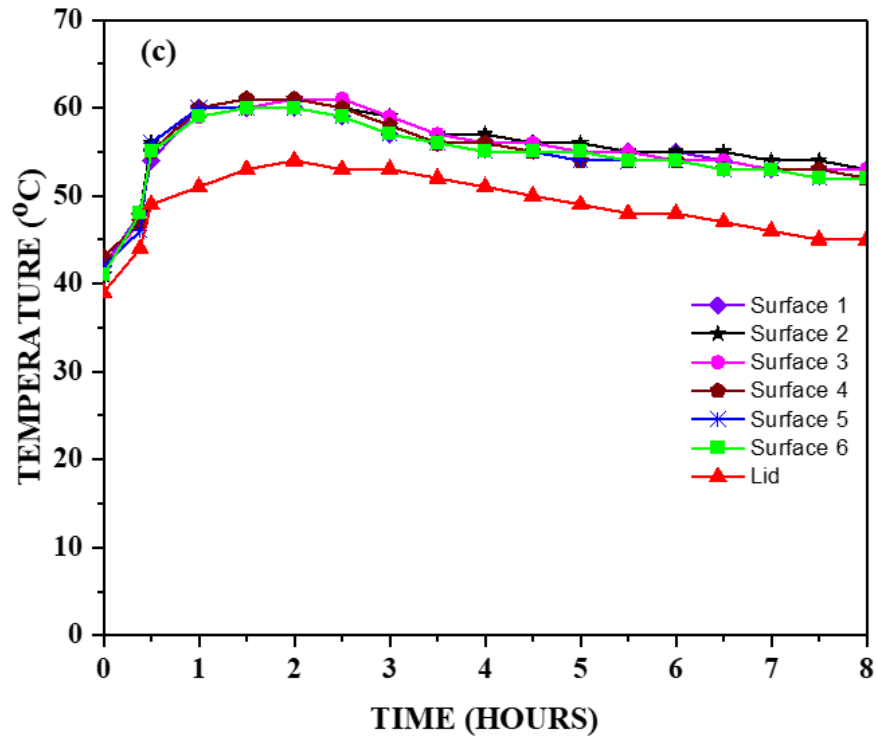
Figure 5.8 Variation of surface temperature of different geometries of TES unit with time (a) cylindrical (b) square (c) hexagonal
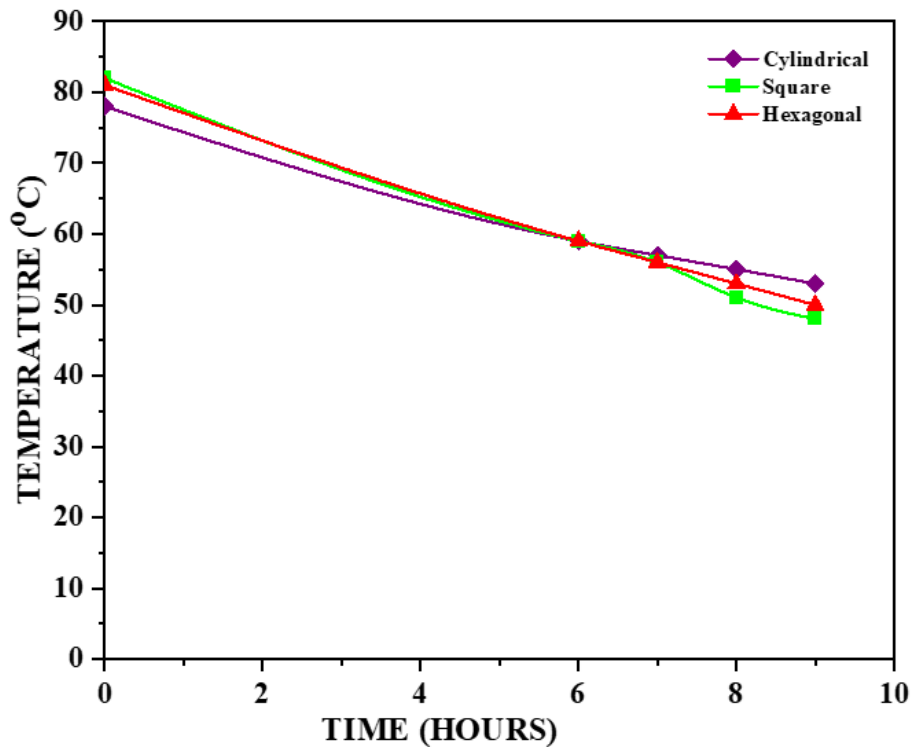
Figure 5.9 Variation of water temperatures in different geometries of TES units with time

Selection of optimum PCM using computational procedure

The mass of PCM and the size of the TES unit required for the evening cooking with SBC by employing different PCMs such as erythritol, magnesium chloride hexa-hydrate and acetanilide (Table 5.7) are determined using the developed computational procedure. The cooking pot of 20 cm diameter and 10 cm height is considered for the study. The optimum mass of PCM (m_{pcm}) and the size of the PCM container (D_i) are computed for keeping the cooking load at the melting temperature of PCM for different duration of time. The melting temperatures of PCMs such as erythritol, magnesium chloride hexa-hydrate and acetanilide are about 118°C, which is necessary for cooking above 100°C during sun-down time. The results indicate that, the designed mass of PCM is less for erythritol (6.06 kg) compared to magnesium chloride hexa-hydrate (16.02 kg) and acetanilide (13.25 kg) for time duration of 9 hours. Therefore, the size of the TES unit employing erythritol, magnesium chloride hexa-hydrate and acetanilide are 31.52 cm, 41.32 cm and 45.33 cm respectively. The same is the case for 6 hours and 3 hours duration.

Table 5.7 Comparison of mass of PCM and size of the TES unit using computational procedure

Sl No.	PCM	Melting point (°C)	Size of the TES unit, D_i (cm)			Mass of PCM (kg)		
			t= 9 hrs	t= 6 hrs	t= 3 hrs	t = 9 hrs	t= 6 hrs	t= 3 hrs
1	Erythritol	118	31.52	27.24	23.39	6.06	3.49	1.5
2	$MgCl_2.6H_2O$	118	41.32	33.17	25.97	16.02	8.58	3.37
3	Acetanilide	118.9	45.33	35.60	27.01	13.25	6.95	2.64

From the results of iterative procedure for the design of TES unit, it is clear that erythritol shows minimum quantity of requirement for maintaining the constant temperature for specific duration of time. Therefore, erythritol is selected as the best PCM to be used for TES unit incorporated with SBC.

5.3.2. Selection of optimum PCM by MCDM methods

Preselection of PCM

A number of PCMs have been tested in SBC for TES unit for the last few years (Nkhonjera et al. 2017; Omara et al. 2020). The melting temperature of PCMs used in the earlier works ranges from 41 to 119°C. Since the cooking is accomplished with the temperature above the boiling point of water, PCM with melting point more than 100°C is essential. This is the only criterion required for the preselection of PCM for heat storage in SBC. Therefore, PCMs having melting temperature in the range 100-119°C are selected for the optimum analysis (Table 5.8).

Table 5.8 Thermo-physical properties of selected PCMs

Properties		Acetanilide	Erythritol	Paraffin wax	Magnesium chloride hexa-hydrate	Oxalic acid di-hydrate
Melting Point, (°C)		118.9	118	100	118	101
LH of fusion, (kJ/kg)		222	339	140	167	370
Density (kg/m³)	solid	1210	1480	880	1569	1650
	liquid	1020	1300	770	1450	1600
Specific heat (kJ/kg K)	solid	2	1.38	1.8	1.72	1.62
	liquid	2	2.76	2.4	2.82	1.62
Thermal conductivity (W/mK)	solid	0.5	0.733	0.21	0.694	0.57
	liquid	0.5	0.326	0.21	0.57	0.57
Thermal stability		Average	High	Very High	Low	Low
Cost Price		Average	High	Low	High	Above average

Criteria for the optimum selection

The quantitative index such as latent heat of fusion (Q_L), thermal conductivity (k_s), density of solid (ρ_s), density of liquid (ρ_l), specific heat of solid (C_{ps}), specific heat of

liquid (C_{pl}) and qualitative index like thermal stability (TS) and cost price (CP) of PCM are identified as the criteria for the optimum selection. Here, Q_L, k_s, ρ_s, ρ_l, C_{ps}, C_{pl} and TS are the beneficial criteria whereas cost price is non-beneficial. The thermo-physical properties of PCMs are obtained from the earlier works (Table 5.8).

Here, thermal stability and cost of PCMs are expressed in qualitative parameter instead of quantitative. Each qualitative parameter is converted to fuzzy scores according to the eleven-point scales as shown in Table 5.9 (Rathod and Kanzaria 2011). The converted numerical values corresponding to each qualitative parameter are shown in Table 5.10.

Table 5.9 Conversion of linguistic terms into fuzzy scores (Rathod and Kanzaria 2011)

Linguistic term	Crisp score
Exceptionally low	0.045
Extremely low	0.135
Very low	0.255
Low	0.335
Below average	0.410
Average	0.500
Above average	0.590
High	0.665
Very high	0.745
Extremely high	0.865
Exceptionally high	0.955

Table 5.10 Numerical values of qualitative parameter

PCM	Thermal stability	Cost Price
Acetanilide	0.50	0.50
Erythritol	0.665	0.665
Paraffin wax	0.745	0.335
Magnesium chloride hexa-hydrate	0.335	0.665
Oxalic acid di-hydrate	0.335	0.590

Weight calculation

The weightage of different criteria is obtained by using AHP, CRITIC and ENTROPY method.

AHP method

In this method, firstly pair-wise comparison matrix is formulated which is given by,

$$
\begin{bmatrix}
 & Q_L & k_s & C_{ps} & C_{pl} & \rho_s & \rho_l & TS & CP \\
Q_L & 1 & 5 & 7 & 7 & 5 & 5 & 6 & 9 \\
k_s & 1/5 & 1 & 5 & 5 & 2 & 2 & 3 & 7 \\
C_{ps} & 1/7 & 1/5 & 1 & 1 & 1/5 & 1/5 & 2 & 3 \\
C_{pl} & 1/7 & 1/5 & 1 & 1 & 1/5 & 1/5 & 2 & 3 \\
\rho_s & 1/5 & 1/2 & 5 & 5 & 1 & 1 & 3 & 7 \\
\rho_l & 1/5 & 1/2 & 5 & 5 & 1 & 1 & 3 & 7 \\
TS & 1/6 & 1/3 & 1/2 & 1/2 & 1/3 & 1/3 & 1 & 4 \\
CP & 1/9 & 1/7 & 1/3 & 1/3 & 1/7 & 1/7 & 1/4 & 1
\end{bmatrix}
\quad (5.47)
$$

For TES unit employing PCM as LHS material, latent heat is the most important among all the criteria. Thermal conductivity and density of PCM also play major role in the heat storage. Higher values of latent heat and thermal conductivity results in larger heat transfer and thermal stability. Also, more density indicates lesser volume for the PCM storage. The nine-point scale of Saaty is used to assess the relative importance of the criteria to formulate pair-wise comparison matrix (Karayalcin 1980). Accordingly, comparison has been made by considering absolute importance to latent heat of PCM with reference to cost price and assigned relative importance value of 9 for Q_L over CP. Whereas, with reference to specific heat capacity of PCM, latent heat is considered very strong importance and assigned value of 7 for Q_L over C_{ps} and C_{pl}. Likewise, all the pair-wise comparison has been made and the corresponding matrix is formulated. The normalized weights of each criterion and consistency values are determined (Table 5.11). The consistency ratio (CR) is calculated by dividing consistency index (CI) with random index (RI) value. Finally,

the consistency check of the AHP method is carried out and consistency ratio (CR) is obtained as 0.067 which is lesser than the accepted upper limit value of 0.1. Therefore, the obtained weights are consistent. The weightage for latent heat of fusion and thermal conductivity are found to be 39.9 % and16.8% respectively. Since this method finds the weightage from the pairwise comparison matrix and relative importance scale, it gives more weights to the latent heat of fusion as it is most important criteria for TES unit. We obtained less weightage of 2% for cost of PCM as it is insignificant criteria for the performance of TES unit.

Table 5.11 Weights by AHP method and consistency check

Criteria	Weighted sum value	Criteria weights (W_{AHP})	Consistency values (λ)
Q_L	3.723	0.399	9.339
k_s	1.549	0.168	9.205
C_{ps}	0.395	0.048	8.212
C_{pl}	0.395	0.048	8.212
ρ_s	1.195	0.135	8.850
ρ_l	1.195	0.135	8.850
TS	0.387	0.047	8.286
CP	0.171	0.020	8.324
Average, λ_{max}			8.66
CI			0.094
CR			0.067

CRITIC method

This method normalizes the decision matrix, finds the standard deviation for each criterion and finally calculate the objective weights by following the procedures detailed in methodology section. The criteria weights obtained through CRITIC method is given in Table 5.12. Here, cost, and thermal stability of PCM is found to be more important criteria with weightage of 15.5% and 15.2% respectively. Whereas less weightage is obtained for thermal conductivity of PCM with 10.2%. Also, it is

clear that the weightage of all the criteria varies in small percentage with an average value of 12.5 %.

ENTROPY method

Here, the weightage of each attribute is computed by ENTROPY method. This method normalizes the decision matrix and computes the weight vector from the calculated entropy value of each criterion. The criteria weightage computed using ENTROPY method is given in Table 5.12. The weightage for latent heat of fusion and thermal conductivity are found to be 23% and 22.9 % respectively. The results indicate that latent heat of fusion is more relevant criteria to be focussed while selecting the optimum PCM for TES system. Also, thermal conductivity is equally important that of latent heat of fusion with small decrement in weightage. Here, less weightage is obtained for specific heat of solid PCM having 2.5%.

Compromised weights

The resulting compromised weights of each criterion are shown in Table 5.12. Here, W_j which is the compromised weights between all the three methods is almost similar to $W_{j,AE}$ which is between AHP and ENTROPY method. This is because the variation of weightage obtained through CRITIC method for all criteria is less. Maximum weightage is for latent heat of fusion with 54.8% followed by thermal conductivity of PCM with 19.6%.

Table 5.12 Criteria weights and compromised value

Weights	Q_L	k_s	C_{ps}	C_{pl}	ρ_s	ρ_l	TS	CP
W_{AHP}	0.399	0.168	0.048	0.048	0.135	0.135	0.047	0.020
W_{ENT}	0.230	0.229	0.025	0.067	0.076	0.103	0.178	0.091
W_{CRI}	0.119	0.102	0.131	0.126	0.108	0.106	0.152	0.155
$W_{j,AE}$	0.543	0.227	0.007	0.02	0.061	0.083	0.049	0.011
$W_{j,AC}$	0.409	0.148	0.054	0.052	0.125	0.123	0.061	0.027
W_j	0.548	0.196	0.008	0.021	0.056	0.074	0.063	0.015

Optimum selection of PCM by MCDM methods

The criteria weights obtained by AHP, ENTROPY and CRITIC methods and also compromised values are considered for the optimum selection of PCM by MCDM techniques such as TOPSIS, EDAS and MOORA.

TOPSIS method

To select the optimum PCM among different alternatives, TOPSIS method is used for which normalized decision matrix is shown in Table 5.13. The weighted normalized decision matrix with ideal and non-ideal solutions are given in 5.14. Since the TOPSIS method is distance-based approach, distance from the best and worst alternative are calculated. Finally, the relative closeness (RC) values are computed to rank the alternatives (Table 5.15). In the first stage, criteria weights by AHP method are taken to form the weighted normalized matrix. Therefore, this technique can be referred as AHP-TOPSIS method. As per ranking made by AHP-TOPSIS method, erythritol is selected as best alternative having comparatively higher latent heat of fusion (339 kJ/kg) and thermal conductivity (0.733 W/Mk) which are beneficial criteria.

Table 5.13 Normalized decision matrix

PCM	Q_L	k_s	C_{ps}	C_{pl}	ρ_s	ρ_l	TS	CP
Acetanilide	0.376	0.391	0.521	0.378	0.390	0.366	0.412	0.396
Erythritol	0.574	0.573	0.360	0.522	0.477	0.467	0.548	0.527
Paraffin wax	0.237	0.164	0.469	0.454	0.284	0.277	0.614	0.265
MgCl$_2$.6H$_2$O	0.283	0.542	0.448	0.533	0.506	0.521	0.276	0.527
Oxalic acid di-hydrate	0.627	0.445	0.422	0.306	0.532	0.548	0.276	0.467

By following the same procedure of TOPSIS method, the relative closeness value and ranking are made with other criteria weights. Like AHP-TOPSIS, the MCDM method of optimization using criteria weights obtained through ENTROPY and CRITIC

techniques are referred as ENTROPY-TOPSIS and CRITIC-TOPSIS method respectively. Ranking of different PCMs using AHP-TOPSIS, ENTROPY-TOPSIS, CRITIC-TOPSIS and compromised weights incorporated TOPSIS method are made as shown in Table 5.15. All results give erythritol as optimum PCM from various alternatives for heat storage medium in SBC. Oxalic di-hydrate is found to be the second-best alternative used for TES unit in SBC. But, other three alternatives vary between the four methods of MCDM.

Table 5.14 Weighted Normalized decision matrix with ideal and non -ideal values and distance measurement

PCM	Q_L	k_s	C_{ps}	C_{pl}	ρ_s	ρ_l	TS	CP	E_i^+	E_i^-
Acetanilide	0.150	0.066	0.025	0.018	0.053	0.049	0.019	0.008	0.110	0.071
Erythritol	0.229	0.096	0.017	0.025	0.064	0.063	0.026	0.011	0.027	0.156
Paraffin wax	0.095	0.028	0.023	0.022	0.038	0.037	0.029	0.005	0.177	0.019
$MgCl_2.6H_2O$	0.113	0.091	0.022	0.026	0.068	0.070	0.013	0.011	0.138	0.081
Oxalic acid di-hydrate	0.250	0.075	0.020	0.015	0.072	0.074	0.013	0.009	0.029	0.170
Y_j^+	0.250	0.096	0.025	0.026	0.072	0.074	0.029	0.005		
Y_j^-	0.095	0.028	0.017	0.015	0.038	0.037	0.013	0.011		

Table 5.15 Ranking of PCMs using TOPSIS method with different criteria weights

PCM	AHP-TOPSIS		ENTROPY-TOPSIS		CRITIC-TOPSIS		Compromised weights (W_j) - TOPSIS	
	RC	Rank	RC	Rank	RC	Rank	RC	Rank
Acetanilide	0.392	3	0.447	4	0.450	4	0.383	3
Erythritol	0.854	1	0.813	1	0.628	1	0.871	1
Paraffin wax	0.096	5	0.328	5	0.482	3	0.087	5
$MgCl_2.6H_2O$	0.368	4	0.477	3	0.439	5	0.3	4
Oxalic acid di-hydrate	0.852	2	0.619	2	0.497	2	0.869	2

EDAS method

In this method, firstly the average solution (AV_j) of each criterion is evaluated. Then positive and negative distances from average solution (PDA and NDA) are calculated for each cell in the decision matrix as shown in Table 5.16 and 5.17.

Table 5.16 PDA values

PCM	Q_L	k_s	C_{ps}	C_{pl}	ρ_s	ρ_l	TS	CP
Acetanilide	0	0	0.174	0	0	0	0	0.093
Erythritol	0.369	0.354	0	0.190	0.090	0	0.289	0
Paraffin wax	0	0	0.056	0.034	0	0	0.444	0.392
MgCl$_2$.6H$_2$O	0	0.282	0.009	0.216	0.156	0.068	0	0
Oxalic acid di-hydrate	0.494	0.053	0	0	0.215	0.123	0	0

Table 5.17 NDA values

PCM	Q_L	k_s	C_{ps}	C_{pl}	ρ_s	ρ_l	TS	CP
Acetanilide	0.103	0.076	0	0.138	0.109	0.159	0.031	0
Erythritol	0	0	0.190	0	0	0	0	0.207
Paraffin wax	0.435	0.612	0	0	0.352	0.365	0	0
MgCl$_2$.6H$_2$O	0.326	0	0	0	0	0	0.351	0.207
Oxalic acid di-hydrate	0	0	0.049	0.302	0	0	0.351	0.071

The same criteria weights as obtained by AHP method (Table 5.11) is used to evaluate the weighted PDA and NDA values of each cell. Thus, this method can be referred as AHP-EDAS method. Then the weighted sum of PDA and NDA values is calculated for each alternative (Table 5.18-5.19). In the next step, normalized values of weighted sum of PDA and NDA denoted by NSP_i and NSN_i are calculated. Finally, ranking is made by comparing the average of NSP_i and NSN_i values (Table 5.20).

AHP-EDAS method of MCDM also selects erythritol as the best PCM similar to the results of TOPSIS method.

Table 5.18 Weighted sum of PDA values (SP$_i$)

PCM	Q_L	k_s	C_{ps}	C_{pl}	ρ_s	ρ_l	TS	CP	WS_i^+
Acetanilide	0	0	0.008	0	0	0	0	0.002	0.010
Erythritol	0.147	0.059	0	0.009	0.012	0	0.014	0	0.242
Paraffin wax	0	0	0.003	0.002	0	0	0.021	0.008	0.033
MgCl$_2$.6H$_2$O	0	0.047	0.00008	0.010	0.021	0.009	0	0	0.088
Oxalic acid di-hydrate	0.197	0.009	0	0	0.029	0.017	0	0	0.252

Table 5.19 Weighted sum of NDA values (SN$_i$)

PCM	Q_L	k_s	C_{ps}	C_{pl}	ρ_s	ρ_l	TS	CP	WS_i^-
Acetanilide	0.041	0.013	0	0.007	0.015	0.021	0.001	0	0.098
Erythritol	0	0	0.009	0	0	0	0	0.004	0.013
Paraffin wax	0.173	0.103	0	0	0.048	0.049	0	0	0.373
MgCl$_2$.6H$_2$O	0.130	0	0	0	0	0	0.016	0.004	0.151
Oxalic acid di-hydrate	0	0	0.002	0.014	0	0	0.016	0.001	0.035

Table 5.20 Normalized SP and SN values and final ranking of alternatives using AHP-EDAS method

PCM	SP$_i$	SN$_i$	NSP$_i$	NSN$_i$	AS$_i$	Rank
Acetanilide	0.010	0.098	0.040	0.736	0.388	4
Erythritol	0.242	0.013	0.959	0.964	0.962	1
Paraffin wax	0.033	0.373	0.131	0.000	0.066	5
MgCl$_2$.6H$_2$O	0.088	0.151	0.351	0.597	0.474	3
Oxalic acid di-hydrate	0.252	0.035	1.000	0.907	0.953	2

Like AHP-EDAS, the MCDM method of optimization using criteria weights obtained through ENTROPY and CRITIC techniques are referred as ENTROPY-EDAS and CRITIC-EDAS method respectively. Ranking of different PCMs using AHP-EDAS, ENTROPY-EDAS, CRITIC-EDAS and compromised weights incorporated EDAS method are made as shown in Table 5.21. All results give erythritol as optimum PCM from various alternatives for heat storage medium in SBC. Oxalic di-hydrate, magnesium chloride hexa-hydrate, acetanilde and paraffin wax are second, third, fourth and last preferred PCM among the alternatives. Here, all the methods produce same rankings of alternatives except variation between third and fourth rank in case of EDAS technique with compromised weights as input.

Table 5.21 Ranking of PCMs using EDAS method with different criteria weights

PCM	AHP-EDAS		ENTROPY-EDAS		CRITIC-EDAS		Compromised weights (W_j) - EDAS	
	AS_i	Rank	AS_i	Rank	AS_i	Rank	AS_i	Rank
Acetanilide	0.388	4	0.394	4	0.427	4	0.388	3
Erythritol	0.962	1	0.961	1	0.851	1	0.981	1
Paraffin wax	0.066	5	0.242	5	0.424	5	0.056	5
$MgCl_2.6H_2O$	0.474	3	0.471	3	0.461	3	0.381	4
Oxalic acid di-hydrate	0.953	2	0.697	2	0.562	2	0.963	2

MOORA method

Normalized assessment value (NAV) and ranking of different PCMs using AHP-MOORA, ENTROPY-MOORA, CRITIC-MOORA and compromised weights incorporated MOORA method are made as shown in Table 5.22. All results give erythritol as optimum PCM from various alternatives for heat storage medium in SBC.

The results of three MCDM methods namely TOPSIS, EDAS and MOORA shows that erythritol should be selected as LHS medium for SBC to perform effectively

comparing with other PCMs such as paraffin wax, acetanilide, magnesium chloride hexa-hydrate and oxalic acid di-hydrate.

Table 5.22 Ranking of PCMs using MOORA method with different criteria weights

PCM	AHP-MOORA		ENTROPY-MOORA		CRITIC-MOORA		Compromised weights (W_j) - MOORA	
	NAV	Rank	NAV	Rank	NAV	Rank	NAV	Rank
Acetanilide	0.372	4	0.319	4	0.283	4	0.364	3
Erythritol	0.51	1	0.441	1	0.342	1	0.529	1
Paraffin wax	0.266	5	0.269	5	0.276	5	0.246	5
$MgCl_2.6H_2O$	0.392	3	0.329	3	0.285	3	0.352	4
Oxalic acid di-hydrate	0.509	2	0.381	2	0.299	2	0.521	2

Comparison of optimum results from MCDM methods

The ranking of PCMs using MCDM methods such as TOPSIS, EDAS and MOORA with respect to different criteria weights are made. It is observed that first, second and fifth ranks are same for all the optimization methods. There is an interchange of third and fourth ranks with respect to different MCDM methods. The weights of criteria also effect the rankings of alternatives.

Spearman rank correlation coefficients (Table 5.23) are calculated between the ranks obtained by different MCDM methods (Madhua et al. 2020). This correlation coefficient confirms the dominance of MCDM method which is having closest ranking from all other MCDM methods. Spearman's rank correlation coefficient (r_s) is calculated by using the equation as given below: (Madhua et al. 2020)

$$r_s = 1 - \frac{6 \sum d^2}{n(n^2 - 1)} \tag{5.48}$$

where, 'n' is the number of alternatives and 'd' is the difference in the rank for an alternative found by two methods.

Table 5.23 Spearman rank correlation coefficient between different MCDM methods

| | | | TOPSIS | | | | EDAS | | | | MOORA | | |
		AHP	CRI	EN	CW	AHP	CRI	EN	CW	AHP	CRI	EN	CW
TOPSIS	**AHP**	1	0.9	0.7	1	0.9	0.9	0.9	1	0.9	0.9	0.9	1
	CRI	-	1	0.6	0.9	1	1	1	0.9	1	1	1	0.9
	EN	-	-	1	0.7	0.6	0.6	0.6	0.7	0.6	0.6	0.6	0.7
	CW	-	-	-	1	0.9	0.9	0.9	1	0.9	0.9	0.9	1
EDAS	**AHP**	-	-	-	-	1	1	1	0.9	1	1	1	0.9
	CRI	-	-	-	-	-	1	1	0.9	1	1	1	0.9
	EN	-	-	-	-	-	-	1	0.9	1	1	1	0.9
	CW	-	-	-	-	-	-	-	1	09	0.9	0.9	1
MOORA	**AHP**	-	-	-	-	-	-	-	-	1	1	1	0.9
	CRI	-	-	-	-	-	-	-	-	-	1	1	0.9
	EN	-	-	-	-	-	-	-	-	-	-	1	0.9
	CW	-	-	-	-	-	-	-	-	-	-	-	1

The highest average value of r_s (0.93) is obtained for seven hybrid MCDM methods such as CRITIC-TOPSIS, AHP-EDAS, CRITIC-EDAS, ENTROPY-EDAS, AHP-MOORA, CRITIC-MOORA and ENTROPY-MOORA. The average value of r_s for TOPSIS, EDAS and MOORA methods with compromised criteria weights is obtained as 0.91. Whereas the lowest value of r_s (0.64) is obtained for ENTROPY-TOPSIS method which indicates low similarity in rankings with other methods. Therefore, rankings obtained through ENTROPY-TOPSIS method can be ignored.

In addition to the computational procedure, MCDM techniques select erythritol as the best alternative among various PCMs considered for the TES unit in SBC concerning different performance criteria. Therefore, this study suggests erythritol as an optimum PCM for the TES unit integrated with SBC.

5.4 Summary

Selection of optimum PCM is essential for the development of efficient TES unit incorporated with SBC. The optimum PCM is selected with the aid of different MCDM techniques such as TOPSIS, EDAS and MOORA. The criteria weights required for the optimization algorithm is found by using AHP, ENTROPY and CRITIC methods. Through all MCDM techniques, erythritol is observed as the best alternative among various PCMs based on the different performance criteria. Calculating optimum quantity of PCM and TES unit dimensions is essential for the effective utilization of latent heat. To address this, a computational procedure is developed to solve tedious analytical equations for designing TES units for SBCs. The iterative algorithm built in MATLAB is used to calculate optimal PCM mass and container dimensions. The developed computational procedure is validated by comparing with previous works and with the experimental study. Furthermore, TES units of different geometries such as rectangular, hexagonal, and cylindrical are designed and fabricated. Based on the results, cylindrical geometries are optimal choice for TES units. This iterative procedure also recommends erythritol to be used for TES as it requires lesser quantity (6.06 kg) compared with magnesium chloride hexa-hydrate (16.02 kg) and acetanilide (13.25 kg) for maintaining constant temperature for duration of 9 hours and cooking pot of size 20 cm in diameter and 10 cm height. Therefore, erythritol is selected as the optimum PCM to be selected for TES unit integrated with SBC.

6. PERFORMANCE ASSESSMENT OF OPTIMIZED THERMAL ENERGY STORAGE SYSTEM INTEGRATED WITH SOLAR BOX COOKER

The optimized thermal energy storage (TES) unit is now tested with the trapezoidal shaped solar box cooker (TSBC) for the performance assessment. The optimum selected PCM erythritol is used as the latent heat storage (LHS) medium. As a preliminary study, the TES incorporated cooking pot is tested with cylindrical SBC (CSBC) using paraffin wax as the LHS medium. Further, the rectangular SBC (RSBC) with optimum mixture of sensible heat storage materials (SHSMs) is experimentally investigated for performance evaluation. A more detailed discussion is presented in the following sections.

6.1. Background

The optimization of TES for SBC has been presented in chapter 5. Based on the computational procedure, the TES unit is designed and fabricated. Also, optimum PCM is selected using MCDM techniques. Now it is required to test the performance of the optimized TES system by experimental study.

This chapter presents the experimental investigations of TES incorporated SBCs using sensible and latent heat storage materials. First, RSBC incorporated with optimum SHSMs such as sand, brick, charcoal, and iron grits are tested with water as cooking load. Next, the optimized TES system is tested with CSBC using paraffin wax as the LHS medium. Further, the optimized TES system with optimum PCM (erythritol) is experimentally assessed the performance using TSBC.

6.2. Performance assessment of RSBC with optimum mixture of SHSMs

In the present study, sand, charcoal, iron grits, and brick powder are used as the heat storage materials which are placed below the absorber plate of cooker. These materials are selected as they have high melting point, high specific heat capacity (Table 6.1), low cost and availability. The materials are taken in different proportion

by mass and are mixed thoroughly. They are kept above the absorber plate in different trays. The peak stagnant temperature of different composition is measured using thermocouple. The mixture composition which gives maximum temperature is selected as the optimum proportion of storage materials.

Table 6.1 Thermo-physical properties of heat storage materials (Bergman et al. 2011)

Properties	Materials			
	Sand	Iron grits	Brick	Charcoal
Density (kg/m^3)	1515	1550	1920	450
Specific heat (J/kg K)	800	460	835	709

Comparing heat storage of different proportions of SHSMs at regular interval of time, the optimum proportion of mixtures of iron grits, sand, brick powder and charcoal is found to be 1:2:2:3 respectively. For a desirable temperature of water at 80°C for about 2 hours, mass of heat storage materials is found to be 1.24 kg, 2.48 kg, 2.48 kg and 3.72 kg respectively for iron grits, sand, brick powder and charcoal.

The RSBC with heat storage material is open to the solar radiation from 10 AM to 3 PM and store the heat absorbed. A cooking pot containing 1kg of water is placed over the absorber plate and recorded the temperatures of water and absorber plate at regular intervals from 3 PM to 7 PM. From experiments, it is found that the water in the cooking pot maintains temperature above 70˚C till 6 PM (Figure 6.1). The developed RSBC incorporated with SHSMs can be best utilized for cooking the food during daytime and also during late evening hours even in situations where there is scarcity of cooking fuel.
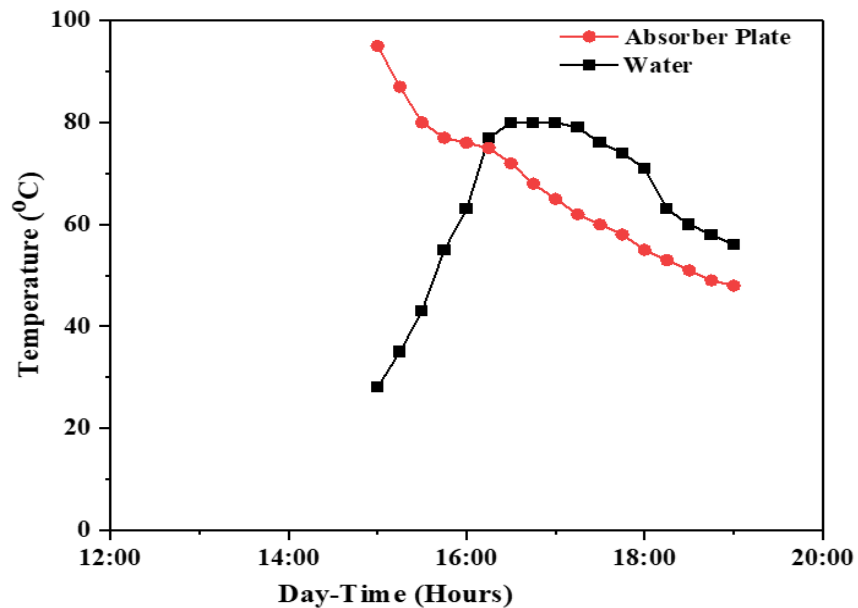
Figure 6.1 Variation of absorber plate and water temperature with time during heat retention test

6.3. Performance test of optimized TES unit containing paraffin wax charged with CSBC

The performance test of the optimized TES unit with paraffin wax as the PCM is conducted by charging with CSBC (Figure 6.2). The specifications of CSBC used in this study are already presented in section 3.2.2.2 of chapter 3. This study uses a 16 cm diameter and 18 cm high cooking vessel surrounded by the TES system. Table 5.1 of chapter 5 lists the thermo-physical parameters of commercial-grade paraffin wax, which is utilized as a PCM for heat storage. The fabrication and design of the TES are discussed in chapter 5.

Figure 6.2 Experimental setup (TES incorporated with CSBC)

The cooking pot having 1 kg of water is placed on the top of the absorber plate, and the whole assembly is open to direct sunlight. Figure 6.3 shows the variation of solar irradiance and temperatures of the absorber plate, cooking pot, water, and ambient air measured during the experiment conducted on 10th June 2021. The experiments began at 10 AM (IST) and took measurements at 15-minute intervals. The ambient, water, TES surface, and absorber plate temperatures reached 32°C, 86°C, 91°C, and 104°C, respectively at 1:15 PM, and the corresponding solar irradiance is observed to be 830 W/m². Water, absorber plate, and cooking pot temperatures gradually decrease as the day progresses. At 3 PM (IST), the cooking pot integrated TES unit is taken from the CBSC and placed in the thermal insulation box. Then, the water and TES container surface temperatures are respectively 62 and 65°C. Experimentation revealed that water keeps the temperature in the 55-60°C range until 9 PM (IST).

148
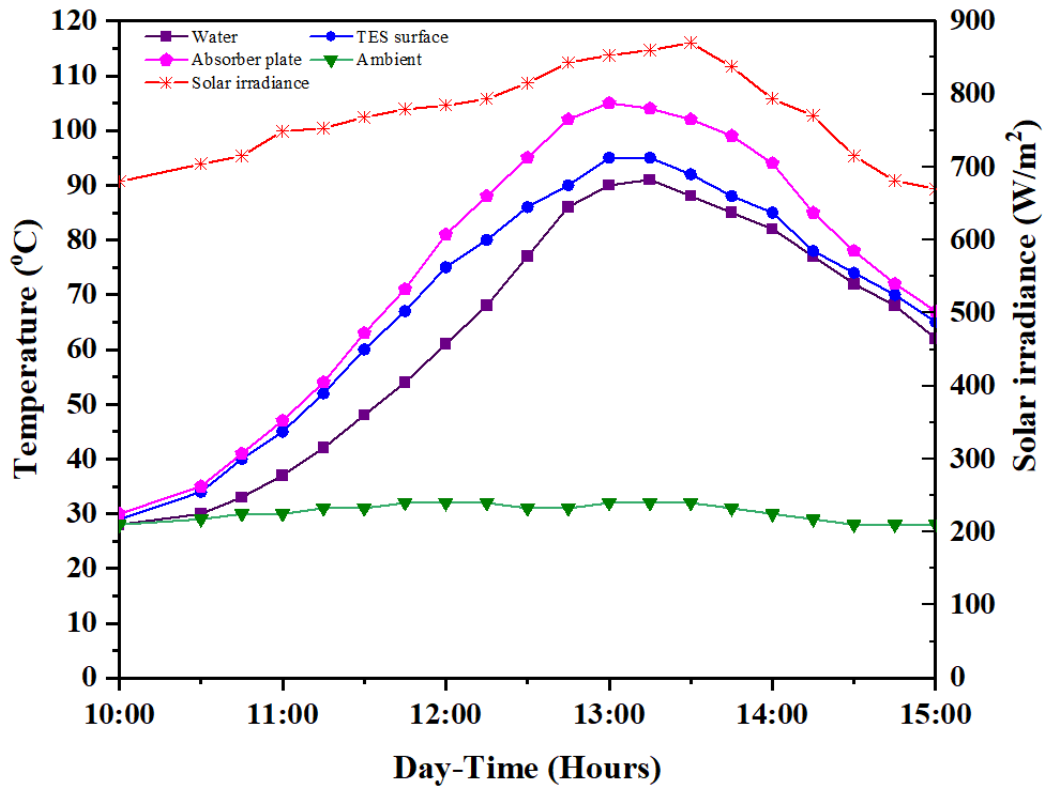
Figure 6.3 Variation of water temperature and solar irradiance with time (10th June 2021)

6.4. Performance test of optimized TES system containing erythritol as PCM integrated with TSBC

6.4.1. Phase change material (Erythritol)

In this study, TES uses erythritol ($C_4H_8O_4$) as heat storage material, a naturally occurring polyalcohol sugar found in fruits and fermented foods. The low-calorie content of erythritol makes it an attractive sugar substitute and food additive. Erythritol is considered as TES material for medium-temperature applications (Narayanan et al. 2017) and is known for its good thermal stability (Barrio et al. 2017). The melting point of erythritol makes it an excellent TES medium for SCs (around 100-120°C), ensuring temperatures higher than 100°C needed for cooking. Also, the material is non-toxic and edible. A study showed that noon cooking did not affect energy storage and that evening cooking with erythritol is faster than noon cooking (Sharma et al. 2009).

6.4.2. Thermal properties of erythritol

The melting point and latent heat of fusion of erythritol are determined by the differential scanning calorimetry (DSC) instrument NETZSCH DSC 404F1 (Figure 6.4). The measurement conditions are heating rate 5 K / min in an inert atmosphere of nitrogen, K-type temperature sensor with accuracy 0.1; testing temperature range 25 to 150°C and the sample crucible made of aluminium with lid pierced and sealed. Two different samples 7.4 and 9.5 mg of erythritol is used for testing with DSC and shows similar kind of melting phase. The numerical integration of area between heat flow and extrapolated baseline in the DSC curve is used to calculate the latent heat of specimens (Figure 6.5). The melting point in any heating process is determined by the temperature at the farthest location from base line. The thermo-physical properties of erythritol found using DSC is given in Table 6.2. The melting starts at 119.7°C and reached its peak value at 128°C for sample 1. The melting point and peak temperature for sample 2 are 117.96°C and 126.65°C respectively. Whereas the latent heat of fusion for sample 1 and 2 are respectively 328.2 and 326.8 J/g. The present DSC results are in close agreement with the properties illustrated in previous studies (Table 6.2).
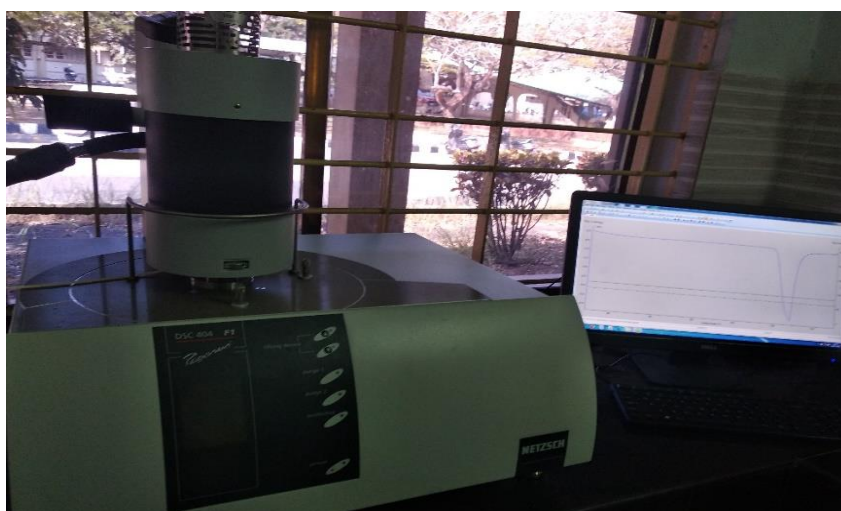
Figure 6.4 NETZSCH DSC 404F1 instrument

Table 6.2 Properties of erythritol from DSC heating curve

Properties	Present study		(Coccia et al. 2020)	(Mawire et al. 2022)
	Sample 1	Sample 2		
Melting temperature (°C)	119.7-128.0	117.9-126.6	108.7	118.4-122.0
Latent heat of fusion (kJ/kg)	328.2	326.8	312.8	310.6
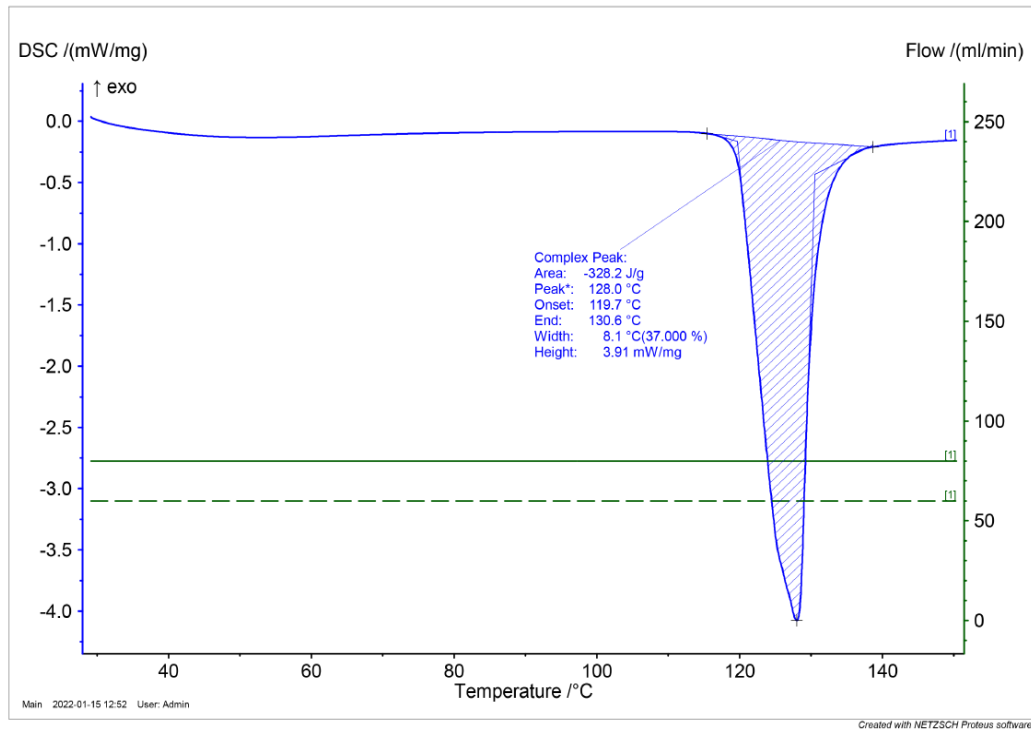
Figure 6.5 DSC heating curve of erythritol (Sample 1) by NETZSCH DSC 404F1

6.4.3. Fabrication of TES Unit

TES unit is designed using the computational procedure explained in chapter 5. TES containers are sized according to the properties of the heat storage material and the time required for evening and night cooking. Table 6.3 shows the mass of erythritol needed and size of the TES container enclosing the cooking vessel (16 cm diameter, 9 cm height). Figure 6.6 shows the pictorial view of TES incorporated cooking pot. The system utilizes two stainless steel cylindrical containers. The outer container is

painted black to enhance solar energy absorption and has diameter 20 cm and height 11.5 cm. The cooking load (water or glycerol) is contained within the inner container measuring 16 cm in diameter and 9 cm high. Then the two pots are joined by the tungsten inert gas (TIG) welding process at the top using flange. The top of the container is drilled with two holes so that PCM can be inserted into the cavity. The PCM can be loaded on both lateral and bottom sides. Erythritol is heated in an electric furnace above the melting temperature before being inserted into the TES unit. Liquid erythritol is then poured into the annular cavity of TES unit. K-type thermocouples are mounted in each of the two holes to measure PCM temperature. Through the hole in the glass lid, a thermocouple is inserted to measure the temperature of the cooking load.

Figure 6.6 Cooking pot with TES unit and glass lid

Table 6.3 Dimensions of TES units and required mass of PCM

Inner pot dimensions (cm)		Outer pot dimensions (cm)		Mass of PCM (kg)		
Diameter	Height	Diameter	Height	Lateral side	Bottom side	Total
16	9	20	11.5	1.322	0.827	2.149

6.4.4. Performance of TSBC with TES unit

The performance test is conducted with the TES unit charged with TSBC having four reflectors (Figure 6.7). The details of TSBC are given in section 3.2 of chapter 3. The TES-integrated cooking pot containing one kg of load (glycerol) is placed inside the TSBC, and the whole assembly is open to direct sunlight. Figure 6.8 shows the variation in temperatures of SBC components, glycerol, and PCM measured during the experiment conducted on 10th February 2022. The experiments began at 10 AM (IST) and took measurements at one-hour intervals. The absorber plate attained maximum temperature of 135°C at 2.00 PM, while the glycerol and PCM temperatures reached 124°C and 129°C, respectively. At 3 PM (IST), the cooking pot integrated TES unit is taken from the cooker and placed in the thermal insulation box. Then, the cooking load and PCM temperatures are respectively 119 and 121°C. Figure 6.9 (a) shows the variation of the glycerol and PCM temperatures measured up to 8 PM during the experiment. Experimentation revealed that the cooking load kept the temperature in the 113-117°C range until 8 PM (IST). Similar results are also obtained for the test conducted on 17th February 2022, as shown in Figure 6.9 (b). The cooking load maintains temperature above 114°C during evening hours.
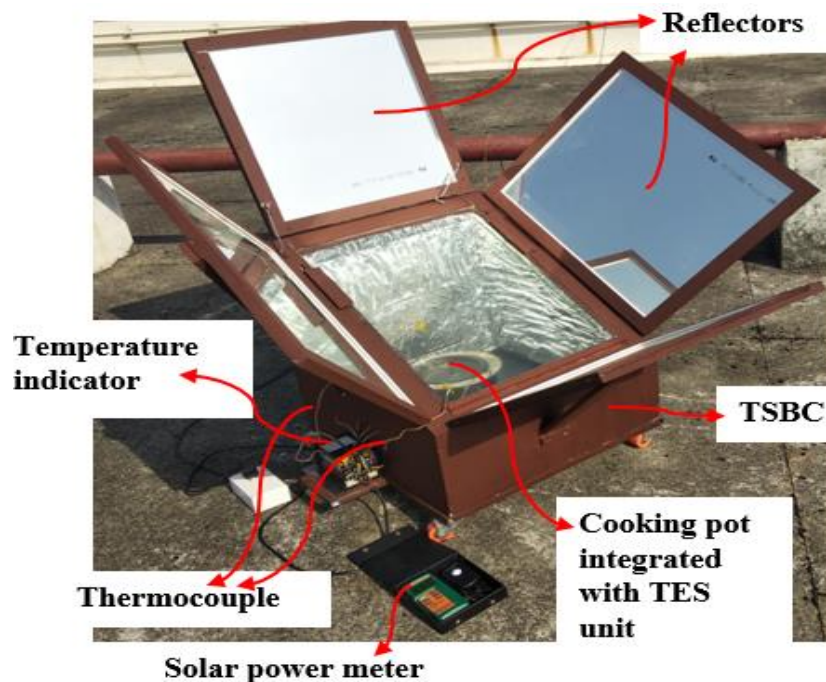
Figure 6.7 Experimental setup (TES incorporated with TSBC)

Figure 6.8 Variation of temperature and solar irradiance during performance test of TES with glycerol as cooking load (10th February 2022)
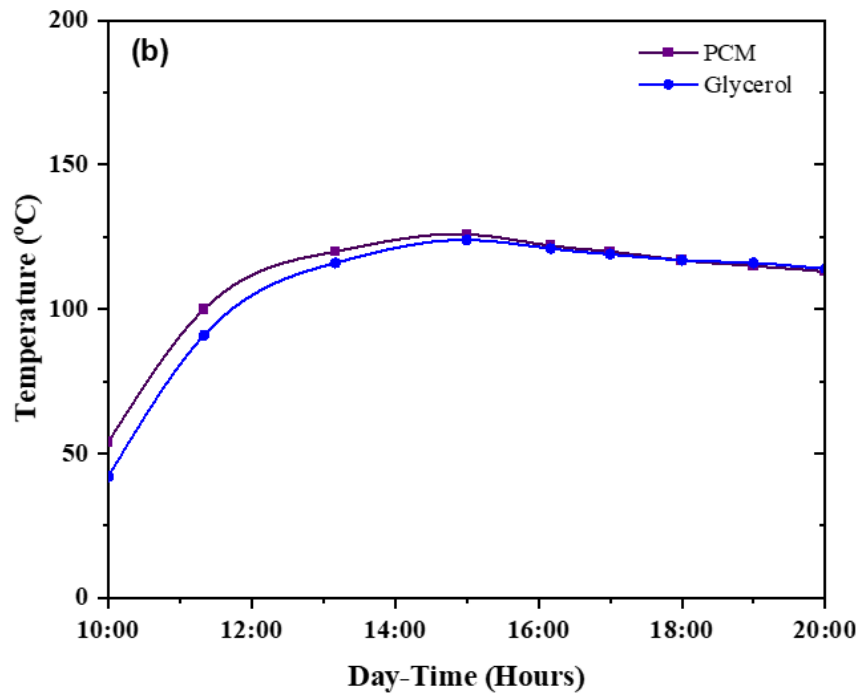
Figure 6.9 Variation of cooking load (glycerol) and PCM temperatures with time (a) 10th February 2022 (b) 17th February 2022

Figure 6.10 shows the variation of temperatures of SBC components, cooking load (water) and PCM. The absorber plate shows maximum temperature of 131°C at 2.00 PM, and the corresponding PCM and water temperatures are 121°C and 97°C. At 3 PM, the cooking pot is taken from the cooker and placed inside the thermal insulation box. The PCM and water temperatures are noted up to 8 PM and are shown in Figure 6.11. At 8 PM, the water temperature is over 90°C. Similar results of water temperature more than 90°C is obtained for the experiments conducted on 27th January and 2nd February 2022.
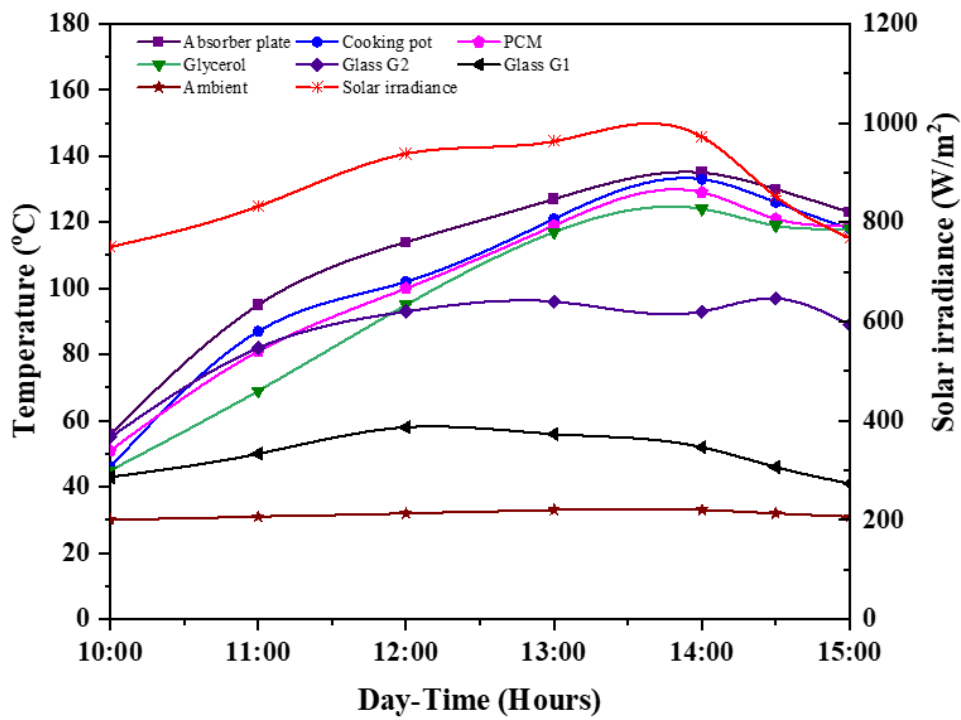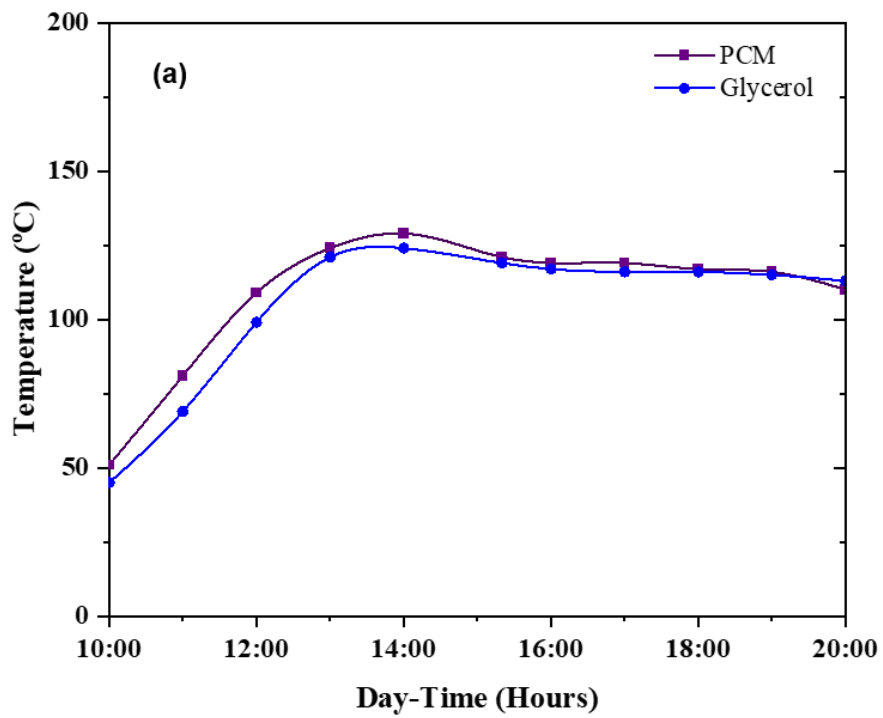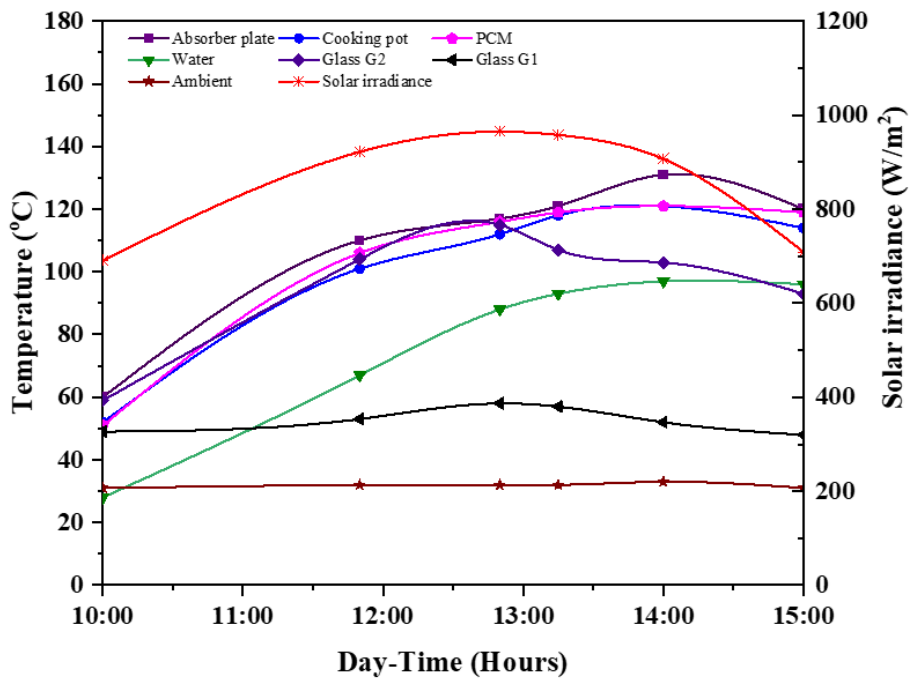
Figure 6.10 Variation of temperature and solar irradiance during performance test of TES with water as cooking load (20th February 2022)
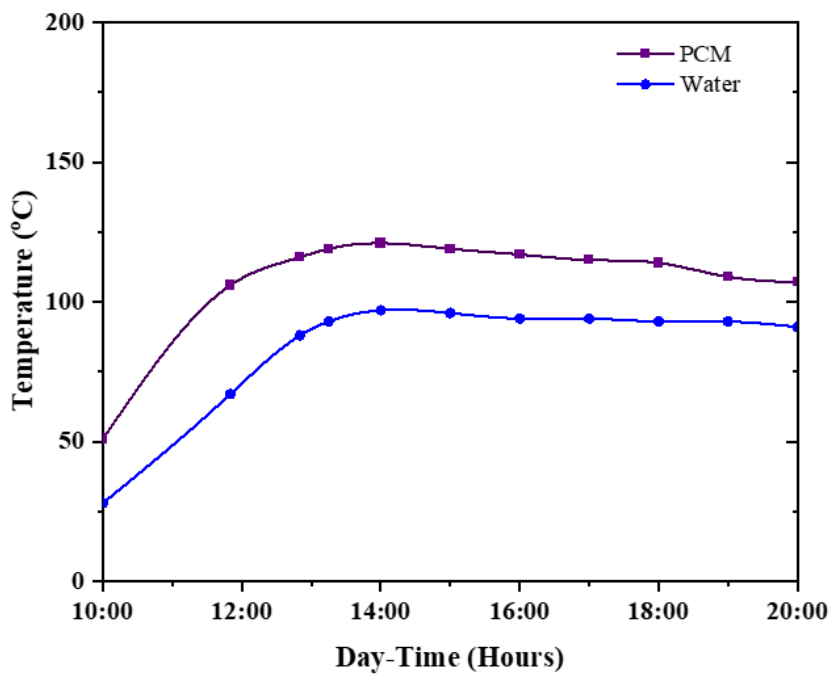
Figure 6.11 Variation of cooking load (water) and PCM temperatures with time (20th February 2022)

6.5 Summary

First, the rectangular SBC (RSBC) with optimum mixture of sensible heat storage materials (SHSMs) is experimentally investigated for performance evaluation. An optimal mixture of four SHSMs namely iron grits, sand, brick powder and charcoal in the ratio 1:2:2:3 is used to store heat in the RSBC. Though the RSBC with heat storage material gains the absorber plate temperature slowly compared to the ordinary SBCs, water temperatures above 70°C are maintained till 6 PM. Next the thermal energy storage (TES) incorporated cooking pot is tested with cylindrical SBC (CSBC) using paraffin wax as the LHS medium. The CBSC is used to charge the heat storage material during the daytime up to 3 PM (IST), and the TES unit discharges the thermal energy required for the night cooking. The results show that TES unit keep the water temperature at the same level as the melting point of paraffin wax (55-60°C) until 9 PM (IST). Then the optimized TES unit is tested with the TSBC for the performance assessment. The optimum selected PCM erythritol is used as the LHS medium. The melting temperature and latent heat of fusion of erythritol are measured using differential scanning calorimetry (DSC) instrument. The TSBC charges the PCM up to 3 PM (IST) during the day, while the TES unit discharges the thermal energy at evening hours. The TSBC integrated with the TES unit keeps the cooking load (glycerol) temperature at 113-117°C at 8 PM (IST). Similarly, the TES system integrated TBC maintains temperature of more than 90°C for water as cooking load.

7. CONCLUSION

The prime objective of the present work is to design, optimize, develop and test a solar box cooker (SBC) incorporated with optimized thermal energy storage (TES) unit using phase change material (PCM). This study uses experimental, numerical, and machine learning-based analysis as provided in Chapters 3 to 6. A summary of each chapter is presented below.

7.1. Experimental analysis of various shaped solar box cookers

In Chapter 3, rectangular, cylindrical, and trapezoidal shaped SBCs are designed, fabricated, and studied for performance evaluation. Experiments are conducted on various shaped SBCs to familiarize them with the test procedure and performance assessment.

A rectangular-shaped solar box cooker (RSBC) is developed as a preliminary work. The optimum cooker surface area is calculated using analytical heat loss and energy balance equations. The heat loss factors are computed by an iterative procedure using MATLAB programming. Based on the anticipated average value of solar irradiance and mass of water to be boiled, the absorber plate area is 0.34 m^2. The RSBC having an outer reflector is fabricated according to the design considerations. The first and second figures of merit are obtained from experimental investigations as 0.085 and 0.319, respectively, which is lower than that of A-grade SBC as per the Bureau of Indian Standards (BIS). This is because sensible heat storage materials (SHSMs) absorb a large amount of heat from the absorber plate.

Next, the performance evaluation of cylindrical solar box cooker (CSBC) fitted with decahedron-shaped outer reflector is carried out. The CSBC is designed and fabricated based on the principle of the minimum entropy generation (MEG) method. The absorber plate area obtained through the MEG method is 0.146 m^2. The experimental investigation is conducted to check the effectiveness of decahedron reflector on the performance of cooker, including stagnation, sensible heat, and cooking performance tests. The average values of the first and second figures of merit are 0.13 and 0.39, respectively, which satisfies the requirements of A-grade SBC. The

energy and exergy efficiency and standardized cooking power are 21.93 %, 3.04 %, and 24.84 W. The developed cooker shows better-standardized cooking power and energy efficiency performance than the conventional rectangular and trapezoidal-shaped SBCs. The heat loss coefficient is computed through an iterative procedure and compared with the experimentally obtained value. The time for boiling 0.5 kg of water and cooking 100g of rice is 80 and 100 minutes. Cooking above 100°C with minimum boiling time is possible with the CSBC fitted with decahedron reflector. The developed CSBC is a promising device that can be further optimized for better performance. One of the remarkable findings is that the present CSBC fitted with decahedron reflector attained boiling temperature in a shorter time than previously developed models cited in the literature. It is suggested that the proposed method of MEG theory could be used as a starting point for further research on the optimum design of SCs that minimize energy loss. Computational methods for estimating heat loss coefficients will also assist in improving the efficiency of SCs.

Trapezoidal-shaped SBC (TSBC) is designed and fabricated in the next stage. The absorber plate area of 0.2256 m^2 is set based on the MEG method. Tests are performed on the TSBC with and without outer reflectors. The absorber plate temperature increases 37.9% when passing from one configuration to another. It shows maximum absorber plate temperature of 171°C under mean solar irradiance and surrounding temperature of 841.8 W/m^2 and 32°C, respectively. The cooker with outer reflectors is more optically efficient, as indicated by the first figure of merit of 0.135. Different SBCs are compared concerning standardized cooking power, energy efficiency, and the first figure of merit. TSBC fitted with four outer reflectors performs more than the CSBC fitted with decahedron reflector.

The economic analysis of TSBC and CSBC is carried out. Annualized life cycle cost (ALCC) of $14.3 (₹1,066.00) and $18.16 (₹1354.00) are obtained respectively for the TSBC and CSBC, which is economically feasible. Considering 50% of time where SBC is used, the payback period for TSBC and CSBC are respectively 2.61 and 3.31 years. Therefore, TSBC is more cost-effective option than CSBC.

7.2. Prediction model development for SBC using computational and machine learning techniques

Chapter 4 presented prediction model development for SBC by combining numerical simulation and machine learning (ML) techniques. This study uses ML techniques such as random forest, decision tree, linear regression, and k-nearest neighbor (k-NN).

The use of ML techniques in solar thermal energy conversion applications is of significant importance in developing effective prediction models. Many data are involved in solar thermal device analysis, depending on the day, time, and location. Developing an ML-based prediction model is essential to forecast the system performance in a short time, which motivates the present study. Accordingly, prediction models for SBC have been developed using ML techniques such as RF, decision tree, linear regression, and k-NN. For this, first, a numerical model based on thermal balances at different components of SBC is developed to generate the input data required for ML models. Experiments are carried out on the TSBC from January to March 2022 to validate the numerical model. Across all component temperatures, the difference between experimental and numerical results is less than 7%, indicating the accuracy of the numerical model. Then, the ML prediction models are trained, validated, and tested using the simulation results. The root mean square error (RMSE), determination coefficient (R^2), mean absolute error (MAE), and mean square error (MSE) are used to assess ML prediction results. The RMSE, R^2, MAE and MSE for the prediction using RF model are 1.61 (^{o}C), 0.996, 1.21 (^{o}C) and 2.60 (^{o}C), respectively. It indicates that the RF model can accurately predict the thermal parameters of SBCs with great precision. In light of the performance evaluation results, the RF procedure might be viewed as a feasible and practical method for predicting the temperatures of different components in SBC. Further, based on the analysis of input variables and their effects in ML modeling, it is found that the present TSBC is more effective in regions with latitudes less than 30° and longitudes greater than 25°. This kind of approach will be beneficial in solar thermal applications for early and faster prediction of performance parameters.

7.3. Design optimization of PCM-based thermal energy storage unit for solar box cooker

Chapter 5 presents optimization of TES system for SBCs for evening or night cooking. A computational procedure is developed to simplify the exhaustive calculations required to optimize and design the TES unit employing PCM as the heat storage medium. Different geometries of TES units are fabricated, and experiments are conducted to validate the computational procedure. The optimum PCM for TES is also selected using multi-criteria decision-making (MCDM) methods.

Calculating optimum quantity of PCM and TES unit dimensions is essential for the effective utilization of latent heat. A computational procedure is developed to solve tedious analytical equations for designing TES units for SBCs. The iterative algorithm implemented in MATLAB computes optimal PCM mass and container dimensions. The developed computational procedure is validated by comparing with previous works and the present experimental study. TES units of various shapes (cylindrical, hexagonal, and square) incorporated with the cooking vessel are designed, fabricated, and tested for the comparative performance study. This novel TES unit features PCM storage on all sides, even on the lid, which increases heat transfer to the cooking load. Commercial grade paraffin wax is used as the latent heat storage (LHS) material. The results of the indoor test show that after 6 hours, all geometries of TES units keep the water temperature at the same level as the melting point of paraffin wax (55-60°C). However, cylindrical TES unit perform best, followed by hexagonal, while square TES unit perform least. The surface area to volume ratio is lowest for cylindrical geometry and highest for a square shape. The computational procedure will simplify the exhaustive calculations in designing TES units of different shapes employing any LHS material. The developed iterative solver will be helpful for researchers to do the optimum design of the TES unit for SBC for the effective utilization of latent heat stored in PCM.

Selection of optimum PCM is also essential for developing an efficient TES unit incorporated with SBC. This study selects the optimum PCM with the aid of different MCDM techniques such as TOPSIS, EDAS, and MOORA. The criteria weights required for the optimization algorithm is found using AHP, ENTROPY, and CRITIC

methods. Through all MCDM techniques, erythritol is the best alternative among various PCMs based on the different performance criteria. The iterative procedure also recommends erythritol to be used for TES surrounding the cooking pot of dimensions 20 cm diameter and 10 cm height as it requires lesser quantity (6.06 kg) compared with magnesium chloride hexahydrate (16.02 kg) and acetanilide (13.25 kg) for maintaining a constant temperature for 9 hours. Therefore, the present study suggests erythritol as the optimum PCM to be selected for the TES unit integrated with SBC.

7.4. Performance assessment of optimized thermal energy storage system integrated with solar box cooker

In chapter 6, performance analysis of optimized TES systems incorporated with SBC is presented. The TES unit is designed and fabricated using iterative procedure as discussed in chapter 5.

First, the RSBC with optimum SHSMs is investigated for the performance evaluation. An optimal mixture of SHSMs namely iron grits, sand, brick powder and charcoal in the ratio 1:2:2:3 is used to store the heat energy in the cooker. Though the RSBC with heat storage material gains the absorber plate temperature slowly compared to the ordinary SBCs, water temperatures above 70°C are maintained till 6 PM. Therefore, it is concluded that the heat retention capacity is sufficient for RSBC with SHS to maintain higher temperatures during late evening compared to conventional SBCs.

Next, as a preliminary study, the optimized TES unit discussed in chapter 5 is tested with CSBC using paraffin wax as the LHS medium. The CBSC is used to charge the heat storage material during the daytime up to 3 PM (IST), and the TES unit discharges the thermal energy required for the night cooking. The experimental results show that TES unit keep the water temperature at the same level as the melting point of paraffin wax (55-60°C) until 9 PM (IST). Finally, the optimized TES unit is tested with the TSBC for the performance assessment. The optimum selected PCM erythritol is used as the LHS medium. The melting temperature and latent heat of fusion of erythritol are measured using differential scanning calorimetry (DSC) instrument. The TSBC charges the PCM up to 3 PM (IST) during the day, while the TES unit

discharges the thermal energy at evening hours. The TSBC integrated with the TES unit keeps the cooking load (glycerol) temperature at 113-117°C at 8 PM (IST). Similarly, the TES system integrated TBC maintains temperature of more than 90°C for water as cooking load.

7.5. Summary

This study focused on the design, fabrication, and experimental assessment of the performance of a novel solar box cooker (SBC) incorporated with the optimized thermal energy storage (TES) unit using phase change material (PCM). It includes experimental, numerical, and machine learning-based analysis. Rectangular, cylindrical, and trapezoidal shaped SBCs are designed, fabricated, and studied for performance evaluation. The trapezoidal shaped SBC is found to be more efficient and cost-effective compared with rectangular and cylindrical. Next, the temperature at different elements of the SBC is predicted using computational and machine learning (ML) techniques. The ML models can easily predict the performance without further simulations to test the same kind of solar cooker at different geographical locations. This kind of approach will be beneficial in solar thermal applications for early and faster prediction of performance parameters. Next, the optimization of TES system for SBCs for evening or night cooking is carried out. For this, a computational procedure is developed to simplify the exhaustive calculations required to optimize and design the TES unit employing PCM as the heat storage medium. Different geometries of TES units are fabricated, and experiments are conducted to validate the computational procedure. The optimum PCM for TES is selected using multi-criteria decision-making (MCDM) methods. The study suggests erythritol as the optimum PCM for the TES unit integrated with SBC. Finally, the optimized TES unit is tested with the trapezoidal SBC for the performance assessment which keeps the cooking load (glycerol) temperature at 113-117°C during night hours.

REFERENCES

Abd-Elhady, M.S., Abd-Elkerim, A.N.A., Ahmed, S., Halim, M.A., and Okail, A.I. (2019). Study the thermal performance of solar cookers by using metallic wires and nano graphene. *Renewable Energy,* 153, 108-116.

Abu-Hamdeh, N.H., and Alnefaie, K.A. (2019). Assessment of thermal performance of PCM in latent heat storage system for different applications. *Solar Energy,* 177, 317-323.

Adelard, L., Pignolet-Tardan, F., Mara, T., Lauret, P., Garde, F., and Boyer, H. (1998). Sky temperature modelisation and applications in building simulation. *Renewable Energy,* 15, 418–430.

Adetifa, B.O., and Aremu, A.K. (2016). Investigating the effect of different heat storage media on the thermal performances of double exposure box-type solar cookers. *International Journal of Renewable Energy Research*, 6(3), 1109-1118.

Agrawal, H., and Yadav, A. (2015). Thermal Analysis of a Solar Cooker with Sensible Heat Storage unit. *Journal of Material Science and Mechanical Engineering*, 2(6), 9-12.

Ahmad, M.W., Reynolds, J., and Rezgui, Y. (2018). Predictive modelling for solar thermal energy systems: A comparison of support vector regression, random forest, extra trees and regression trees. *Journal of Cleaner Production,* 203, 810-821.

Ahmed, S.M.M., Al-Amin, M.R., Ahammed, S., Ahmed, F., Saleque, A.M., and Rahman, M.A. (2020). Design, construction and testing of parabolic solar cooker for rural households and refugee camp. *Solar Energy,* 205, 230–240.

Algifri, A.H., and Al-Towaie, H.A. (2001). Efficient orientation impacts of box-type solar cooker on the cooker performance. *Solar Energy*, 70(2), 165-170.

Al-Nehari, H.A., Mohammed, M.A., Odhah, A.A., Al-attab, K.A., Mohammed, B.K., Al-Habari, A.M., and Al-Fahd, N.H. (2021). Experimental and numerical analysis of

tiltable box-type solar cooker with tracking mechanism. *Renewable Energy,* 180, 954-965.

Apaolaza-Pagoaga, X., Carrillo-Andres, A., and Ruivo, C.R. (2021b). New approach for analysing the effect of minor and major solar cooker design changes: Influence of height trivet on the power of a funnel cooker. *Renewable Energy,* 179, 2071-2085.

Apaolaza-Pagoaga, X., Carrillo-Andres, A., Ruivo, C.R., and Fernández-Hernández, F. (2023). The effect of partial loads on the performance of a funnel solar cooker. *Applied Thermal Engineering*, 219, Part C, 119643.

Apaolaza-Pagoaga, X., Sagade, A.A., Ruivo, C.R., and Carrillo-Andres, A. (2021a). Performance of solar funnel cookers using intermediate temperature test load under low sun elevation. *Solar Energy,* 225, 978-1000.

Arabacigil, B., Yuksel, N., Avci, A. (2015). The use of paraffin wax in a new solar cooker with inner and outer reflectors. *Thermal Science*, 19(5) 1663-1671.

Aramesh, M., Ghalebani, M., Kasaeian, A., Zamani, H., Lorenzini, G., Mahian, O., and Wongwises, S. (2019). A review of recent advances in solar cooking technology. *Renewable Energy,* 140, 419-435.

Arif, M.R., Khan, M.A., Azhar, M., Akhtar, N., and Meraj, M. (2021). Thermal Performance Comparison and Augmentation of Two Identical Box-Type Solar Cookers Operating in Tropical Climatic Conditions. *Journal of thermal science and engineering applications,* 13(6), 061004.

Arunachala, U.C., and Kundapur, A. (2020). Cost-effective solar cookers: A global review. *Solar Energy,* 207, 903-916.

Atmane, I., El Moussaoui, N., Kassmi, K., Deblecker, O., and Bachiri, N. (2021). Development of an innovative cooker (hot plate) with photovoltaic solar energy. *Journal of Energy Sto*rage, 36, 102399.

Bejan, A., Kearney, D.W., and Kreith, F. (1981). Second Law Analysis and Synthesis of Solar Collector Systems. *Journal of Solar Energy Engineering*, 103 (23).

Bergman, T.L., Lavine, A.S., Incropera, F.P., and Dewitt, D.P. (2017). Fundamentals of Heat and Mass Transfer, 7th Edition, John Wiley & Sons.

Bhavani, S., Shanmugan, S., Chithambaram, V., Essa, F.A.E., Kabeel, A., and Selvaraju, P. (2021). Simulation study on thermal performance of a Solar Box Cooker using nanocomposite for natural Food invention. *Environmental Science and Pollution Research*, 28, 50649-50667.

Bhave, A.G., and Kale, C.K. (2020). Development of a thermal storage type solar cooker for high temperature cooking using solar salt. *Solar Energy Materials and Solar Cells,* 208,110394.

Bhave, A.G., and Thakare, K.A. (2018). Development of a solar thermal storage cum cooking device using salt hydrate. *Solar Energy,* 171, 784-789.

Binark, A.K., and Turkmen, N. (1996). Modelling of a hot box solar cooker. *Energy Conversion Management,* 37(3), 303-310.

Breiman, L. (2001). Random forests. Machine Learning, 45, 5-32.

Buddhi, D., and Sahoo, L.K. (1997). Solar cooker with Latent heat storage: Design and Experimental Testing. *Energy Conversion Management,* 38 (5), 493-498.

Buddhi, D., Sharma, S.D., and Sharma, A. (2003). Thermal performance evaluation of a latent heat storage unit for late evening cooking in a solar cooker having three reflectors. *Energy Conversion Management,* 44(6), 809-817.

Channiwala, S.A., and Doshi, N.I. (1989). Heat loss coefficients for box-type solar cooker. *Solar Energy*, 42(6), 495-501.

Chatelain, T., Mauree, D., Taylor, S., Bouvard, O., Fleury, J., Burnier, L., and Schuler, A. (2019). Solar cooking potential in Switzerland: Nodal modelling and optimization. *Solar Energy,* 194, 788-803.

Chauhan, A., Tyagi, V.V., and Anand, S. (2019). Minimum entropy generation and its validation against Hottel Whillier model for PV/T and FPC collectors. *Solar Energy,* 188, 143–157.

Chen, C.R., Sharma, A., Tyagi, S.K., and Buddhi, D. (2008). Numerical heat transfer studies of PCMs used in a box-type solar cooker. *Renewable Energy,* 33, 1121-1129.

Churchill, S.W., and Chu, H.H. (1975). Correlating equations for laminar and turbulent free convection from a vertical plate. *International Journal of Heat and Mass Transfer,* 18, 1323–1329.

Coccia, G., Aquilanti, A., Tomassetti, S., Comodi, G., and Nicola, G.D. (2020). Design, realization, and tests of a portable solar box cooker coupled with an erythritol-based PCM thermal energy storage. *Solar Energy,* 201, 530–540.

Coccia, G., Aquilanti, A., Tomassetti, S., Ishibashi, A., and Di Nicola, G. (2021). Design, manufacture and test of a low-cost solar cooker with high-performance light-concentrating lens. *Solar Energy,* 224, 1028–1039.

Coccia, G., Nicola, G.D., Pierantozzi, M., Tomassetti, S., and Aquilanti, A. (2017). Design, manufacturing, and test of a high concentration ratio solar box cooker with multiple reflectors. *Solar Energy,* 155, 781–792.

Collares-Pereira, M., Cavaco, A., and Tavares, A. (2018). Figures of merit and their relevance in the context of a standard testing and performance comparison methods for solar box-cookers. *Solar Energy,* 166, 21-27.

Cuce, E. (2018a). Improving thermal power of a cylindrical solar cooker via novel micro/nano porous absorbers: A thermodynamic analysis with experimental validation. *Solar Energy,* 176, 211-219.

Cuce, P.M. (2018b). Box type solar cookers with sensible thermal energy storage medium: A comparative experimental investigation and Thermodynamic analysis. *Solar Energy*, 166, 432-440.

Cuce, P.M., Kolayli, S., and Cuce, E. (2020). Enhanced performance figures of solar cookers through latent heat storage and low-cost booster reflectors. *International Journal of Low-Carbon Technologies*, 00:1-7.

Diakoulaki, D., Mavrotas, G., and Papayannakis, L. (1995). Determining Objective Weights in Multiple Criteria Problems: the CRITIC Method, *Computers and Operations Research,* 22(7) 763–770.

Domanski, R., El-Sebaii, A.A., and Jaworski, M. (1995). Cooking during off-sunshine hours using PCMs as storage media. *Energy,* 20(7), 607-616.

Duffie, J.A., and Beckman, W.A. (2013). Solar Engineering of Thermal Processes, fourth ed., John Wiley & Sons, New York.

Ebersviller, S.M., and Jetter, J.J. (2020). Evaluation of performance of household solar cookers. *Solar Ener*gy, 208, 166-172.

Ekechukwu, O.V., and Ugwuoke, N.T. (2003). Design and measured performance of a plane reflector augmented box-type solar-energy cooker. *Renewable Energy,* 28, 1935-1952.

El-Sebaii, A.A., Al-Amir, S., Al-Marzouki, F.M., Faidah, A.S., Al-Ghamdi, A.A.M., and Al-Heniti, S. (2009). Fast thermal cycling of acetanilide and magnesium chloride hexa-hydrate for indoor solar cooking. *Energy Conversion and Management,* 50(12), 3104–3111.

El-Sebaii, A.A., and Ibrahim, A. (2005). Experimental testing of a box-type solar cooker using the standard procedure of cooking power. *Renewable Energy,* 30, 1861-1871.

Emovon, I., and Oghenenyerovwho, O.S. (2020). Application of MCDM method in material selection for optimal design: A review. *Results in Materials,* 7, 100115.

Engoor, G.G., Shanmugam, S., and Veerappan, A.R. (2020). Experimental investigation of a box-type solar cooker incorporated with Fresnel lens magnifier. *Energy Sources, Part A: Recovery, Utilization, and Environmental effects,* https://doi.org/10.1080/15567036.2020.1826009.

Engoor, G.G., Shanmugam, S., Veerappan, A.R. (2022). Energy and exergy based study on a box type solar cooker coupled with a Fresnel lens magnifier. *International Journal of Green Energy*, https://doi.org/10.1080/15435075.2022.2043868.

Funk, P.A. (2000). Evaluating the International standard procedure for testing solar cookers and reporting performance. *Solar Energy,* 68(1), 1-7.

Gadhave, P., Prabhune, C., and Pathan, F. (2020). Selection of phase change material for domestic water heating using multi criteria decision approach. *Australian Journal of Mechanical Engineering*, doi: 10.1080/14484846.2020.1842297

Geddam, S., Dinesh, G.K., and Sivasankar, T. (2015). Determination of thermal performance of a box type solar cooker. *Solar Energy*, 113, 324-331.

Goswami, A., Basu, S., and Sadhu, P.K. (2019). Improvement of Energy Efficiency and Effectiveness of Cooking for Parabolic-Type Solar Cooker Used with Activated-Carbon-Coated Aluminium Cooking Pot. *Global Challenges*, 1900047.

Guidara, Z., Souissi, M., Stern, A.M., and Maalej, A. (2017). Thermal performance of a solar box cooker with outer reflectors: Numerical and Experimental Investigation. *Solar Energy,* 158, 347-359.

Harmim, A., Merzouk, M., Boukar, M., and Amar, M. (2013). Design and experimental testing of an innovative building-integrated box type solar cooker. *Sol Energy*, 98, 422-433.

Herez, A., Ramadan, M., and Khaled, M. (2018). Review on solar cooker systems: Economic and environmental study for different Lebanese scenarios. *Renewable and Sustainable Energy Reviews,* 81, 421–432.

Hollands, K.G.T., Unny, T.E., Raithby, G.D., and Konicek, L. (1976). Free convective heat transfer across inclined air layers. *ASME Trans. J. Heat Transfer* 98, 189-193.

Hosseinzadeh, M., Faezian, A., Mirzababaee, S.M., Zamani, H. (2020c). Parametric analysis and optimization of a portable evacuated tube solar cooker. *Energy,* 194, 116816.

Hosseinzadeh, M., Sadeghirad, R., Zamani, H., Kianifar, A., and Mirzababaee, S.M. (2020a). The performance improvement of an indirect solar cooker using multi-walled carbon nanotube-oil nanofluid: an experimental study with thermodynamic analysis. *Renewable Energy*, 165, 14-24.

Hosseinzadeh, M., Sadeghirad, R., Zamani, H., Kianifar, A., Mirzababaee, S.M., and Faezian, A. (2020b). Experimental study of a nanofluid-based indirect solar cooker: Energy and exergy analyses. *Solar Energy Materials & Solar Cells*, 221, 110879.

Hottel, H.C. (1976). A simple model for estimating the transmittance of direct solar radiation through clear atmosphere. *Solar Energy,* 18, 129-134.

Indora, S., and Kandpal, T.C. (2018). Institutional and community solar cooking in India using SK-23 and Scheffler solar cookers: A financial appraisal. *Renewable Energy*, 120, 501-511.

Kajumba, P.K., Okello, D., Nyeinga, K., and Nydal, O.J. (2020). Experimental investigation of a cooking unit integrated with thermal energy storage system. *Journal of Energy Storage*, 32, 101949.

Kandpal, T.C., and Mathur, S.S. (1986). The economics of box-type solar cookers. *Energy Conversion Management*, Vol.26, No.2, pp. 233-235.

Kandpal, T.C., and Mathur, S.S. (1986). The economics of box-type solar cookers. *Energy conversion management*, 26(2), 233-235.

Kanyowa, T., Nyakujara, G.V., Ndala, E., and Das, S. (2021). Performance analysis of Scheffler dish type solar thermal cooking system cooking 6000 meals per day. *Solar Energy,* 218, 563–570.

Karayalcin, I.I. (1982). The Analytic Hierarchy Process: Planning, Priority Setting, Resource Allocation: T. L. SAATY. McGraw-Hill, New York, 1980, xiii+ 287 pages. *European Journal of Operational Research,* 9(1), 97–98.

Kaushika, N.D., Tomar, R.K., and Kaushik, S.C., (2014). Artificial neural network model based on interrelationship of direct, diffuse and global solar radiations. *Solar Energy,* 103, 327-342.

Kedida, D.K., Amibe, D.A., and Birhane, Y.T. (2019). Performance of a Pebble Bed Thermal Storage Integrated with Concentrating Parabolic Solar Collector for Cooking. *Hindawi Journal of Renewable Energy*, Article ID 4238549.

Keshavarz Ghorabaee, M., Zavadskas, E.K., Olfat, L., and Turskis, Z. (2015). Multi-criteria inventory classification using a new method of evaluation based on distance from aver- age solution (EDAS), *Informatica,* 26 (3), 435–451.

Khallaf, A.M., Tawfik, M.A., El-Sebaii, A.A., and Sagade, A.A. (2020). Mathematical modeling and experimental validation of the thermal performance of a novel design solar cooker. *Solar Energy,* 207, 40–50.

Kolhe, M., Kolhe, S., and Joshi, J.C. (2002). Economic viability of stand-alone solar photovoltaic system in comparison with diesel-powered system for India. *Energy Economics,* 24, 155-165.

Kumar, A., Saxena, A., Pandey, S.D., and Joshi, S.K. (2022). Design and performance characteristics of a solar box cooker with phase change material: A feasibility study for Uttarakhand region, India. *Applied Thermal Engineering*, 208, 118196.

Kumar A, Shukla SK, Kumar A (2018) Heat loss analysis: An approach toward the revival of parabolic dish type solar cooker. International Journal of Green Energy, DOI: 10.1080/15435075.2018.1423978.

Kumar, S. (2004a). Natural convective heat transfer in trapezoidal enclosure of box-type solar cooker. *Renewable Energy,* 29, 211-222.

Kumar, S. (2004b). Thermal Performance study of box type solar cooker from heating characteristic curves. *Energy Conversion and Management,* 45, 127-139.

Kumar, S. (2005). Estimation of design parameters for thermal performance evaluation of box-type solar cooker. *Renewable Energy* ,30, 1117-1126.

Kumar, S., Rubaib, S., Kandpal, T.C., and Mullick, S.C. (1996). Financial feasibility analysis of box-type solar cookers in India. *Energy*, l21, 1257-1264.

Kurt, H., Atik, K., Ozkaymak, M., and Recebli, Z. (2008). Thermal performance parameters estimation of hot box type solar cooker by using artificial neural network. *International Journal of Thermal Science,* 47, 192-200.

Kurt, H., Deniz, E., and Recebli, D. (2008a). An investigation into the effects of box geometries on the thermal performance of solar cookers. *International Journal of Green Energy*, 5, 508-519.

Lecuona, A., Nogueira, J., Ventas, R., Rodríguez-Hidalgo, M. and Legrand, M. (2013). Solar cooker of the portable parabolic type incorporating heat storage based on PCM. *Applied Energy,* 111, 1136–1146.

Lee, H., and Chang, C. (2018). Comparative analysis of MCDM methods for ranking renewable energy sources in Taiwan. *Renewable and Sustainable Energy Reviews,* 92, 883–896.

Lotfi, F.H., and Fallahnejad, R. (2010). Imprecise Shannon's entropy and multi attribute decision making. *Entropy (Basel, Switzerland),* 12(1), 53–62.

Madhua, P., Dhanalakshmia, C.S., and Mathew, M. (2020). Multi-criteria decision-making in the selection of a suitable biomass material for maximum bio-oil yield during pyrolysis, *Fuel,* 277, 118109.

Mahavar, S., Sengar, N., Rajawat, P., Verma, M., and Dashora, P. (2012). Design development and performance studies of a novel Single Family Solar Cooker. *Renewable Energy*, 47, 67-76.

Mardani, A., Jusoh, A., Nor, K.M.D., Khalifah, Z., Zakwan, N., and Valipour, A. (2015). Multiple criteria decision-making techniques and their applications – a review of the literature from 2000 to 2014. *Economic Research-Ekonomska Istraživanja,* 28 (1), 516-571.

Mawire, A., Lentswe, K., Owusu, P. (2022). Performance of two solar cooking storage pots using parabolic dish solar concentrators during solar and storage cooking periods with different heating loads. *Results in Engineering,* 13,100336.

Mawire, A., Lentswe, K., Owusu, P., Shobo, A., Darkwa, J., Calautit, J. and Worall, M. (2020). Performance comparison of two solar cooking storage pots combined with wonderbag slow cookers for off-sunshine cooking. *Solar Energy,* 208, 1166–1180.

Mawire, A., Simelane, S.M., and Abedigamba, P.O. (2021). Energetic and exergetic performance comparison of three solar cookers for developing countries. *Environment, Development and Sustainability*, 23, 14528-14555.

Mbodji, N., and Ali Hajji (2017). Modeling, testing, and parametric analysis of a parabolic solar cooking system with heat storage for indoor cooking. *Energy, Sustainability and Society*, 7, 32.

Mendoza, J.M.F., Gallego-Schmid, A., Rivera, X.C.S, Rieradevall, J., and Azapagic, A. (2019). Sustainability assessment of home-made solar cookers for use in developed countries. *Science of the Total Environment,* 648, 184-196.

Milikias, E., Bekele, A., and Venkatachalam, C. (2020). Performance investigation of improved box-type solar cooker with sensible thermal energy storage. *International Journal of Sustainable Engineering,* 14(3), 507-516.

Mishra, P.K., Nadda, R., Kumar, R., Rana, A., Sethi, M., and Ekilesk, A. (2018). Optimization of multiple arcs protrusion obstacle parameters using AHP-TOPSIS approach in an impingement jet solar air passage. *Heat and Mass Transfer*, 54, 3797-3808.

Mostafaeipour, A., Behzadian, M., Fakhrzad, M.B., Techato, K., and Najafi, F. (2021). A strategic model to identify the factors and risks of solar cooker

manufacturing and use: A case study of Razavi Khorasan, Iran. *Energy Strategy Reviews,* 33, 100587.

Mukaro, R. (2021). Comparison of experimental and artificial neural network estimated thermal performance parameters for a hot-box solar cooker. *Informatica,* 32(3), 2-15.

Mukaro, R., and Tinarwo, D. (2008). Performance evaluation of a hot-box reflector solar cooker using a microcontroller-based measurement system. *International Journal of Energy Research,* 32, 1339–1348.

Mullick, S.C., Kandpal, T.C., and Kumar, S. (1997). Top heat-loss factor of double-glazed box-type solar cooker from indoor experiments. *Energy,* 22(6), 559-565.

Mullick, S.C., Kandpal, T.C., and Saxena, A.K. (1987). Thermal Test Procedure for Box-Type Solar Cookers. *Solar Energy,* 39(4),353-360.

Nahar, N.M. (2001). Design, development and testing of a double reflector hot box solar cooker with a transparent insulation material. *Renewable Energy,* 23, 167-179.

Nahar, N.M. (2003). Performance and testing of a hot box storage solar cooker. *Energy Conversion and Management,* 44, 1323–31.

Narayanan, S.S., Kardam, A., Kumar, V., Bhardwaj, N., Madhwal, D., Shukla, P., Amit, K., Verma, A., and Jain, V.K. (2017). Development of sunlight-driven eutectic phase change material nanocomposite for applications in solar water heating. *Resource-Efficient Technologies,* 3, 272-279.

Nayak, N., Abu Jarir, H., and Al Ghassani, H. (2016). Solar cooker study under Oman conditions for late evening cooking using stearic acid and acetanilide as PCM materials. *Hindawi Journal of Solar Energy, 2016, 2305875*.

Neto, R.V.P., de Souza, L.G.M., de Lima, J.C., de Souza, L.G.V.M., and Mendes, E.V. (2021). Theoretical-experimental study of a box-type solar oven made from disused recyclable elements. *Solar Energy,* 230, 732–746.

Nkhonjera, L., Bello-Ochende, T., John, G., and King'ondu, C.K. (2017). A review of thermal energy storage designs, heat storage materials and cooking performance of solar cookers with heat storage. *Renewable and Sustainable Energy Reviews,* 75, 157–167.

Nyahoro, P.K., Johnson, R.R., and Edwards, J. (1997). Simulated performance of Thermal storage in a solar cooker. *Solarl Energy*, 59,11-7.

Omara, A.A.M., Abuelnuor, A.A.A., Mohammed, H.A., Habibi, D., and Younis, O. (2020). Improving solar cooker performance using phase change materials: A comprehensive review. *Solar Energy,* 207, 539–563.

Ozturk, H.H. (2004). Second law analysis for solar cookers. *International Journal of Green Energy,* 1, 227-239.

Palanikumar, G., Shanmugan, S., Chithambaram, V., Gorjian, S., Pruncu, C.I., Essa, F.A., Kabeel, A.E., Panchal, H., Janarthanan, B., Ebadi, H., Elsheikh, A.H., and Selvaraju, P. (2021). Thermal Investigation of a Solar Box-type Cooker with Nanocomposite Phase Change Materials Using Flexible Thermography. *Renewable Energy,* 178, 260-282.

Panchal, H., Patel, J and Chaudhary, S. (2019). A comprehensive review of solar cooker with sensible and latent heat storage materials. *International Journal of Ambient Energy*, 40(3), 329-334.

Panchal, H., and Sadasivuni, K.K. (2018). Investigation and Performance analysis of Scheffler reflector solar cooking system integrated with sensible and latent heat storage materials. *International Journal of Ambient E*nergy, 41(10),1096-1105.

Panwar, N.L., Kothari, S., and Kaushik, S.C. (2013). Techno-economic evaluation of masonry type animal feed solar cooker in rural areas of an Indian state Rajasthan. *Energy Policy*, 52 ;583–586.

Purohit, I. (2010). Testing of solar cookers and evaluation of instrumentation error. *Renewable Energy,* 35, 2053-2064.

Purohit, I., and Purohit, P. (2009). Instrumentation error analysis of a box-type solar cooker. *Energy Conversion and Management,* 50, 365-375.

Ramadan, M.R.I., Aboul-Enein, S., and El-Sebaii, A.A. (1998). A model of an improved low cost indoor solar cooker in Tanta. *Solar and Wind Technology*, 5, 387-393.

Rastogi, M., Chauhan, A., Vaish, R., and Kishan, A. (2015). Selection and performance assessment of Phase Change Materials for heating, ventilation and air-conditioning applications. *Energy Conversion and Management,* 89, 260-269.

Rathod, M.K., and Kanzaria, H.V. (2011). A methodological concept for phase change material selection based on multiple criteria decision analysis with and without fuzzy environment. *Materials and Design,* 32(6), 3578-3585.

Riva, F., Rocco, M.V., Gardumi, F., Bonamini, G., and Colombo, E. (2017). Design and performance evaluation of solar cookers for developing countries: the case of Mutoyi, Burundi. *International Journal of Energy Research*, 1-15.

Ruivo, C.R., Apaolaza-Pagoaga, X., Nicola, G.D., and Carrillo-Andres, A. (2022). On the use of experimental measured data to derive the linear regression usually adopted for determining the performance parameters of a solar cooker. *Renewable Energy,* 181, 105-115.

Ruivo, C.R., Carrillo-Andres, A., and Apaolaza-Pagoaga, X. (2021). Experimental determination of the standardised power of a solar funnel cooker for low sun elevations. *Renewable Energy,* 170, 364-374.

Sagade, A.A., Samdarshi, S.K., and Lahkar, P.J. (2019). Ensuring the computation of solar cooking process under unexpected reduction in solar irradiance. *Solar Energy,* 179, 286-297.

Sagade, A.A., Samdarshi, S.K., Lahkar, P.J., and Sagade, N.A. (2019). Experimental determination of the thermal performance of a Solar Box Cooker with a modified Cooking Pot. *Renewable Energy*, 150, 1001-1009.

Sagade, A.A., Samdarshi, S.K., and Panja, P.S. (2018). Experimental determination of effective concentration ratio for solar box cookers using thermal tests. *Solar Energy,* 159, 984-991.

Sagade, A.A., Samdarshi, S.K., Sagade, N.A., and Panja. P.S. (2021). Enabling open sun cooling method-based estimation of effective concentration factor/ratio for concentrating type solar cookers. *Solar Energy,* 227, 568–576.

Samdarshi, S.K., and Mullick, S.C. (1991). Analytical equation for the top heat loss factor of a flat-plate collector with double glazing. *Journal of Solar Energy Engineering*, 113(2), 117-122.

Saxena, A., and Agarwal, N. (2018) Performance characteristics of a new hybrid solar cooker with air duct. *Solar Energy*, 159, 628-637.

Saxena, A., and Karakilcik, M. (2017) Performance Evaluation of a Solar Cooker with Low Cost Heat Storage Material. *International Journal of Sustainable and Green Energy,* 6(4), 57-63.

Saxena, A., Cuce, E., Tiwari, G.N., and Kumar, A. (2020). Design and thermal performance investigation of a box cooker with flexible solar collector tubes: An experimental research. *Energy,* 206, 118144.

Shanmugan, S., Gorjian, S., Elsheikh, A.H., Essa, F.A., Omara, Z.M., and Raghu, A.V. (2020). Investigation into the effects of SiO_2/TiO_2 nanolayer on the thermal performance of solar box type cooker. *Energy Sources, Part A: Recovery, Utilization, and Environmental Effect,s* 43(21), 2724-2737.

Sharma, A., Chen, C.R., Murty, V.V.S., and Shukla, A. (2009). Solar cooker with latent heat storage systems: A review. *Renewable and Sustainable Energy Reviews,* 13, 1599–1605.

Sharma, A., Muqeem, M., Sherwani, A.F., and Ahmad, M. (2018). Optimization of diesel engine input parameters running on Polanga biodiesel to improve performance and exhaust emission using MOORA technique with standard deviation, *Energy*

Sources, Part A: Recovery, Utilization, and Environmental Effects, 40 (22), 2753-2770.

Sharma, S.D., Buddhi, D., Sawhney, R.L., and Sharma, A. (2000). Design, development and performance evaluation of a latent heat storage unit for evening cooking in a solar cooker. *Energy Conversion Management,* 41(14), 1497-1508.

Sharma, S.D., Iwata, T., Kitano, H., and Sagara, K. (2005). Thermal performance of a solar cooker based on an evacuated tube solar collector with a PCM storage unit. *Solar Energy*, 78, 416-426.

Siddique, M.Z., Badar, A.W., Jakhrani, S.A., Khan, M.Y., Butt, F.S., and Siddiqui, M.S. (2020). Development and experimental investigation of a novel combined solar cooker and dryer unit, *Energy Sources, Part A: Recovery, Utilization, and Environmental Effects*. https://doi.org/10.1080/15567036.2020.1777222

Singh, M., and Sethi, V.P. (2018). On the design, modelling and analysis of multi-shelf inclined solar cooker cum- Dryer. *Solar Energy,* 162, 620–636.

Singh, O.K. (2021). Development of a solar cooking system suitable for indoor cooking and its exergy and enviroeconomic analyses. *Solar Energy,* 217, 223–234.

Sivaraja, C.M., Sakthivel, G., and Warke, V.R. (2018). Selection of optimum fuel blend to empower the energy efficiency in IC engine using decision system. *Energy Sources, Part A: Recovery Utilization, and Environmental Effects,* 40(6), 693-708.

Socaciu, L., Giurgiu, O., Banyai, D., and Simion, M. (2016). PCM selection using AHP method to maintain thermal comfort of the vehicle occupants. *Energy Procedia,* 85, 489-497.

Soria-Verdugo, A. (2015). Experimental analysis and simulation of the performance of a box type solar cooker. *Energy for sustainable Development,* 29, 65-71.

Tawfik, M.A., Sagade, A.A., Palma-Behnke, R., Abd Allah, W.E., and El-Shal, H.M. (2022). Performance evaluation of solar cooker with tracking type bottom reflector

retrofitted with a novel design of thermal storage incorporated absorber plate. *Journal of Energy Storage,* 51, 104432.

Tawfik, M.A., Sagade, A.A., Palma-Behnke, R., El-Shal, H.M., and Abd Allah, W.E. (2021). Solar Cooker with Tracking-Type Bottom Reflector: An Experimental Thermal Performance Evaluation of a New Design. *Solar Energy,* 220, 295-315.

Thirugnanam, C., Karthikeyan, S., and Kalaimurugan, K. (2020). Study of phase change materials and its application in solar cooker. *Materials Today: Proceedings*, 33(7), 2890-2896.

Tibebu, S., Hailu, A. (2021). Design, Construction, and Evaluation of the Performance of Dual-Axis Sun Trucker Parabolic Solar Cooker and Comparison of Cooker. *Journal of Renewable Energy*, Article ID 8944722.

Torres-Reyes, E., Gortari, J.G.C., Ibarra-Salazar, B.A., and Picon-Nunez, M. (2001). A design method of flat-plate solar collectors based on minimum entropy generation, *Exergy Int. J.* 1(1), 46–52.

Trilok, G., and Gnanasekaran, N. (2021). Numerical study on maximizing heat transfer and minimizing flow resistance behavior of metal foams owing to their structural properties, *International Journal of Thermal Sciences,* 159, 106617.

Vaishya, J.S., Tripathi, T.C., Singh, D., Bhawalker, R.H., and Hegde M.S. (1985). A hot box solar cooker: Performance analysis and testing. *Energy Conversion Management,* 25(3), 373-379.

Vengadesan E., and Senthil, R. (2021). Experimental investigation of the thermal performance of a box type solar cooker using a finned cooking vessel. *Renewable Energy,* 171, 431-446.

Venugopal, D., Chandrasekaran, J., Janarthanan, B., Shanmugan, S., and Kuma, S. (2012). Parametric optimization of a box-type solar cooker with an inbuilt paraboloid reflector using Cramer's rule. *Int J Sustain Energy*, 31(4), 213-227.

Verma, S., Banerjee, S., and Das, R. (2022). A fully analytical model of a box solar cooker with sensible thermal storage. *Solar Energy,* 233, 531–542.

Vigneswaran, V.S., Kumaresan, G., Sudhakar, P., and Santosh, R. (2017). Performance evaluation of solar box cooker assisted with latent heat energy storage system for cooking application. *IOP Conf. Series: Earth and Environmental Science,* 67, 012017.

Weldu, A., Zhao, L., Deng, S., Mulugeta, N., Zhang, Y., Nie, X., and Xu, W. (2019). Performance evaluation on solar box cooker with reflector tracking at optimal angle under Bahir Dar climate. *Solar Energy*, 180, 664-677.

Xu, H., Jia, Y.S., Romagnoli, A., and Py, X. (2017). Selection of phase change material for thermal energy storage in solar air conditioning systems. *Energy Procedia,* 105, 4281-4288.

Yadav, V., Kumar, Y., Agrawal, H., Yadav, A. (2015). Thermal Performance evaluation of solar cooker with latent and sensible heat storage unit for evening cooking. *Australian Journal of Mechanical Engineering,* 28.

Yang, K., Zhu, N., Chang, C., Wang, D., Yang, S. and Ma, S. (2018). A methodological concept for phase change material selection based on multi-criteria decision making (MCDM): A case study. *Energy,* 165, 1085-1096.

Yazdani, M., Torkayesh, A.E., Santibanez-Gonzalez, E.D.R., and Otaghsara, S.K. (2020). Evaluation of renewable energy resources using integrated Shannon Entropy-EDAS model. *Sustainable Operations and Computers* 1, 35–42.

Yettou, F., Azoui, B., Malek, A., Panwar, N.L., Gama, A., Arrif, T., and Merarda, H. (2015). Comparative assessment of two different designs of box solar cookers under algerian sahara conditions. *Revue des Energies Renouvelables,* 18 (2), 227 -234.

Yuksel, N., Arabacigil, B., and Avci, A. (2012). The thermal analysis of paraffin wax in a box-type solar cooker. *Journal of Renewable and Sustainable Energy,* 4, 063126: 1-9.

Zafar, H.A., Badar, A.W., Butt, F.S., Khan, M.Y., and Siddiqui, M.S. (2019). Numerical modeling and parametric study of an innovative solar oven. *Solar Energy,* 187, 411-426.

Zamani, H., Mahian, O., Rashidi, I., Lorenzini, G., and Wongwises, S. (2017). Exergy Optimization of a Double- Exposure Solar Cooker by Response Surface Method. *Journal of Thermal Science and Engineering Applications,* 9, 011003.

LIST OF PUBLICATIONS BASED ON PH.D. RESEARCH WORK

Sl. No.	Title of the paper	Authors (in the same order as in the paper. Underline the Research Scholar's name)	Name of the Journal/ Conference, Vol., No., Pages	Month, Year of Publication	Category*
1	Design, fabrication, and performance assessment of a solar cooker with optimum composition of heat storage materials.	<u>Anil Kumar B C</u>, Ranjith Maniyeri and Anish S	Environmental Science and Pollution Research, 28, pp. 63629 – 63637. (SCI Indexed)	October 2020	1
2	Optimum selection of phase change material for solar box cooker integrated with thermal energy storage unit using multi-criteria decision-making technique.	<u>Anil Kumar B C</u>, Ranjith Maniyeri and Anish S	Journal of Energy Storage, 40: 102807. (SCIE Indexed)	June 2021	1
3	Thermal performance assessment of a cylindrical box solar cooker fitted with decahedron outer reflector.	<u>Anil Kumar B C</u>, Ranjith Maniyeri and Anish S	Energy and Environment, DOI:10.1177/0958305X211070779 (SSCI Indexed)	December 2021	1
4	Modified thermal energy storage unit for solar cookers using iterative design algorithm	<u>Anil Kumar B C</u>, Ranjith Maniyeri and Anish S	Materials Today: Proceedings, 58 (1), pp. 39-45 (SCOPUS Indexed)	January 2022	1
5	Numerical investigation on the effect of various geometries in a solar box-type cooker: A comparative study.	<u>Anil Kumar B C</u>, Ranjith Maniyeri and Anish S	Book chapter, Fluid mechanics and fluid power, Lecture notes in mechanical Engineering, Springer Nature, pp. 81 – 89. https://doi.org/10.1007/978-981-16-0698-4_9 (SCOPUS Indexed) (Research article presented in 46th National Conference on Fluid Mechanics and Fluid Power (FMFP 2019), PSG College of Technology, Coimbatore, India.)	2020	3

6	Experimental investigation on the effect of decahedron frustum shaped reflector on the performance of a cylindrical solar box-type cooker.	Anil Kumar B C, Ranjith Maniyeri and Anish S	4th International Conference on Sustainable Energy and Environmental Challenges (SEEC-2019), CSIR-NEERI, Nagpur, India.	November 27-29, 2019	3
7	Design, fabrication, and performance assessment of a solar cooker with optimum composition of heat storage materials.	Anil Kumar B C, Ranjith Maniyeri and Anish S	5th International Conference on Recent Advancements in Chemical, Energy and Environmental Engineering (RACEEE 2020), SSN College of Engineering, Chennai.	February 13 - 14, 2020	3
8	Performance evaluation of solar cookers using multi-criteria decision-making methods	Anil Kumar B C, Ranjith Maniyeri and Anish S	International Conference on Advance in Mechanical Engineering: Transcending Boundaries (ICAMET 2021), Mangalam College of Engineering, Kottayam, Kerala, India.	July 22 - 23, 2021	3
9	Performance comparison of different geometries of thermal energy storage unit for solar cooker	Anil Kumar B C, Ranjith Maniyeri and Anish S	2nd National and 1st International conference on Fluid Flow and Thermal Sciences, (ICAFFTS 2021), SVNIT Surat, Gujarat, India.	September 24 - 25, 2021	3
10	Solar cooker with low-cost sensible heat storage medium	Anil Kumar B C, Ranjith Maniyeri and Anish S	Best Poster Presentation Award (Poster presentation in Mahindra University Research Symposium (MURS-2020), Mahindra University, Hyderabad. Telangana, India.)	November 26-27, 2020	4

*Category: 1: Journal paper, full paper reviewed   2: Journal paper, Abstract reviews   3: Conference/Symposium paper, full paper reviewed
4: Conference/Symposium paper, abstract reviewed   5: Others (including papers in Workshops, NITK Research Bulletins, Short notes etc.)

BIODATA

NAME: ANIL KUMAR B C

DATE OF BIRTH: 26-09-1982

Mobile No.: +91 9496358213

Email: anilkbc20031@gmail.com

ADDRESS:

Balakandam House, Karadka Post, Kasaragod Dist, Kerala, India - 671542

QUALIFICATION:

Examination	Board/Institute	Year	Percentage / CGPA
Ph. D (course work)	NITK, Surathkal	2019	8.75
M. Tech (Thermal Sciences)	NIT Calicut	2010-2012	9.1
BTech (Mechanical Engg)	LBSCE Kasaragod	2000-2004	76.87%
XII	CBSE	2000	81.4%
X	CBSE	1998	80%

PROFESSIONAL EXPERIENCE:

Name of the College	Designation	From	To
SNGCET Payyanur, Kerala	Lecturer	June 2005	October 2007
LBSCE Kasaragod, Kerala	Assistant Professor	January 2008	July 2019

ACHIEVEMENTS:

1. **Second Rank** in the Kannur University BTech Degree (Mechanical Engineering) in the year 2004.
2. **Best Teacher Award** for the year 2015-16 in LBS College of Engineering Kasaragod.
3. **Best poster presentation** award for the paper titled 'Solar cooker with low-cost sensible heat storage medium' in the Mahindra University Research Symposium (MURS 2020).